NASA CR-159,135

NASA Contractor Report 159135

NASA-CR-159135
19800006812

Exploratory Studies of the Cruise Performance of Upper Surface Blown Configurations

Experimental Program - High-Speed Pressure Tests

J. A. Braden, J. P. Hancock,
K. P. Burdges, and J. E. Hackett

LOCKHEED-GEORGIA COMPANY
Marietta, Georgia 30063

NASA Contract NAS1-13871
OCTOBER 1979

National Aeronautics and
Space Administration

Langley Research Center
Hampton, Virginia 23665
AC 804 827-3966

FOREWORD

This document is submitted in accordance with the requirements of NASA Contract NAS1-13871, Exploratory Studies of the Cruise Performance of Upper Surface Blown Configurations. W. C. Sleeman, Jr. is the NASA-Langley Contract Monitor and J. A. Braden is the Lockheed-Georgia Project Manager.

The technical results under this contract are presented in five reports. For convenience, the overall program documentation is summarized below:

DOCUMENTATION SUMMARY

CR Number	Title
CR-3193	Summary Report
CR-3192	Experimental Program - Test Facilities, Model Design, Instrumentation, and Low-Speed, High-Lift Tests
CR-159134	Experimental Program - High-Speed Force Tests
CR-159135	Experimental Program - High-Speed Pressure Tests
CR-159136	Program Analysis and Conclusions

N80-15071 #

TABLE OF CONTENTS

LIST OF FIGURES

LIST OF FIGURES (CONT'D)

LIST OF FIGURES (CONT'D)

LIST OF FIGURES (CONT'D)

LIST OF FIGURES (CONT'D)

LIST OF FIGURES (CONT'D)

LIST OF FIGURES (CONT'D)

LIST OF FIGURES (CONT'D)

LIST OF FIGURES (CONT'D)

LIST OF FIGURES (CONT'D)

LIST OF FIGURES (CONT'D)

SUMMARY

The purpose and scope of the Cruise Performance Data Base Contract (NAS1-13871) are reviewed briefly in Section 1 of this document. Pertinent model and installation details are then described briefly. Objectives of the pressure test are discussed and the run schedule is outlined. Data are presented for both the standard type of nozzle installation fed by the wing duct and the upstream pipe test arrangement. The purpose of the latter was to permit testing of nacelles mounted on thin pylons on nacelles with nozzles too large for the wing duct supply. Additional variations in nacelle geometry covered by the data of this report are nacelle chordwise position and nozzle shape. Data for both straight and swept wing installations are included. Nacelle and wing pressures in both scrubbed and unscrubbed areas are presented. Wake isobars from data measured one chord length downstream of the wing trailing edge are presented for a number of the test configurations.

1.0 INTRODUCTION

In early 1975, the NASA awarded a contract (NAS1-13871) to the Lockheed-Georgia Company for the acquisition of a high-speed, experimental data base for aircraft configurations featuring nacelles mounted on the upper wing surface. This design concept, known as USB (upper-surface blowing), had received earlier, experimental endorsements as a viable means of achieving moderate-to-good powered lift performance along with beneficial noise reduction in the STOL environment. In the interest of further development of the USB-system, the contractual work performed by the Lockheed-Georgia Company emphasizes an exploratory investigation of the transonic cruise characteristics of USB nacelle-wing combinations. The total program is detailed in the Program Plan of Reference 1. Included in this Program Plan is the commitment to perform two-dimensional pressure tests of a selected range of wing/nacelle combinations. This effort is an important part of the Task II, Cruise Performance Data Base, which is described in Reference 1. To properly analyze the performance trends obtained in the force tests, local pressures on the nacelle and wing surfaces are required. In addition, wake total pressure patterns downstream of the model are also useful. It is to meet these needs as well as the pressure test requirements delineated in Task II that the data in this report are provided.

2.0 SYMBOLS

Dimensional data are presented herein in both the International System of Units (SI) and the U.S. Customary Units. The measurements and calculations were made in the U.S. Customary Units.

A	area, cm^2 ($in.^2$)
AR	aspect ratio
b	model span, cm (in.)
BL	abbreviation: boundary layer
c, C	local wing chord, cm (in.)
$\bar{c}$	mean aerodynamic chord, cm (in.)
C_p, CP	pressure coefficient, $(p_l - p_\infty)/q_\infty$
H_l/H_∞, HL/HO	jet wake local total pressure ratio
M_∞, M	freestream Mach number
p_∞	freestream static pressure, N/m^2 (lb/ft^2)
q_∞	freestream dynamic pressure, N/m^2(lb/ft^2)
R_{NC}	Reynolds number based on $\bar{c}$.
x, X	distance parallel to tunnel centerline, cm (in.)
y, Y	transverse (spanwise) distance, cm (in.)
z, Z	vertical distance, cm (in.)
α	angle of attack, degrees
η	percent semispan

Note: Symbols following commas were employed on computer plots only.

3.0 MODEL AND INSTRUMENTATION DETAILS

The basic objective of the model design effort was to develop a wing-nacelle arrangement which could accommodate a wide range of USB nozzle types for comparative evaluation. An arrangement for metering smooth-profile, high-pressure air to the nozzle entrance was considered necessary. Means for obtaining static pressure distribitions on key surface areas were also required.

3.1 Model Design

To accomplish the desired objectives, the high-speed test configurations were developed around two wing-body configurations with untapered wings swept 0 and 25 degrees. These basic test vehicles could be combined in build-up fashion with a series of nacelle fore-bodies to form a wide range of powered or unpowered configurations. The choice of piped-in nozzle supply air over a powered simulator was made for simplicity and economy. A smooth flow profile at the nozzle entry is ensured by a choke plate with 0.159 cm (1/16 in.) diameter holes evenly distributed over the plate. The substitution of nacelles with other configuration designs, as well as conversion to the clean wing configurations, is made possible by the build-up design of the nacelle pylon, and nozzle mounting block. A re-mote-controlled traversing wake rake is positioned one chord length downstream to provide for complete mapping of the model/jet wake pattern.

A front view of the 2-D pressure model configuration mounted in the tunnel is presented in Figure 1. As the model is viewed in this photograph, nozzle supply air is ducted in from the right-hand side, while pressure tubes are routed out the left-hand side. The traversing wake rake can be seen in the background. A complete description of the model test arrangement including design details of all the model components is contained in Reference 2, which is Volume IIA of this same report.

3.2 Pressure Instrumentation Details

A layout of the straight wing planform along with spanwise locations of the 5 rows of static pressure taps is presented in Figure 2. Row A is directly behind the nacelle and immersed

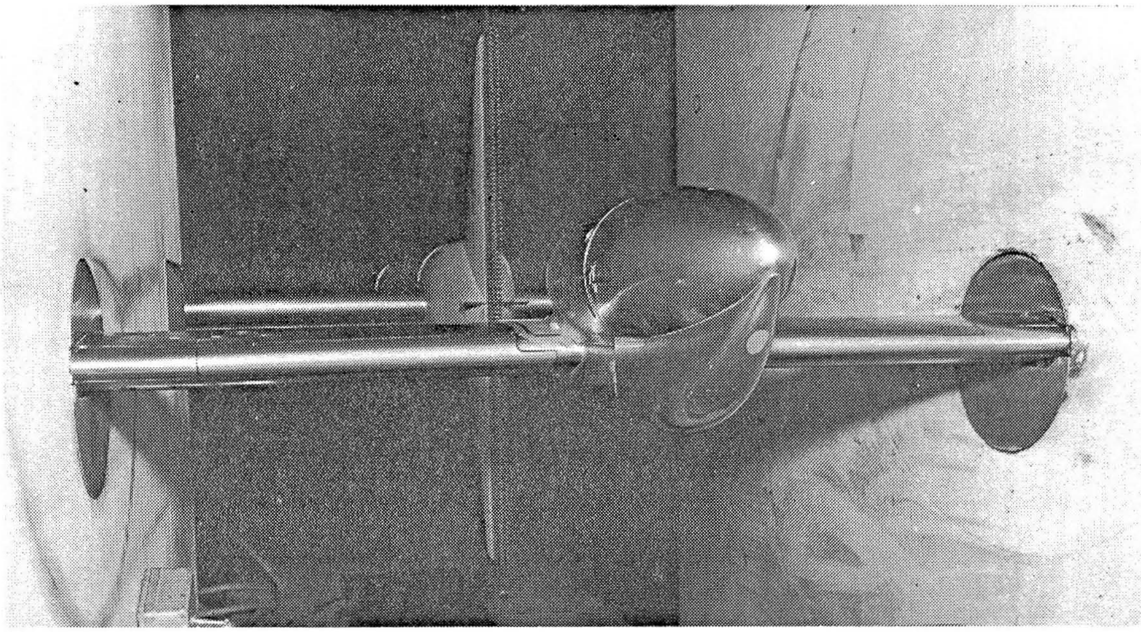

Figure 1. Two-dimensional pressure model and traversing wake rake mounted in CFF

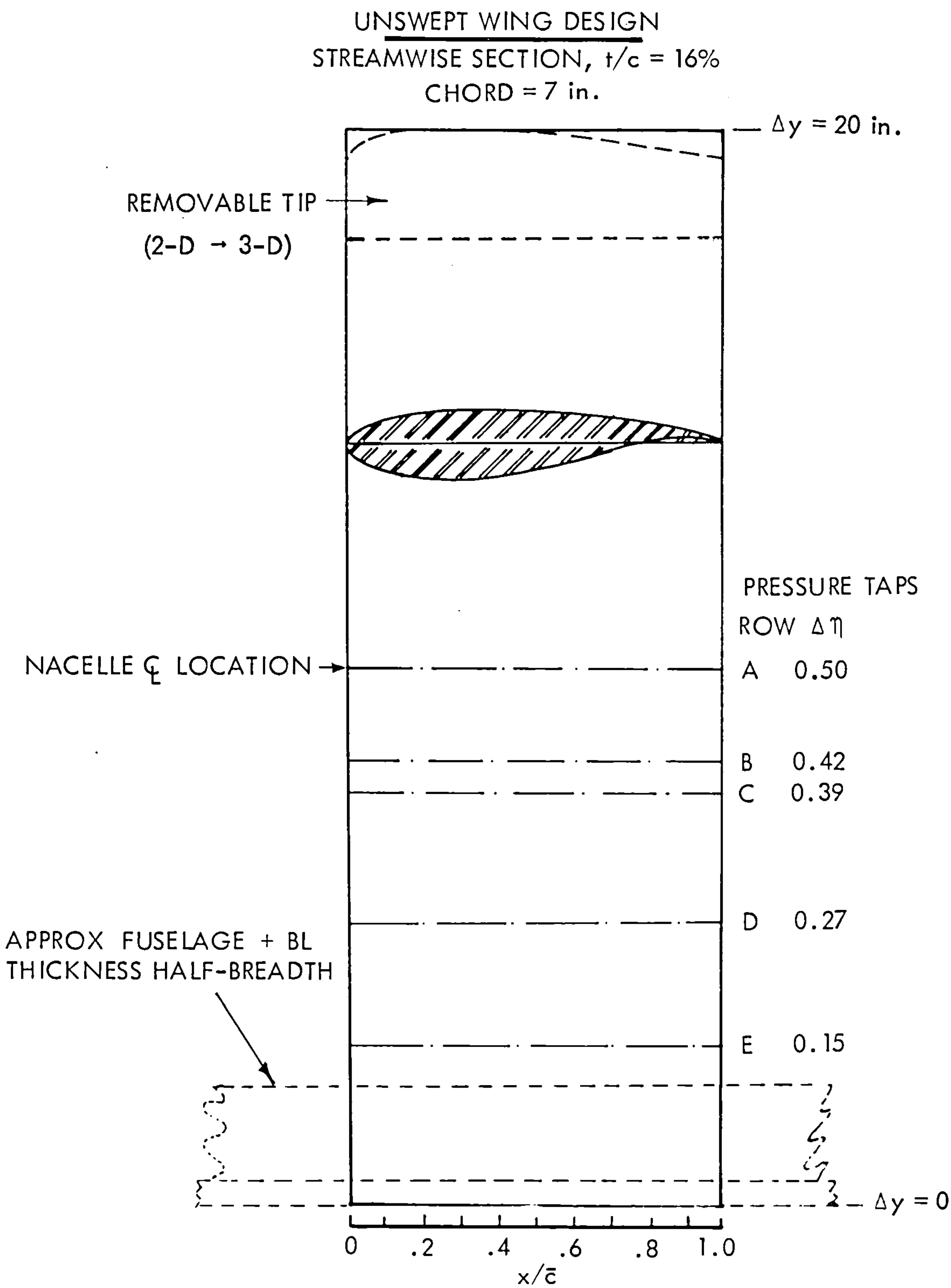

Figure 2. Straight wing planform and instrumentation layout

in the jet, while rows B and C are positioned to obtain jet and nacelle interference effects. Rows D and E are outside the wing/nacelle interference region. Figure 3 shows the chordwise positions for the pressure taps in each of the designated rows.

The planform for the swept wing is laid out in Figure 4 so that the corresponding information shown for the straight wing in Figure 2 is presented. Distribution of pressure tube rows is distinctly different from that carried out on the straight wing due to the provision for a dual nacelle arrangement. Rows A and A' are situated along the nacelle exhaust centerlines, while rows B and C' are between the two nacelles and between the inboard nacelle and the fuselage. Row C is just outboard of the outer engine. Chordwise positions for the pressure taps are presented in Figure 5.

The nozzles are instrumented with static pressure taps along their upper, outer centerlines. Locations of these surface orifices are provided in Figure 6. Nozzles designated with "E" subscripts have six pressure taps, while the standard, long nozzles have only five. In both cases the distributions are essentially linear except as dictated by hardware design constraints. Internal nozzle pressure instrumentation is detailed in Reference 2.

USB CRUISE PROGRAM

ROW A		ROW B		ROW C		ROWS D AND E	
UPPER	LOWER	UPPER	LOWER	UPPER	LOWER	UPPER	LOWER
0.65	--	0.01	0.025	0.01	0.05	0.01	0.05
0.70		0.02	0.050	0.02	0.20	0.05	0.20
0.75		0.05	0.10	0.05	0.40	0.10	0.40
0.80		0.10	0.20	0.10	0.60	0.15	0.60
0.85		0.15	0.30	0.15	0.80	0.20	0.80
0.90		0.20	0.40	0.20		0.30	
0.95		0.25	0.50	0.30		0.45	
1.00	--	0.30	0.60	0.40		0.55	
		0.35	0.70	0.45		0.60	
		0.40	0.80	0.50		0.70	
		0.45	0.90	0.55		0.80	
		0.50		0.60		0.90	
		0.55		0.70		1.00	
		0.60		0.80			
		0.65		0.90			
		0.70		0.95			
		0.80		1.00			
		0.95					
		1.00					

Figure 3. Chordwise pressure tube locations for straight wing measured in $x/\bar{c}$ from leading edge

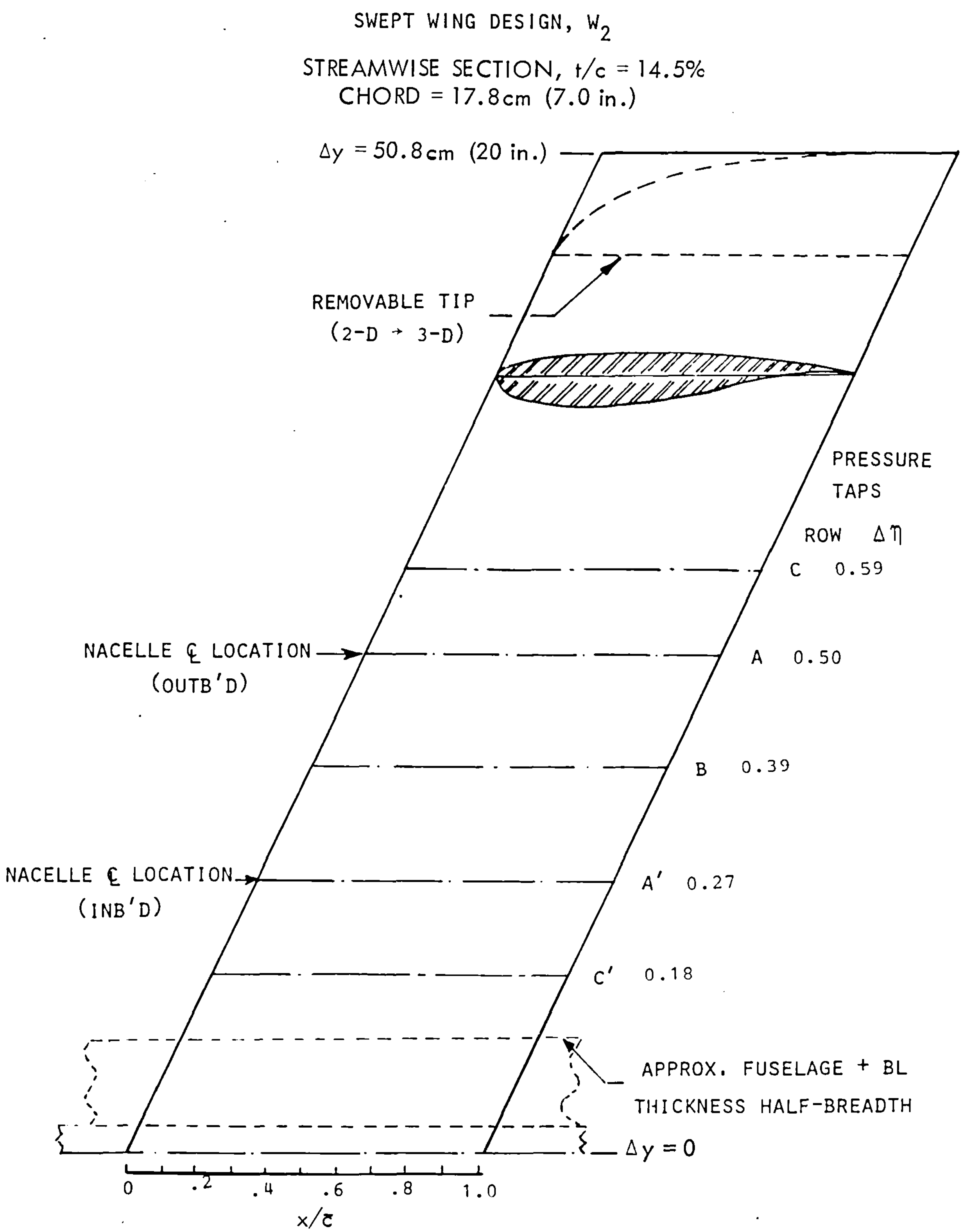

Figure 4. Swept wing planform and instrumentation layout

ROWS A AND A'		ROWS B AND B'		ROWS C AND C'	
UPPER	LOWER	UPPER	LOWER	UPPER	LOWER
0.65	--	0.01	0.025	0.01	0.05
0.70		0.02	0.05	0.02	0.20
0.75		0.05	0.10	0.05	0.40
0.80		0.10	0.20	0.10	0.60
0.85		0.15	0.30	0.15	0.80
0.90		0.20	0.40	0.20	
0.95		0.25	0.50	0.30	
1.00		0.30	0.60	0.40	
		0.35	0.70	0.45	
		0.40	0.80	0.50	
		0.45	0.90	0.55	
		0.50		0.60	
		0.55		0.70	
		0.60		0.80	
		0.65		0.90	
		0.70		0.95	
		0.80		1.00	
		0.90			
		0.95			
		1.00			

Figure 5. Chordwise pressure tube locations for swept wing measured in $x/\bar{c}$ from leading edge

NEW NOZZLES, x/l	EXISTING NOZZLES, x/l
0.186	0.369
0.353	0.479
0.559	0.582
0.745	0.699
0.932	0.807
-	0.903

NOTES: (1) x IS DISTANCE MEASURED AFT FROM NACELLE JOINT.

(2) l IS NOZZLE LENGTH.

(3) EXISTING NOZZLES ARE DESIGNATED WITH "E" SUBSCRIPTS.

Figure 6. Nozzle pressure tube locations along nacelle upper surface

4.0 TEST DESCRIPTION

Both the pressure and force test phases of the USB Cruise Program were formulated around the use of minimum-cost, powered models in a porous-wall, blowndown test facility. This combination permitted a test program covering a comprehensive series of test configurations and parameter variations over an extensive range of test conditions. The test facility is described in detail in Reference 2.

4.1 Test Objectives

The primary objective of the pressure test program was to generate surface static pressure distributions in the jet along the wing surface and outside the jet in the critical interference regions around the nacelle-wing and jet-wing junctures. These would be used to analyze and explain various trends developed in the force test data analysis. They would also provide the means by which measured drag quantities could be broken down into their various components. A secondary objective of the pressure test was to obtain wake total pressure patterns downstream of the model test configurations.

4.2 Run Schedule Summary

The USB pressure tests were broken down into three separate programs -- the straight wing with the short nozzle series (Test 07), the straight wing with the long nozzle series (Test 23), and the swept wing which was tested only with long nozzles (Test 22). Test 23 could be further broken down into those configurations which utilized the standard wing air-supply duct and those with air supplied by the upstream pipe. Reynolds numbers were held constant at 3.5 million to match the pressure tests and a porosity of 4% was maintained throughout the program. The entire pressure test program is summarized in Figure 7.

USB CRUISE PROGRAM

TEST DESCRIPTION	CONFIGURATION DESCRIPTION	CONFIGURATION DEFINITION	TEST NO.	TEST SERIES	RUN NOS.	MACH NO. M_∞	ANGLE OF ATTACK α ~ DEG	NOZZLE PRES. RATIO, H_j/p_∞	REMARKS
Pressure --Surface Static + Wake Total	2-D Clean, Straight Wing	W_1	07	0	1 - 81	0.2 - 0.78	-1 to 20		
	+ Circular Nacelle	$W_1 B_4 P_7 C_1 N_{2E}$		1	82 - 139	Static + 0.6 - 0.75	0 to 2	1.1 - 2.6	
	+ Short D-Duct Nacelle	$W_1 B_4 P_7 C_1 N_{3E}$		2	140 - 183	0.6 - 0.75	1 & 2	1.4 - 2.6	
	+ AR 4 Nacelle	$W_1 B_4 P_7 C_1 N_{4E}$		3	184 - 234	0.6 - 0.75	1 & 2	1.4 - 2.6	
	+ Short Circular Nacelle	$W_1 B_4 P_7 C_1 N_{1E}$		4	235 - 296	0.6 - 0.75	1 & 2	1.0 - 4.0	Run Nos. 295 & 296 are Oil Flow
	+ Short D-Duct Nacelle	$W_1 B_4 P_7 C_1 N_{3E}$		5	297 - 298	0.72	2	1.4 & 2.6	Oil Flow
	+ AR 4 Nacelle	$W_1 B_4 P_7 C_1 N_{4E}$		6	299 - 300	0.72	2	1.4 & 2.6	Oil Flow
	+ Circular Nacelle	$W_1 B_4 P_7 C_1 N_{2E}$		7	301 - 302	0.72	2	1.4 & 2.6	Oil Flow
	2-D Clean, Straight Wing	W_1		8	303 - 325	0.6 - 0.78	0 to 3		R_{NC} from 3.0 to 12.0 x 10^6
Pressure --Surface Static + Wake Total	2-D Clean, Straight Wing	W_1	23	0	1 - 11	0.60 - 0.68	0 to 4		
	+ Short Pylon & Flo-Thru Nac.	$W_1 B_1 P_1 C_5 N_2$		1	12 - 45	0.60 - 0.75	1 to 4		
	+ Long D-Duct Nacelle	$W_1 B_7 P_8 C_2 N_3$		2	46 - 149	Static + 0.6 - 0.72	1 to 4	1.0 - 4.0	
	+ Long AR 6 Nacelle	$W_1 B_7 P_8 C_2 N_5$		3	150 - 213	0.6 - 0.72	1 to 4	1.0 - 3.4	
	+ Streamlined Nacelle	$W_1 B_9 P_{12} C_6 N_6$		4	214 - 302	Static + 0.6 - 0.72	1 to 4	1.0 - 3.2	
	+ Short Pylon & Powered Nac	$W_1 B_1 P_1 C_9 N_2$		5	303 - 409	Static + 0.6 - 0.72	2.6	1.0 - 3.0	Upstream Pipe Installed
	+ D-Duct Nac. at x/c = 0.35	$W_1 B_1 P_{11} C_9 S_6 N_3$		6	410 - 517	Static + 0.6 - 0.72	2.6	1.0 - 3.0	
	+ D-Duct Nac. at x/c = 0.50	$W_1 B_1 P_{11} C_9 S_7 N_3$		7	518 - 624	Static + 0.6 - 0.72	2.6	1.0 - 3.0	
	+ D-Duct Nac. at x/c = 0.20	$W_1 B_1 P_{11} C_9 S_5 N_3$		8	625 - 718	Static + 0.6 - 0.72	2.6	1.0 - 3.0	
	+ Large D-Duct Nac. at x/c = 0.35	$W_1 B_1 P_{11} C_8 S_2 N_1$		9	719 - 801	Static + 0.6 - 0.72	2.6	1.0 - 3.0	
	+ Large D-Duct Nac. at x/c = 0.20	$W_1 B_1 P_{11} C_8 S_1 N_1$		10	802 - 886	Static + 0.6 - 0.72	2.6	1.0 - 3.0	
	+ Large D-Duct Nac. at x/c = 0.50	$W_1 B_1 P_{11} C_8 S_3 N_1$		11	887 - 958	Static + 0.6 - 0.72	2.6	1.0 - 3.0	
Pressure --Surface Static + Wake Total	2-D Clean, Swept Wing	W_2	22	0	1 - 24	0.6 - 0.8	1 to 4		1st 327 Runs Bad
	+ Pylon Mounted Flo-Thru Nac.	$W_2 B_2 P_5 C_5 N_2$		1	25 - 90	0.6 - 0.8	1 to 4		
	+ Outb'd D-Duct Nacelle	$W_2 B_5 P_9 C_3 N_8^1$		2	91 - 205	Static + 0.6 - 0.75	2 to 4	1.0 - 3.7	
	+ 2 D-Duct Nacelles	$W_2 B_{5,6} P_{9,10} C_{3,4} N_8^1 N_8^2$		3	206 - 430	Static + 0.6 - 0.75	2 to 4	1.0 - 3.5	
	+ Inb'd D-Duct Nacelle	$W_2 B_5 P_9 C_3 N_8^1$		4	431 - 545	Static + 0.6 - 0.75	2 to 4	1.0 - 3.6	
		W_2		5	546 - 571	0.6 - 0.8	1 to 4		
	+ Flo-Thru Inlet + Circular Nac	$W_2 B_2 P_5 C_5 N_2$		6	572 - 619	0.6 - 0.8	1 to 4		
	+ Small AR 6 Nacelle	$W_2 B_5 P_9 C_3 N_{13}$		7	620 - 715	Static + 0.6 - 0.75	2 to 4	1.0 - 3.6	

NOTES: (1) $R_{NC} = 3.5 \times 10^6$, except where noted. (2) Wall porosity 5% for force tests and 4% for pressure tests, except as noted.

Figure 7. Run schedule summary for pressure tests

5.0 STRAIGHT WING TEST RESULTS

The presentation of the straight wing pressure test results is divided into four parts, the first three of which are surface pressure distributions, while the last one is wake isobars in terms of local total pressure ratios. Pressure distributions are presented for the short nozzle test series, the long nozzle test series, and those configurations tested with the upstream pipe air supply.

5.1 Model Pressure Distributions, Short Nozzle Series

Data are presented for the first group of test nozzles in Figure 8 through 44. These consist of the so-called short nozzles, N_{1E} through N_{4E}. Because of their shortness, these nozzles have boattail angles which range from 17 to 36 degrees. Complete details of the model geometric characteristics are contained in Reference 2.

All data in this series are presented at a Reynolds' number of 3.5 million based on wing chord. In this section only, because of the many instances of overlapping, flags are used to denote lower surface pressure distributions. There are, of course, no lower surface pressure taps below the nozzle centerline.

USB CRUISE PROGRAM

CONFIG W_1

SYM	TEST	SERIES	RUN	M_∞	α	H_j/p_∞
O	7	0	27	0.72	2°	-

CONFIG $W_1\ B_4\ P_7\ C_1\ N_{3E}$

SYM	TEST	SERIES	RUN	M_∞	α	H_j/p_∞
△	7	2	164	0.72	2°	1.85

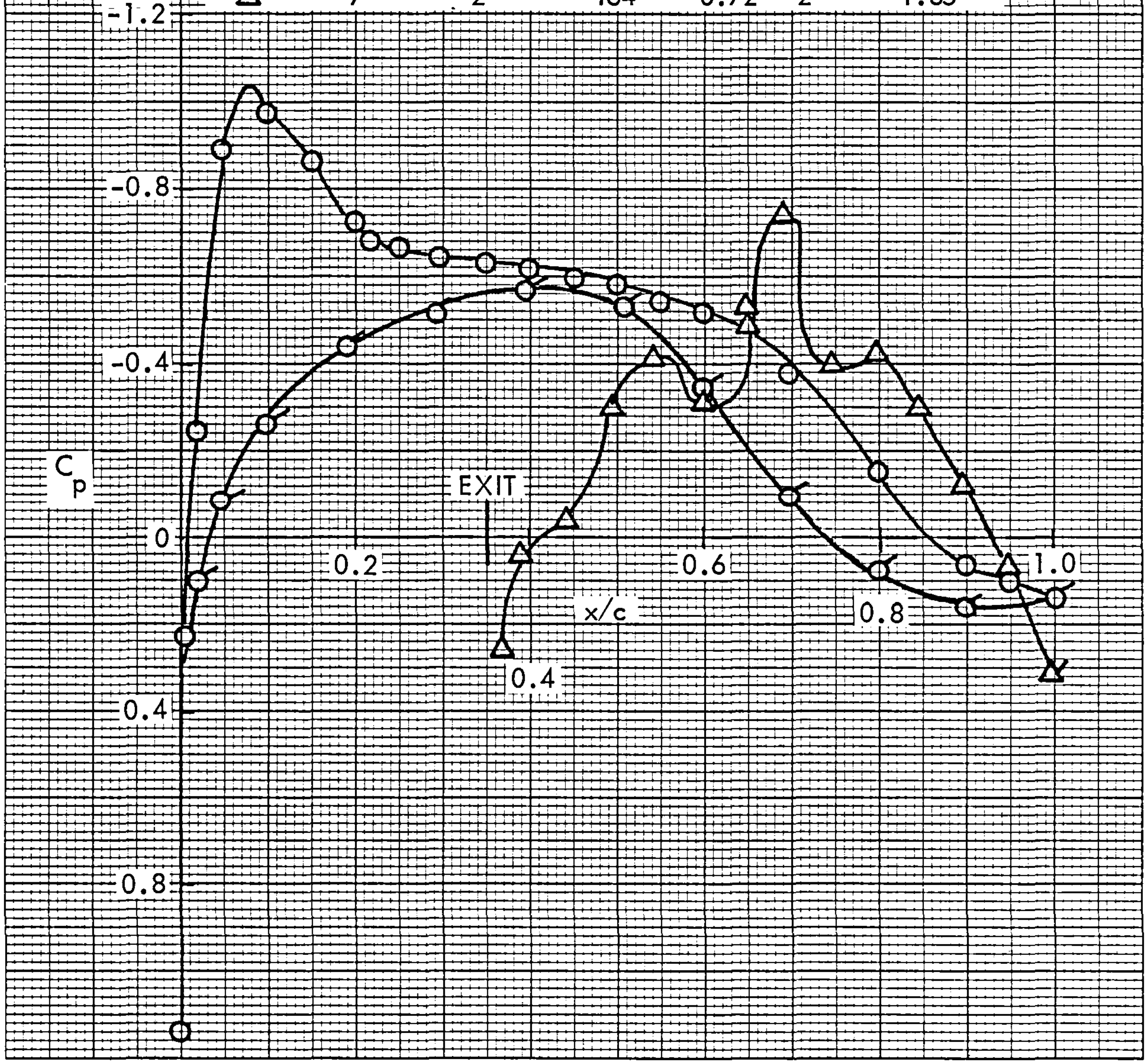

Figure 8. Wing pressure distribution, jet effect on wing pressures aft of nozzle compared to clean wing, η = 0.50

USB CRUISE PROGRAM

CONFIG W_1

SYM	TEST	SERIES	RUN	M_∞	α	H_j/p_∞
○	7	0	27	0.72	2°	-

CONFIG $W_1 B_4 P_7 C_1 N_{3E}$

SYM	TEST	SERIES	RUN	M_∞	α	H_j/p_∞
△	7	2	164	0.72	2°	1.85

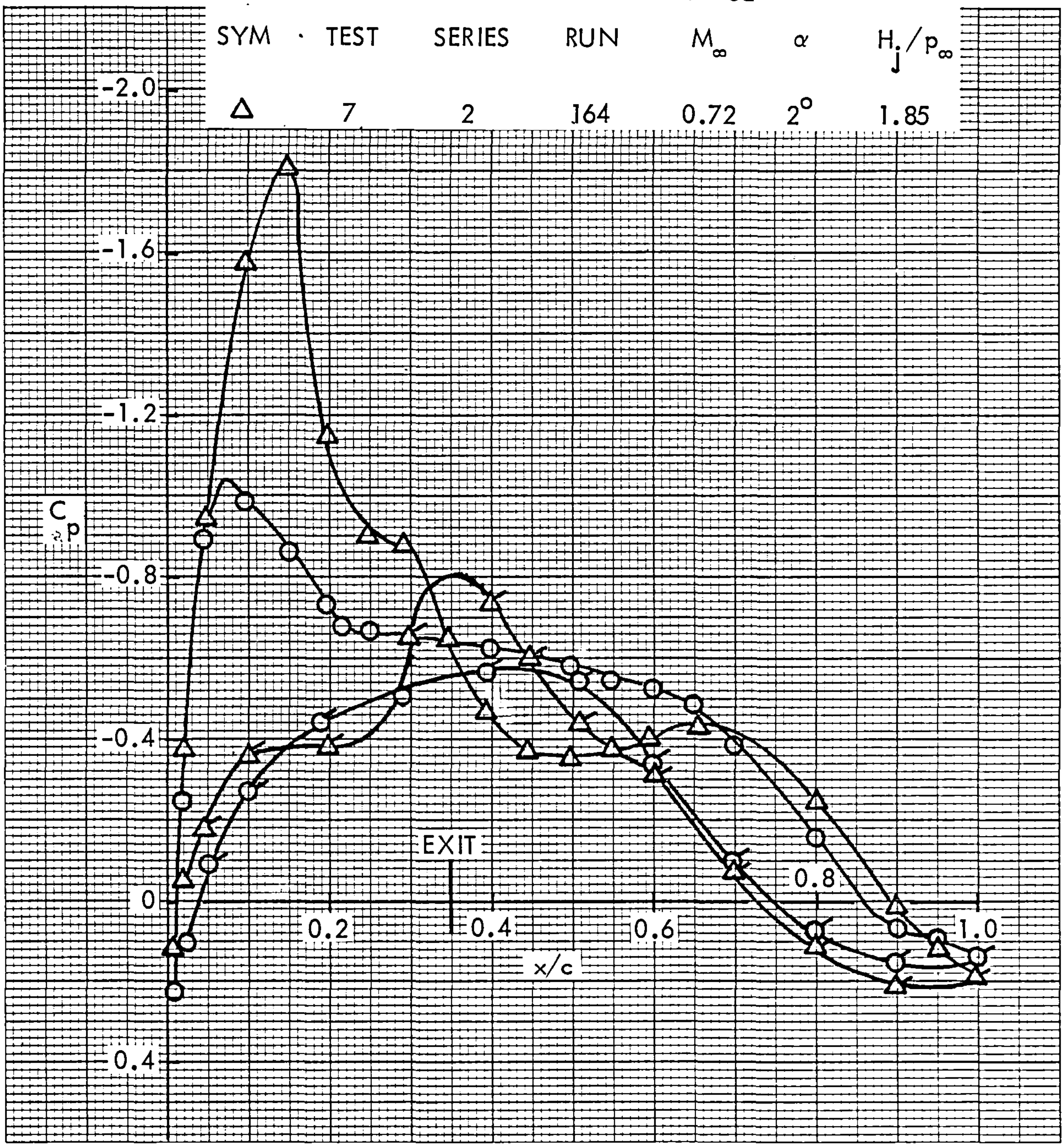

Figure 9. Wing pressure distribution, jet effect on wing pressures aft of nozzle compared to clean wing, $\eta = 0.42$

CONFIG W_1

SYM	TEST	SERIES	RUN	M_∞	α	H_j/p_∞
O	7	0	27	0.72	2°	-

CONFIG $W_1\ B_4\ P_7\ C_1\ N_{3E}$

SYM	TEST	SERIES	RUN	M_∞	α	H_j/p_∞
Δ	7	2	164	0.72	2°	1.85

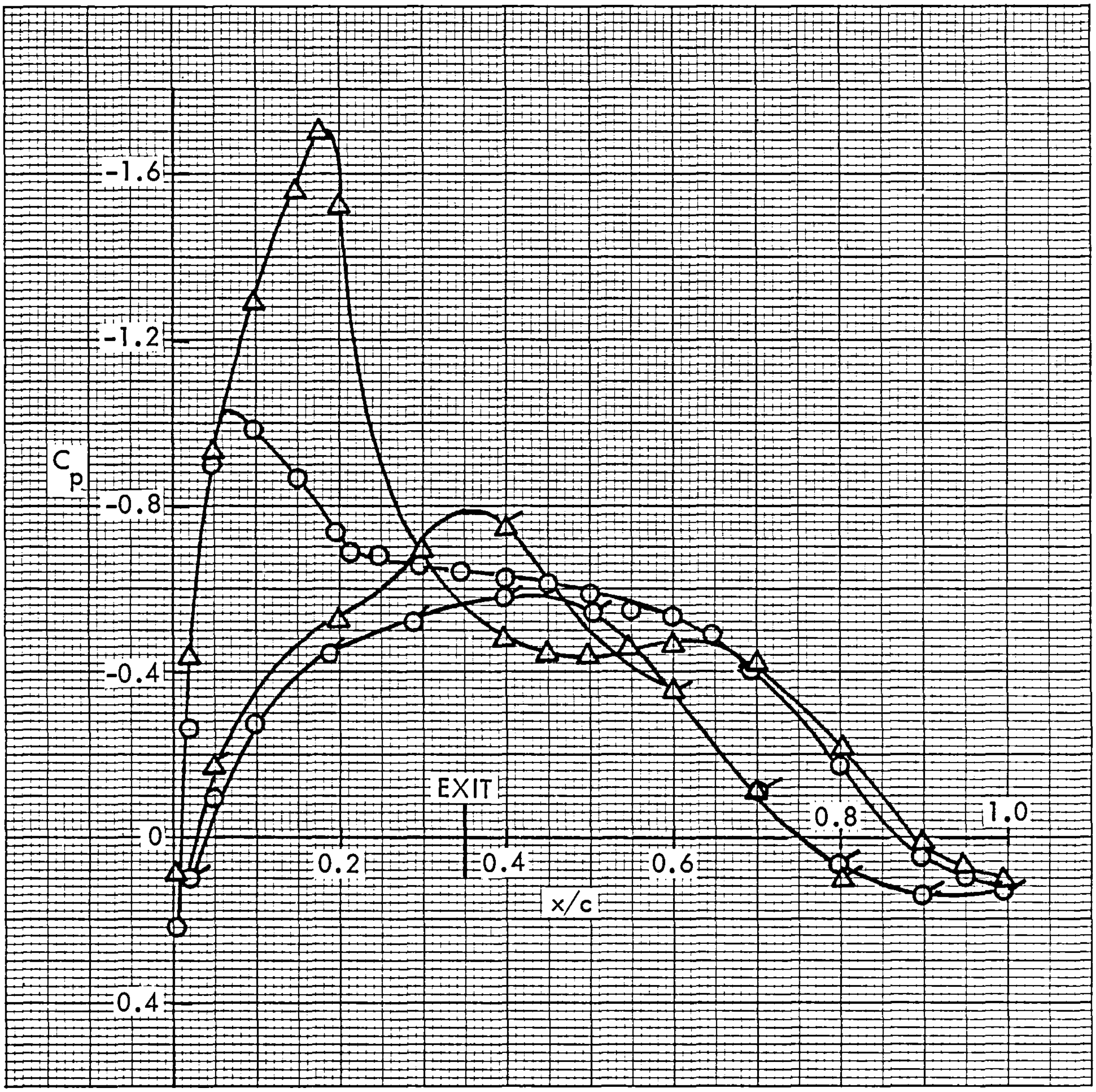

Figure 10. Wing pressure distribution, jet effect on wing pressures aft of nozzle compared to clean wing, $\eta = 0.39$

CONFIG $W_1\ B_4\ P_7\ C_1\ N_{1E}$

SYM	TEST	SERIES	RUN	M_∞	α	H_j/p_∞
O	7	4	237	0.60	2°	2.62
Δ	7	4	293	0.75	2°	2.56

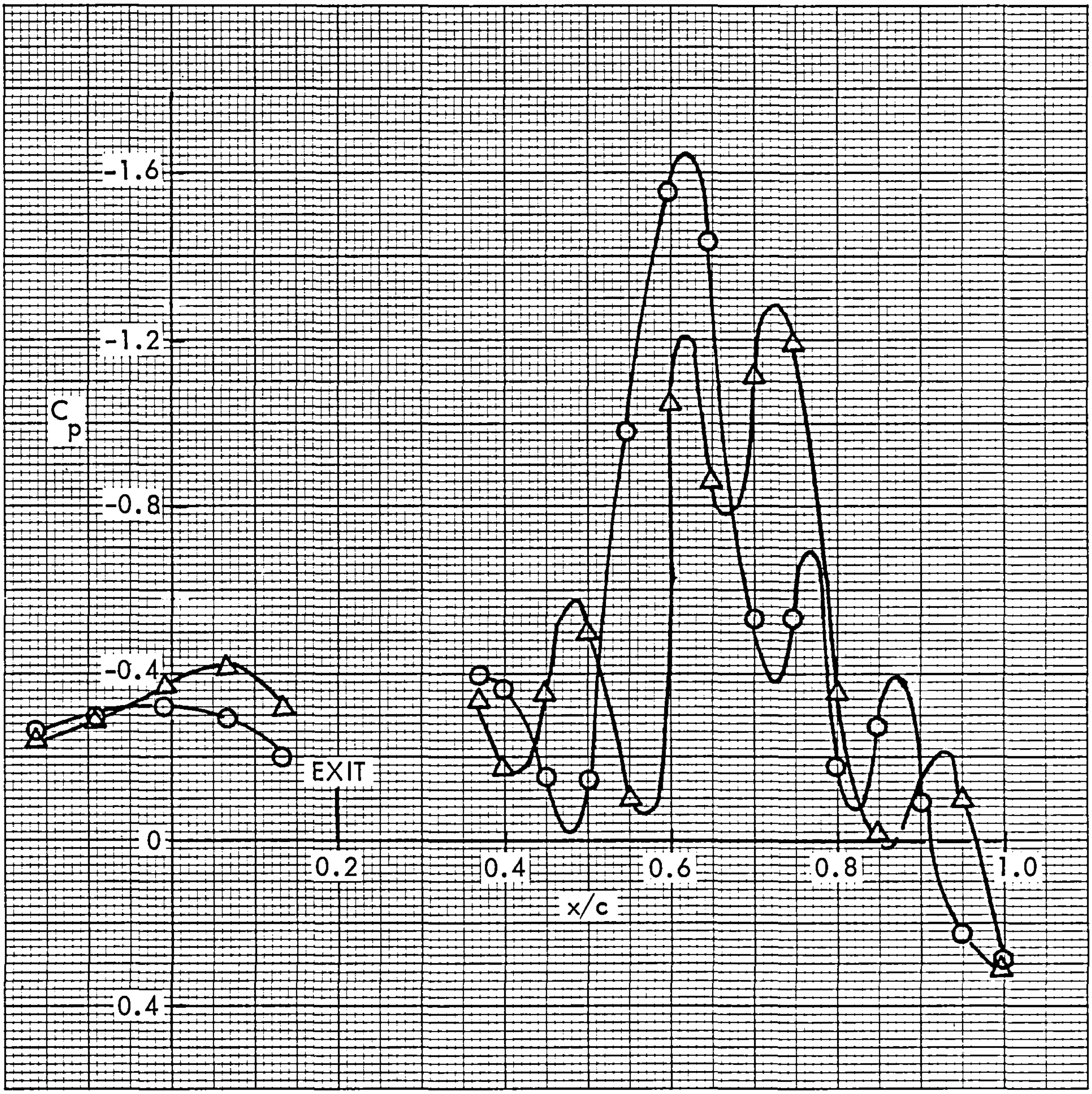

Figure 11. Wing pressure distribution, effect of Mach number, nozzle N_{1E}, $\eta = 0.50$

CONFIG $W_1 B_4 P_7 C_1 N_{1E}$

SYM	TEST	SERIES	RUN	M_∞	α	H_j/p_∞
O	7	4	237	0.60	2°	2.62
Δ	7	4	293	0.75	2°	2.56

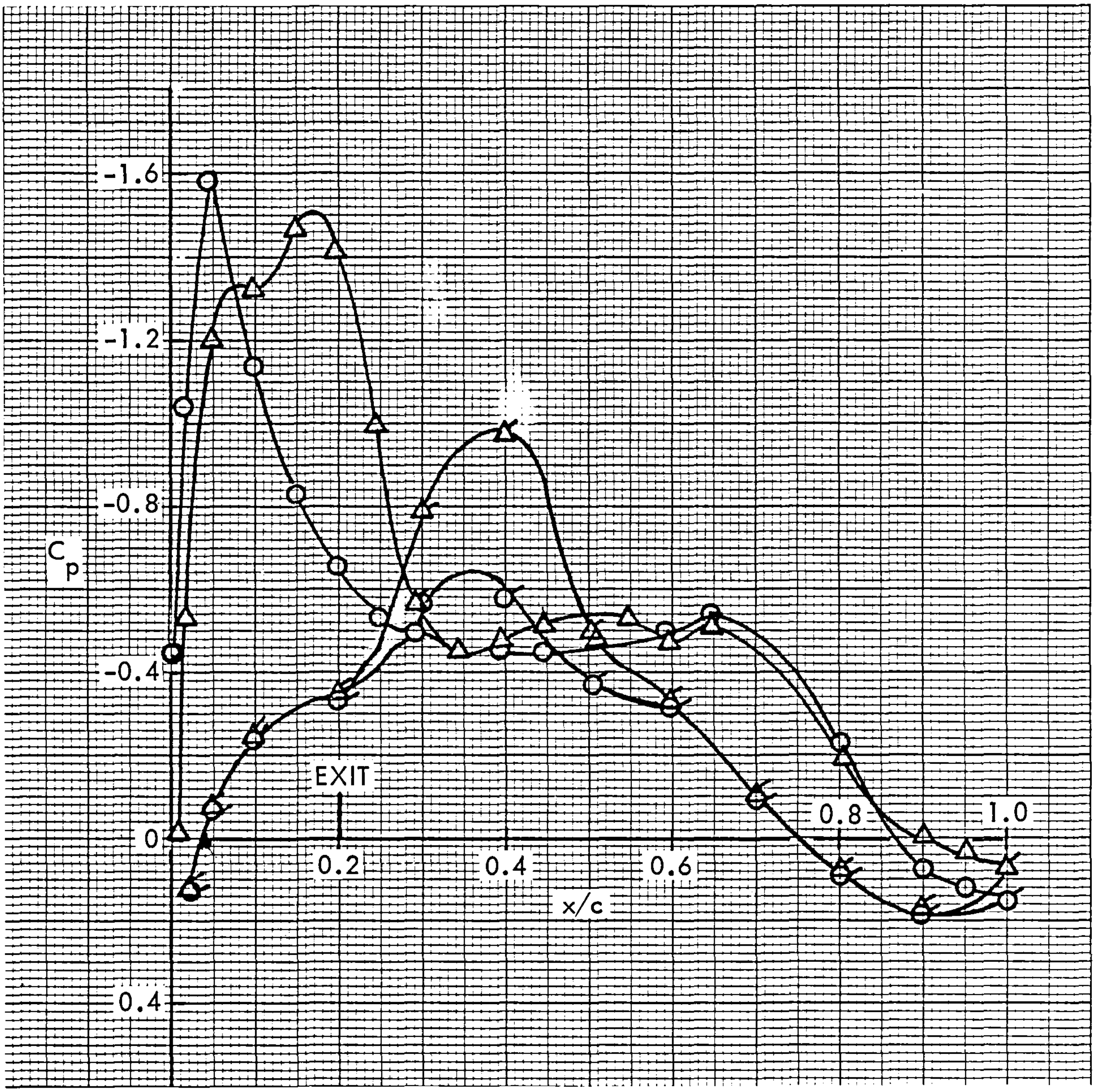

Figure 12. Wing pressure distribution, effect of Mach number, nozzle N_{1E}, $\eta = 0.42$

CONFIG $W_1 B_4 P_7 C_1 N_{1E}$

SYM	TEST	SERIES	RUN	M_∞	α	H_j/p_∞
O	7	4	237	0.60	2°	2.62
Δ	7	4	293	0.75	2°	2.56

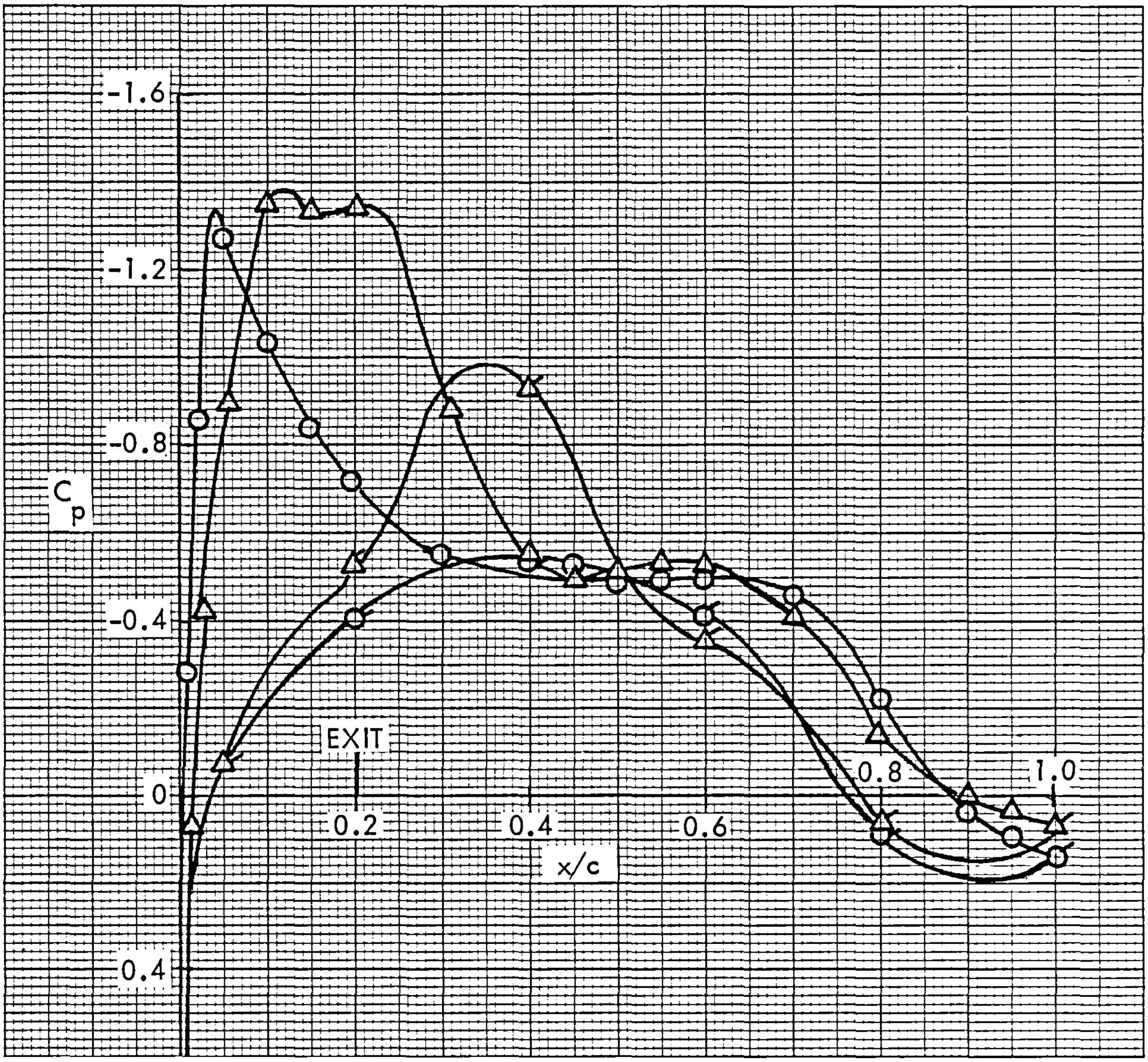

Figure 13. Wing pressure distribution, effect of Mach number, nozzle N_{1E}, $\eta = 0.39$

CONFIG $W_1 B_4 P_7 C_1 N_{2E}$

SYM	TEST	SERIES	RUN	M_∞	α	H_j/p_∞
O	7	1	128	0.60	2°	2.21
△	7	1	123	0.75	2°	2.17

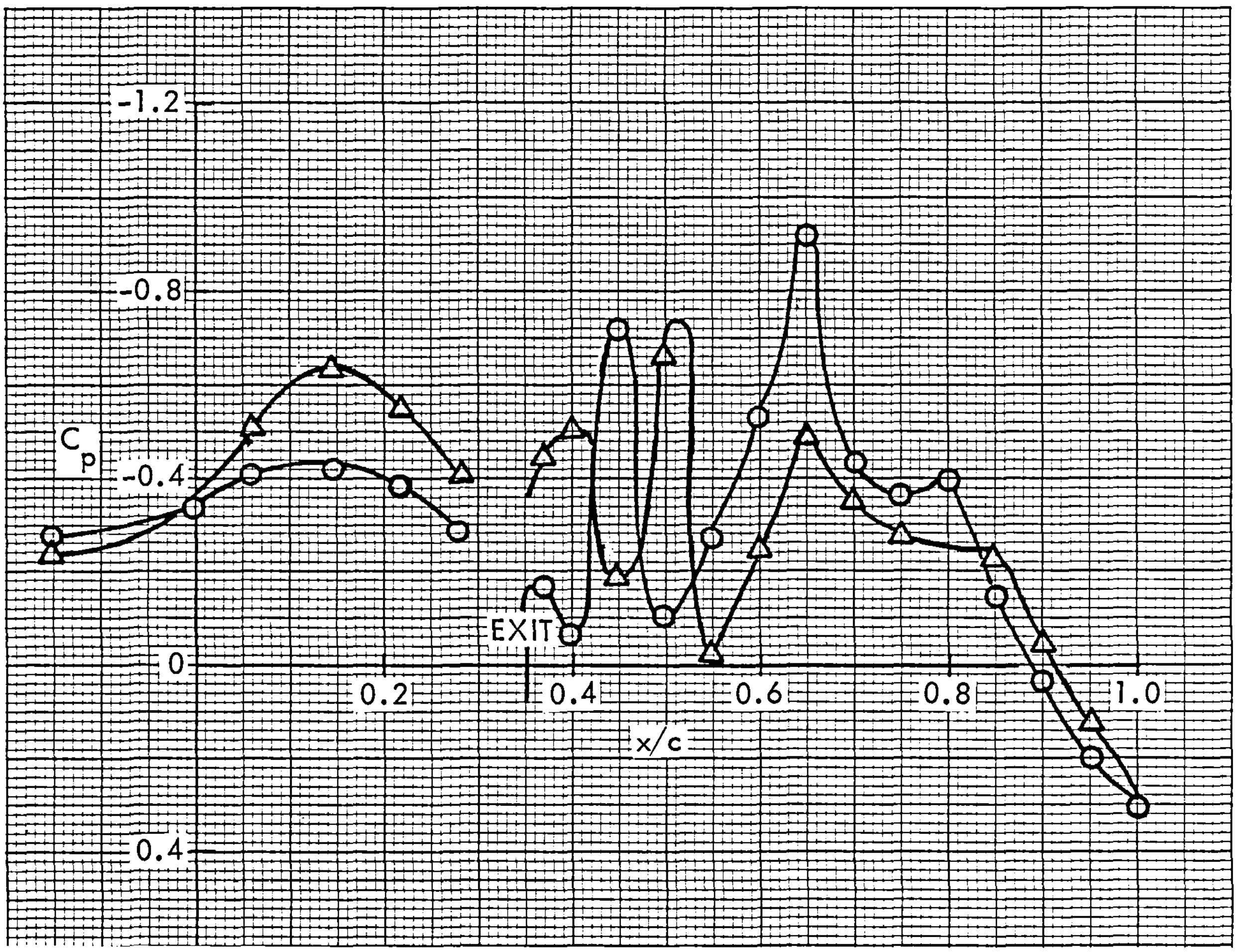

Figure 14. Wing pressure distribution, effect of Mach number, nozzle N_{2E}, $\eta = 0.50$

CONFIG			$W_1\ B_4\ P_7\ C_1\ N_{2E}$			
SYM	TEST	SERIES	RUN	M_∞	α	H_j/p_∞
○	7	1	128	0.60	2°	2.21
△	7	1	123	0.75	2°	2.17

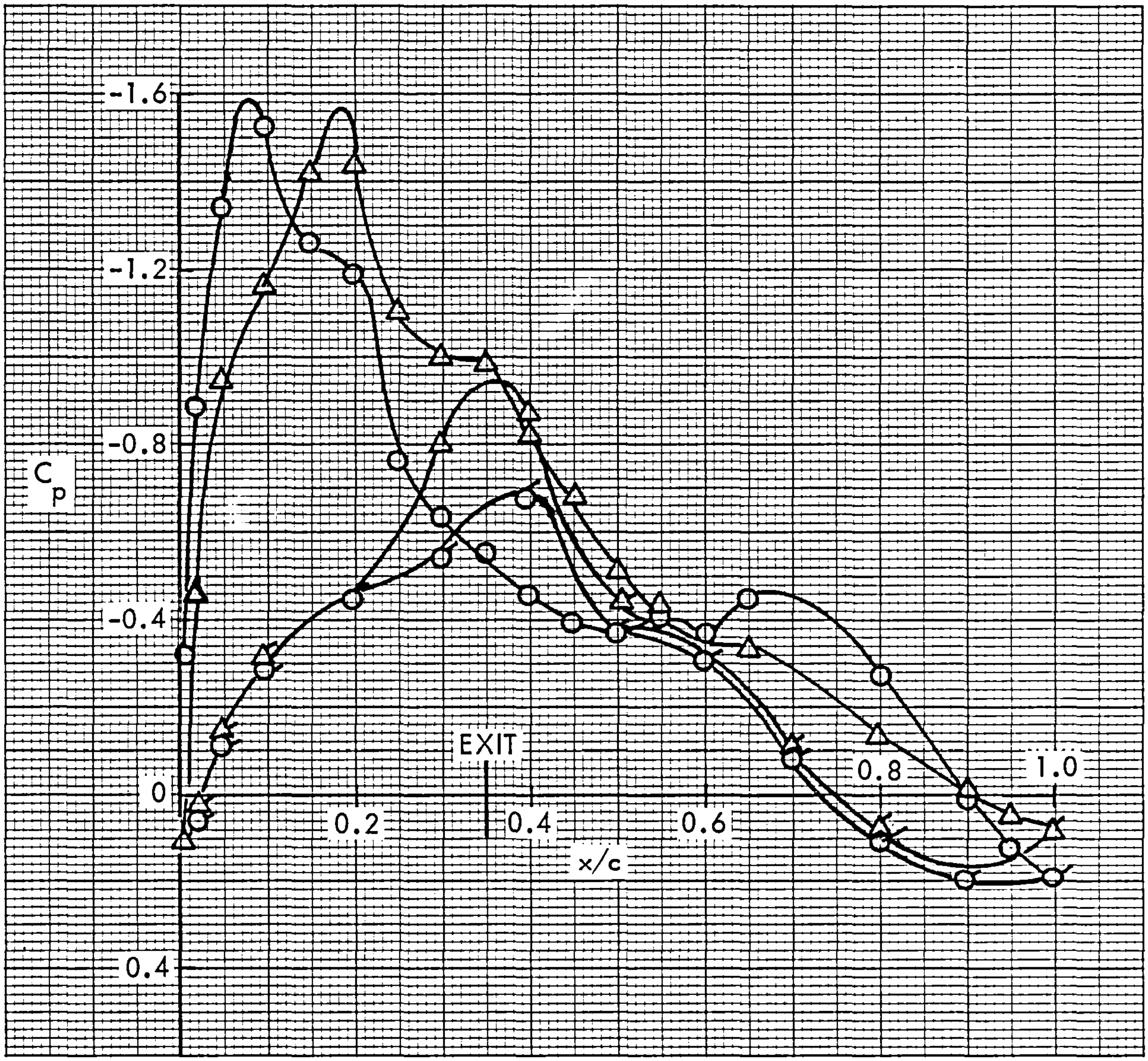

Figure 15. Wing pressure distribution, effect of Mach number, nozzle N_{2E}, $\eta = 0.42$

CONFIG $W_1 B_4 P_7 C_1 N_{2E}$

SYM	TEST	SERIES	RUN	M_∞	α	H_j/p_∞
○	7	1	128	0.60	2°	2.21
△	7	1	123	0.75	2°	2.17

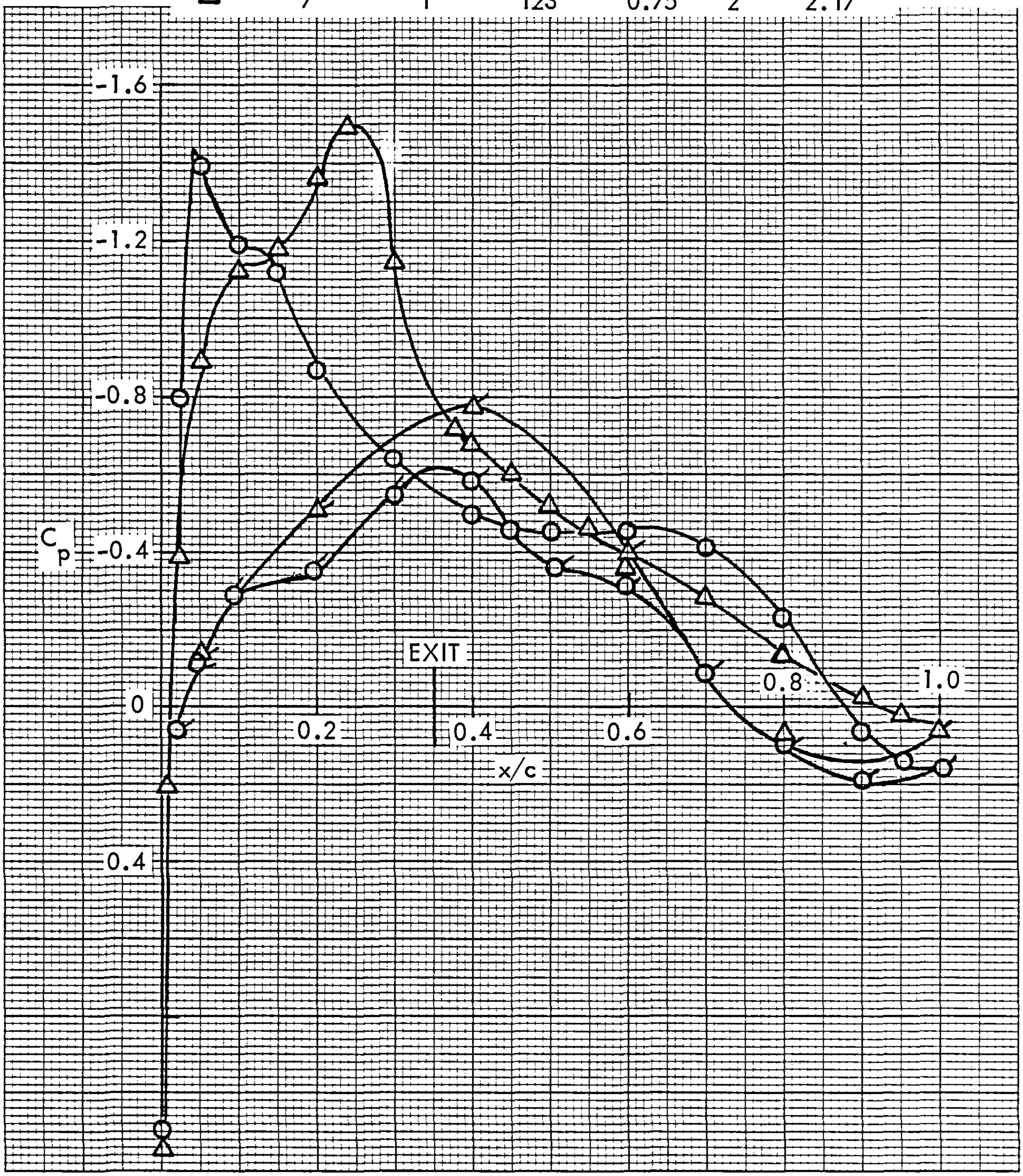

Figure 16. Wing pressure distribution, effect of Mach number, nozzle N_{2E}, $\eta = 0.39$

CONFIG $W_1 B_4 P_7 C_1 N_{3E}$

SYM	TEST	SERIES	RUN	M_∞	α	H_j/p_∞
○	7	2	144	0.60	2°	2.21
△	7	2	155	0.75	2°	2.23

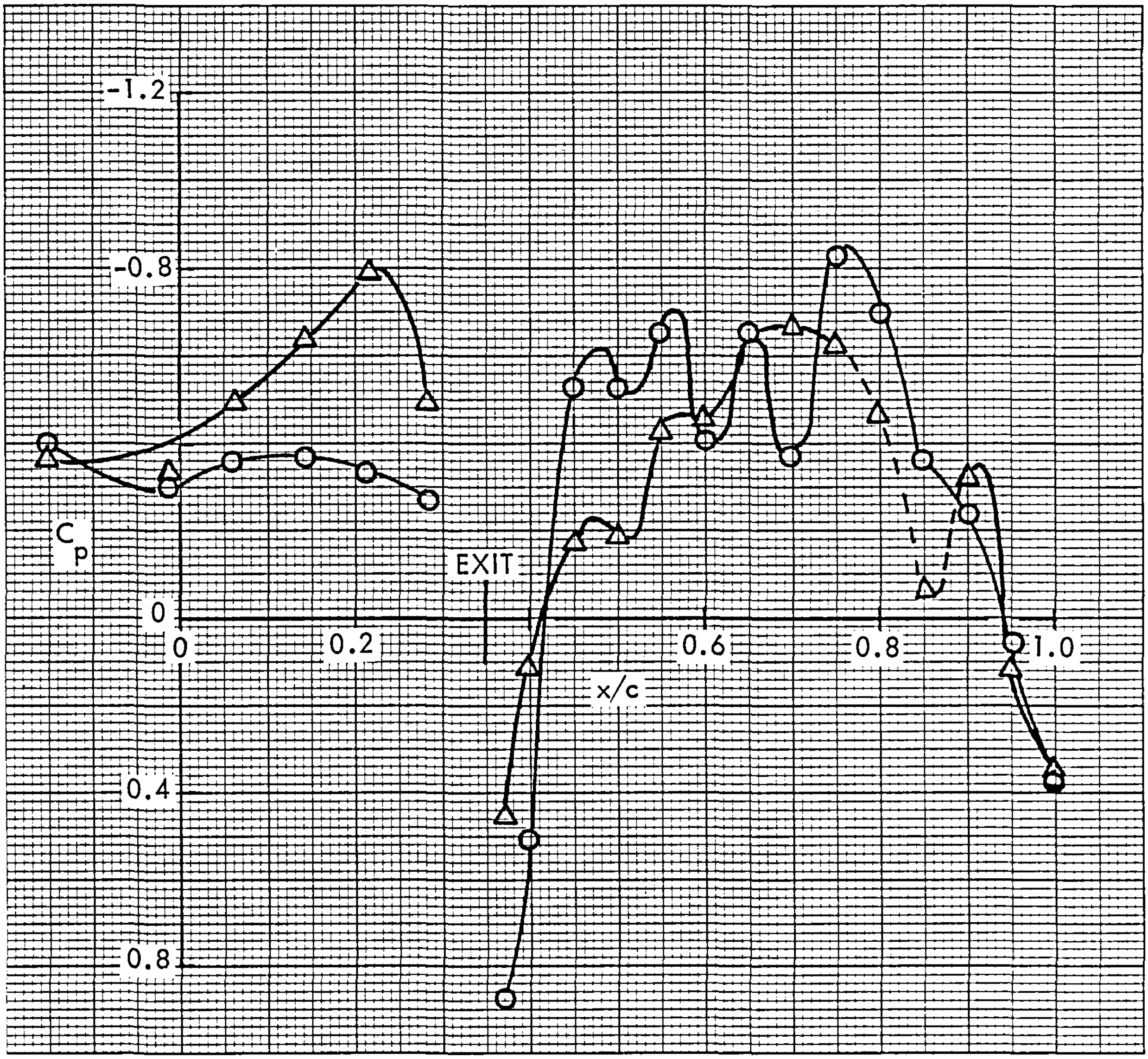

Figure 17. Wing pressure distribution, effect of Mach number, nozzle N_{3E}, $\eta = 0.50$

CONFIG $W_1 B_4 P_7 C_1 N_{3E}$

SYM	TEST	SERIES	RUN	M_∞	α	H_j/p_∞
O	7	2	180	0.60	2°	1.78
Δ	7	2	155	0.75	2°	2.23

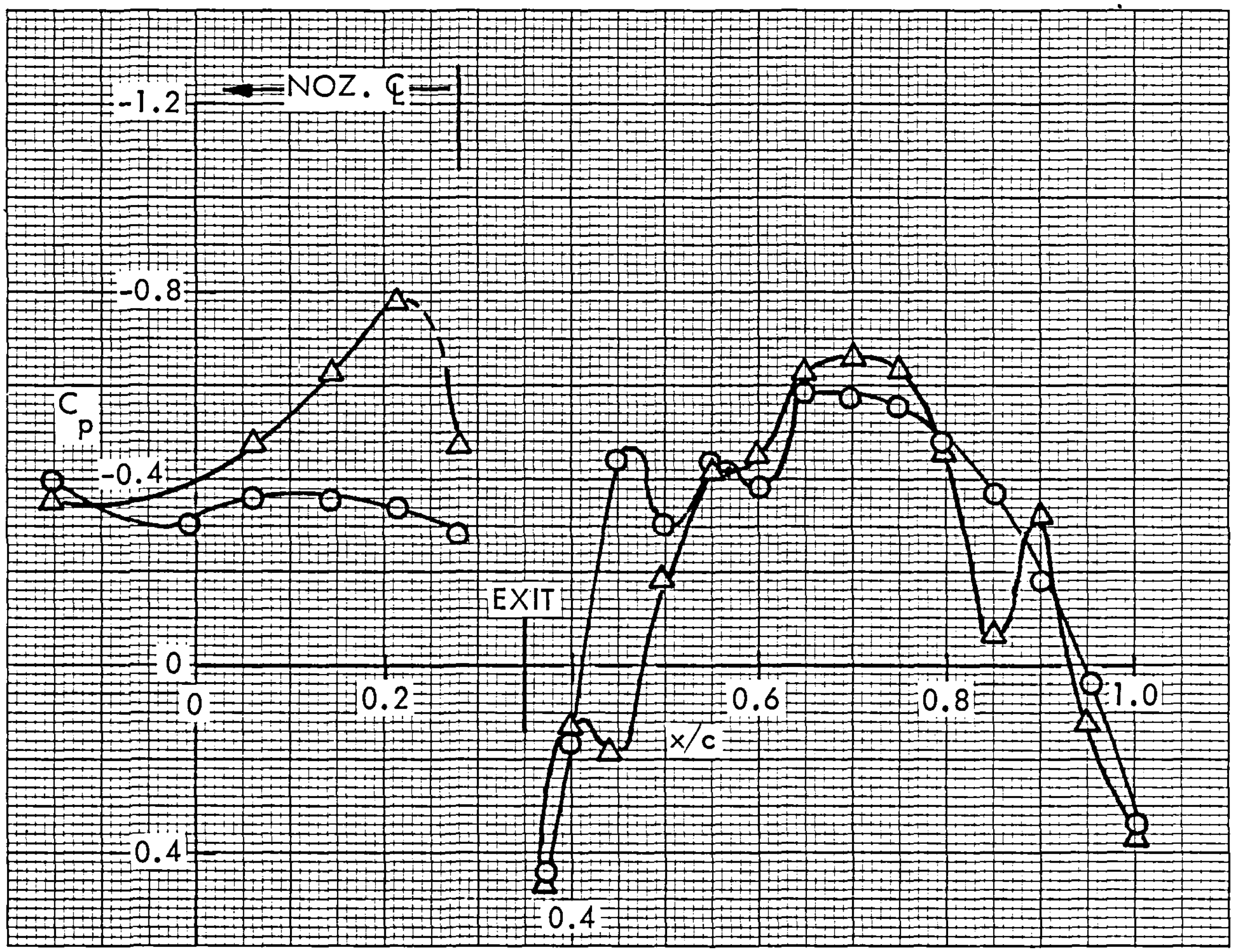

Figure 18. Wing pressure distribution, effect of Mach number, nozzle N_{3E}, q_j/q_∞ = constant, $\eta = 0.50$

CONFIG $W_1 B_4 P_7 C_1 N_{3E}$

SYM	TEST	SERIES	RUN	M_∞	α	H_j/p_∞
O	7	2	144	0.60	2°	2.21
Δ	7	2	155	0.75	2°	2.23

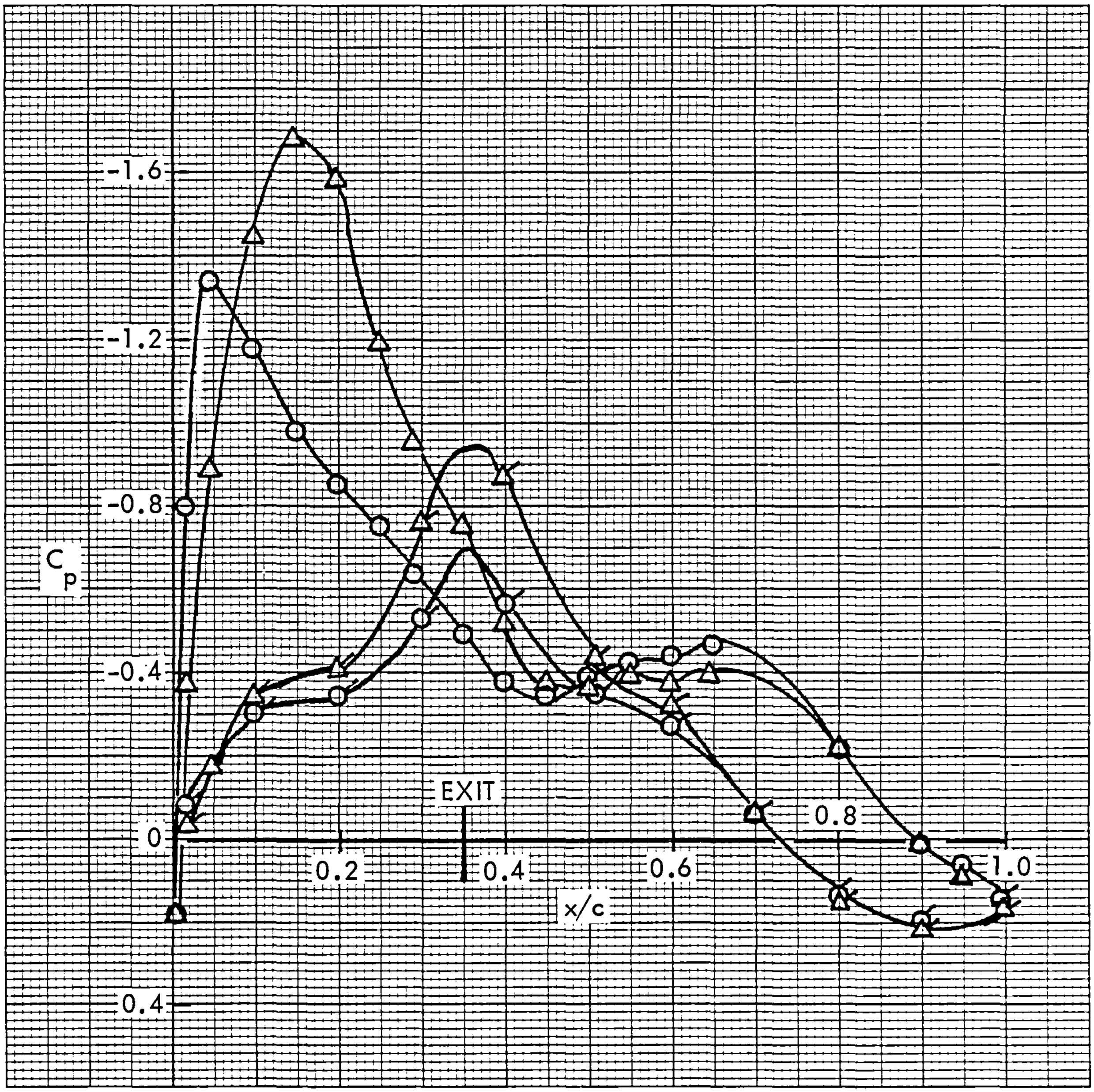

Figure 19. Wing pressure distribution, effect of Mach number, nozzle N_{3E}, $\eta = 0.42$

CONFIG $W_1 B_4 P_7 C_1 N_{3E}$

SYM	TEST	SERIES	RUN	M_∞	α	H_j/p_∞
○	7	2	144	0.60	2°	2.21
△	7	2	155	0.75	2°	2.23

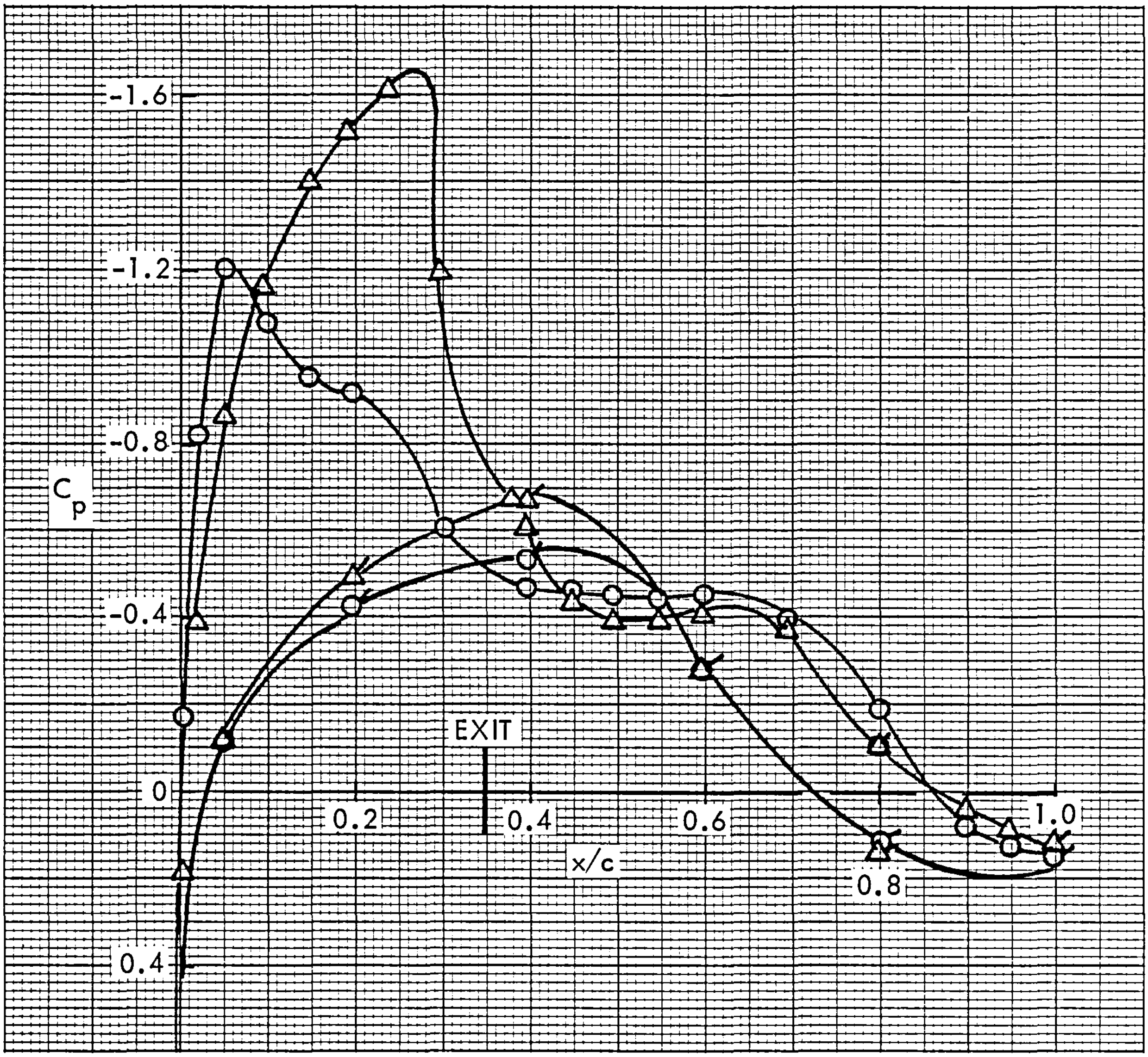

Figure 20. Wing pressure distribution, effect of Mach number, nozzle N_{3E}, $\eta = 0.39$

CONFIG $W_1 B_4 P_7 C_1 N_{4E}$

SYM	TEST	SERIES	RUN	M_∞	α	H_j/p_∞
O	7	6	190	0.60	2°	2.21
△	7	6	215	0.75	2°	2.17

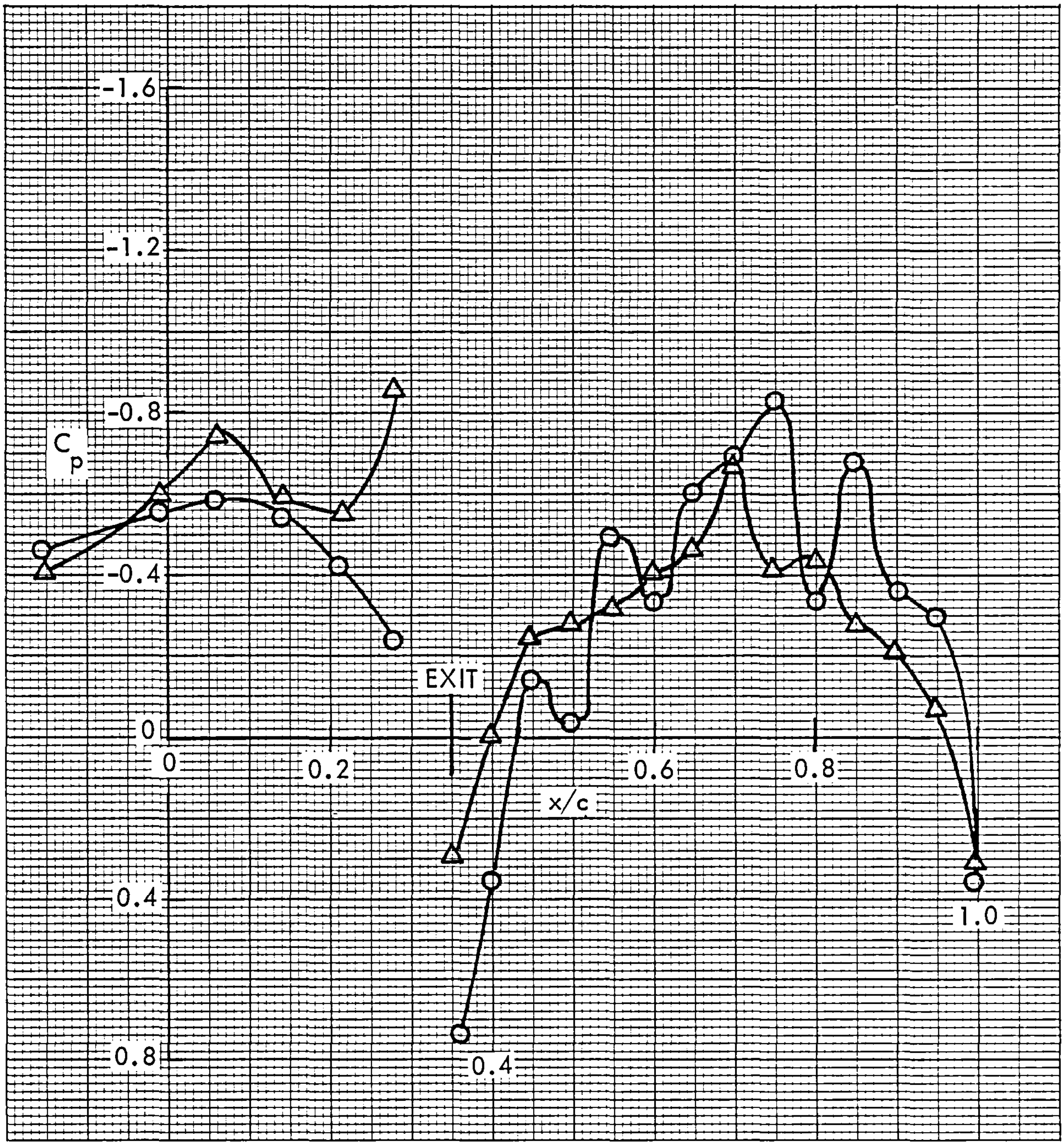

Figure 21. Wing pressure distribution, effect of Mach number, nozzle N_{4E}, $\eta = 0.50$

CONFIG $W_1 B_4 P_7 C_1 N_{4E}$

SYM	TEST	SERIES	RUN	M_∞	α	H_j/p_∞
O	7	6	190	0.60	2°	2.21
Δ	7	6	215	0.75	2°	2.17

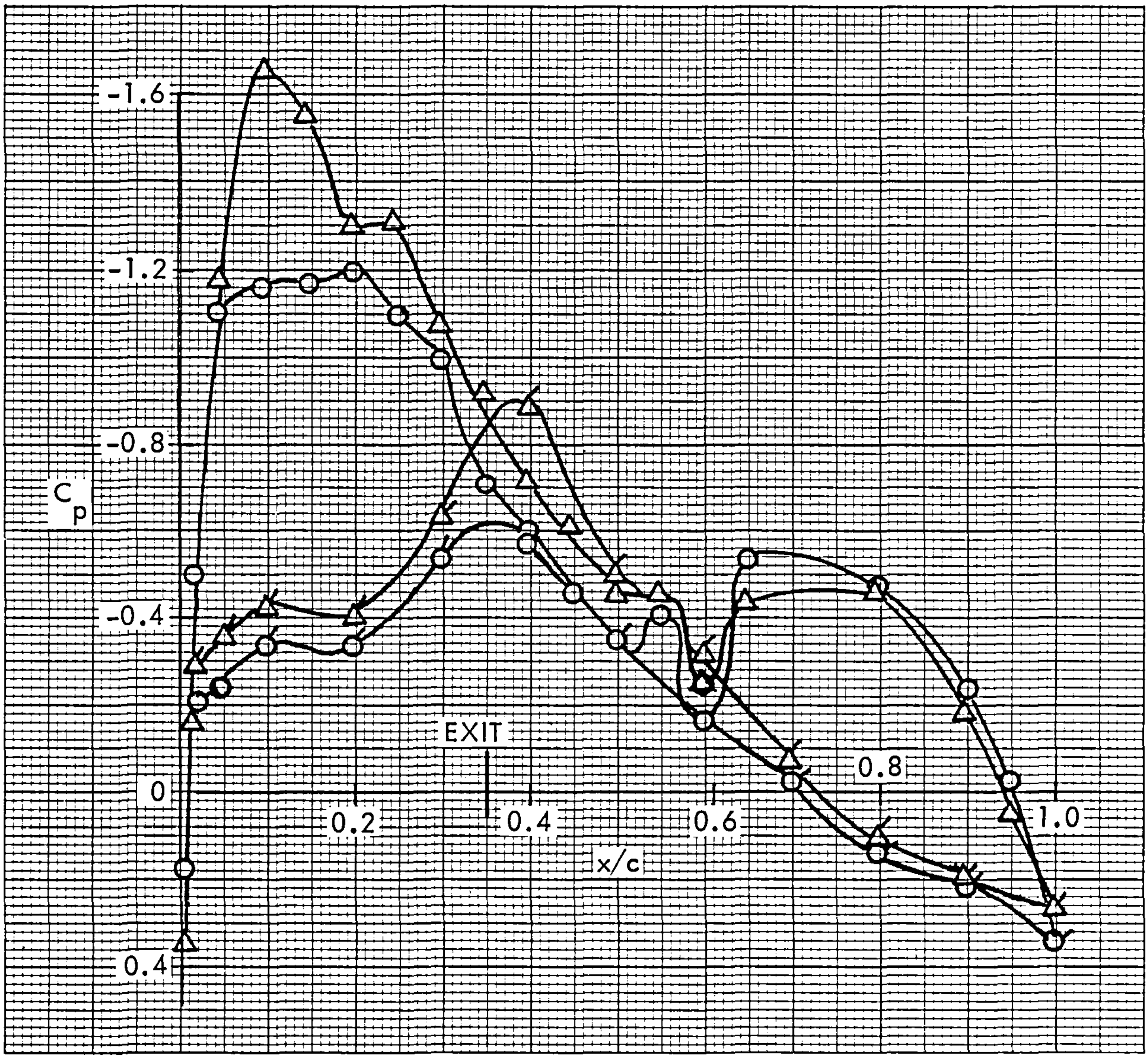

Figure 22. Wing pressure distribution, effect of Mach number, nozzle N_{4E}, $\eta = 0.42$

CONFIG $W_1\ B_4\ P_7\ C_1\ N_{4E}$

SYM	TEST	SERIES	RUN	M_∞	α	H_j/p_∞
○	7	6	190	0.60	2°	2.21
△	7	6	215	0.75	2°	2.17

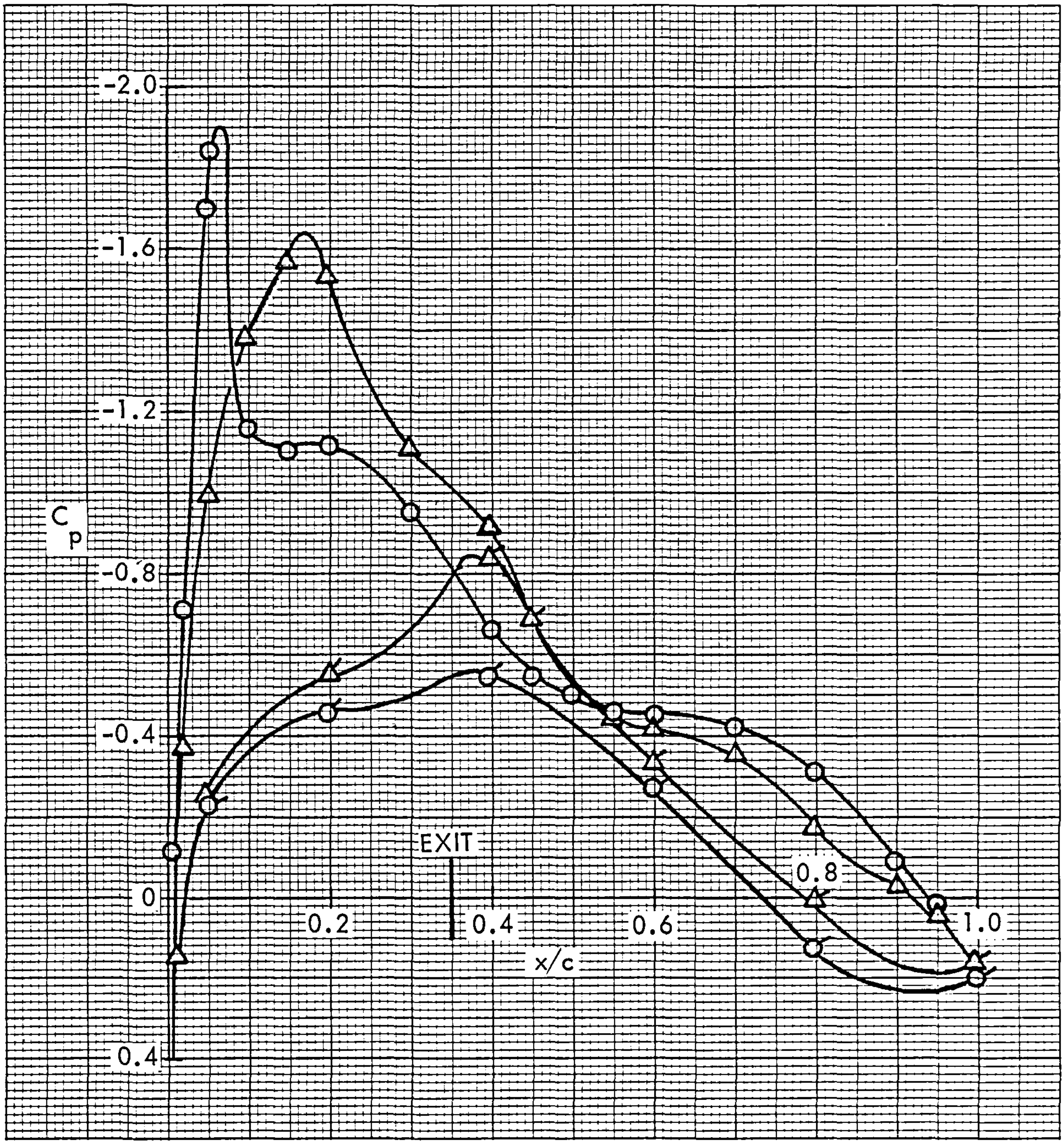

Figure 23. Wing pressure distribution, effect of Mach number, nozzle N_{4E}, $\eta = 0.39$

CONFIG $W_1 B_4 P_7 C_1 N_{1E}$

SYM	TEST	SERIES	RUN	M_∞	α	H_j/p_∞
O	7	4	284	0.72	2°	1.00
Δ	7	4	275	0.72	2°	1.44
+	7	4	282	0.72	2°	2.62

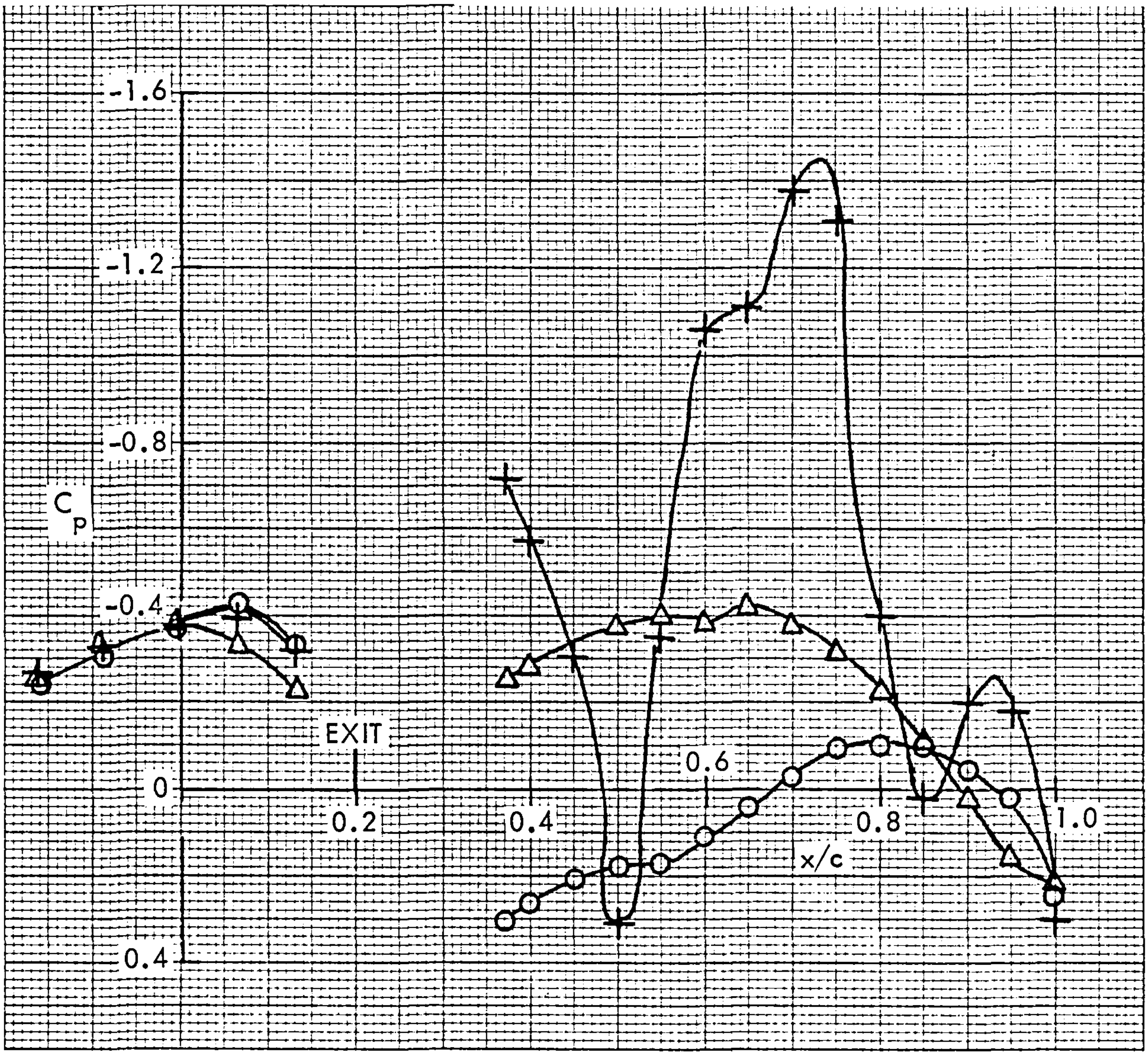

Figure 24. Wing pressure distribution, effect of nozzle pressure ratio, nozzle N_{1E}, $\eta = 0.50$

CONFIG $W_1\ B_4\ P_7\ C_1\ N_{1E}$

SYM	TEST	SERIES	RUN	M_∞	α	H_j/p_∞
○	7	4	284	0.72	2°	1.00
△	7	4	275	0.72	2°	1.44
+	7	4	282	0.72	2°	2.62

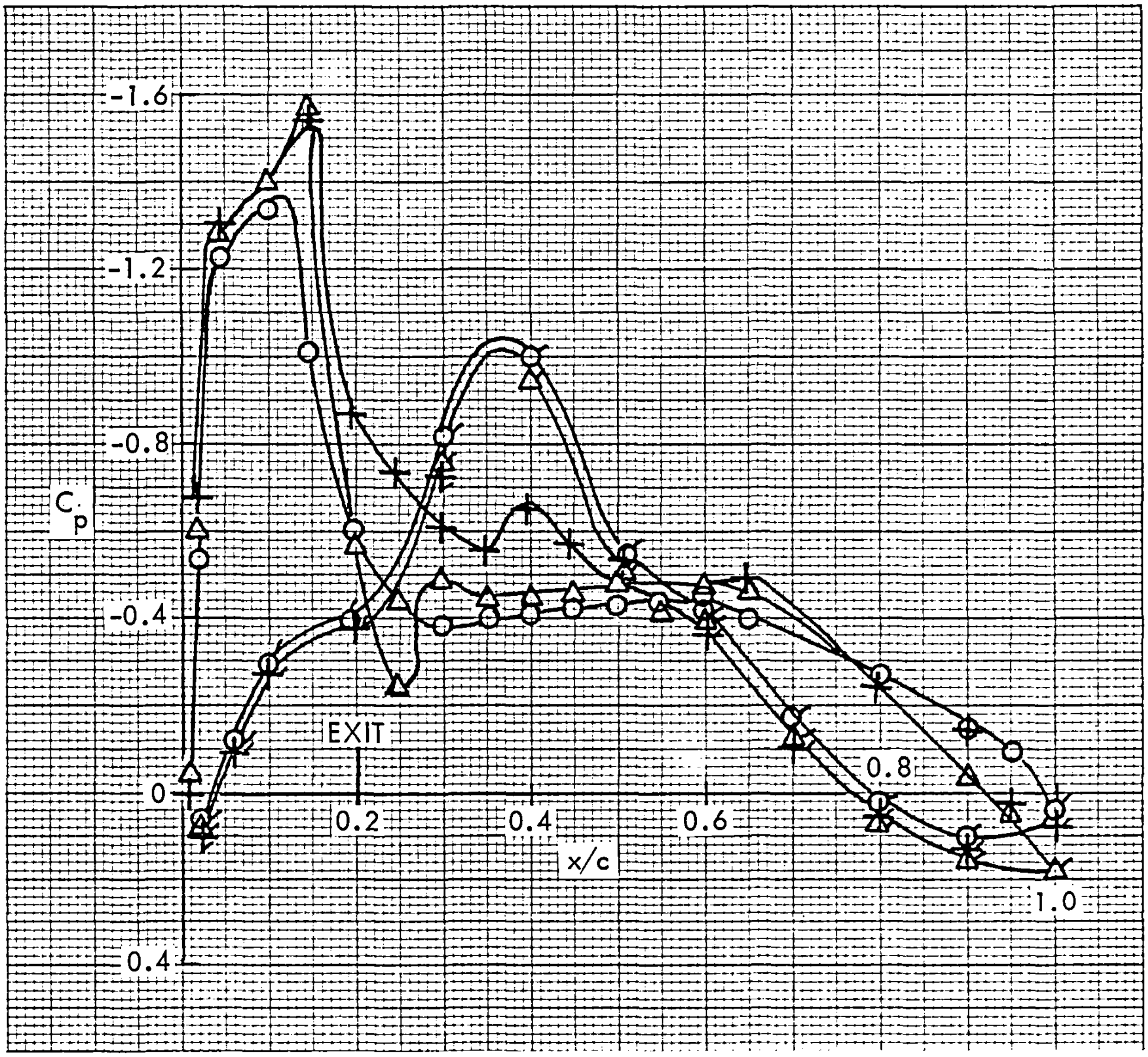

Figure 25. Wing pressure distribution, effect of nozzle pressure ratio, nozzle N_{1E}, η = 0.42

CONFIG $W_1 B_4 P_7 C_1 N_{1E}$

SYM	TEST	SERIES	RUN	M_∞	α	H_j/p_∞
○	7	4	284	0.72	2°	1.00
△	7	4	275	0.72	2°	1.44
+	7	4	282	0.72	2°	2.62

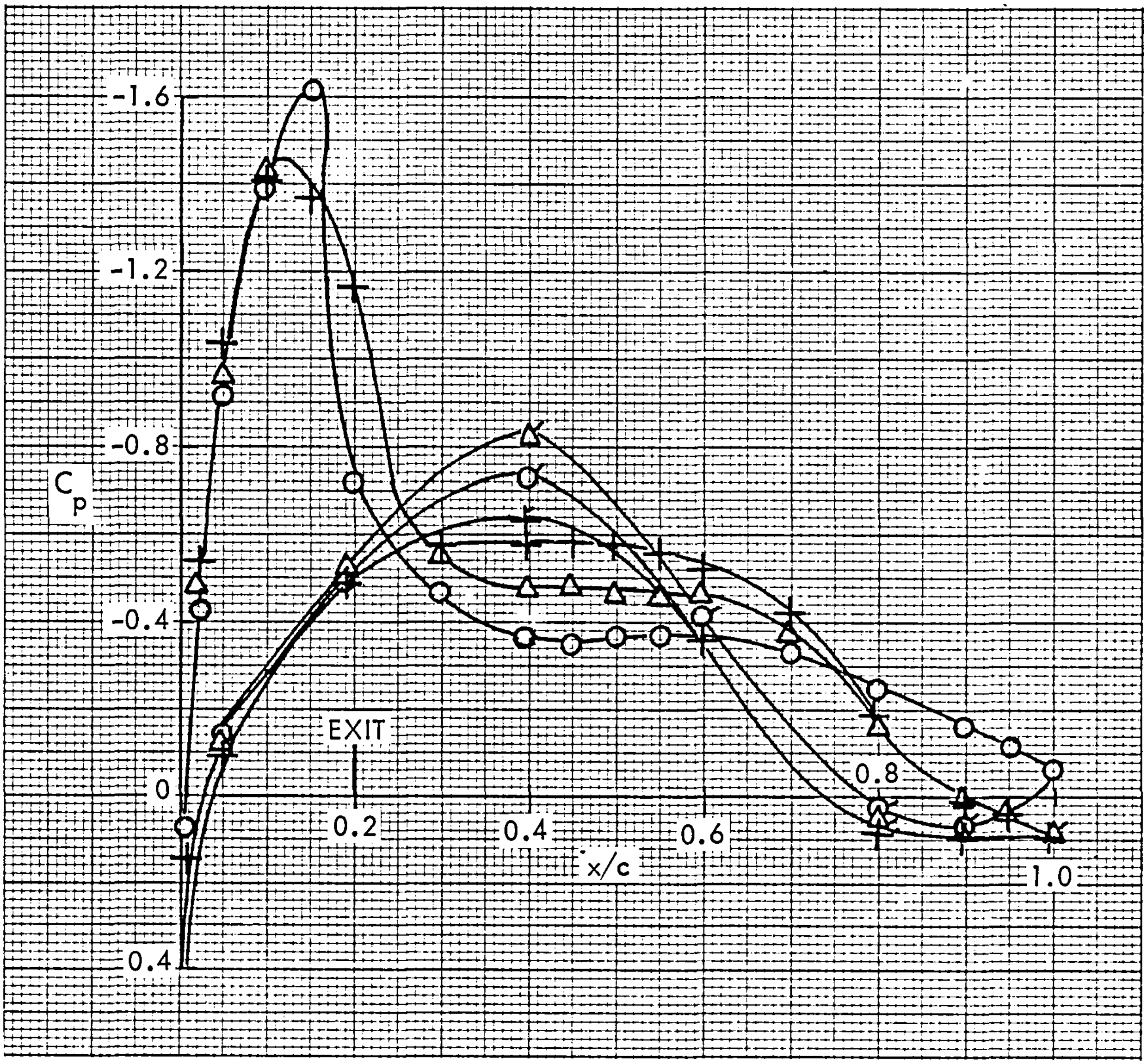

Figure 26. Wing pressure distribution, effect of nozzle pressure ratio, nozzle N_{1E}, η = 0.39

CONFIG $W_1 B_4 P_7 C_1 N_{2E}$

SYM	TEST	SERIES	RUN	M_∞	α	H_j/p_∞
O	7	1	111	0.72	2°	1.44
Δ	7	1	112	0.72	2°	1.85
+	7	1	132	0.72	2°	2.65

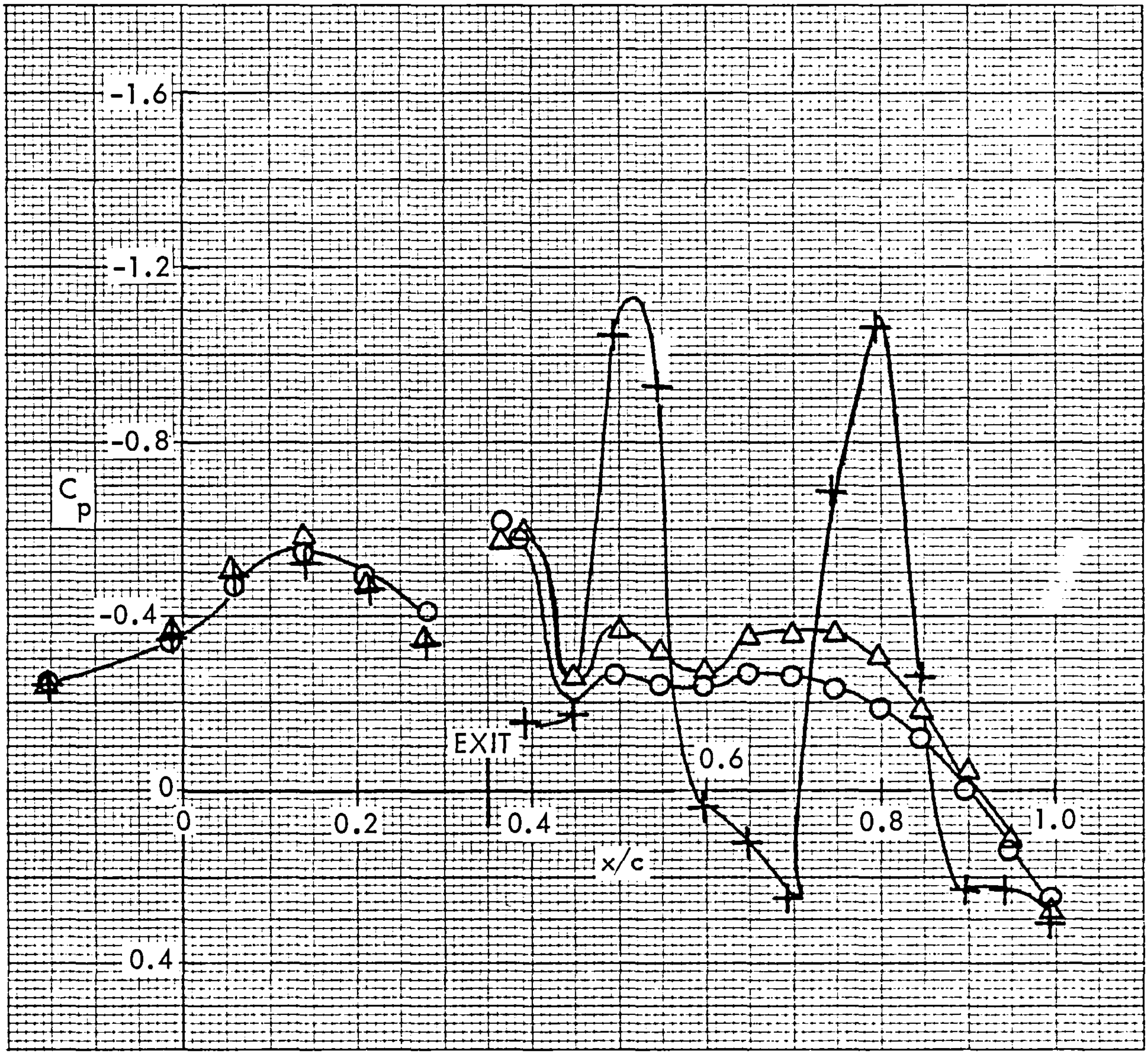

Figure 27. Wing pressure distribution, effect of nozzle pressure ratio, nozzle N_{2E}, $\eta = 0.50$

CONFIG $W_1 B_4 P_7 C_1 N_{2E}$

SYM	TEST	SERIES	RUN	M_∞	α	H_j/p_∞
○	7	1	111	0.72	2°	144
△	7	1	132	0.72	2°	2.65

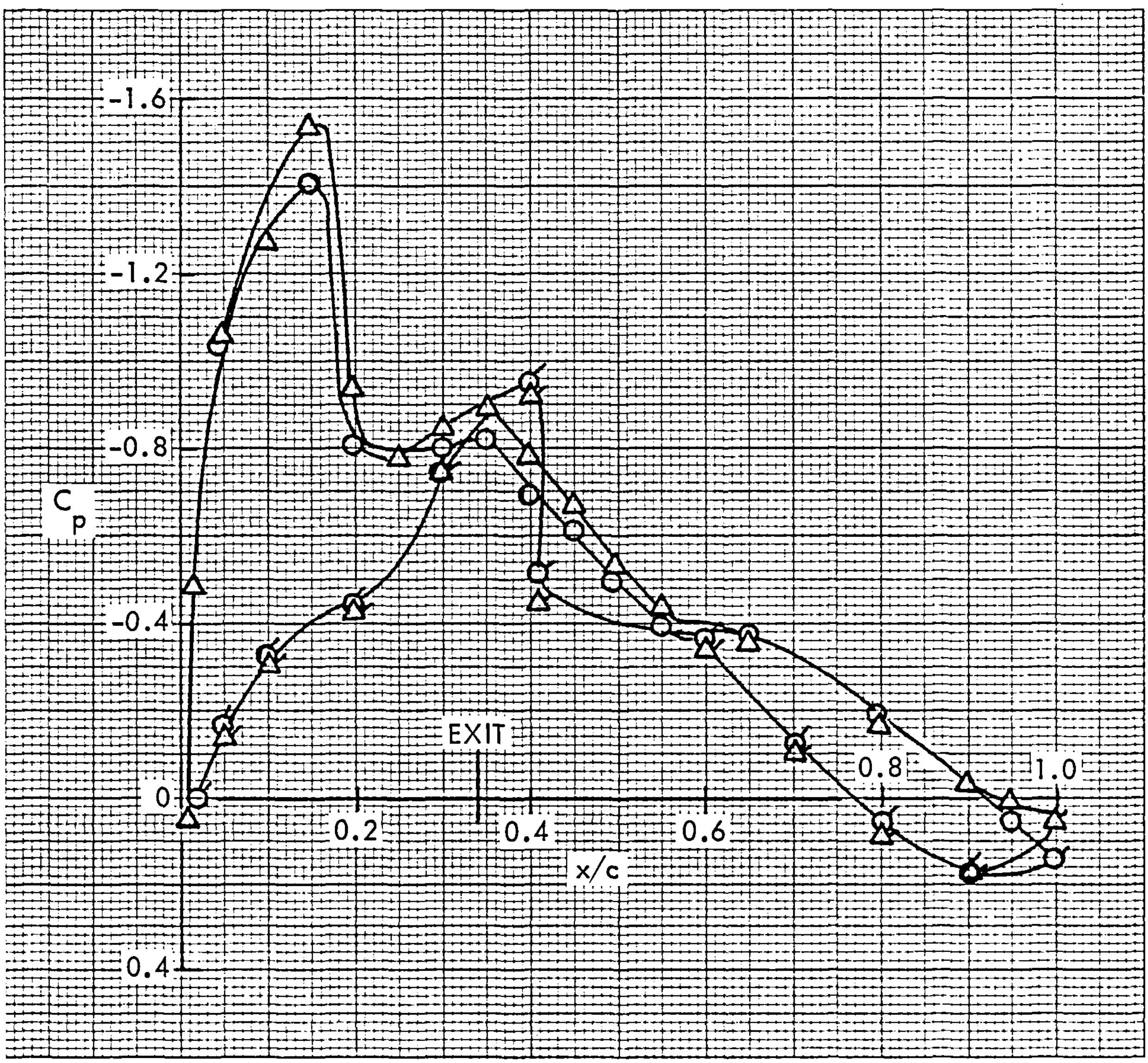

Figure 28. Wing pressure distribution, effect of nozzle pressure ratio, nozzle N_{2E}, $\eta = 0.42$

CONFIG $W_1 B_4 P_7 C_1 N_{2E}$

SYM	TEST	SERIES	RUN	M_∞	α	H_j/p_∞
○	7	1	111	0.72	2°	1.44
△	7	1	132	0.72	2°	2.65

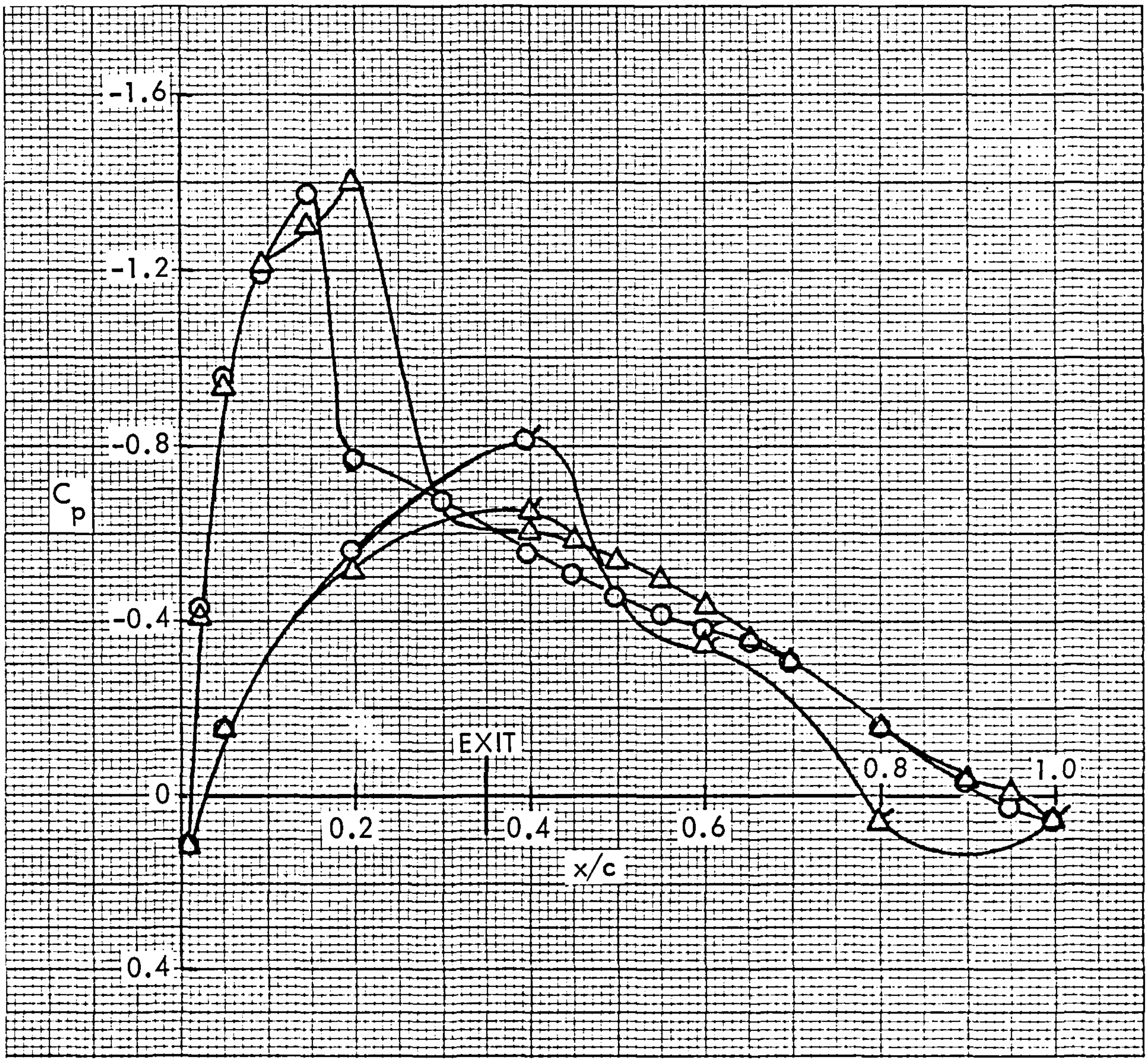

Figure 29. Wing pressure distribution, effect of nozzle pressure ratio, nozzle N_{2E}, η = 0.39

CONFIG $W_1 B_4 P_7 C_1 N_{3E}$

SYM	TEST	SERIES	RUN	M_∞	α	H_j/p_∞
O	7	2	167	0.72	2°	1.44
Δ	7	2	164	0.72	2°	1.85
+	7	2	140	0.72	2°	2.70

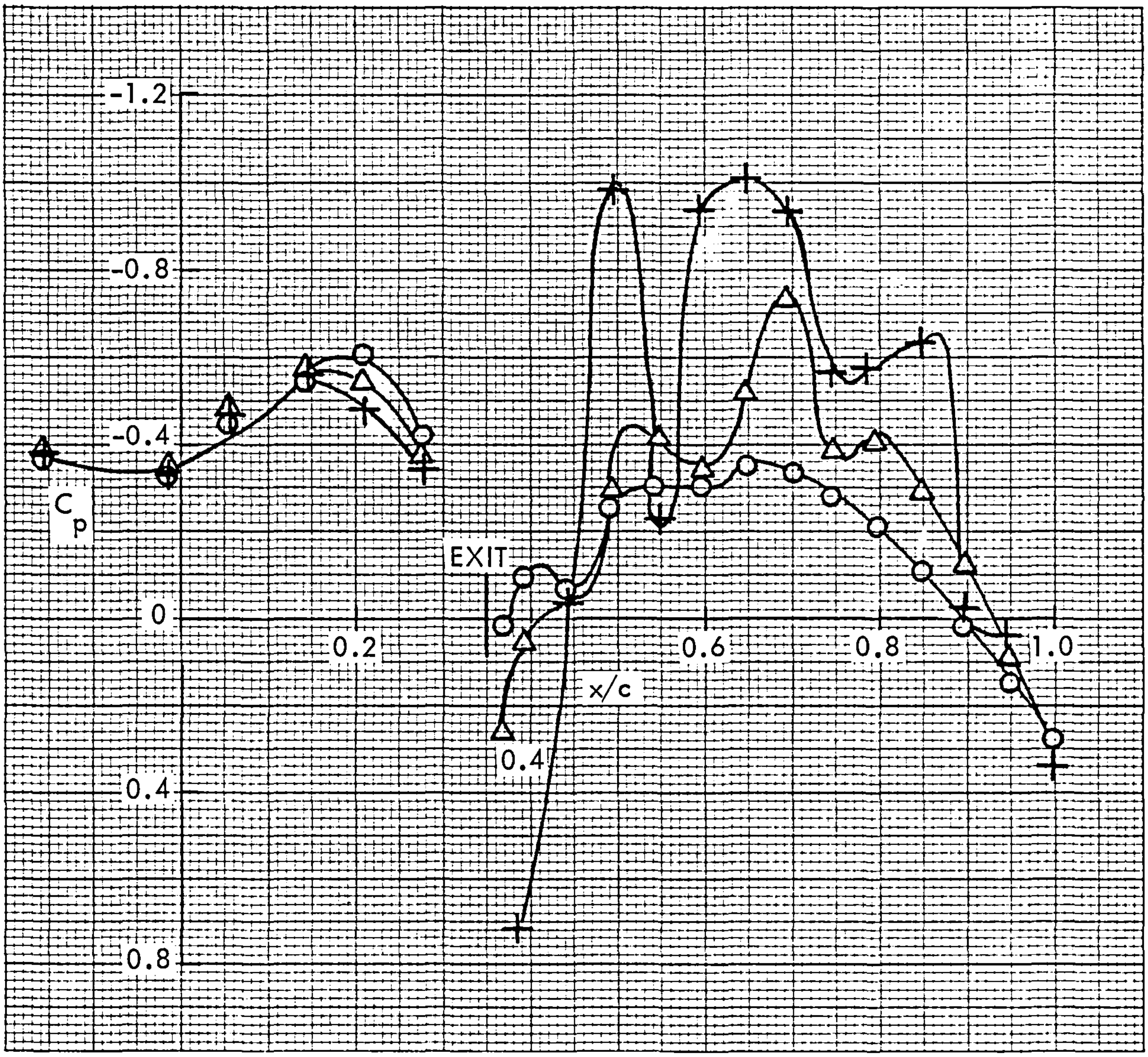

Figure 30. Wing pressure distribution, effect of nozzle pressure ratio, nozzle N_{3E}, η = 0.50

CONFIG $W_1\ B_4\ P_7\ C_1\ N_{3E}$

SYM	TEST	SERIES	RUN	M_∞	α	H_j/p_∞
O	7	2	167	0.72	2°	1.44
Δ	7	2	140	0.72	2°	2.70

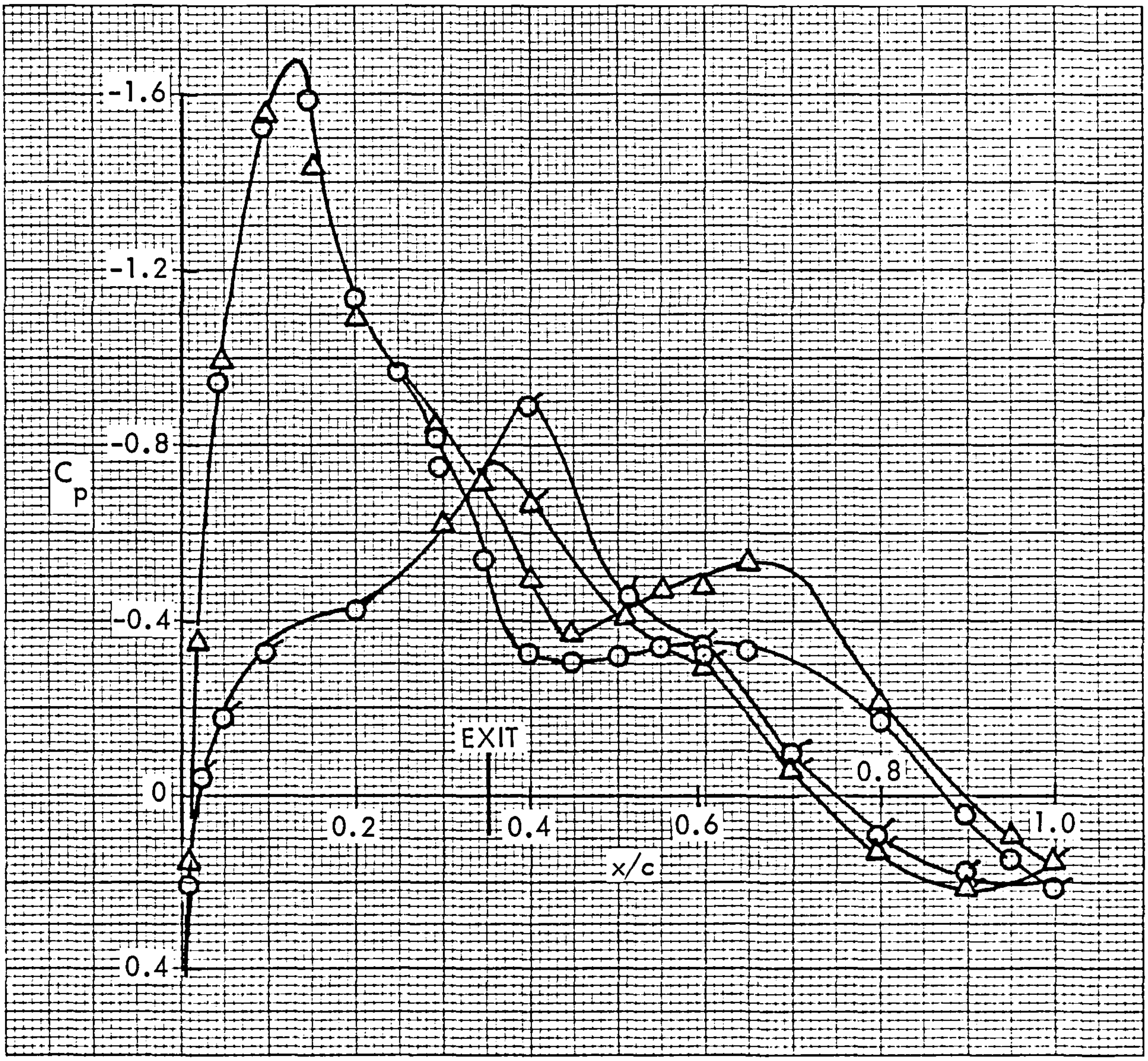

Figure 31. Wing pressure distribution, effect of nozzle pressure ratio, nozzle N_{3E}, $\eta = 0.42$

CONFIG $W_1 B_4 P_7 C_1 N_{3E}$

SYM	TEST	SERIES	RUN	M_∞	α	H_j/p_∞
O	7	2	167	0.72	2°	1.44
Δ	7	2	140	0.72	2°	2.70

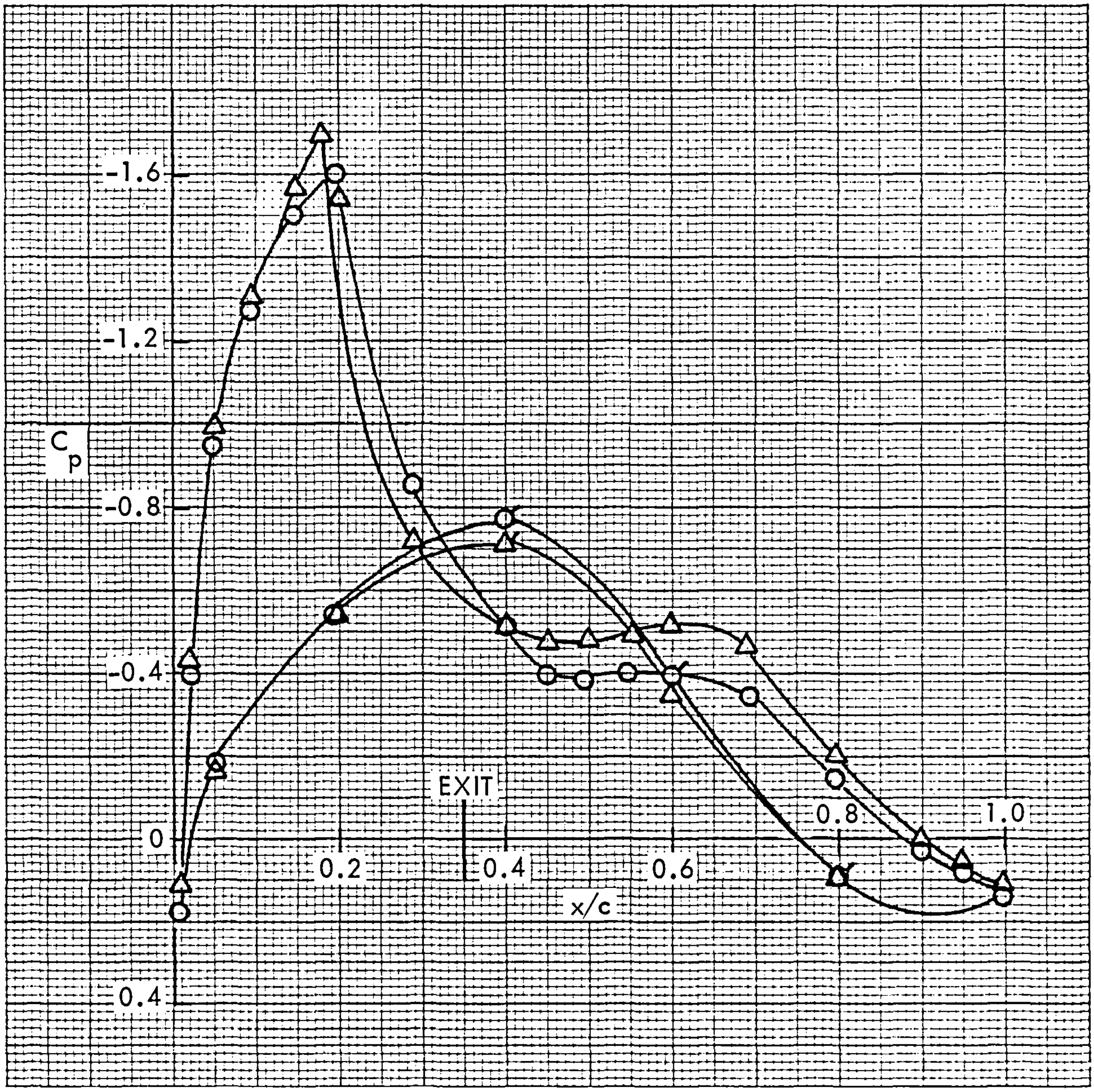

Figure 32. Wing pressure distribution, effect of nozzle pressure ratio, nozzle N_{3E}, $\eta = 0.39$

CONFIG $W_1 B_4 P_7 C_1 N_{4E}$

SYM	TEST	SERIES	RUN	M_∞	α	H_j/p_∞
O	7	3	202	0.72	2°	1.44
Δ	7	3	205	0.72	2°	1.83
+	7	3	234	0.72	2°	2.65

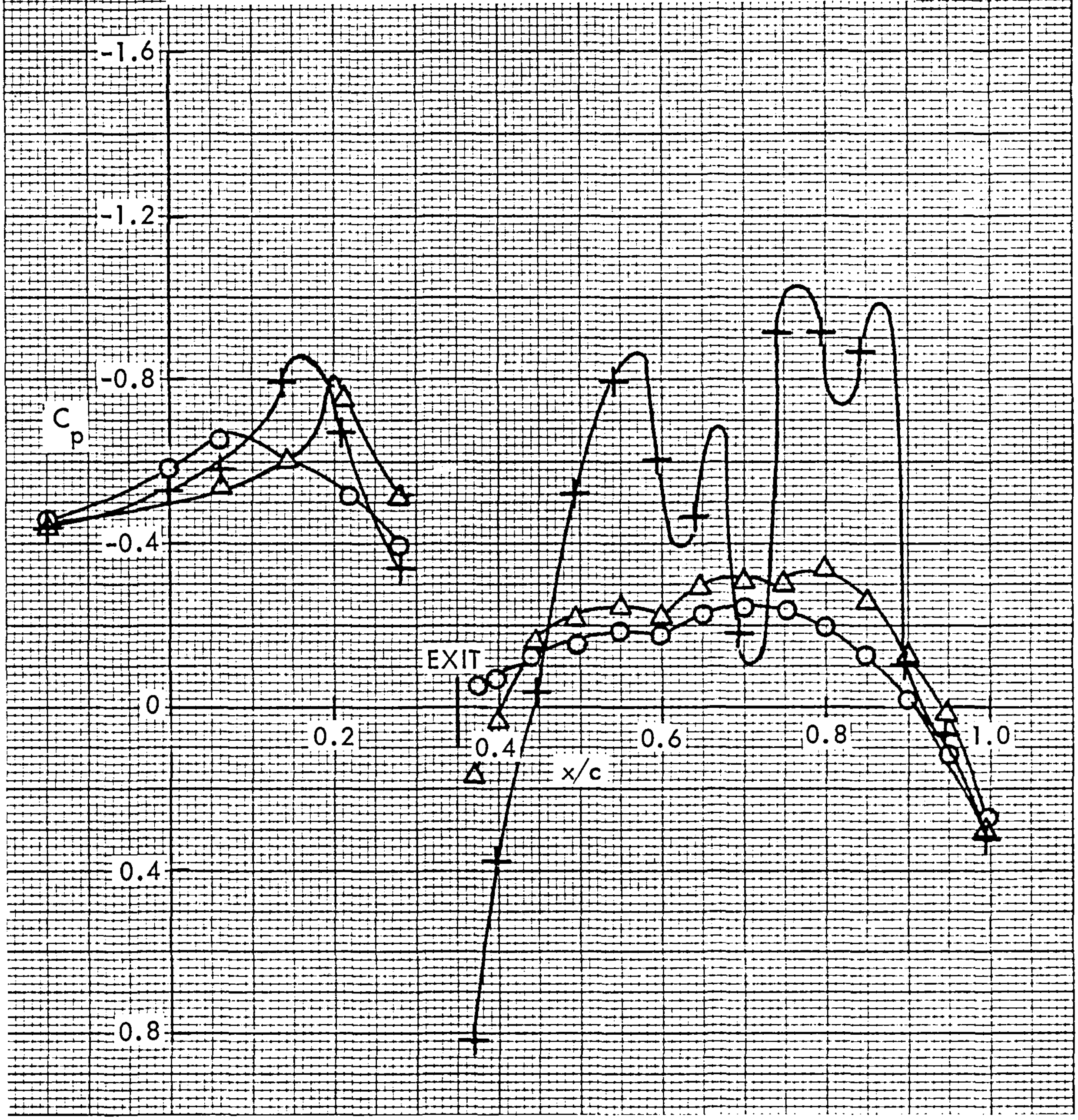

Figure 33. Wing pressure distribution, effect of nozzle pressure ratio, nozzle N_{4E}, $\eta = 0.50$

CONFIG $W_1 B_4 P_7 C_1 N_{4E}$

SYM	TEST	SERIES	RUN	M_∞	α	H_j/p_∞
O	7	3	202	0.72	2°	1.44
△	7	3	234	0.72	2°	2.65

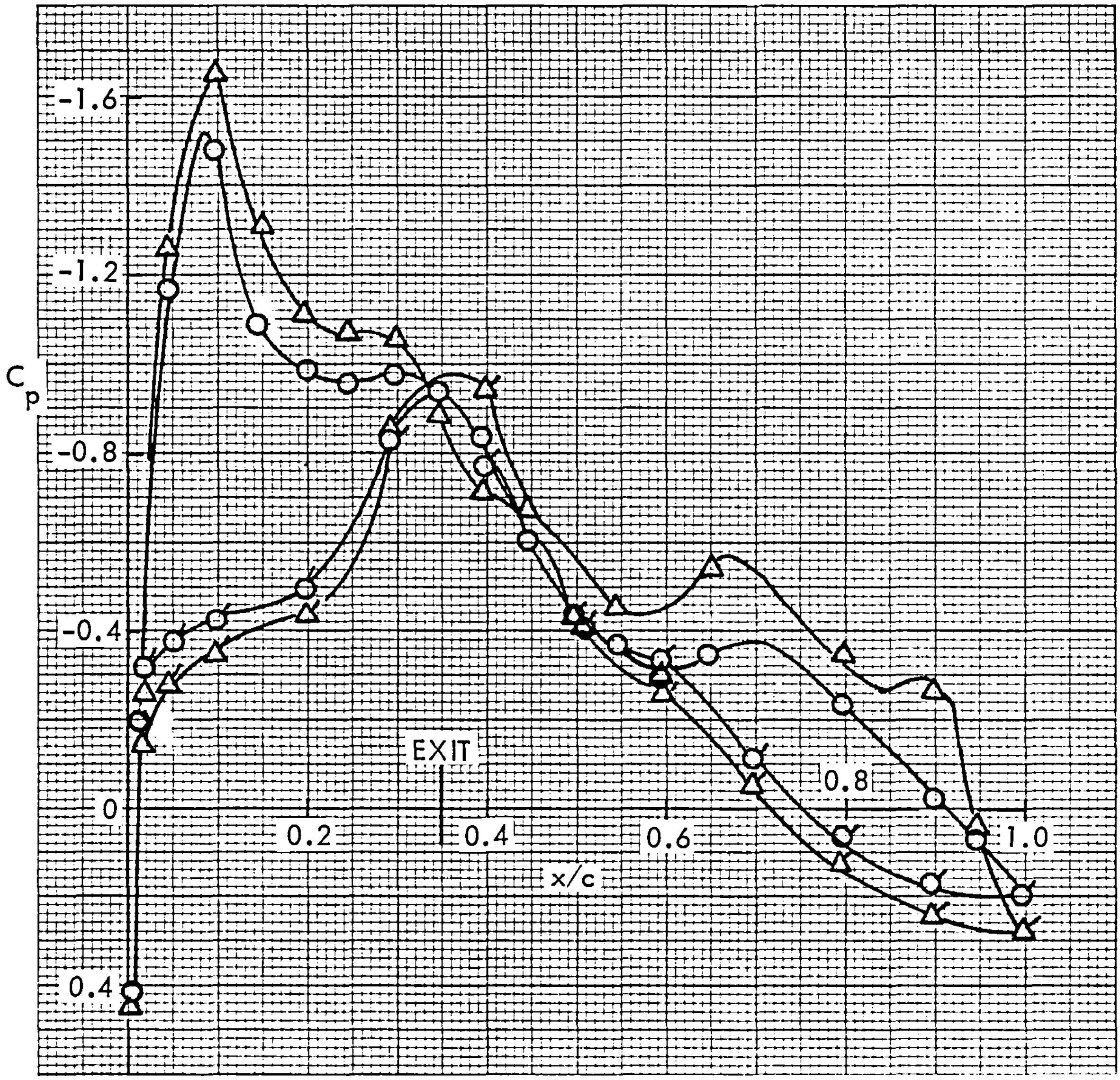

Figure 34. Wing pressure distribution, effect of nozzle pressure ratio, nozzle N_{4E}, $\eta = 0.42$

CONFIG $W_1 B_4 P_7 C_1 N_{4E}$

SYM	TEST	SERIES	RUN	M_∞	α	H_j/p_∞
○	7	3	202	0.72	2°	1.44
△	7	3	234	0.72	2°	2.65

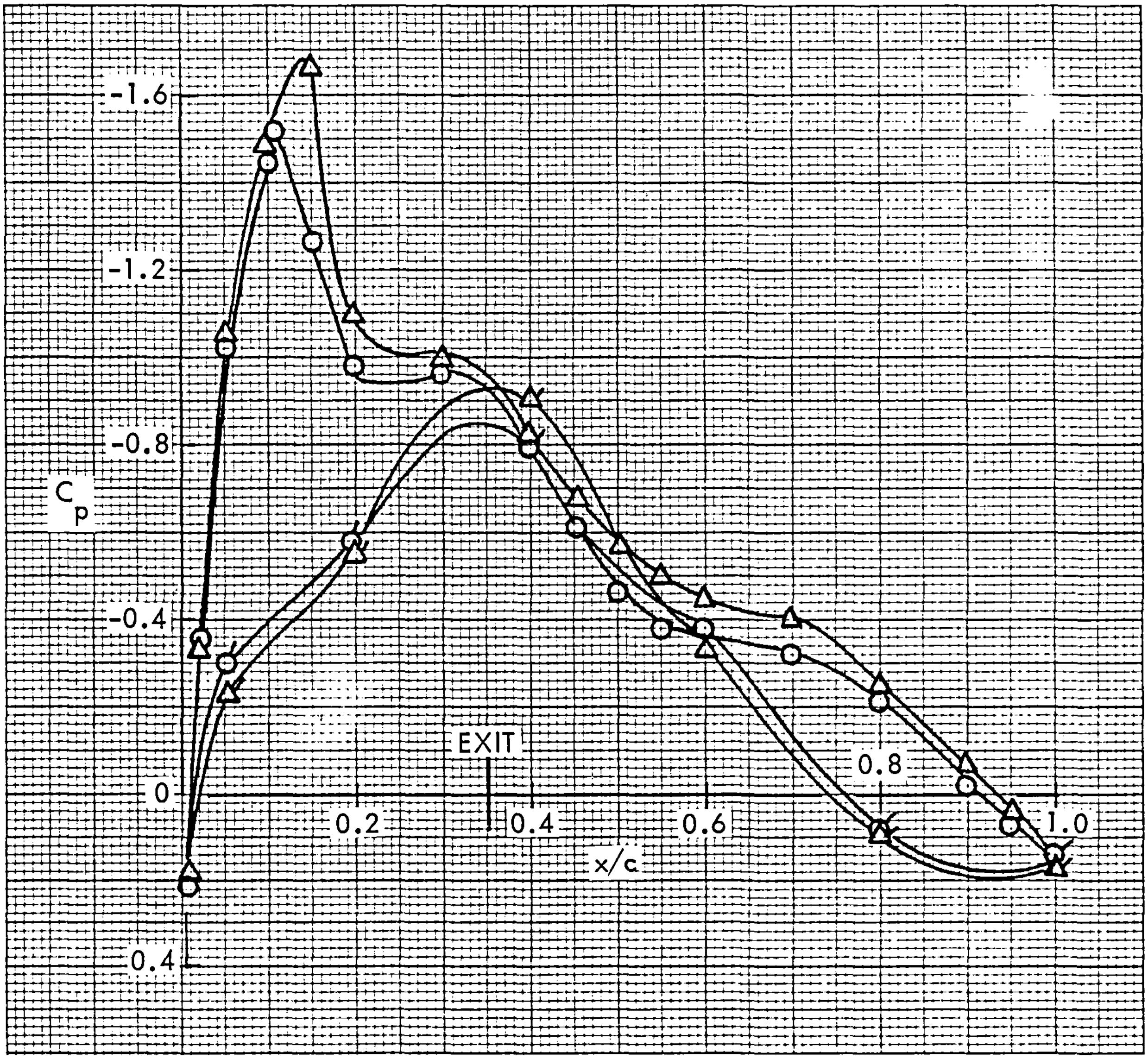

Figure 35. Wing pressure distribution, effect of nozzle pressure ratio, nozzle N_{4E}, $\eta = 0.39$

CONFIG $W_1 B_4 P_7 C_1 N_{4E}$

SYM	TEST	SERIES	RUN	M_∞	α	H_j/p_∞
O	7	3	202	0.72	2°	1.44
△	7	3	205	0.72	2°	1.83
+	7	3	234	0.72	2°	2.65

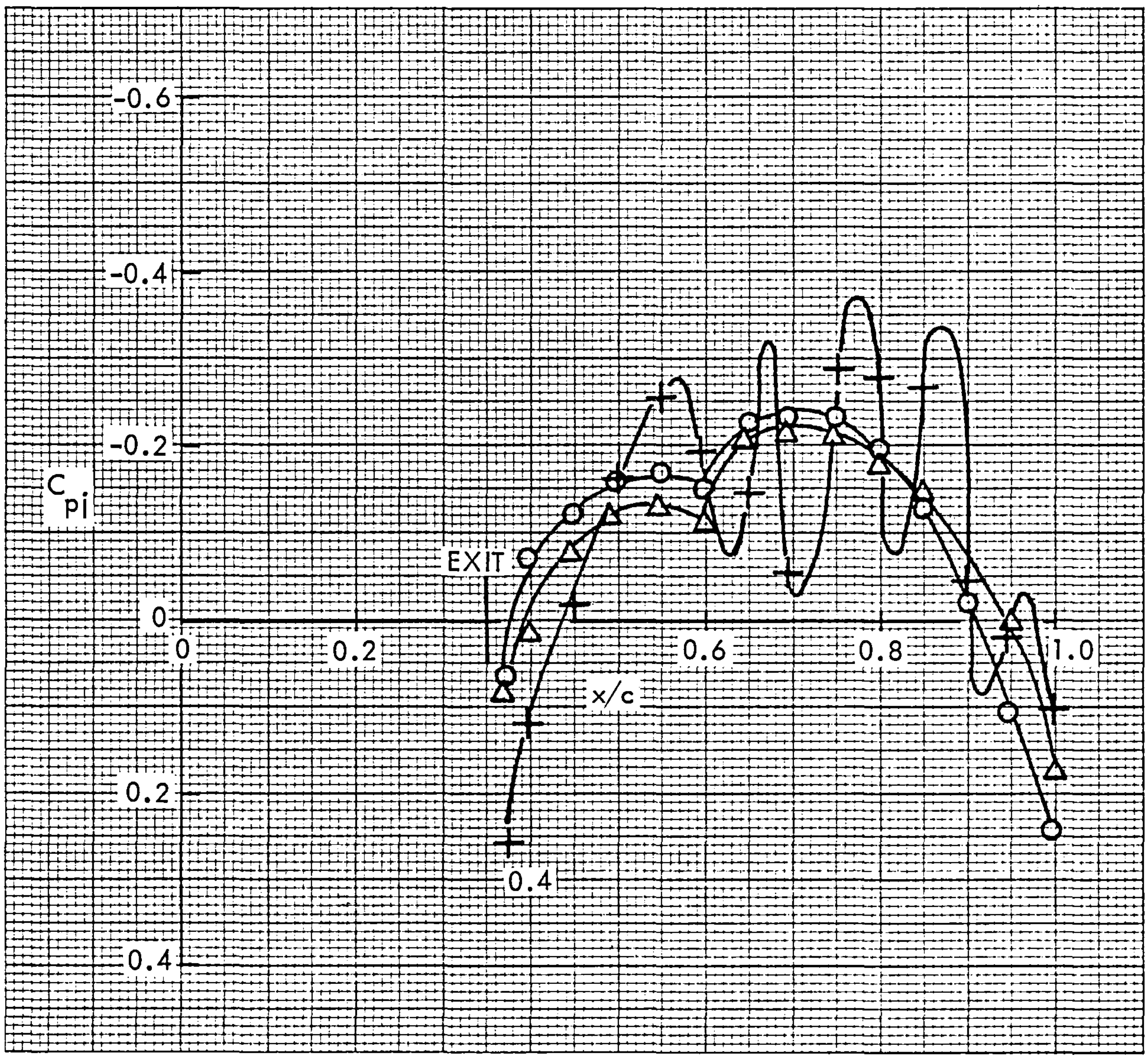

Figure 36. Wing pressure distribution based on q_j, effect of nozzle pressure ratio, nozzle N_{4E}, $\eta = 0.50$

CONFIG $W_1 B_4 P_7 C_1 N_{2E}$

SYM	TEST	SERIES	RUN	M_∞	α	H_j/p_∞
○	7	1	111	0.72	2^o	1.44
△	7	1	112	0.72	2^o	1.85
+	7	1	132	0.72	2^o	2.65

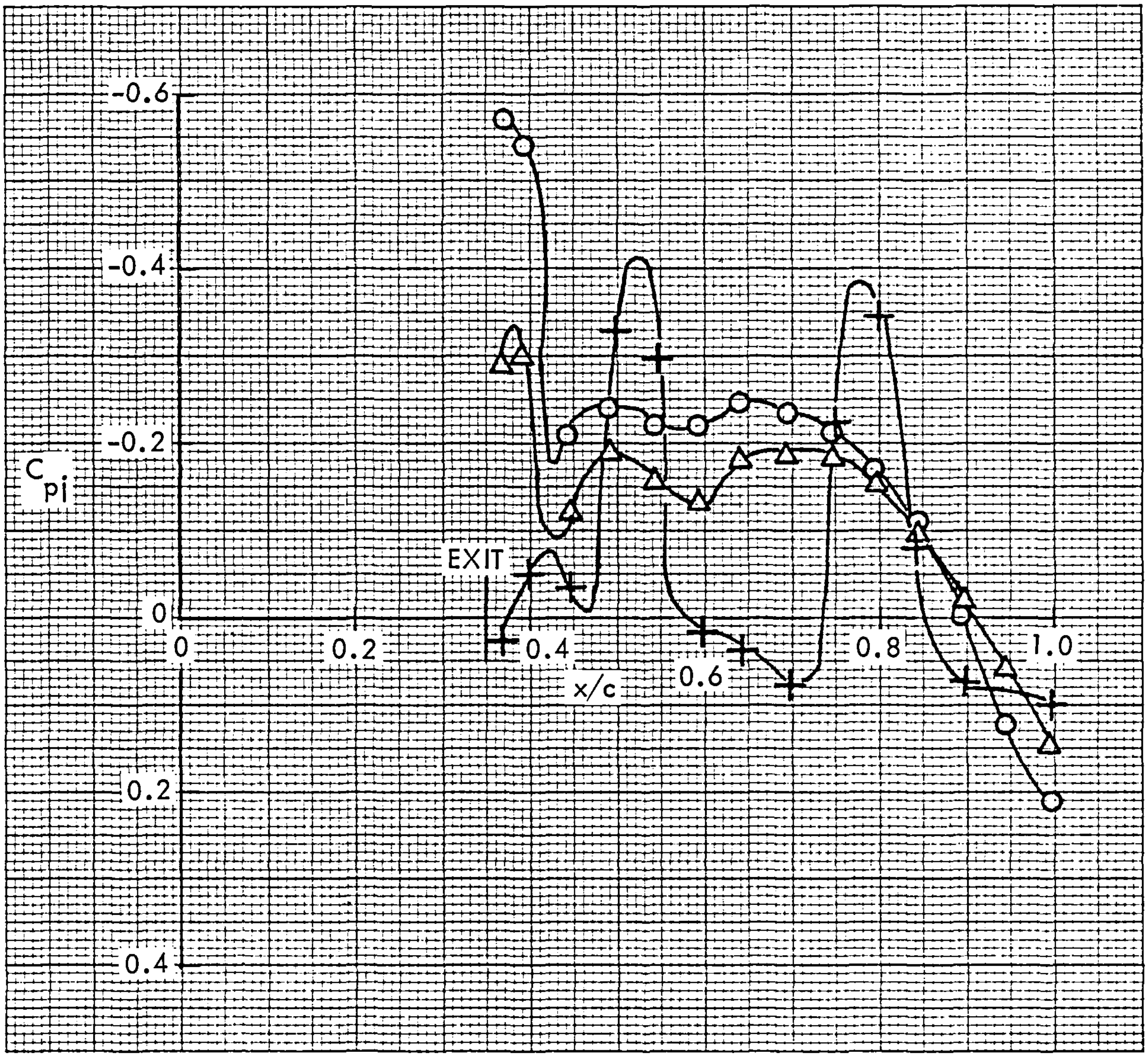

Figure 37. Wing pressure distribution based on q_j, effect of nozzle pressure ratio, nozzle N_{2E}, $\eta = 0.50$

CONFIG	SYM	TEST	SERIES	RUN	M_∞	α	H_j/p_∞
$W_1 B_4 P_7 C_1 N_{2E}$	○	7	1	132	0.72	2°	2.65
$W_1 B_4 P_7 C_1 N_{3E}$	△	7	2	140	0.72	2°	2.67
$W_1 B_4 P_7 C_1 N_{4E}$	+	7	3	234	0.72	2°	2.65

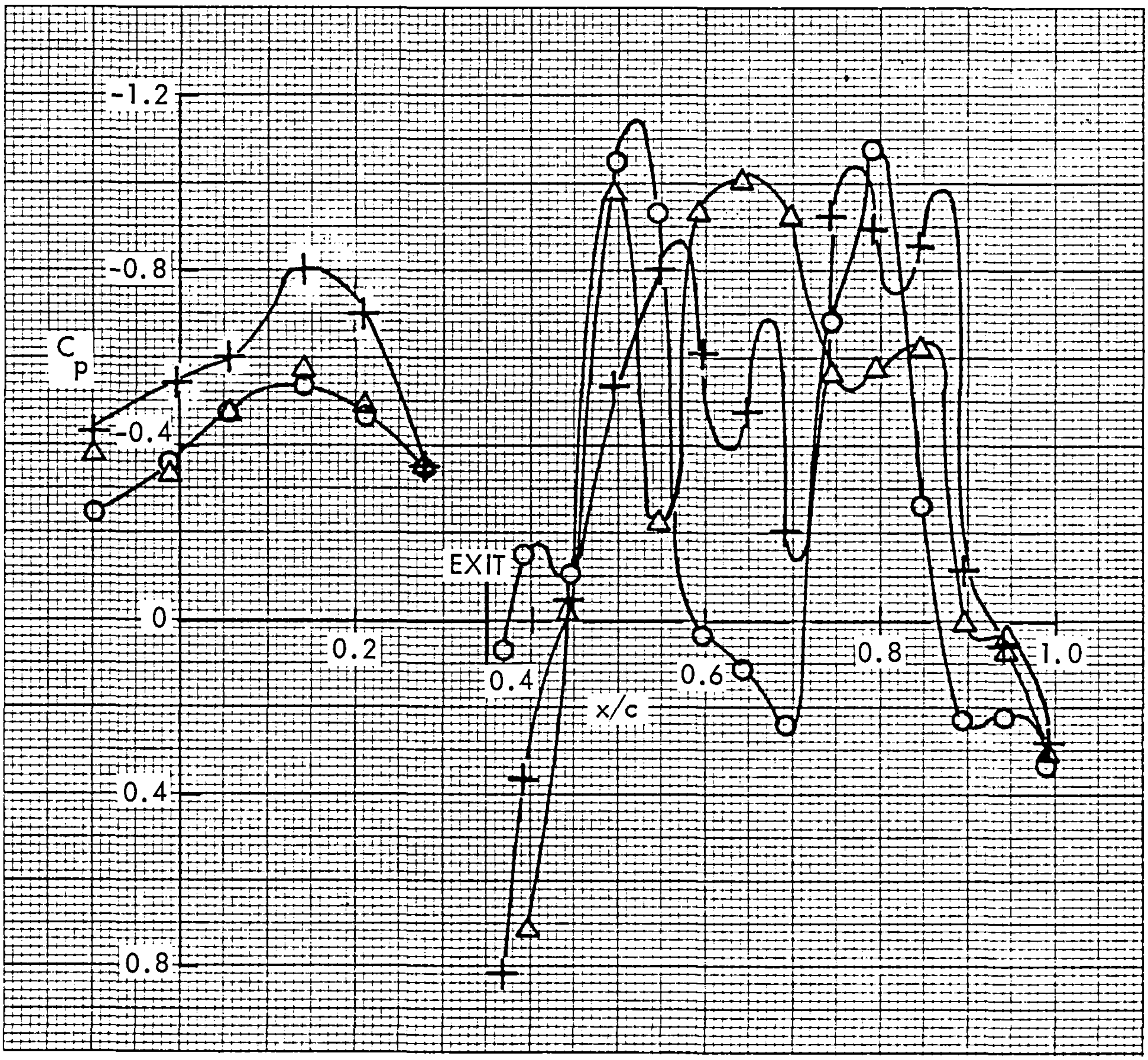

Figure 38. Wing pressure distribution, influence of nozzle shape, η = 0.50

CONFIG	SYM	TEST	SERIES	RUN	M_∞	α	H_j/p_∞
$W_1 B_4 P_7 C_1 N_{2E}$	○	7	1	132	0.72	2°	2.65
$W_1 B_4 P_7 C_1 N_{3E}$	△	7	2	140	0.72	2°	2.67
$W_1 B_4 P_7 C_1 N_{4E}$	+	7	3	234	0.72	2°	2.65

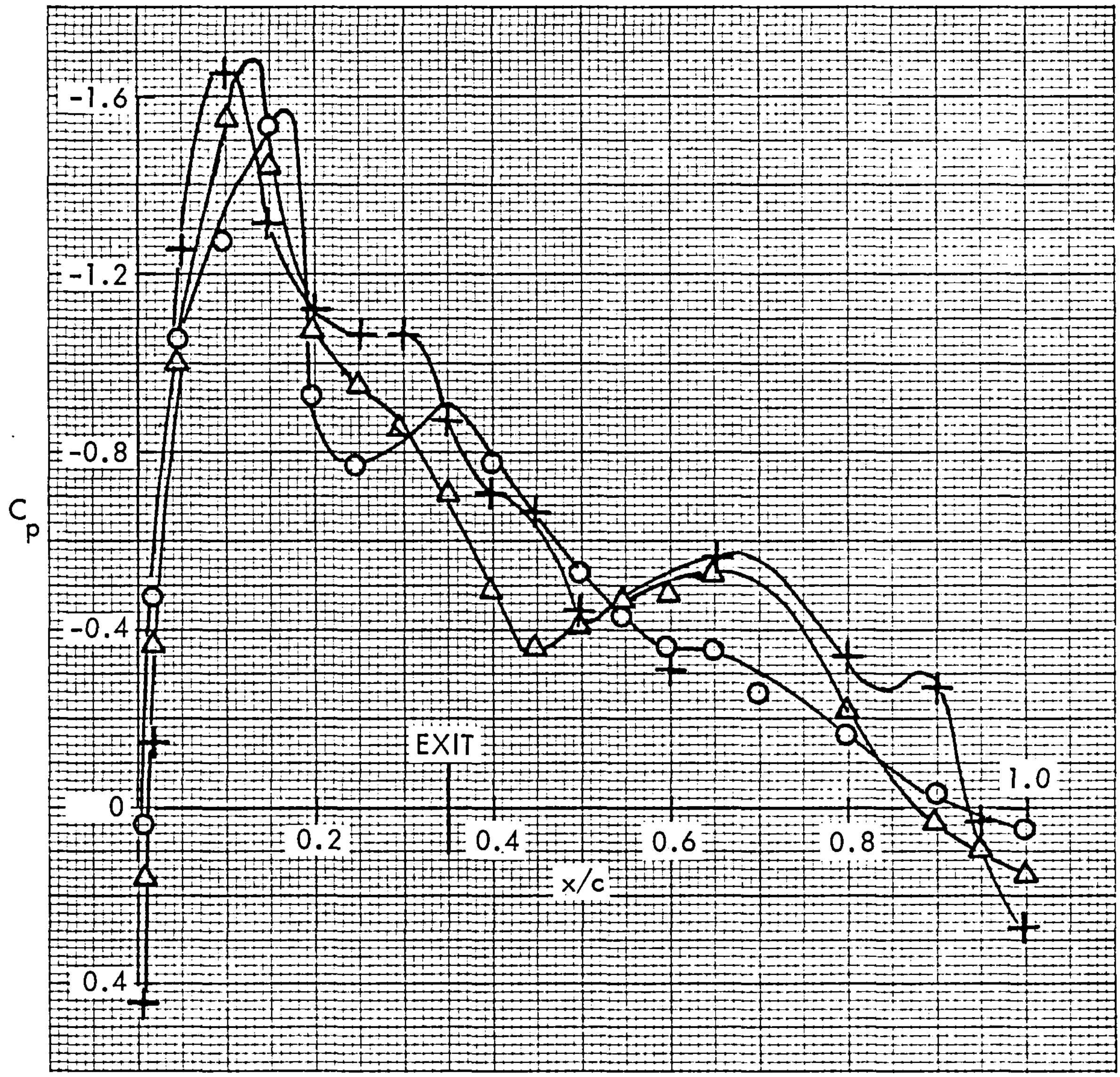

Figure 39. Wing pressure distribution, influence of nozzle shape, η = 0.42

CONFIG	SYM	TEST	SERIES	RUN	M_∞	α	H_j/p_∞
$W_1 B_4 P_7 C_1 N_{2E}$	○	7	1	132	0.72	2°	2.65
$W_1 B_4 P_7 C_1 N_{3E}$	△	7	2	140	0.72	2°	2.67
$W_1 B_4 P_7 C_1 N_{4E}$	+	7	3	234	0.72	2°	2.65

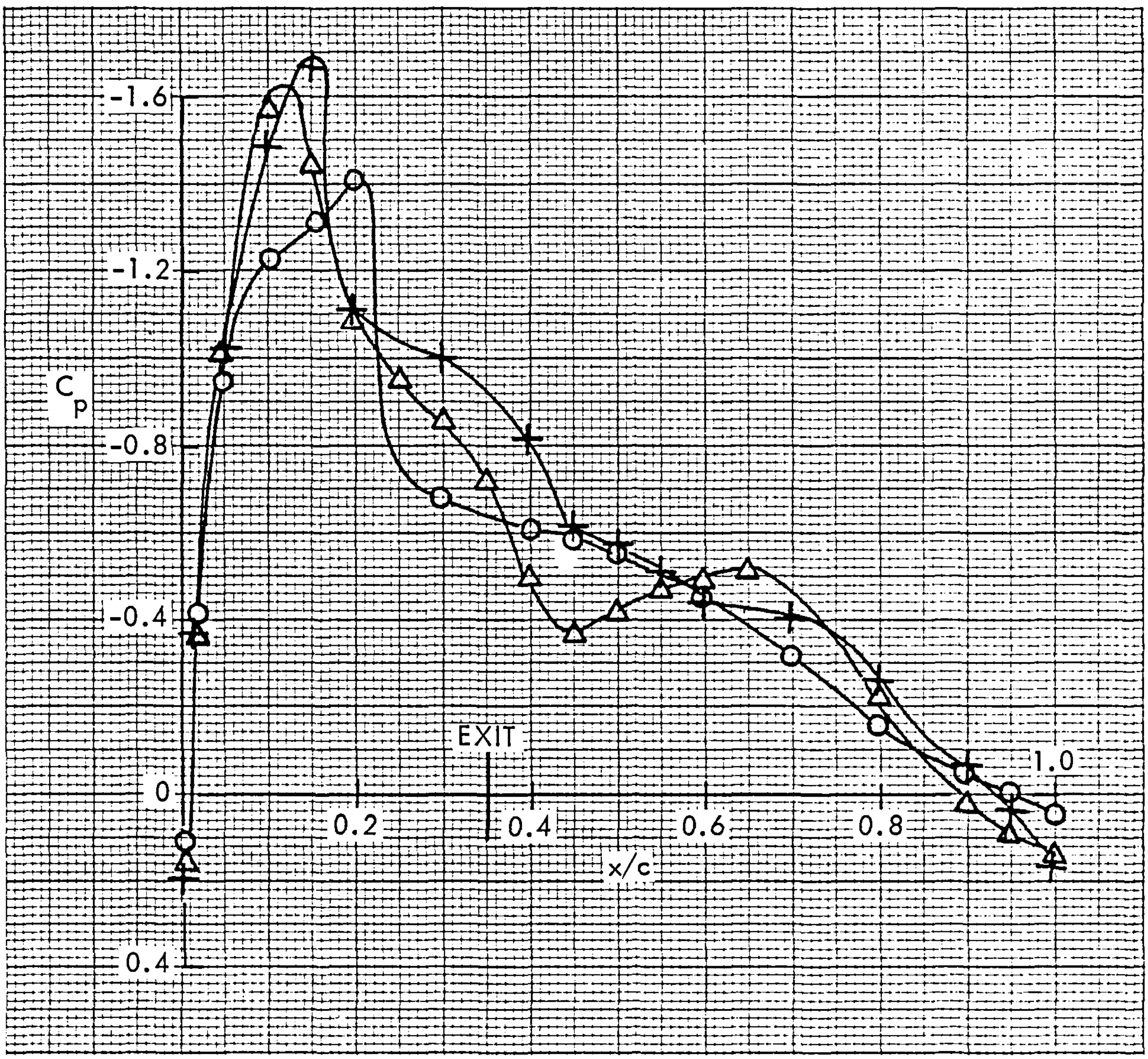

Figure 40. Wing pressure distribution, influence of nozzle shape, η = 0.39

USB CRUISE PROGRAM

CONFIG	SYM	TEST	SERIES	RUN	M_∞	α	H_j/p_∞
$W_1 B_4 P_7 C_1 N_{2E}$	○	7	1	111	0.72	2°	1.44
$W_1 B_4 P_7 C_1 N_{3E}$	△	7	2	167	0.72	2°	1.44
$W_1 B_4 P_7 C_1 N_{4E}$	+	7	3	202	0.72	2°	1.44
$W_1 B_4 P_7 C_1 N_{1E}$	×	7	4	275	0.72	2°	1.44

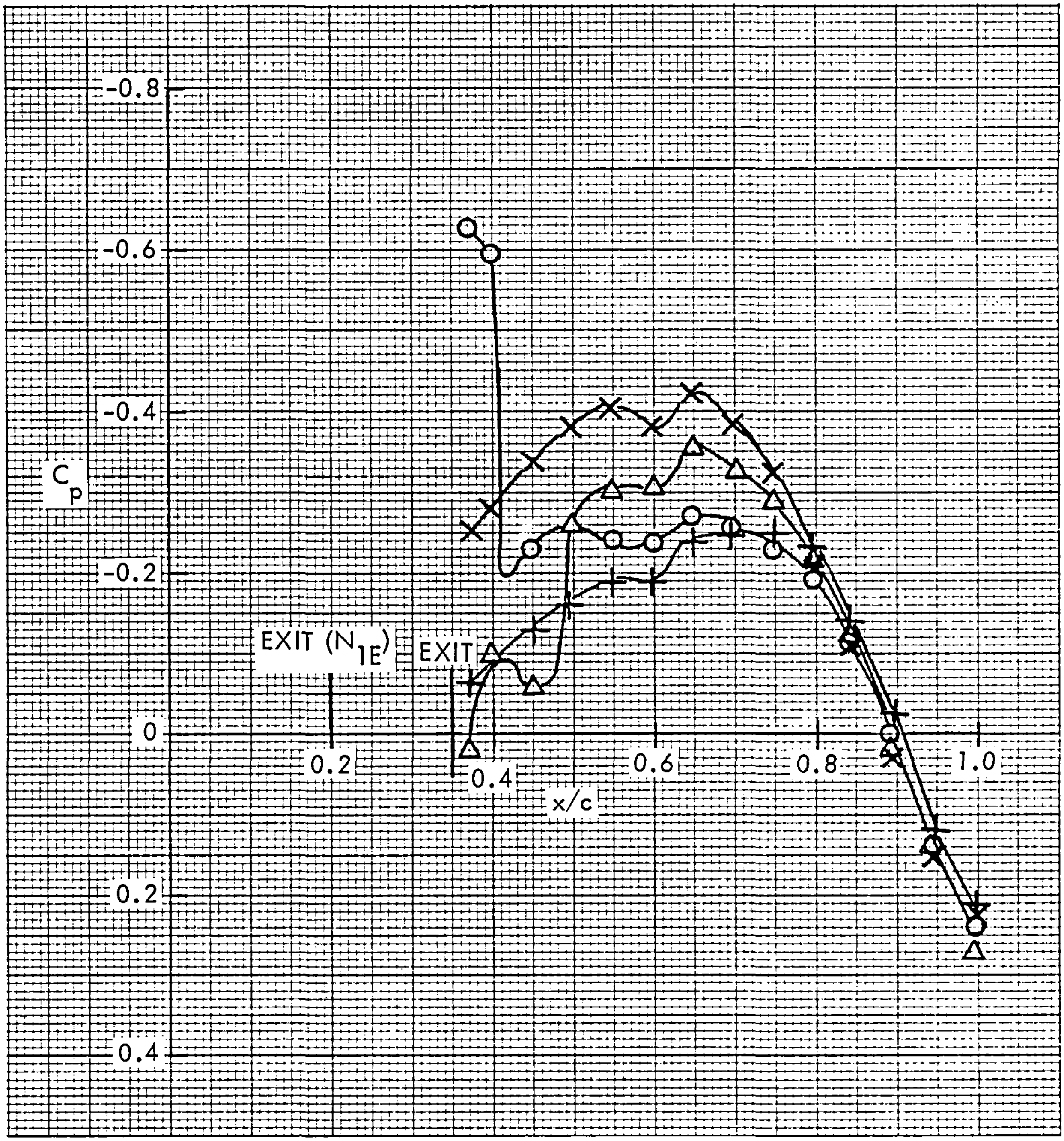

Figure 41. Wing pressure distribution, influence of nozzle shape, flow-through pressure ratio, η = 0.50

USB CRUISE PROGRAM

CONFIG $W_1 B_4 P_7 C_1 N_{2E}$

TEST	SERIES	RUN	M_∞	α	H_j/p_∞
7	1	139	0.72	2°	2.60

SYM	η
O	0.50
Δ	0.42
+	0.39

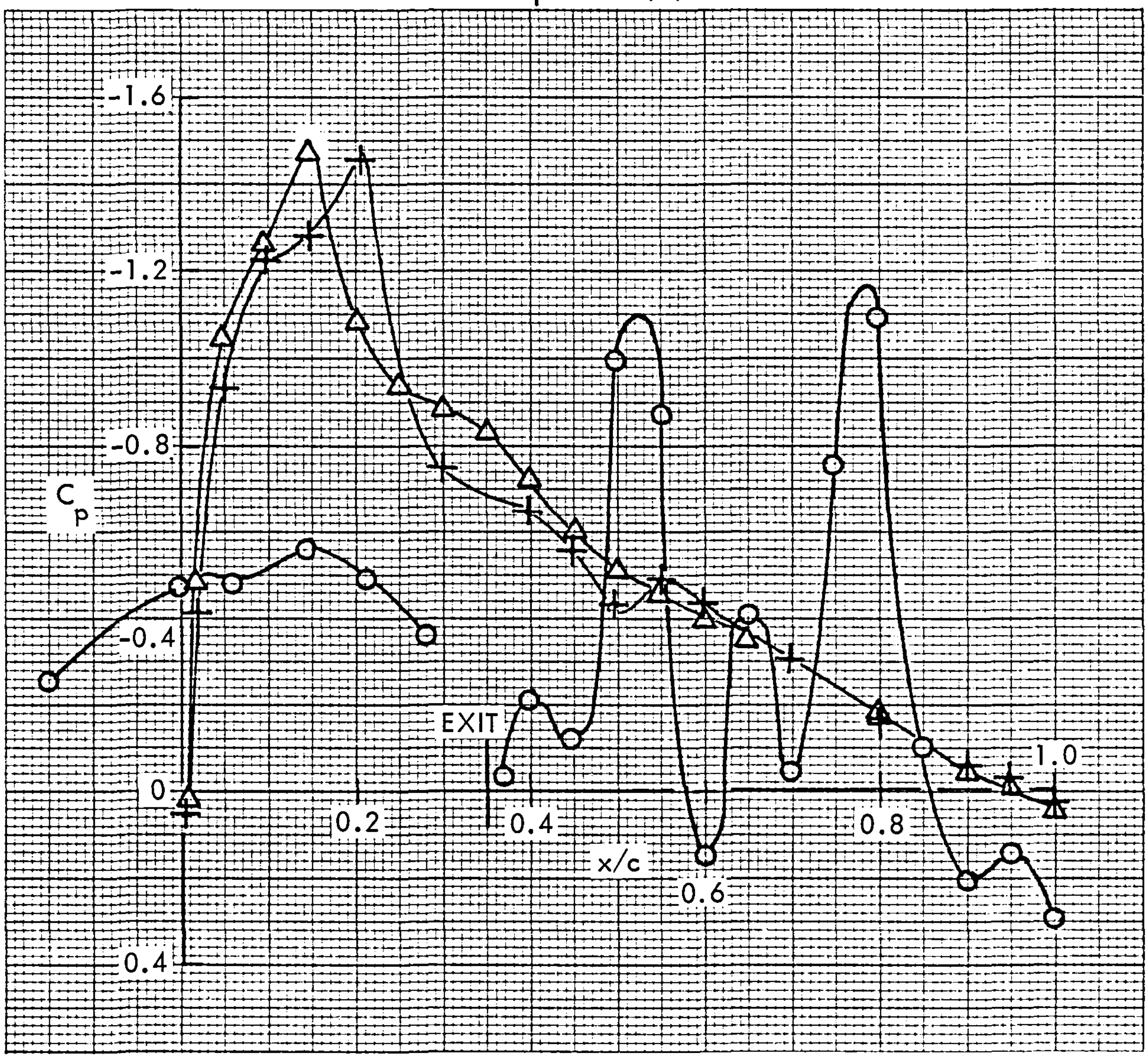

Figure 42. Wing pressure distribution, spanwise influence of jet, nozzle N_{2E}

USB CRUISE PROGRAM

CONFIG $W_1 B_4 P_7 C_1 N_{3E}$

TEST	SERIES	RUN	M_∞	α	H_j/p_∞
7	1	140	0.72	2°	2.67

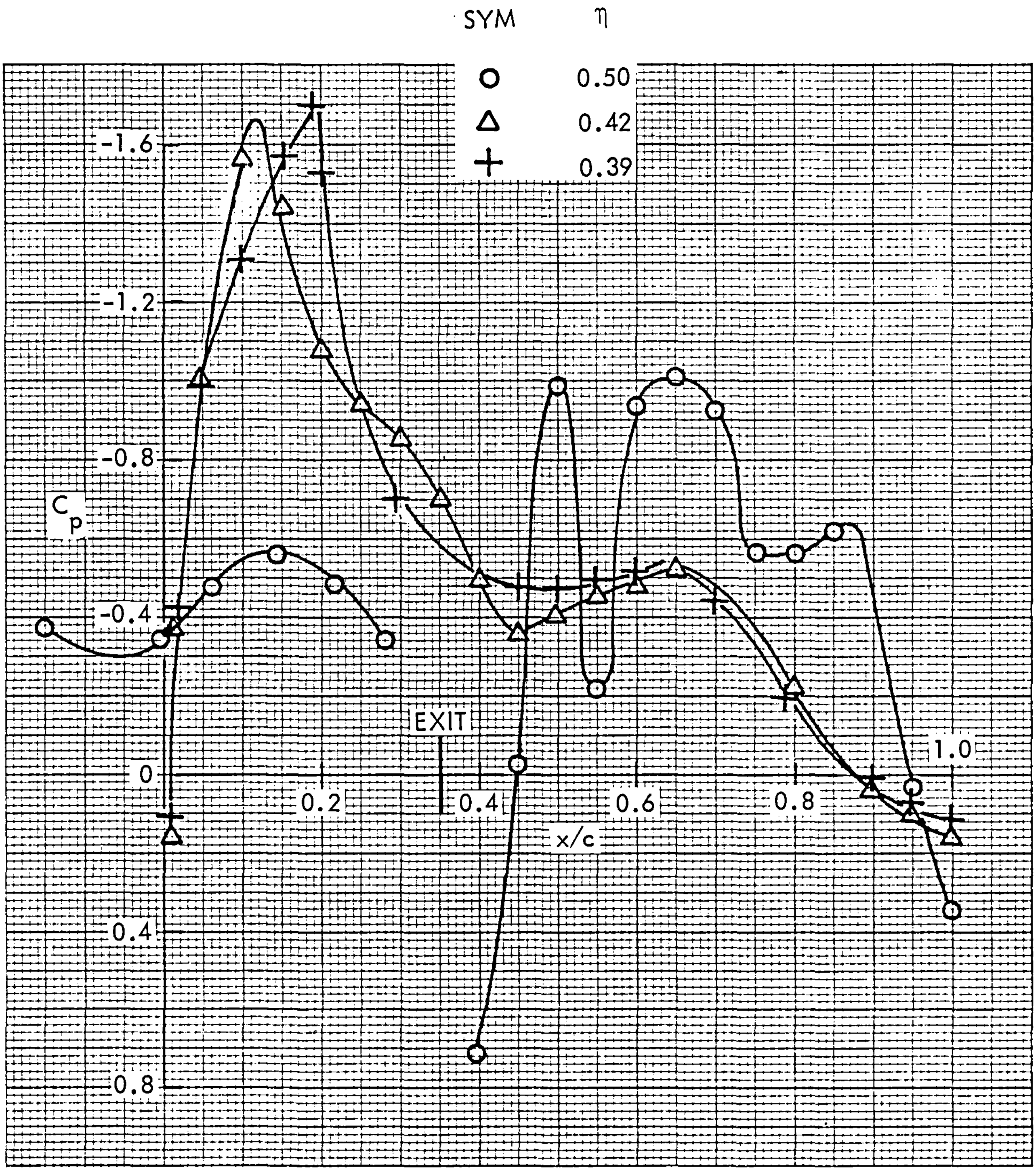

Figure-43. Wing pressure distribution, spanwise influence of jet, nozzle N_{3E}

USB CRUISE PROGRAM

CONFIG $W_1 B_4 P_7 C_1 N_{4E}$

TEST	SERIES	RUN	M_∞	α	H_j/p_∞
7	3	210	0.72	2°	2.60

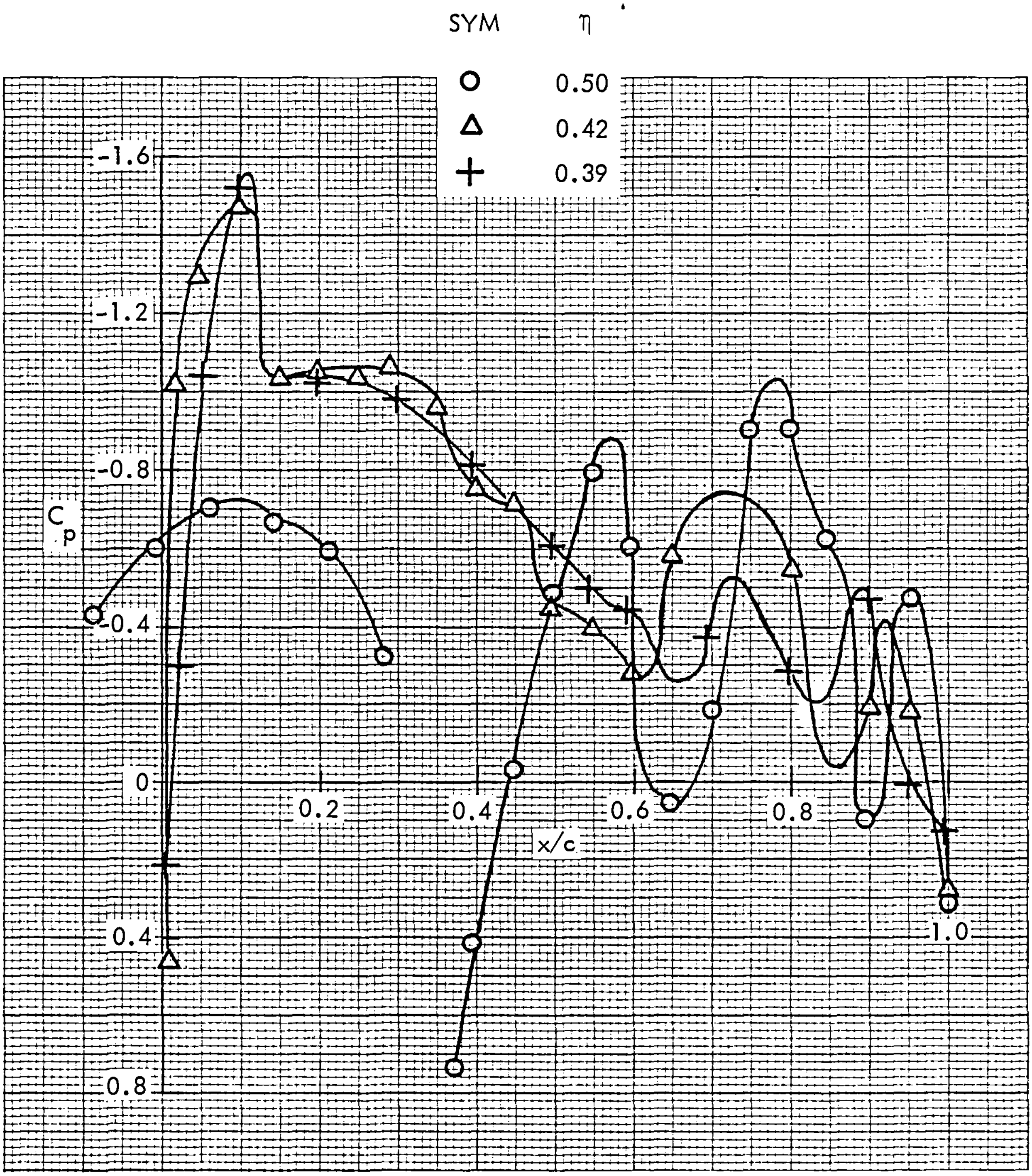

Figure 44. Wing pressure distribution, spanwise influence of jet, nozzle N_{4E}

5.2 Model Pressure Distributions, Long Nozzle Series

Surface static pressure data for the long nozzle series are presented in Figure 45 through 72. The format of presentation for these data is slightly different from that used for the short nozzle series. Two spanwise positions are presented per page as compared to one for the short nozzle series. Since data was taken at four spanwise positions for this group, two pages are required to show the data for each test run.

These data begin with the clean straight wing which is followed by the circular nozzle, N_2, mounted in flow-through configuration on a short pylon. Data are then presented for nozzles N_3, N_5, and N_6 mounted in the standard USB configuration. These are the D-duct, AR = 6, and streamlined D-duct nacelles respectively. All data in this series are presented at a Reynolds' number of 3.5 million based on wing chord.

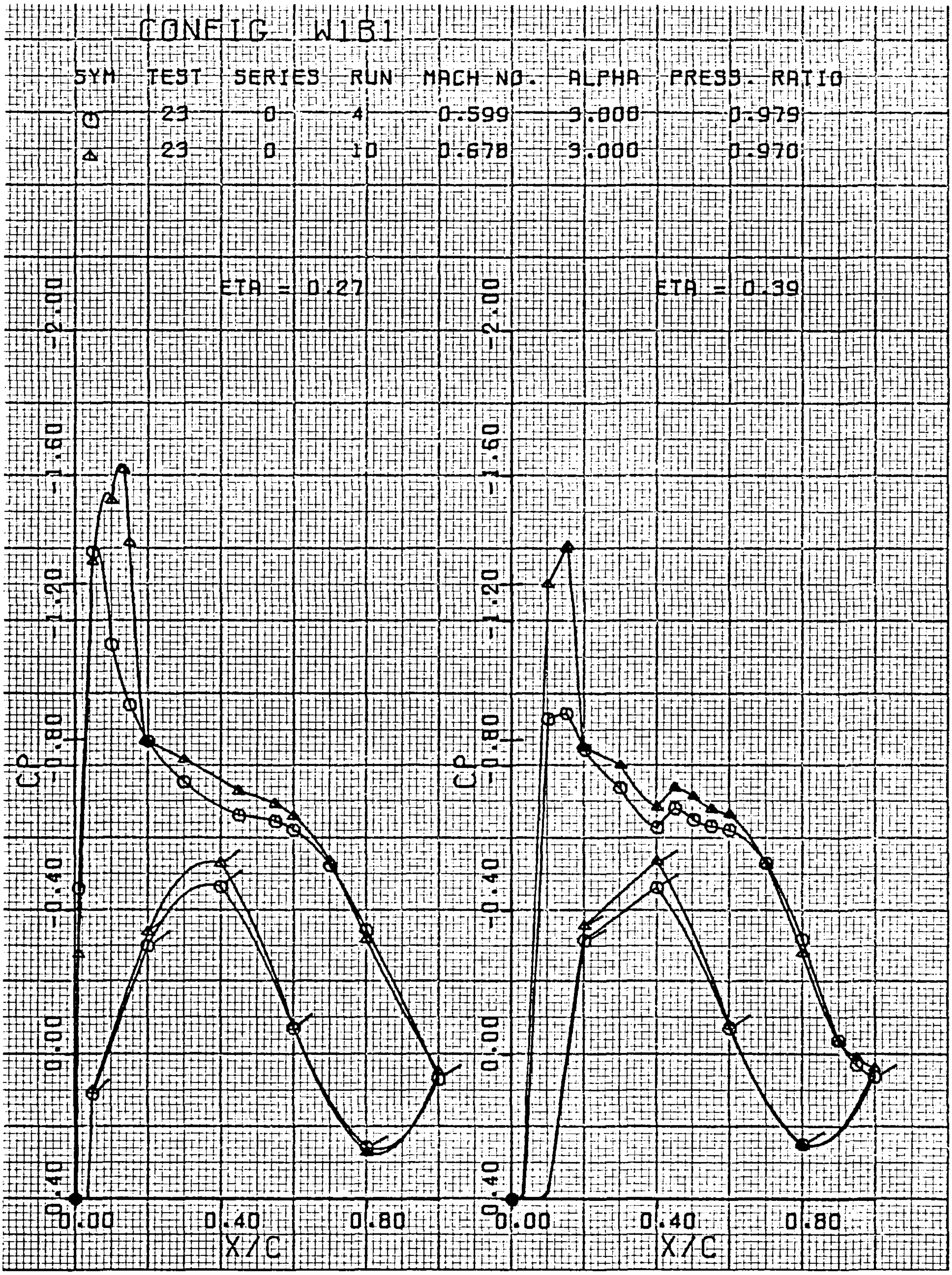

Figure 45. Clean, straight wing pressure distribution, effect of Mach number, η = 0.27, 0.39

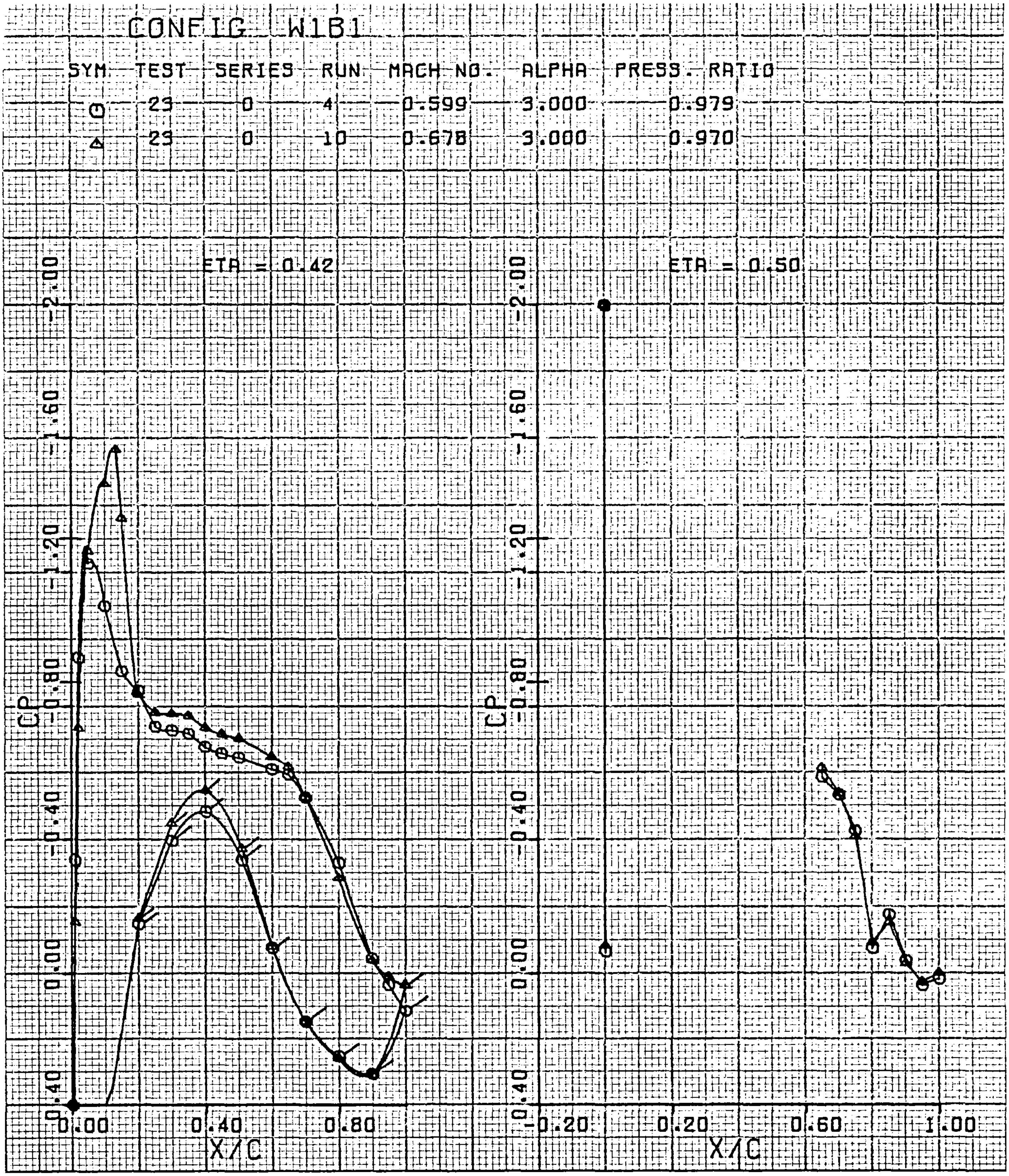

Figure 46. Clean, straight wing pressure distribution, effect of Mach number, η = 0.42, 0.50

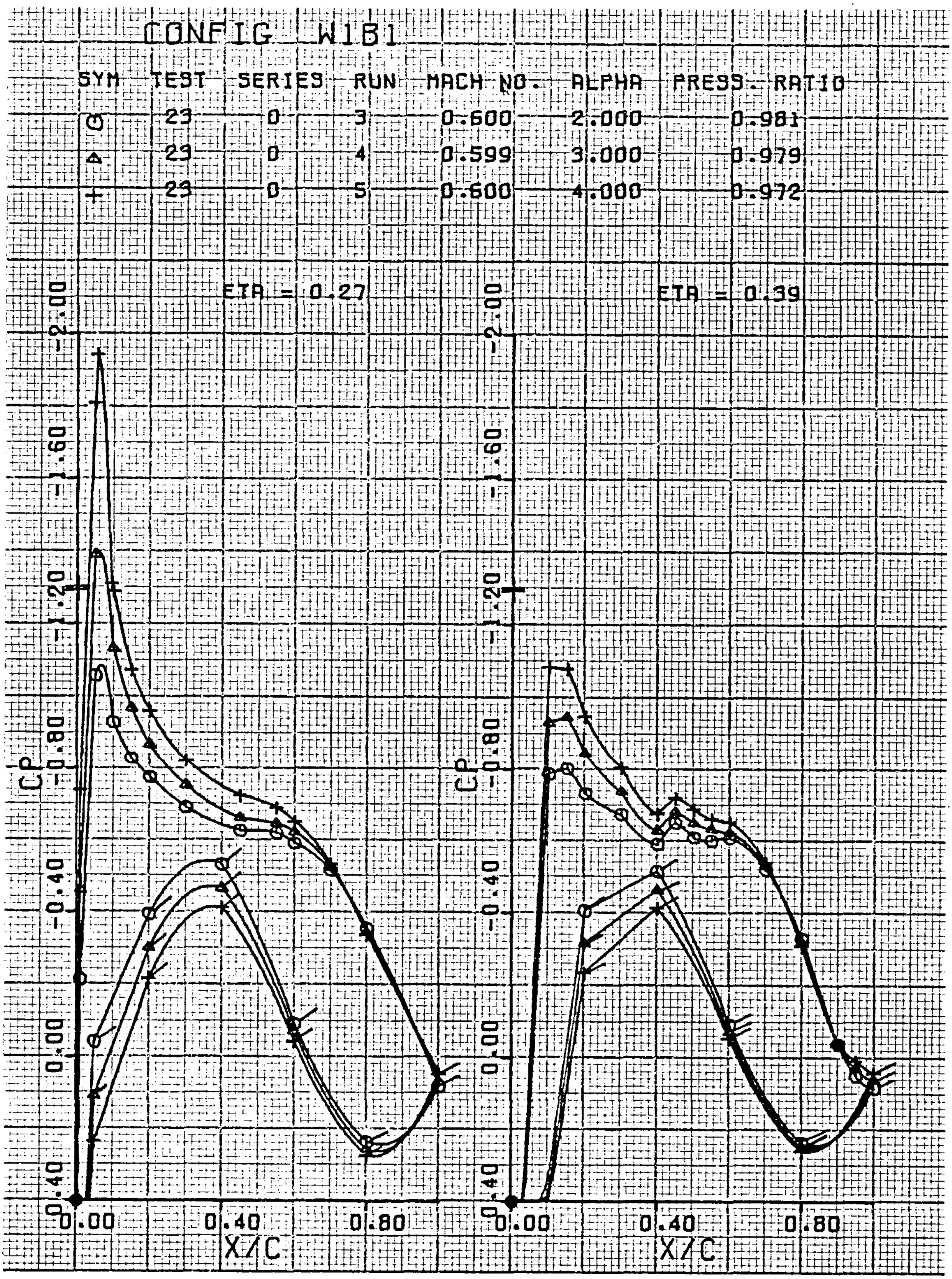

Figure 47. Clean, straight wing pressure distribution, effect of α, $M_\infty = 0.60$, $\eta = 0.27, 0.39$

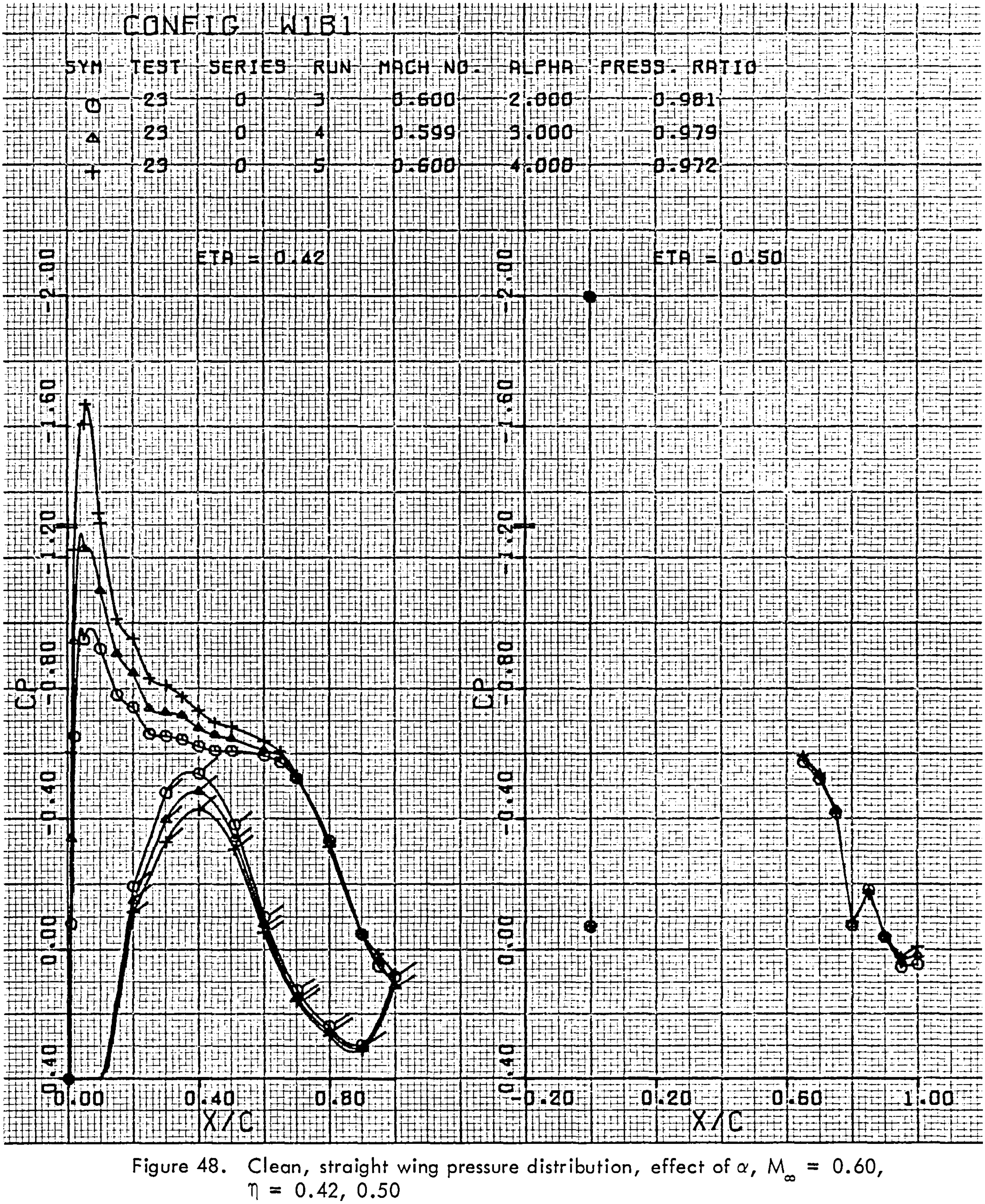

Figure 48. Clean, straight wing pressure distribution, effect of α, M_∞ = 0.60, η = 0.42, 0.50

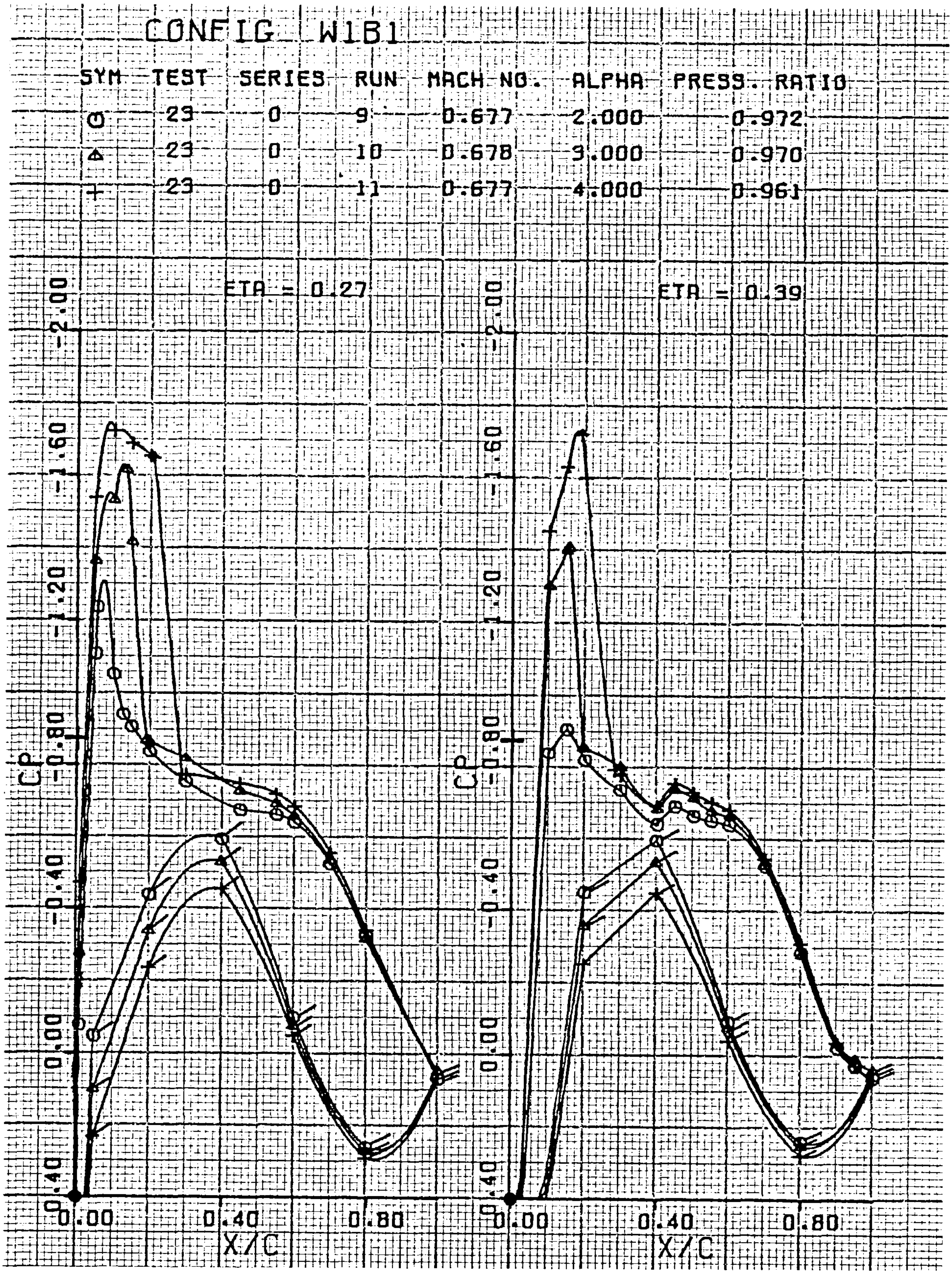

Figure 49. Clean, straight wing pressure distribution, effect of α, $M_\infty = 0.68$, $\eta = 0.27, 0.39$

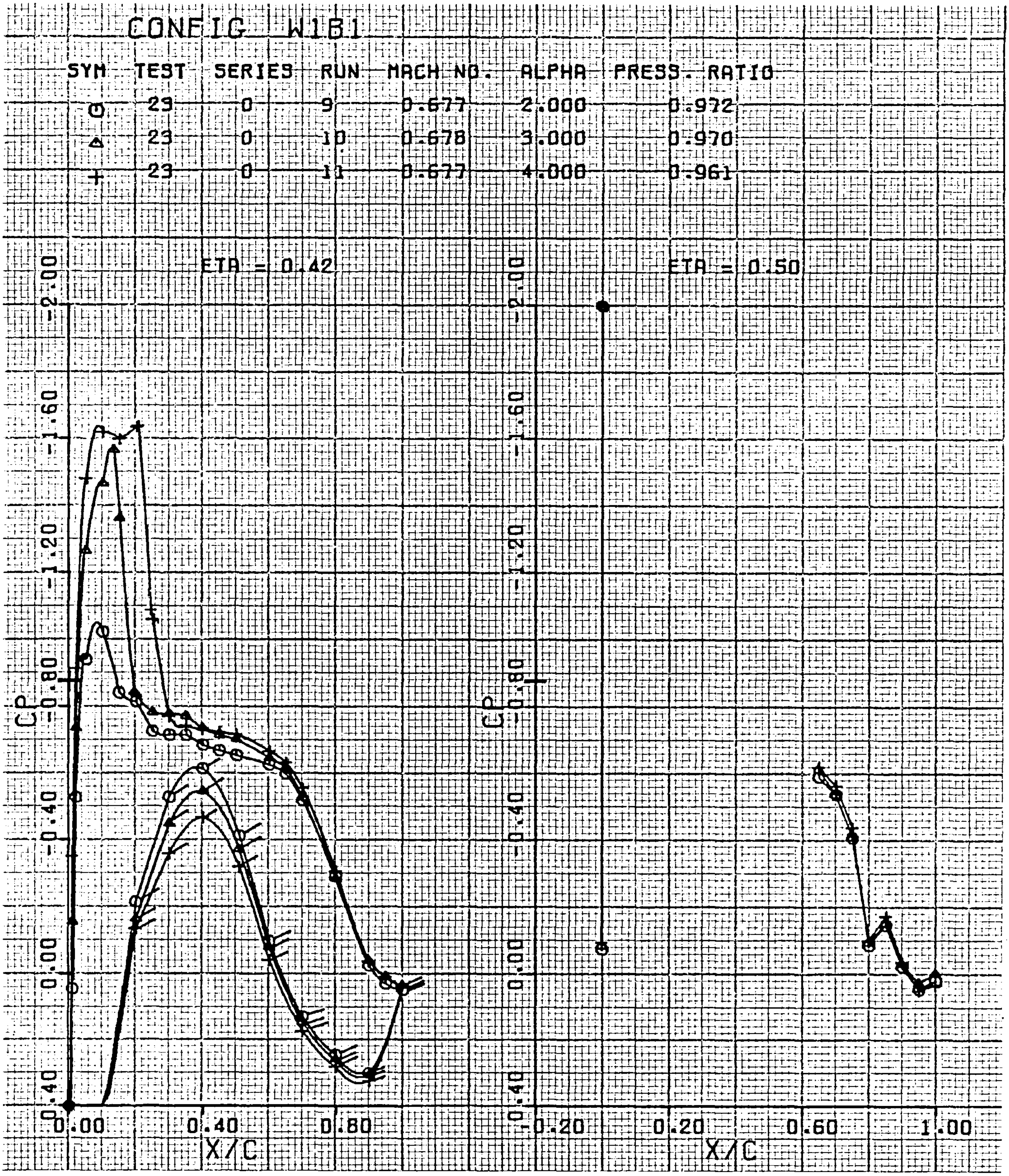

Figure 50. Clean, straight wing pressure distribution, effect of α, $M_\infty = 0.68$, $\eta = 0.42, 0.50$

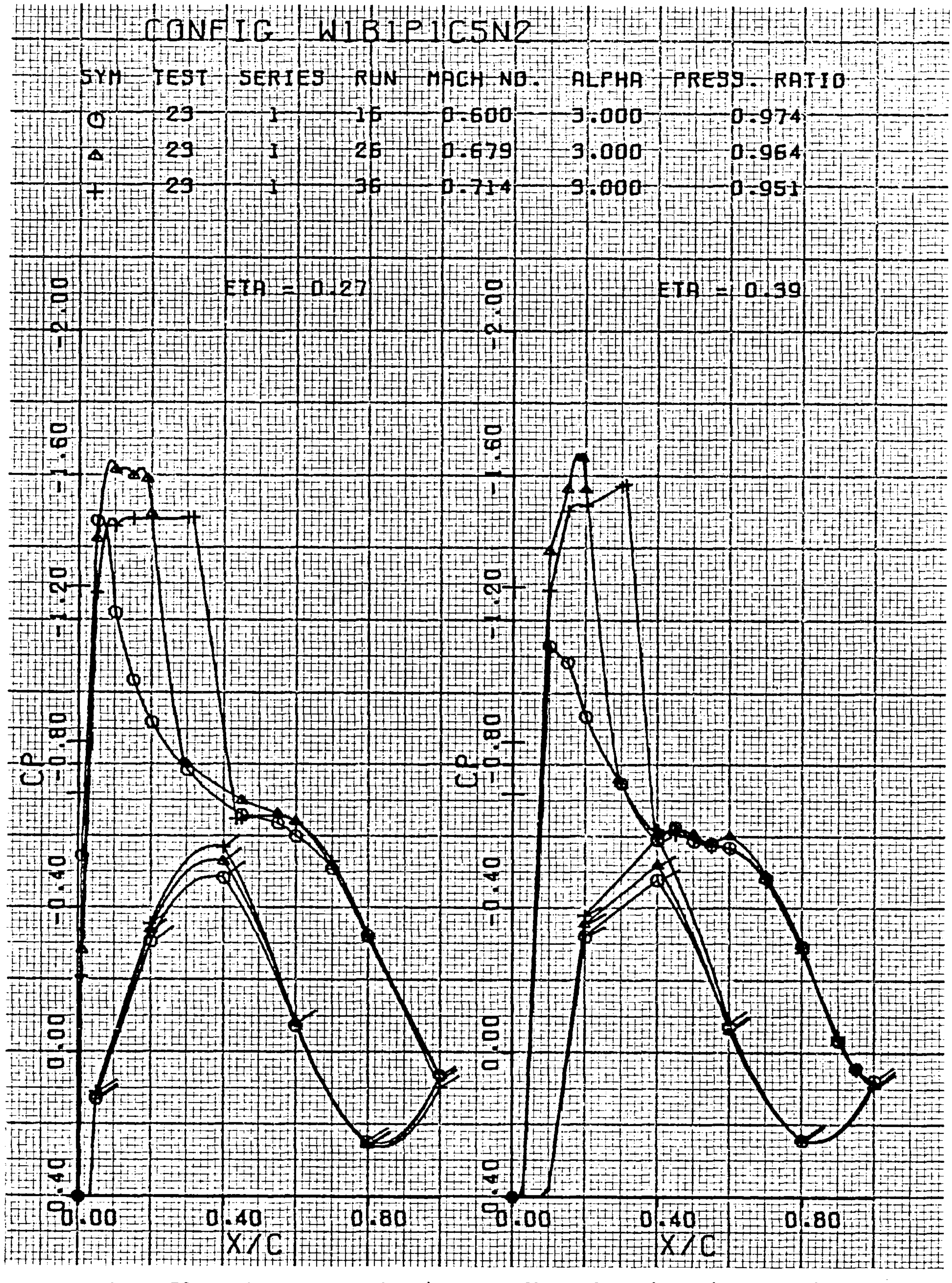

Figure 51. Wing pressure distribution, effect of Mach number, nozzle N_2, η = 0.27, 0.39

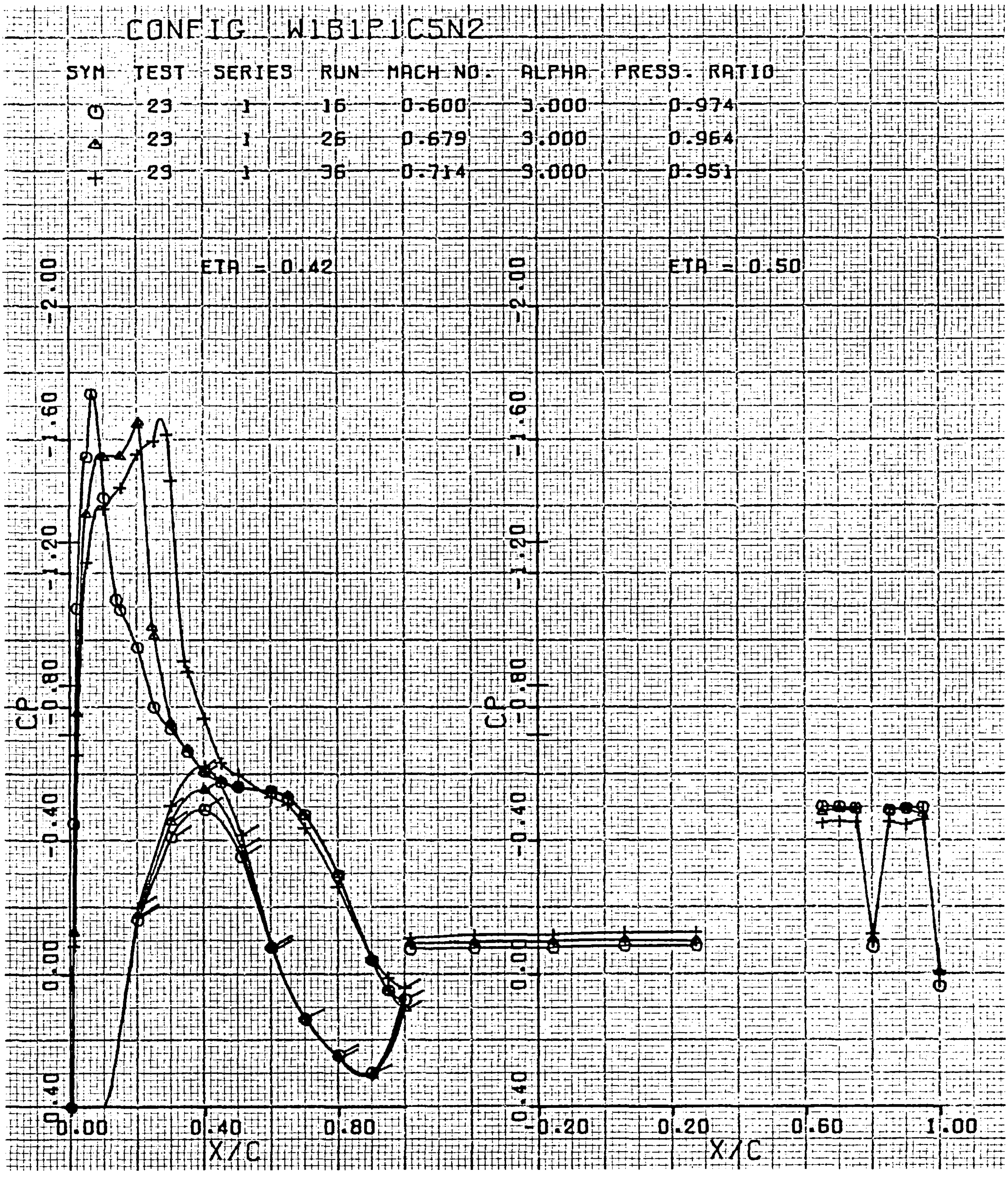

Figure 52. Wing pressure distribution, effect of Mach number, nozzle N_2, η = 0.42, 0.50

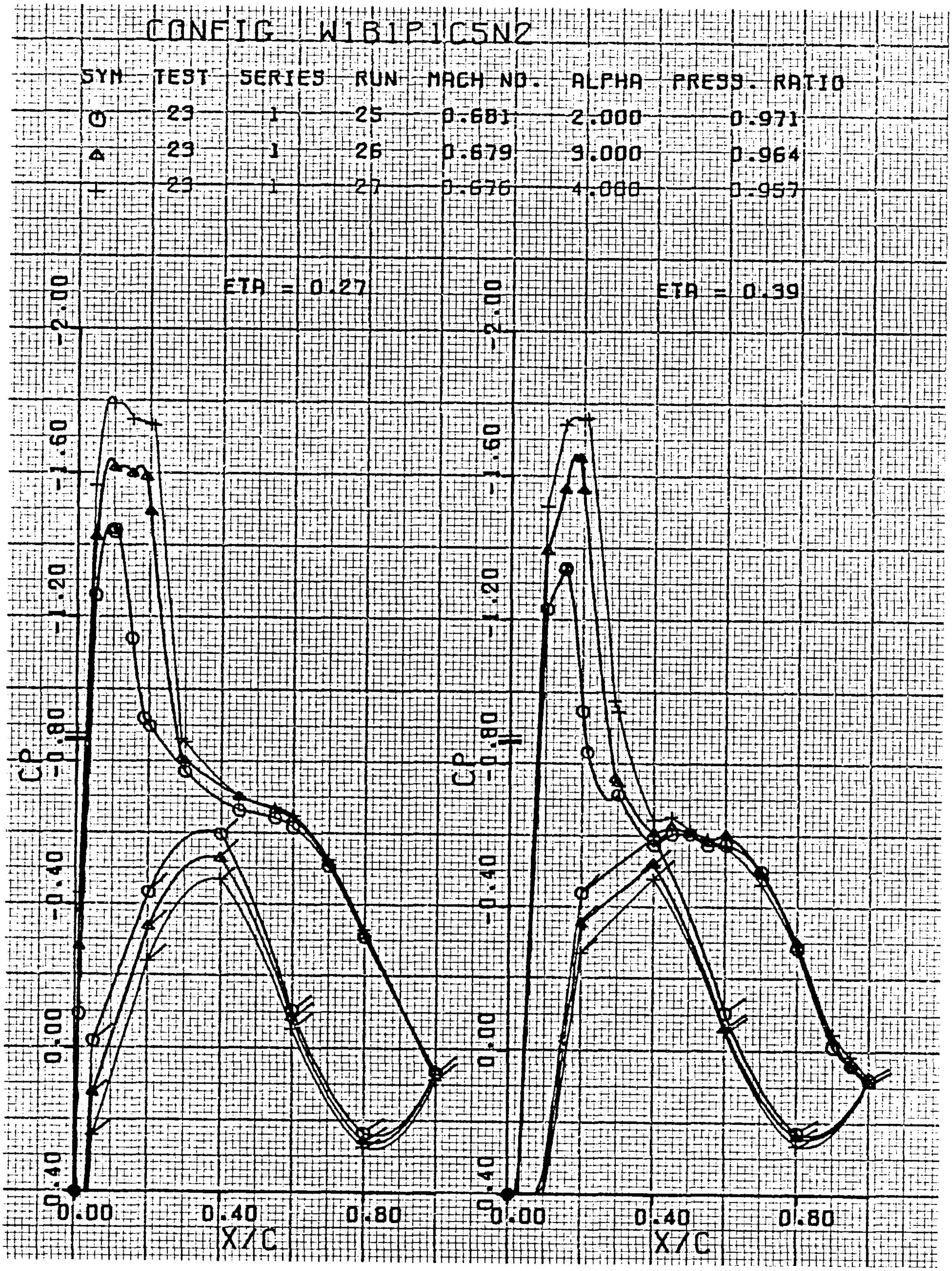

Figure 53. Wing pressure distribution, effect of α, nozzle N_2, η = 0.27, 0.39

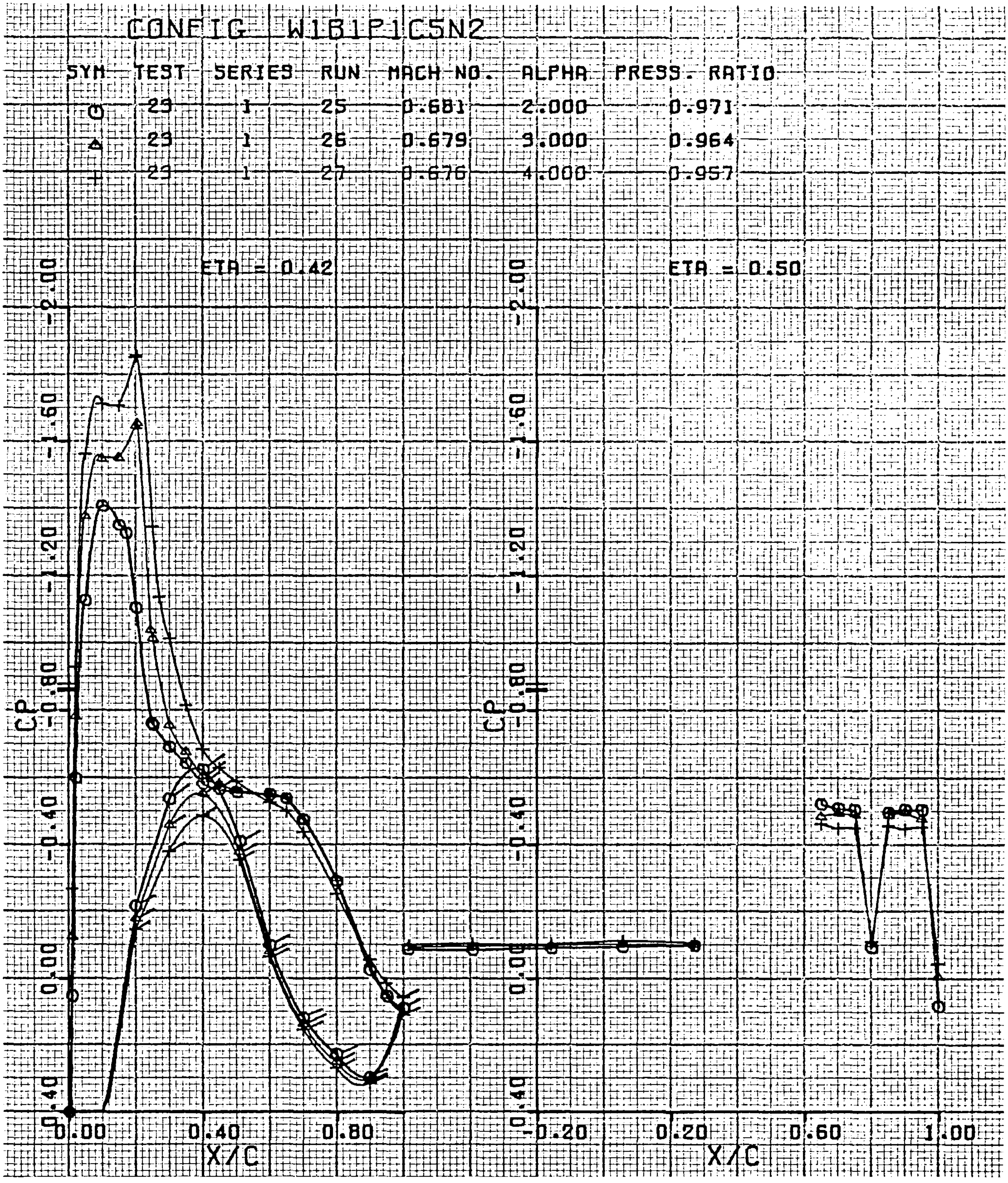

Figure 54. Wing pressure distribution, effect of α, nozzle N_2, η = 0.42, 0.50

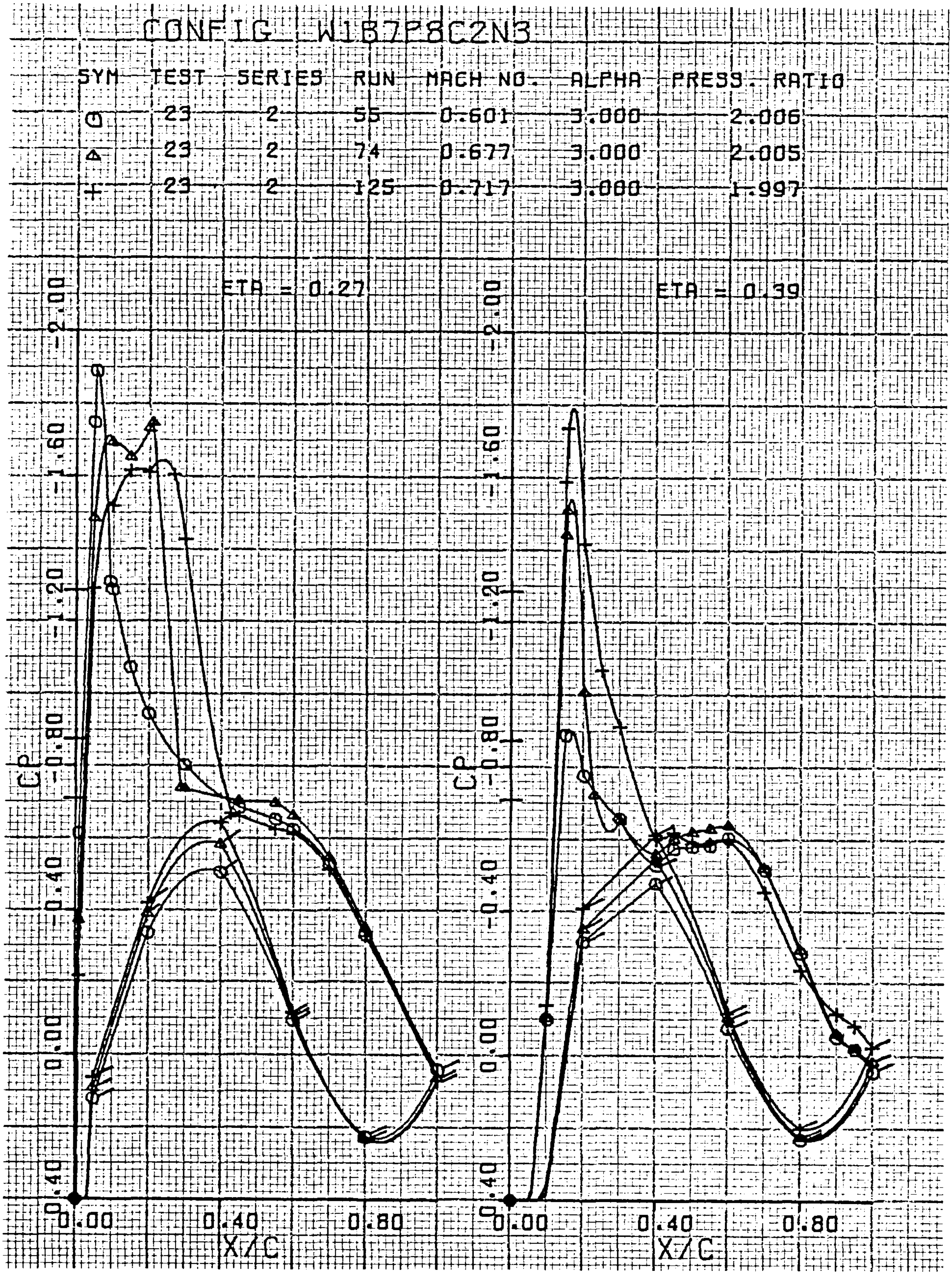

Figure 55. Wing pressure distribution, effect of Mach number, nozzle N_3, $\eta = 0.27, 0.39$

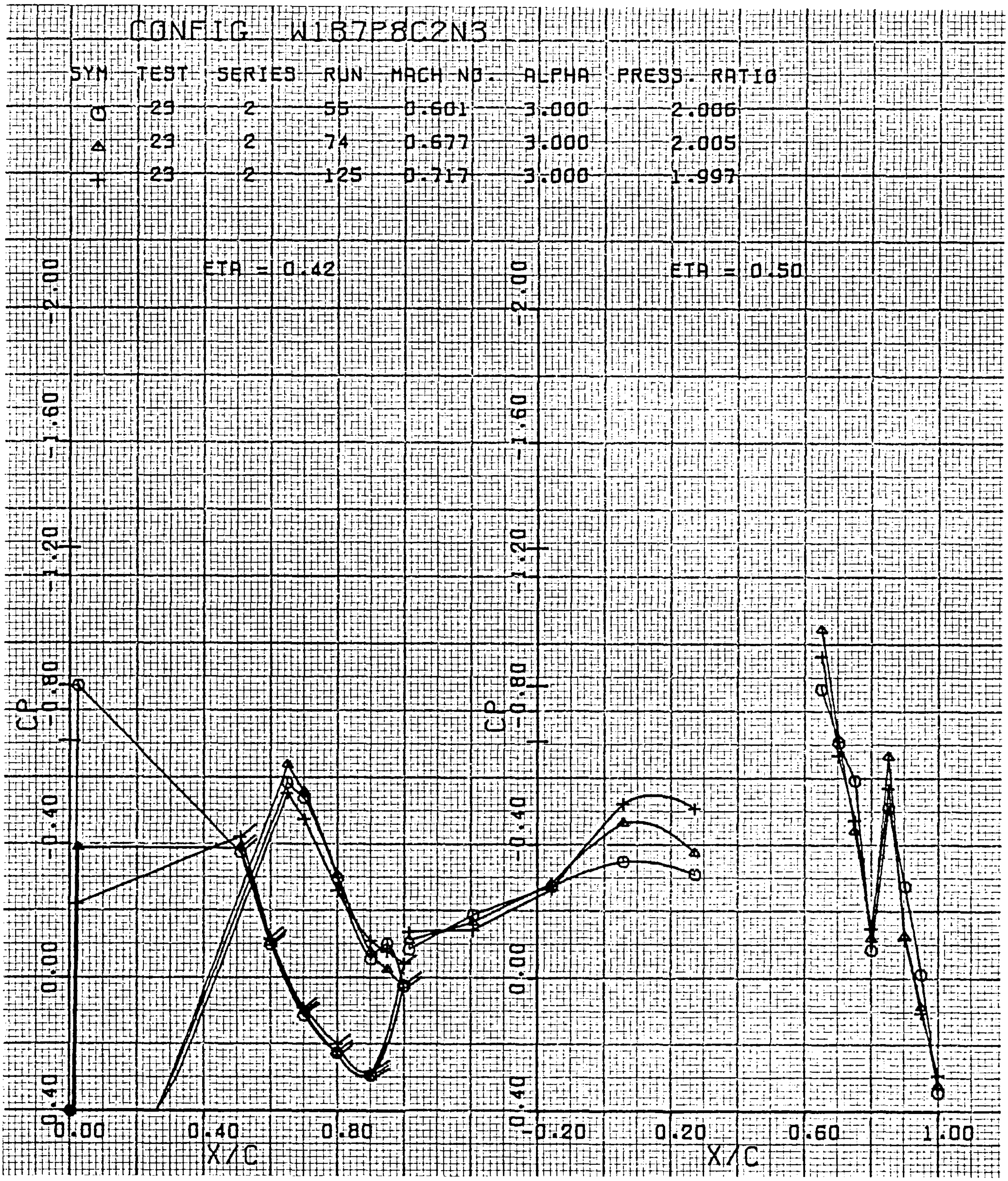

Figure 56. Wing pressure distribution, effect of Mach number, nozzle N_3, $\eta = 0.42, 0.50$

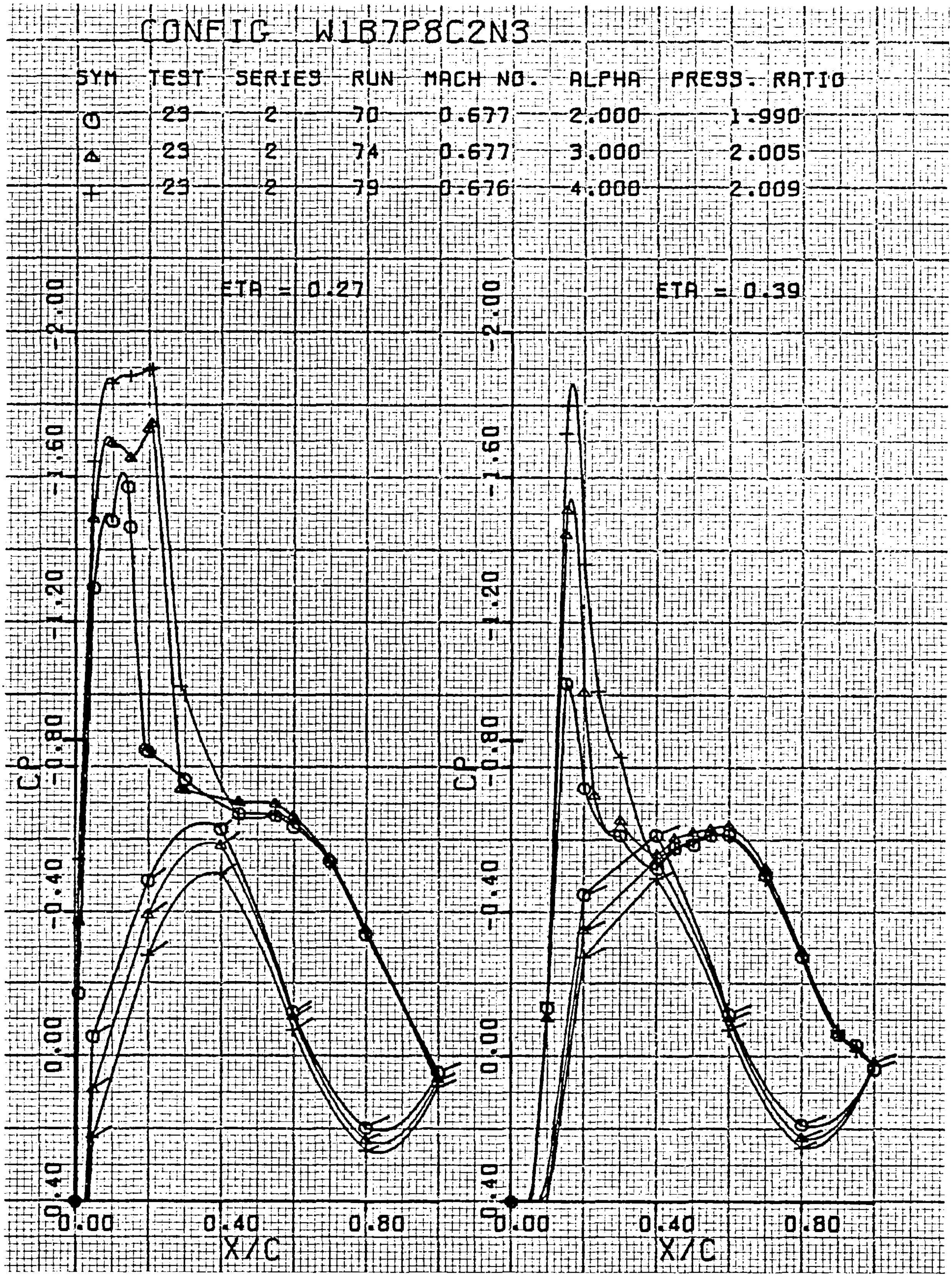

Figure 57. Wing pressure distribution, effect of α, nozzle N_3, η = 0.27, 0.39

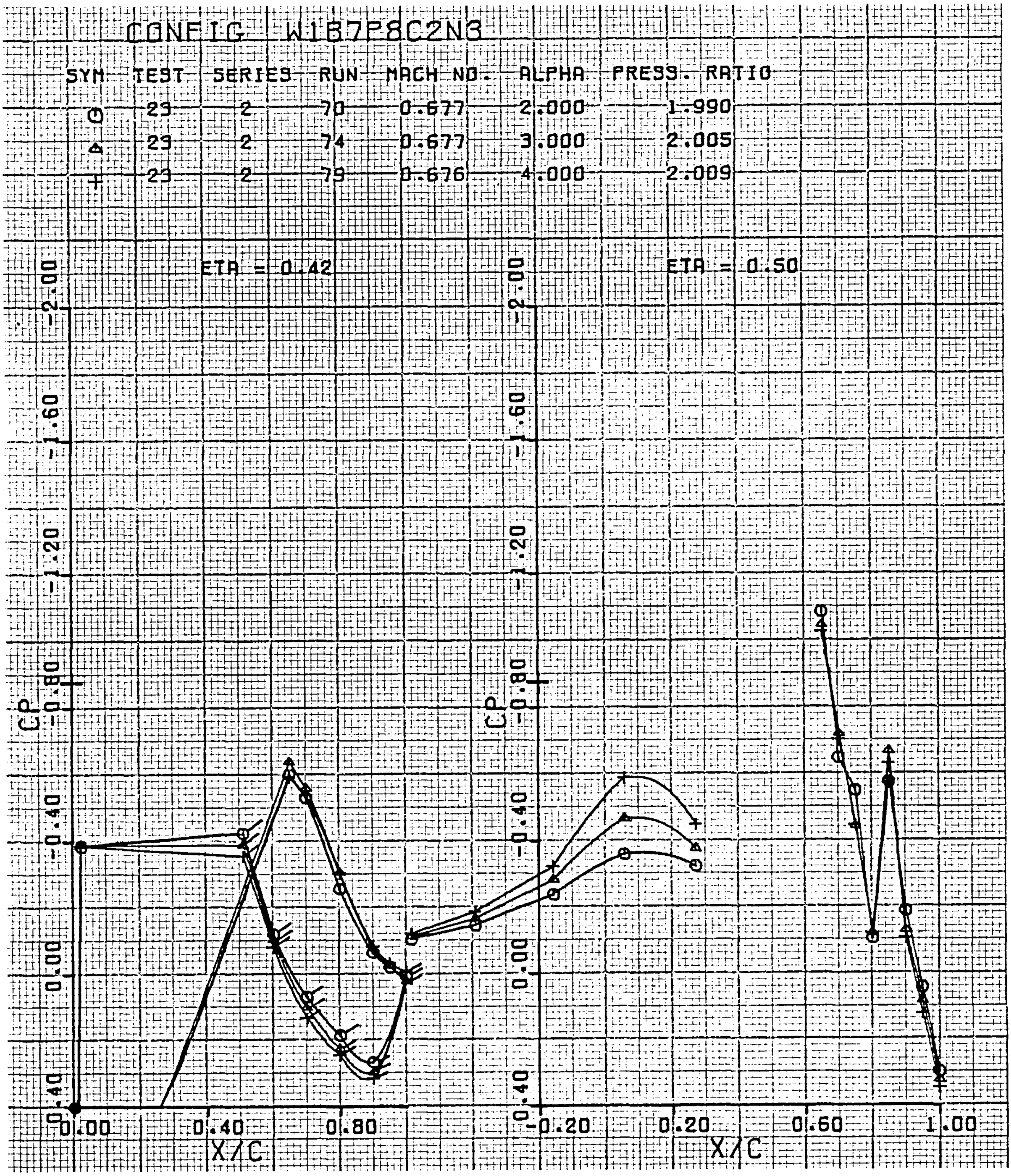

Figure 58. Wing pressure distribution, effect of α, nozzle N_3, $\eta = 0.42,\ 0.50$

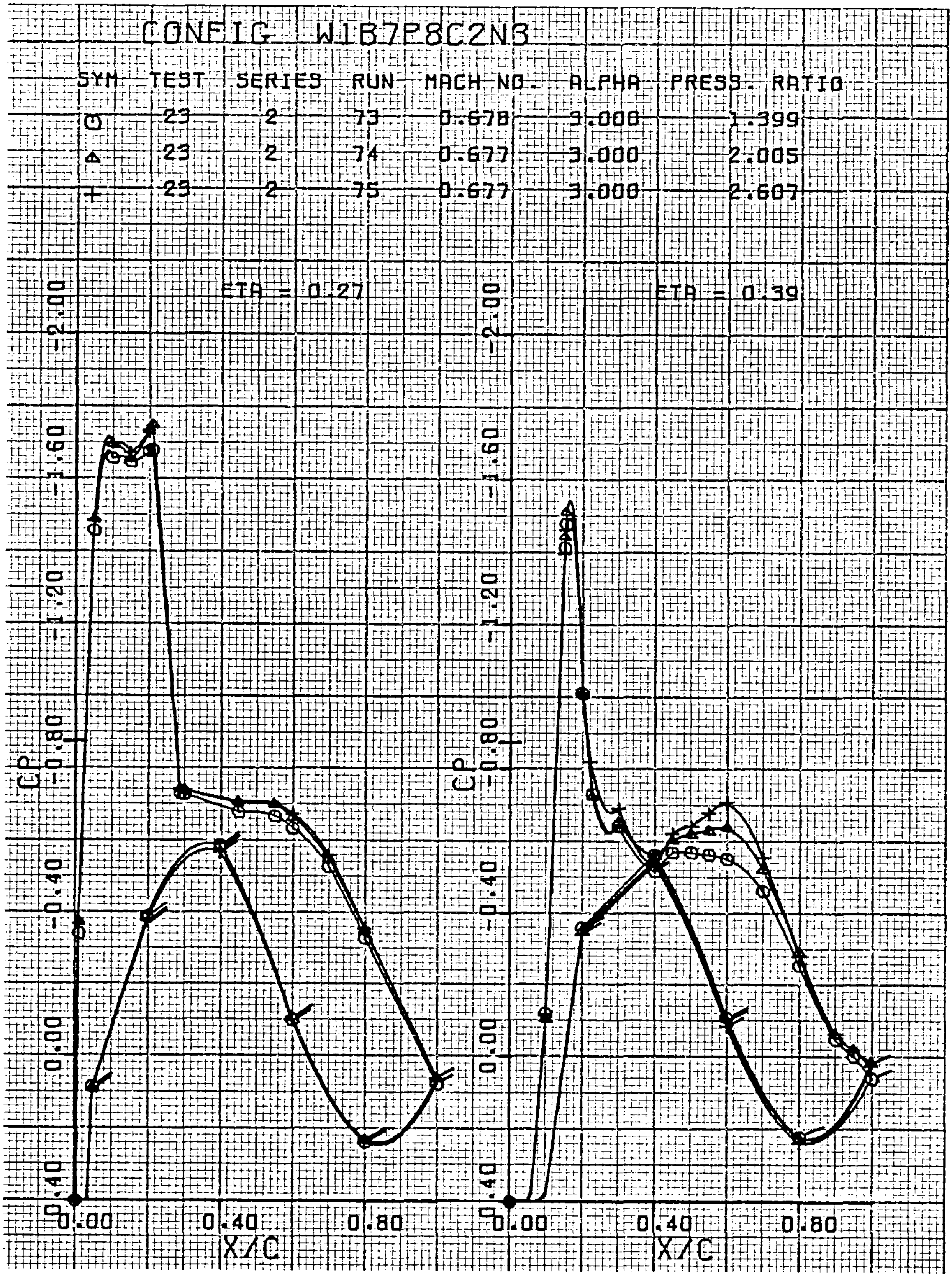

Figure 59. Wing pressure distribution, effect of nozzle pressure ratio, nozzle N_3, η = 0.27, 0.39

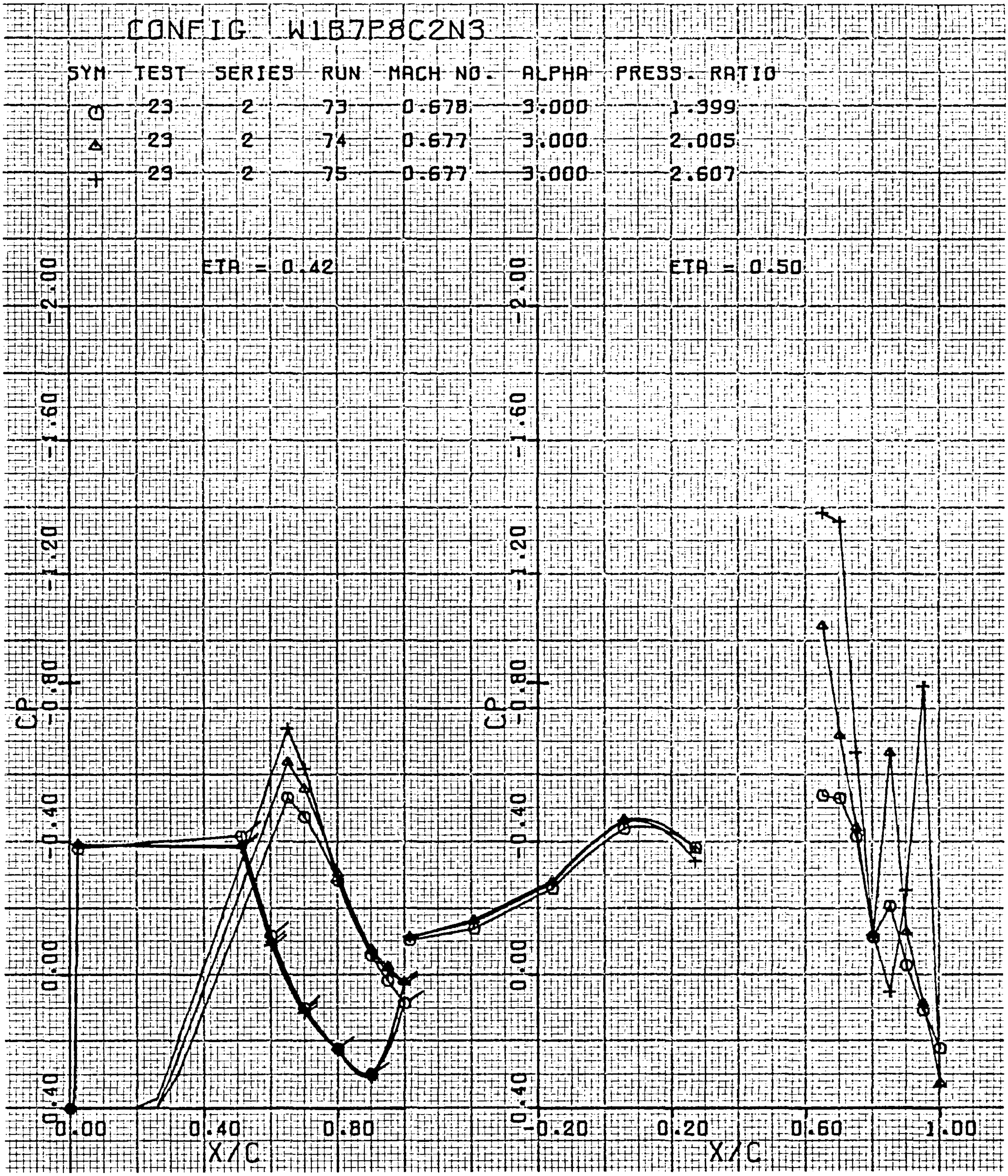

Figure 60. Wing pressure distribution, effect of nozzle pressure ratio, nozzle N_3, η = 0.42, 0.50

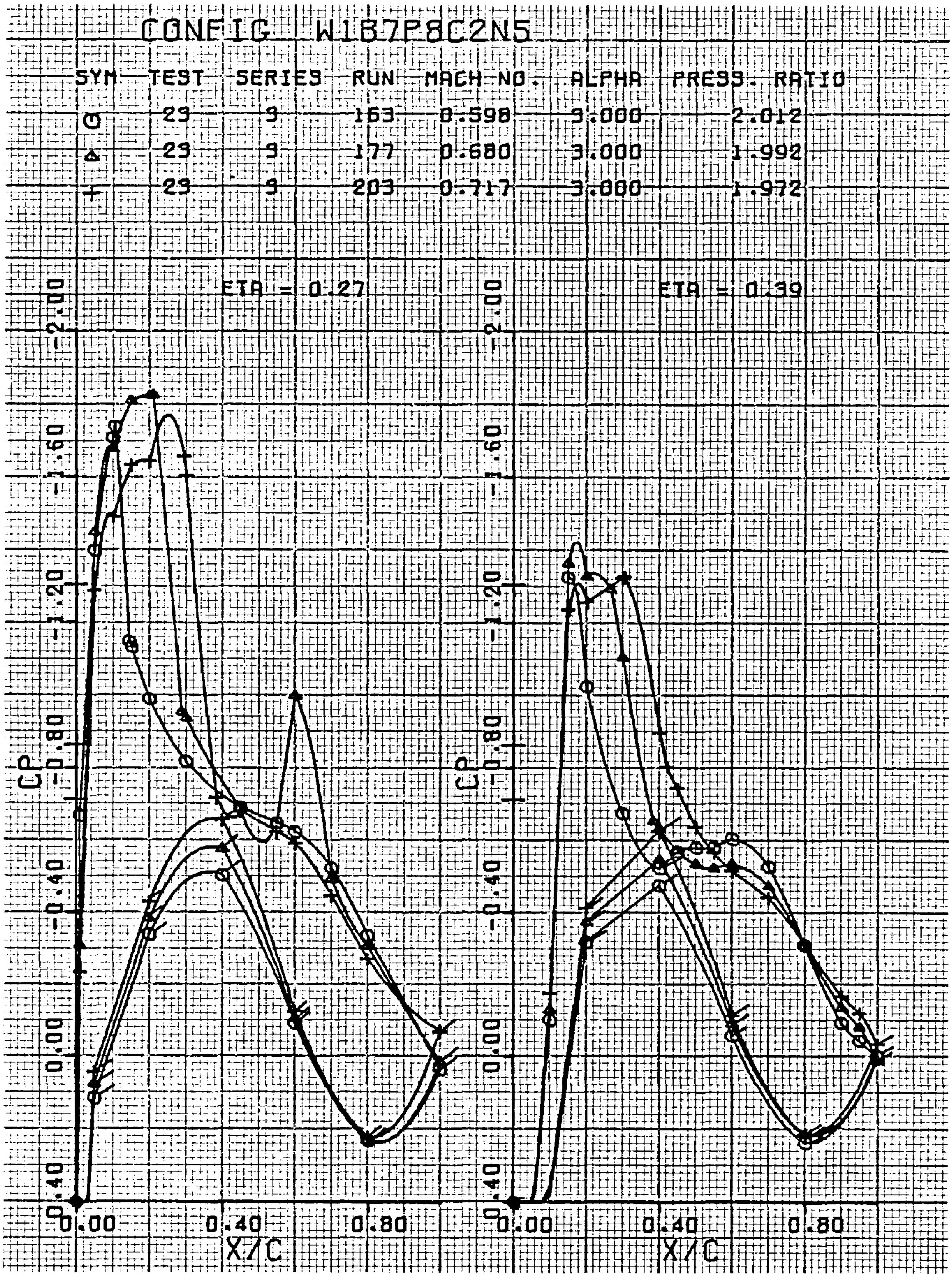

Figure 61. Wing pressure distribution, effect of Mach number, nozzle N_5, η = 0.27, 0.39

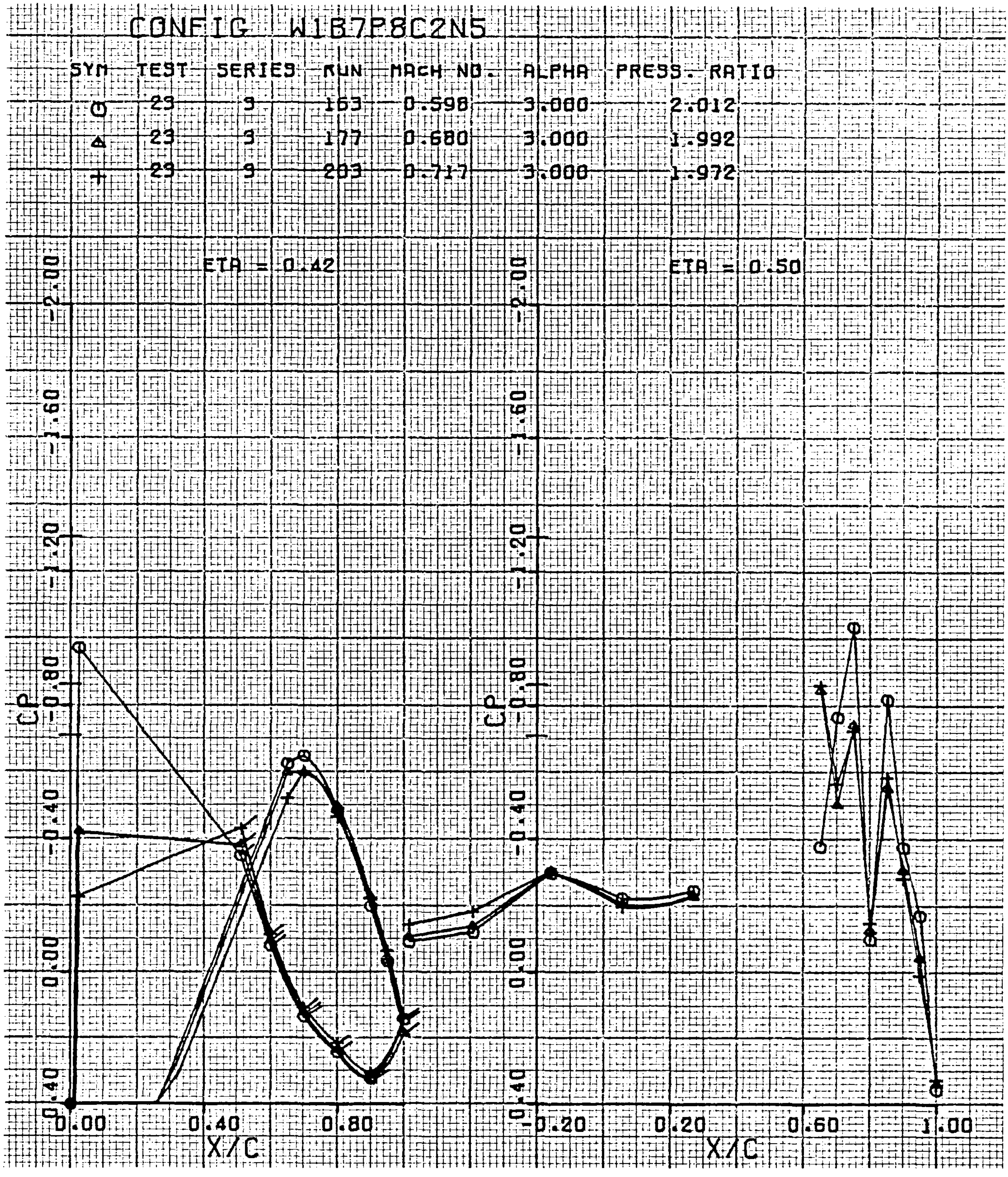

Figure 62. Wing pressure distribution, effect of Mach number, nozzle N_5, η = 0.42, 0.50

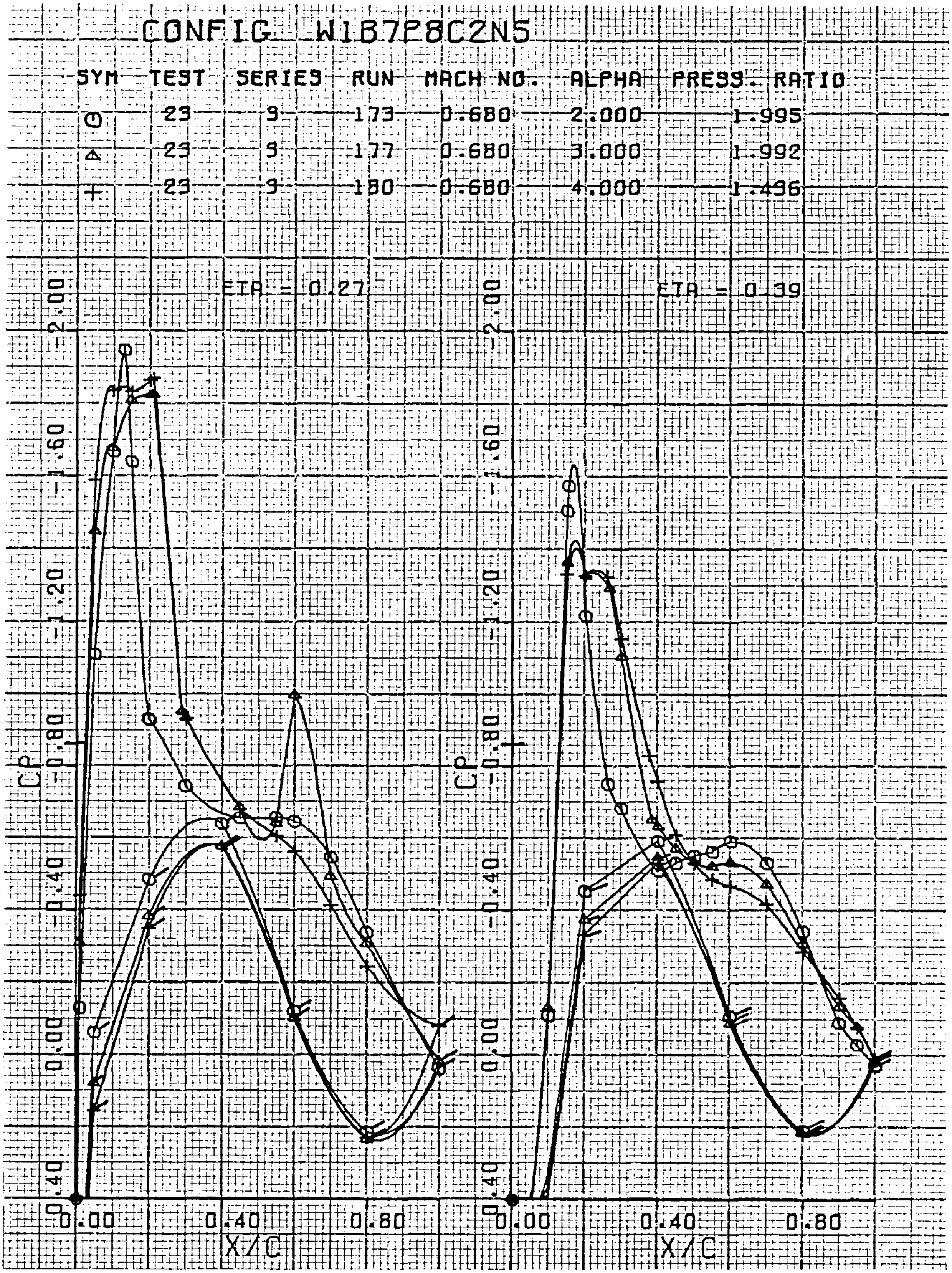

Figure 63. Wing pressure distribution, effect of α, nozzle N_5, η = 0.27, 0.39

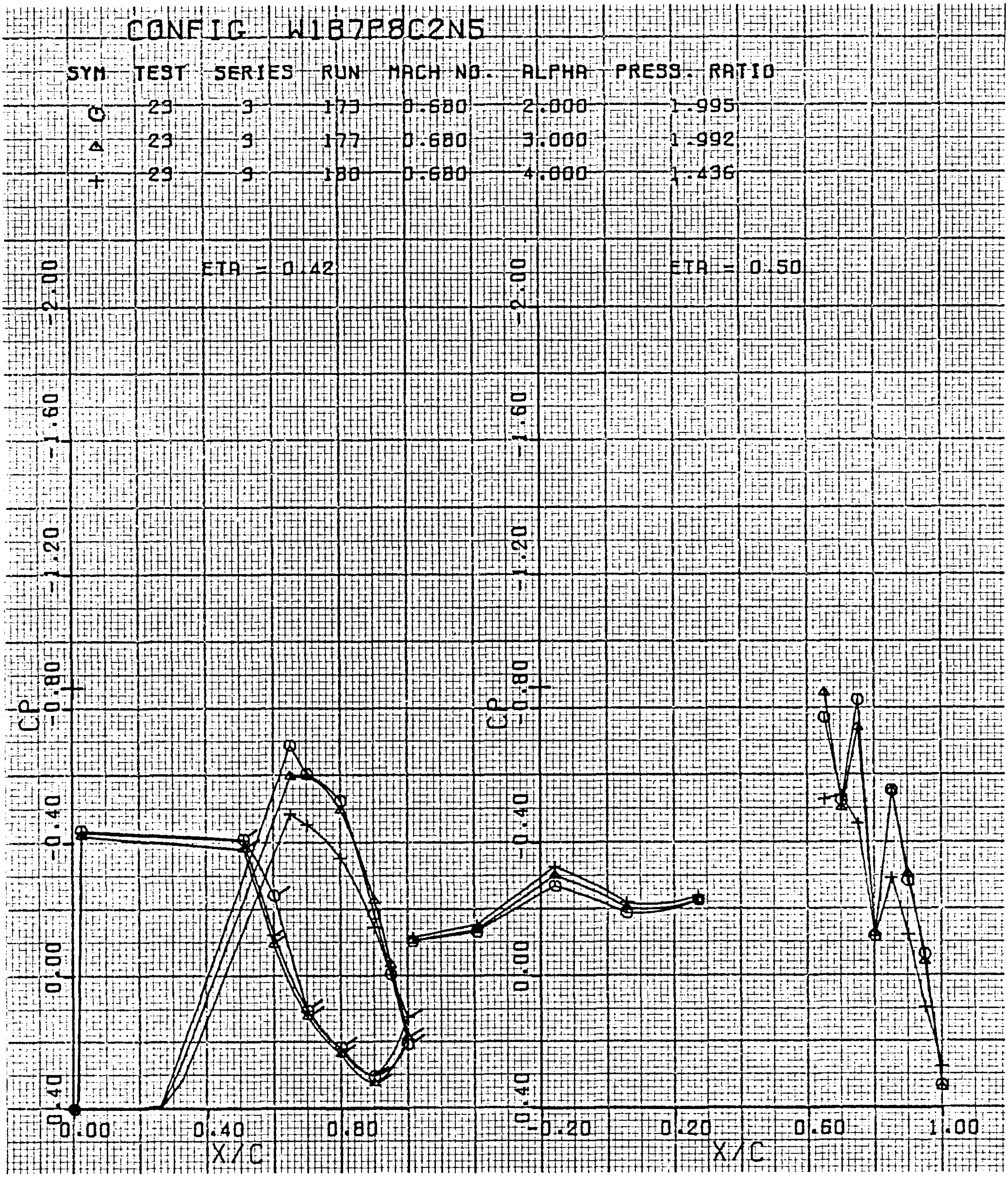

Figure 64. Wing pressure distribution, effect of α, nozzle N_5, η = 0.42, 0.50

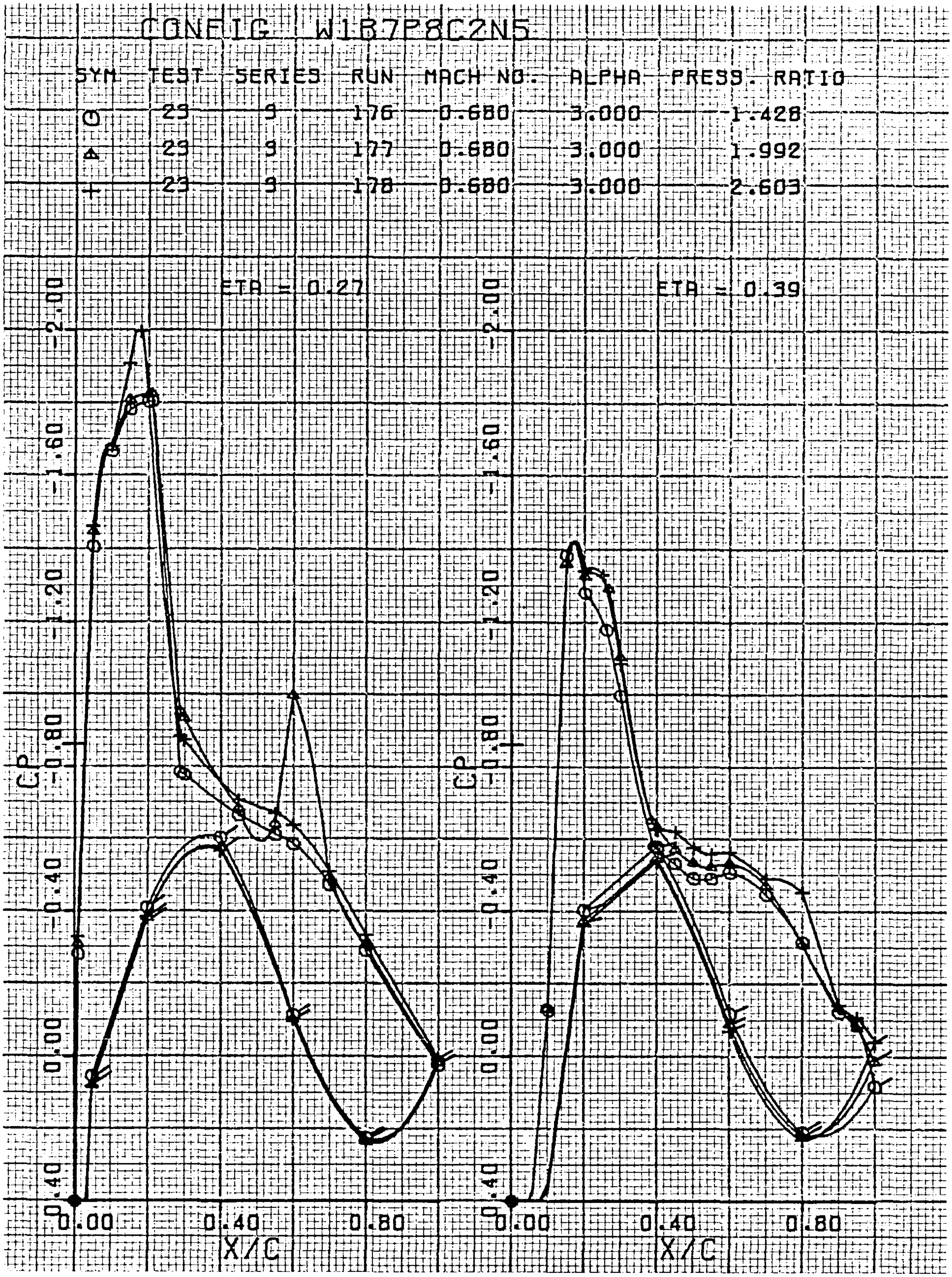

Figure 65. Wing pressure distribution, effect of nozzle pressure ratio, nozzle N_5, $\eta = 0.27, 0.39$

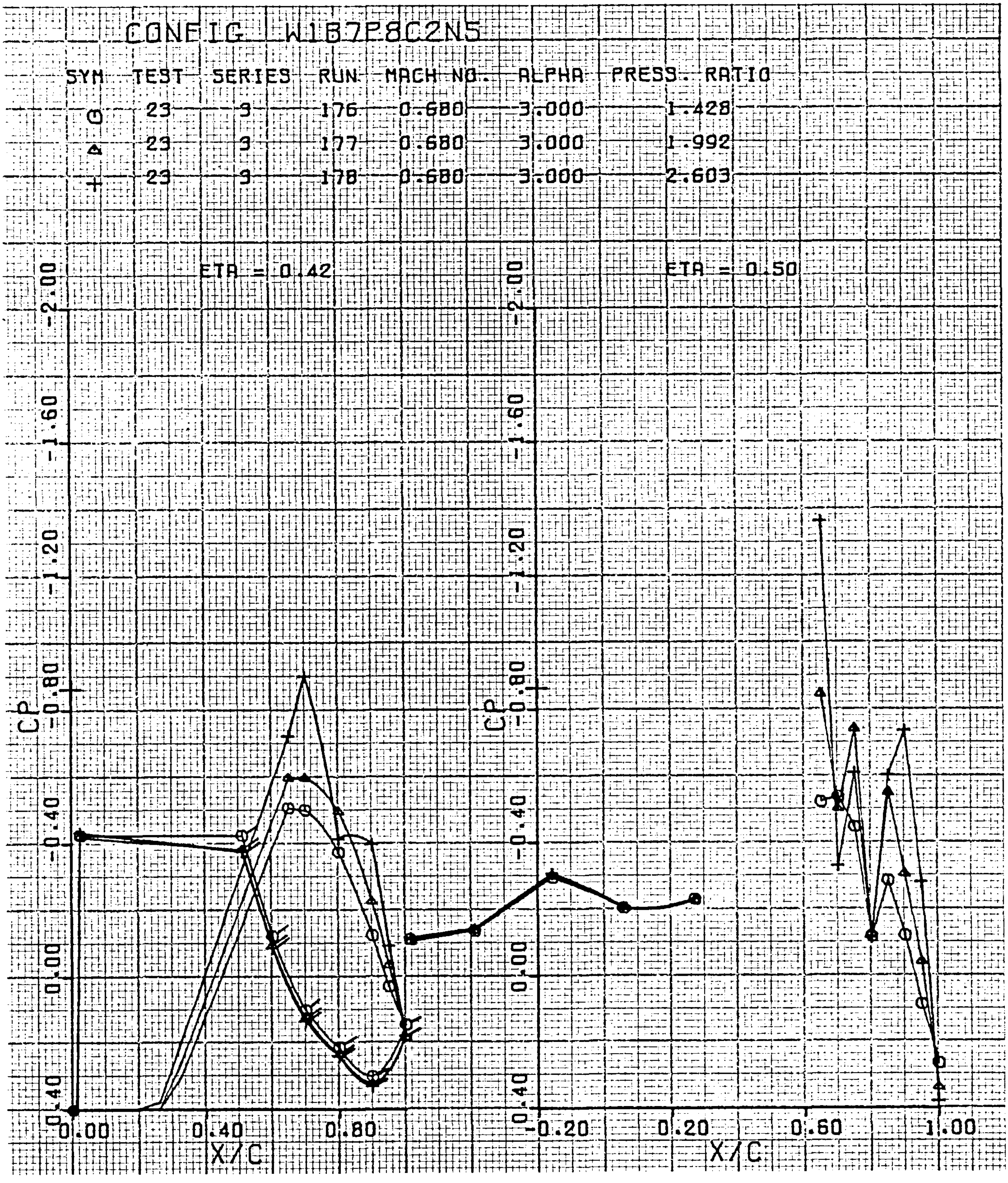

Figure 66. Wing pressure distribution, effect of nozzle pressure ratio, nozzle N_5, η = 0.42, 0.50

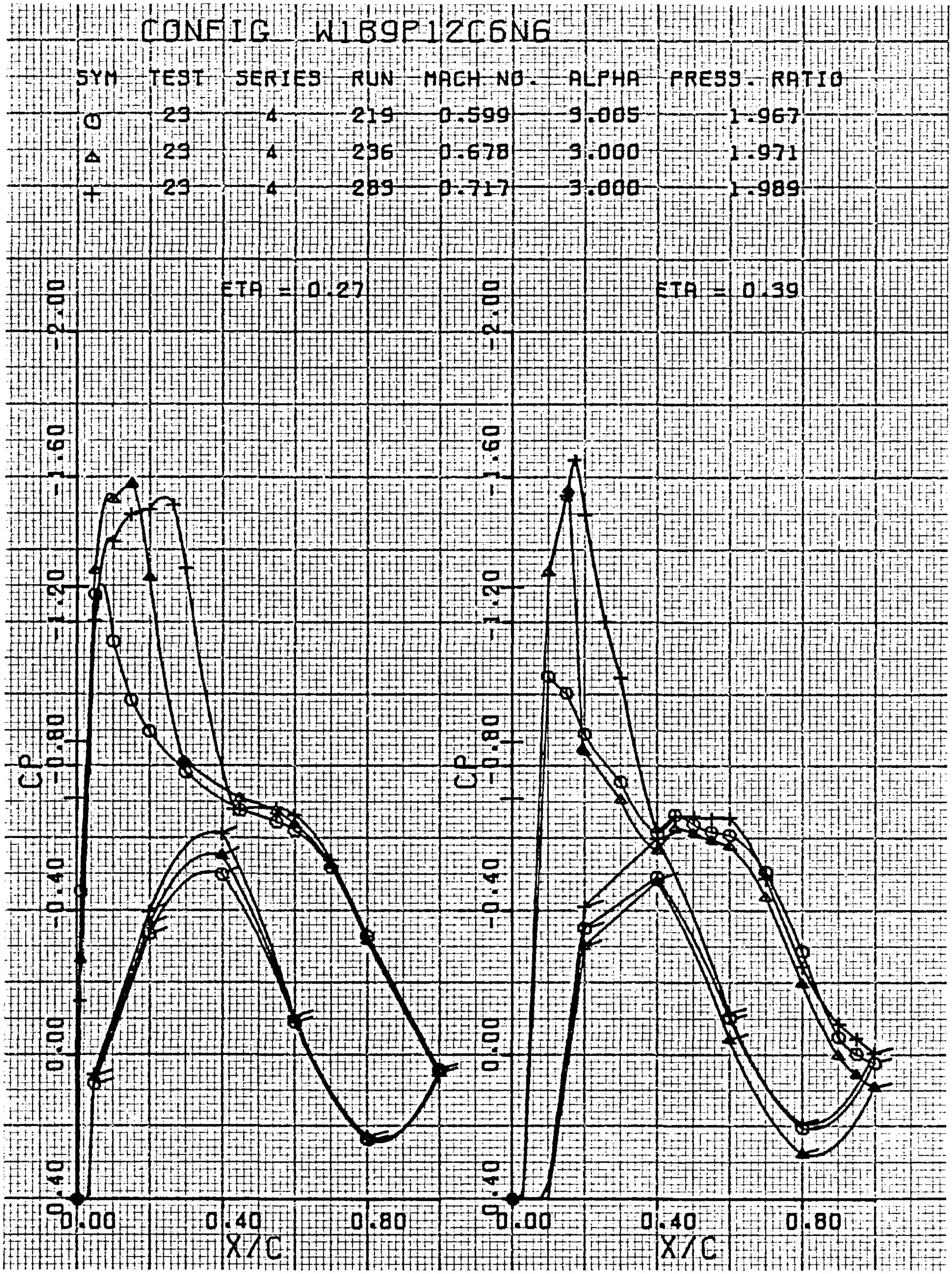

Figure 67. Wing pressure distribution, effect of Mach number, nozzle N_6, η = 0.27, 0.39

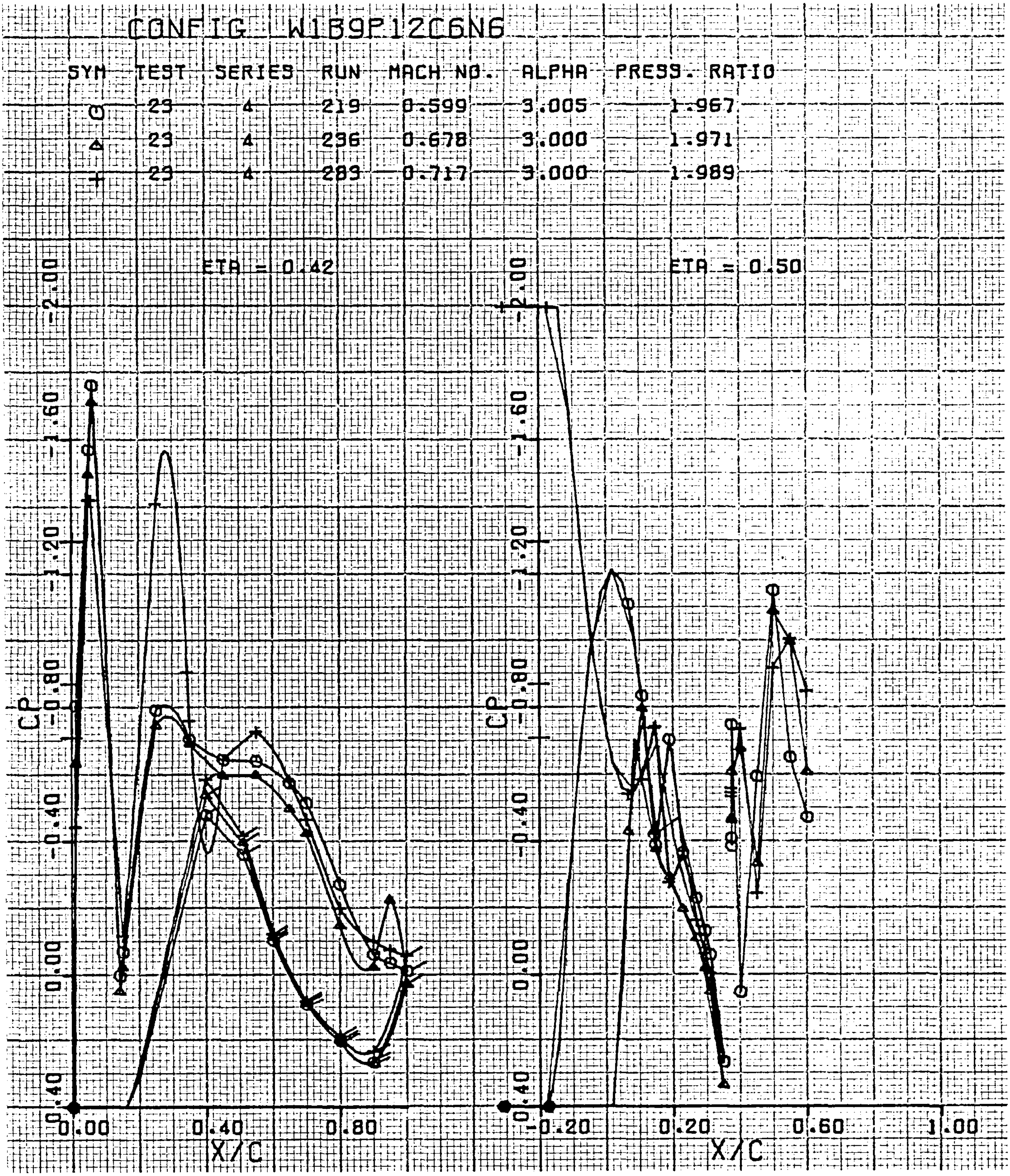

Figure 68. Wing pressure distribution, effect of Mach number, nozzle N_6, η = 0.42, 0.50

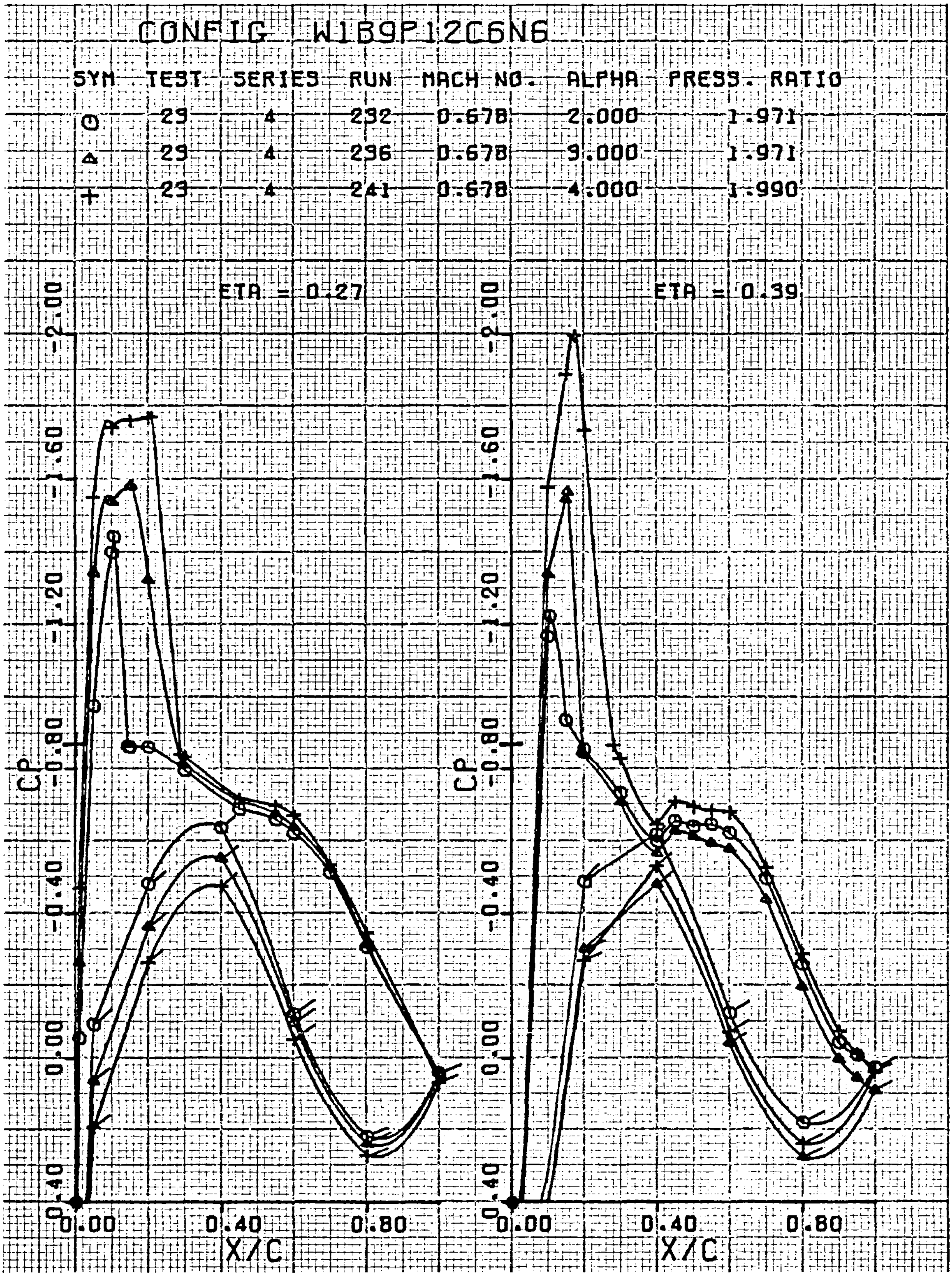

Figure 69. Wing pressure distribution, effect of α, nozzle N_6, η = 0.27, 0.39

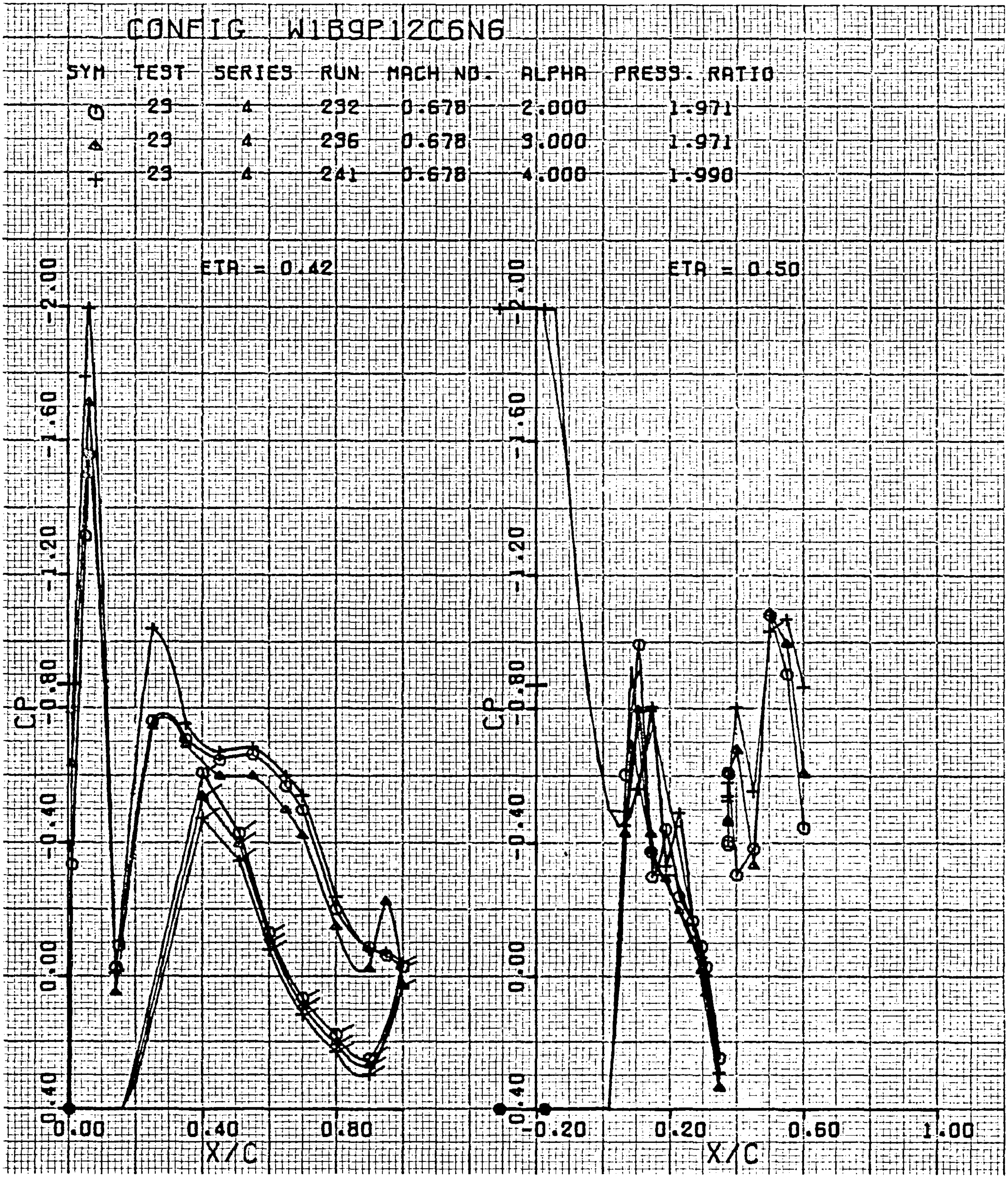

Figure 70. Wing pressure distribution, effect of α, nozzle N_6, η = 0.42, 0.50

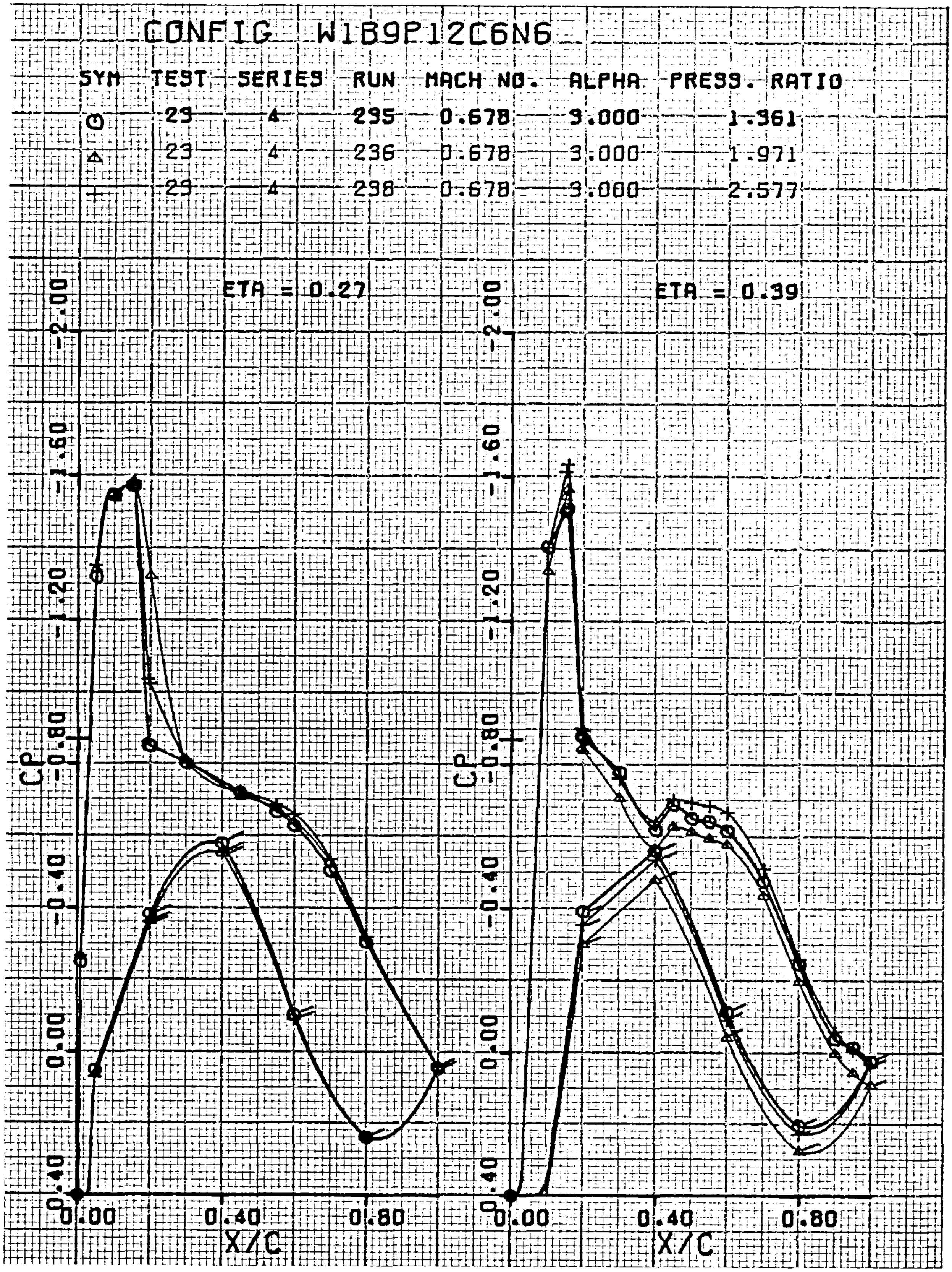

Figure 71. Wing pressure distribution, effect of nozzle pressure ratio, nozzle N_6, η = 0.27, 0.39

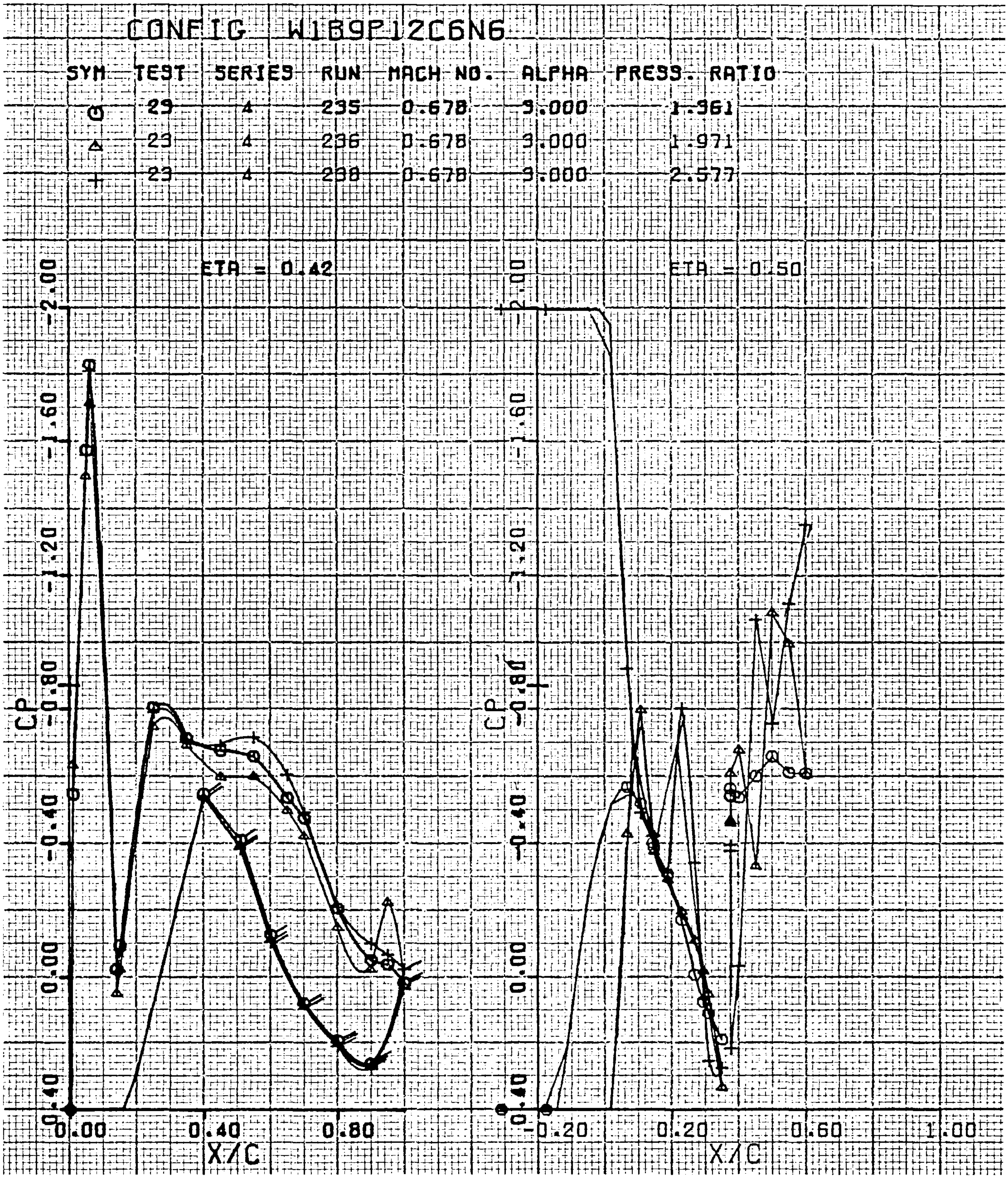

Figure 72. Wing pressure distribution, effect of nozzle pressure ratio, nozzle N_6, η = 0.42, 0.50

5.3 Model Pressure Distributions, Upstream Pipe Installation

Pressure distributions for models tested on the upstream pipe installation are presented in Figures 73 through 104. Presentation format is identical to that used for the long nozzle series. Reasons for use of the upstream pipe arrangement were two-fold. First, it was desired to test over-the-wing nacelles mounted on thin pylons across the complete range of nozzle pressure ratios. Nozzles on these configurations could not be supplied through the wing in the usual manner. Then, second, it was desired to vary the chordwise nozzle discharge position. The upstream pipe in conjunction with various combinations of nacelle spacers and wing mounting pads provided the flexibility required to accomplish this objective.

The first group of data in this section is for a circular nozzle, N_2, mounted on a pylon. This is followed by data for the intermediate D-duct nozzle, N_3, at chordwise positions (x/c noted at top of figures) of 0.35, 0.50, and 0.20. In the last group for this series, data is presented for the large D-duct nozzle, N_1, at the same chordwise positions as for N_3. All data in this series are presented at a Reynold's number of 3.5 million based on wing chord.

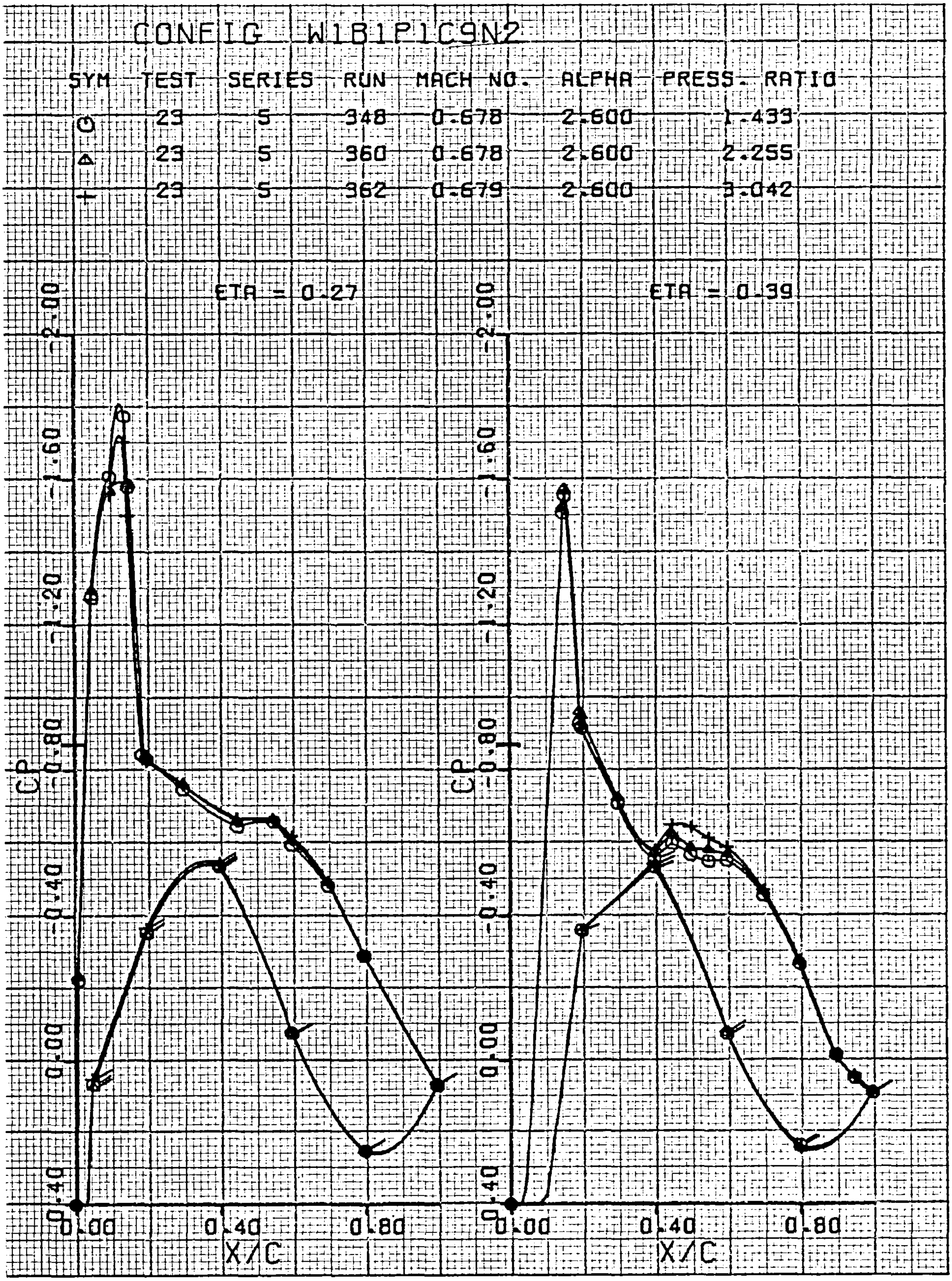

Figure 73. Wing pressure distribution, effect of nozzle pressure ratio, nozzle N_2, η = 0.27, 0.39

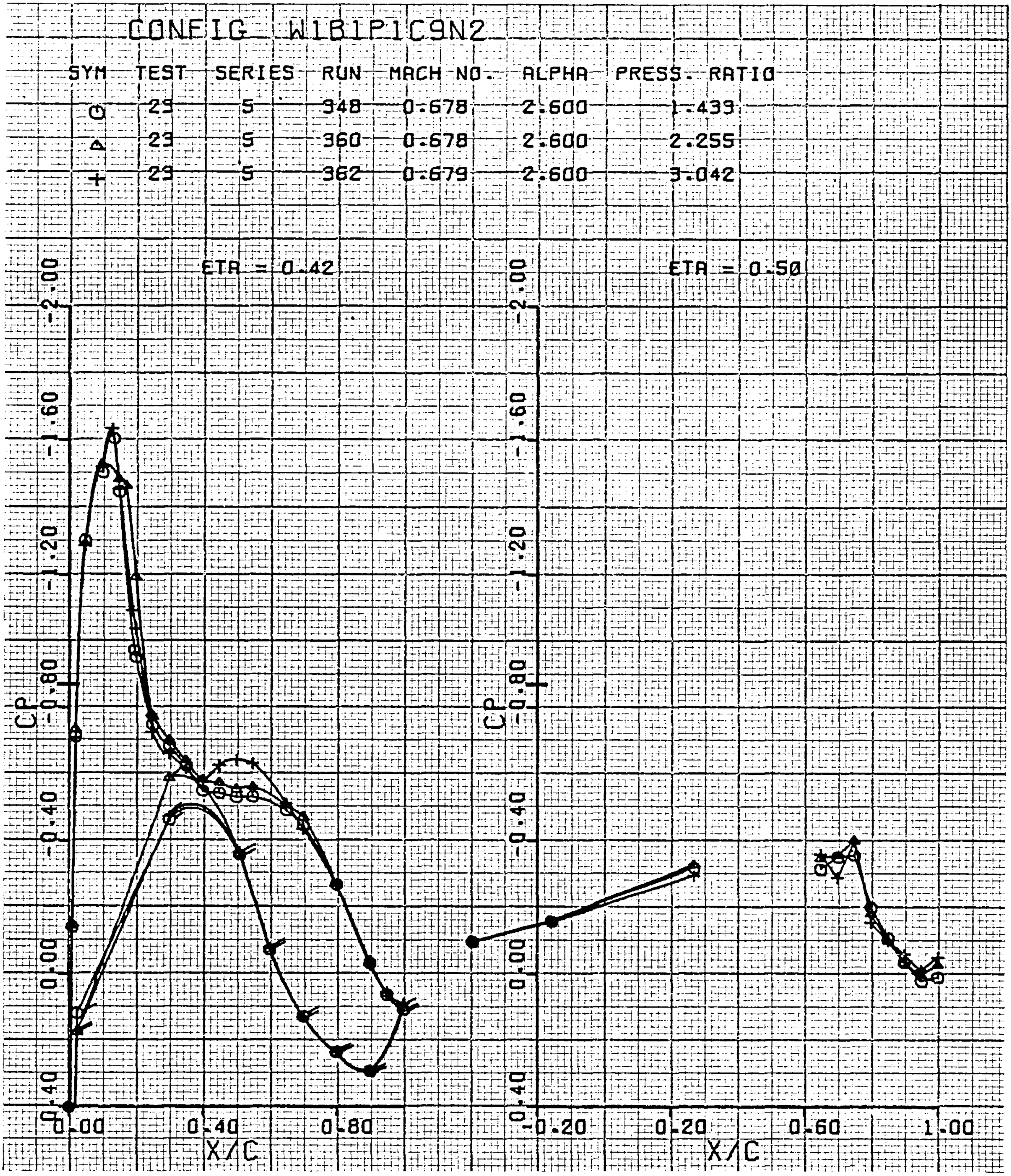

Figure 74. Wing pressure distribution, effect of nozzle pressure ratio, nozzle N_2, η = 0.42, 0.50

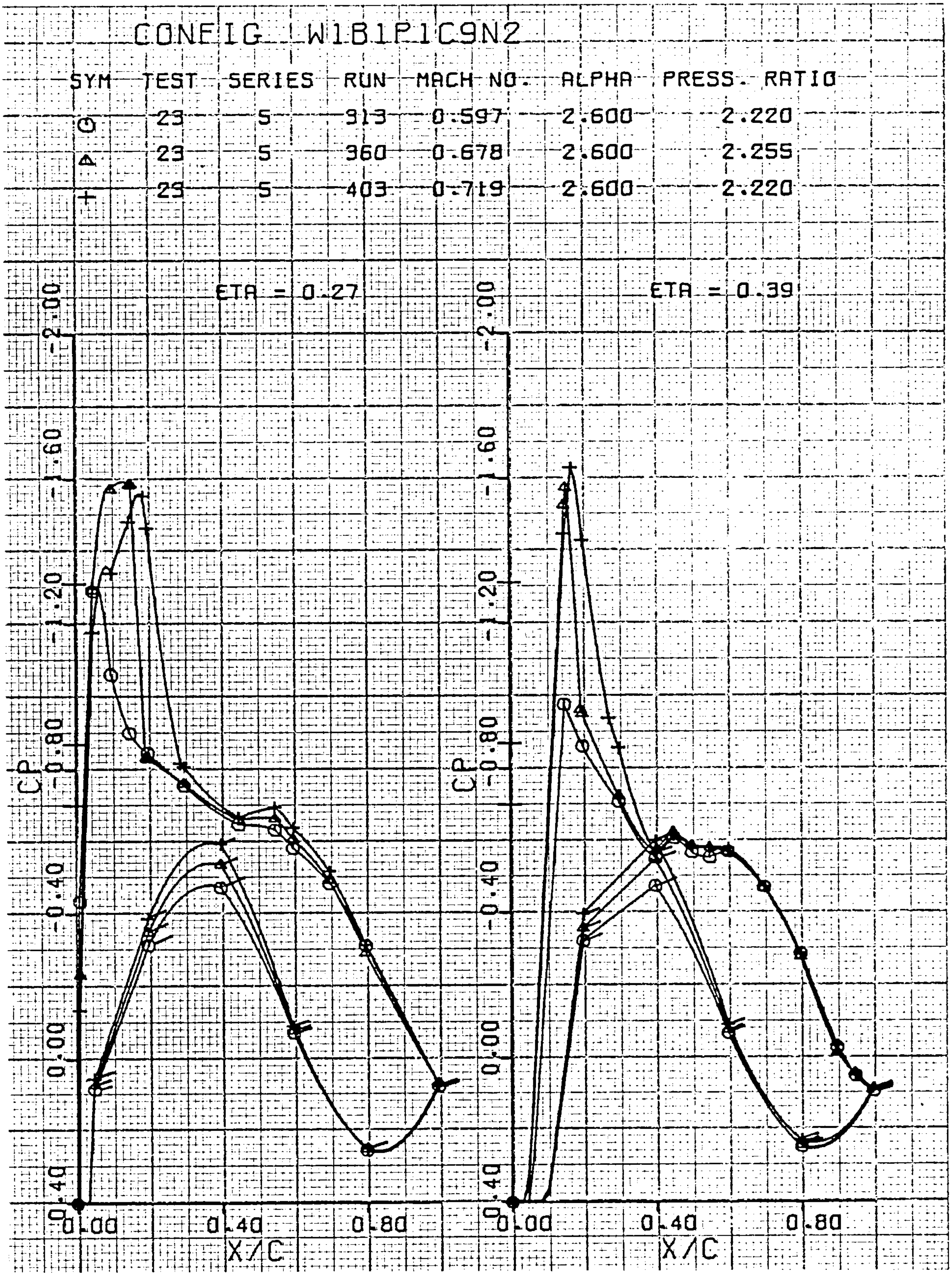

Figure 75. Wing pressure distribution, effect of Mach number, nozzle N_2, η = 0.27, 0.39

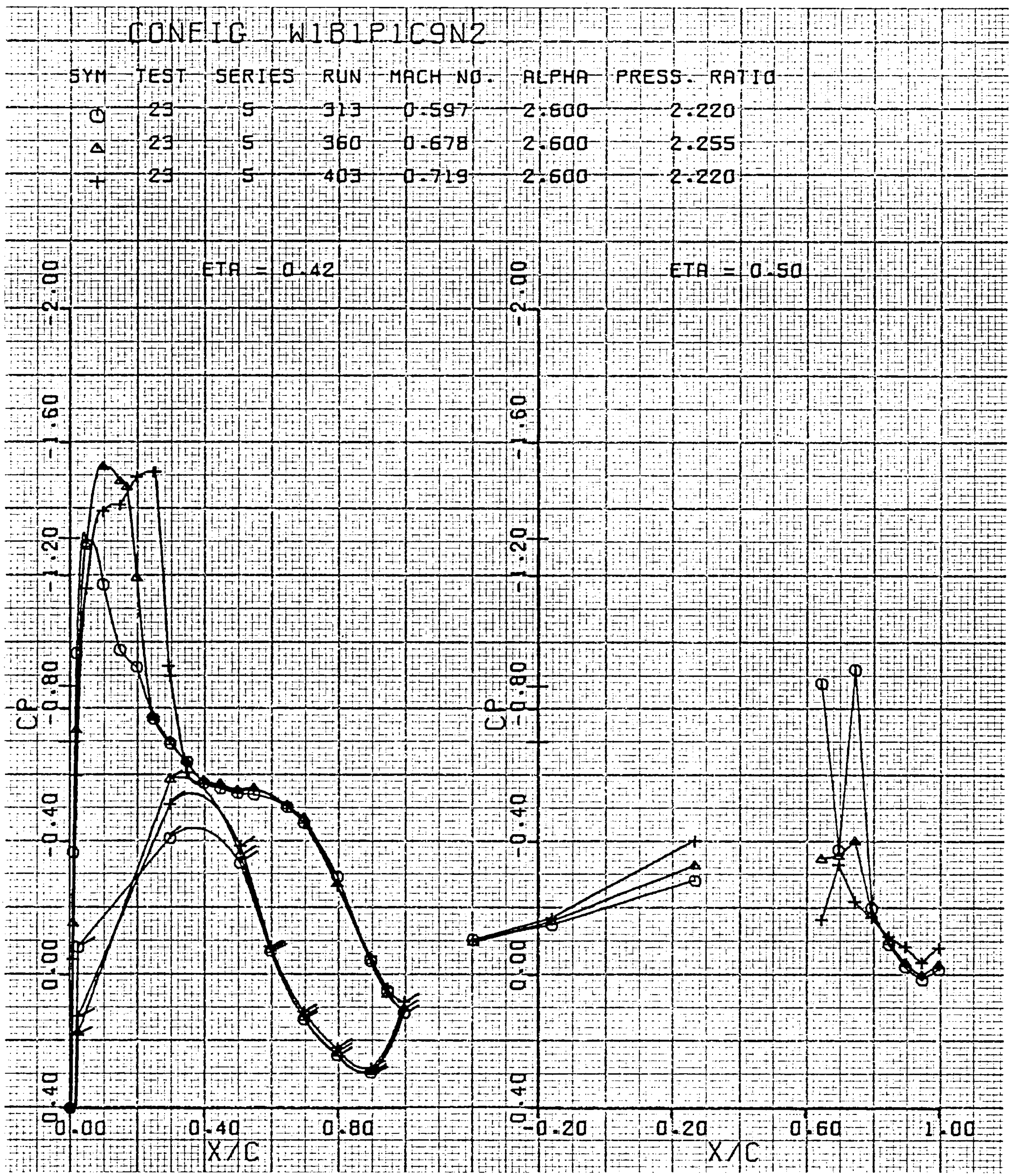

Figure 76. Wing pressure distribution, effect of Mach number, nozzle N_2, η = 0.42, 0.50

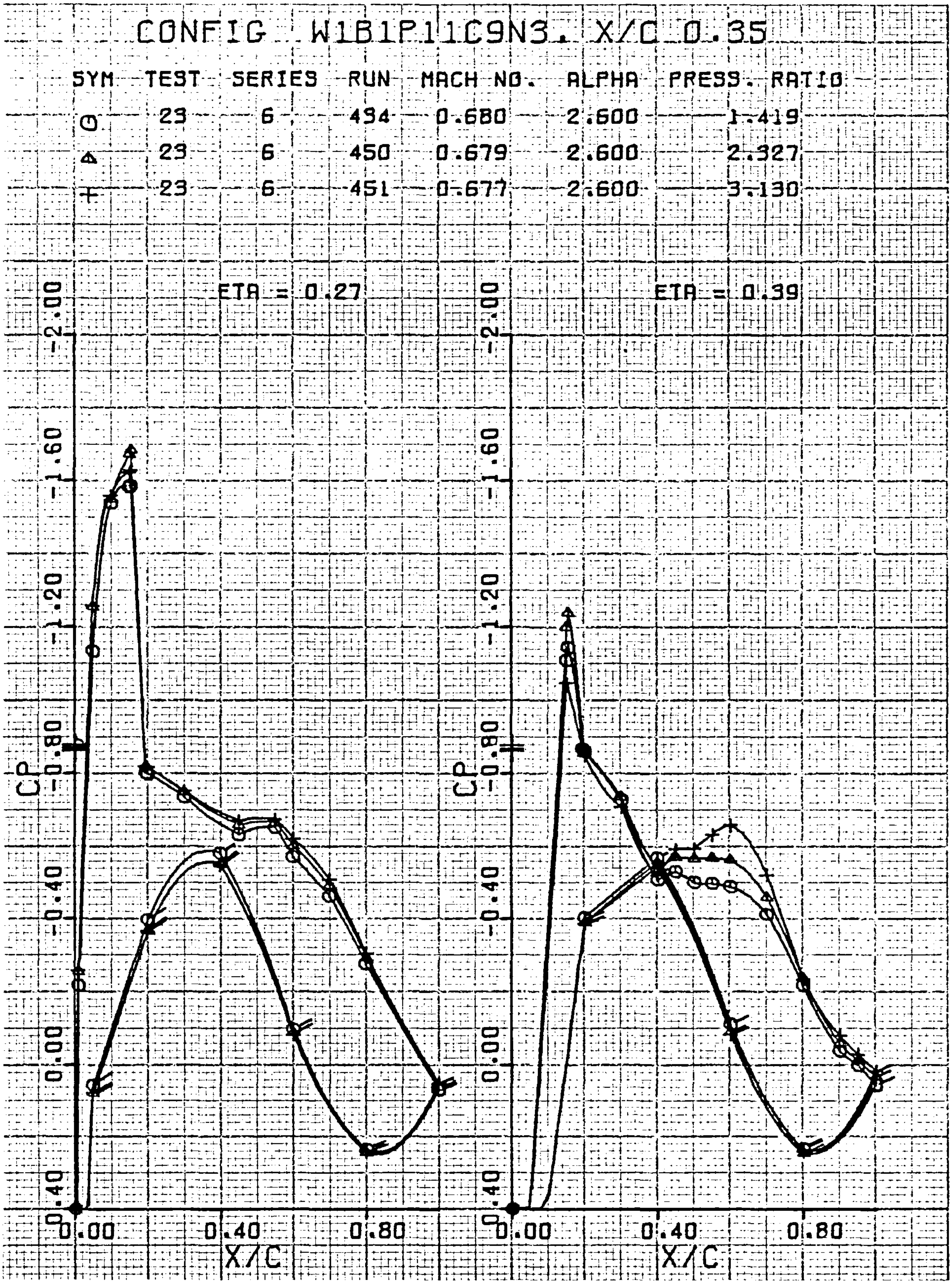

Figure 77. Wing pressure distribution, effect of nozzle pressure ratio, nozzle N_3, $x/c = 0.35$, $\eta = 0.27, 0.39$

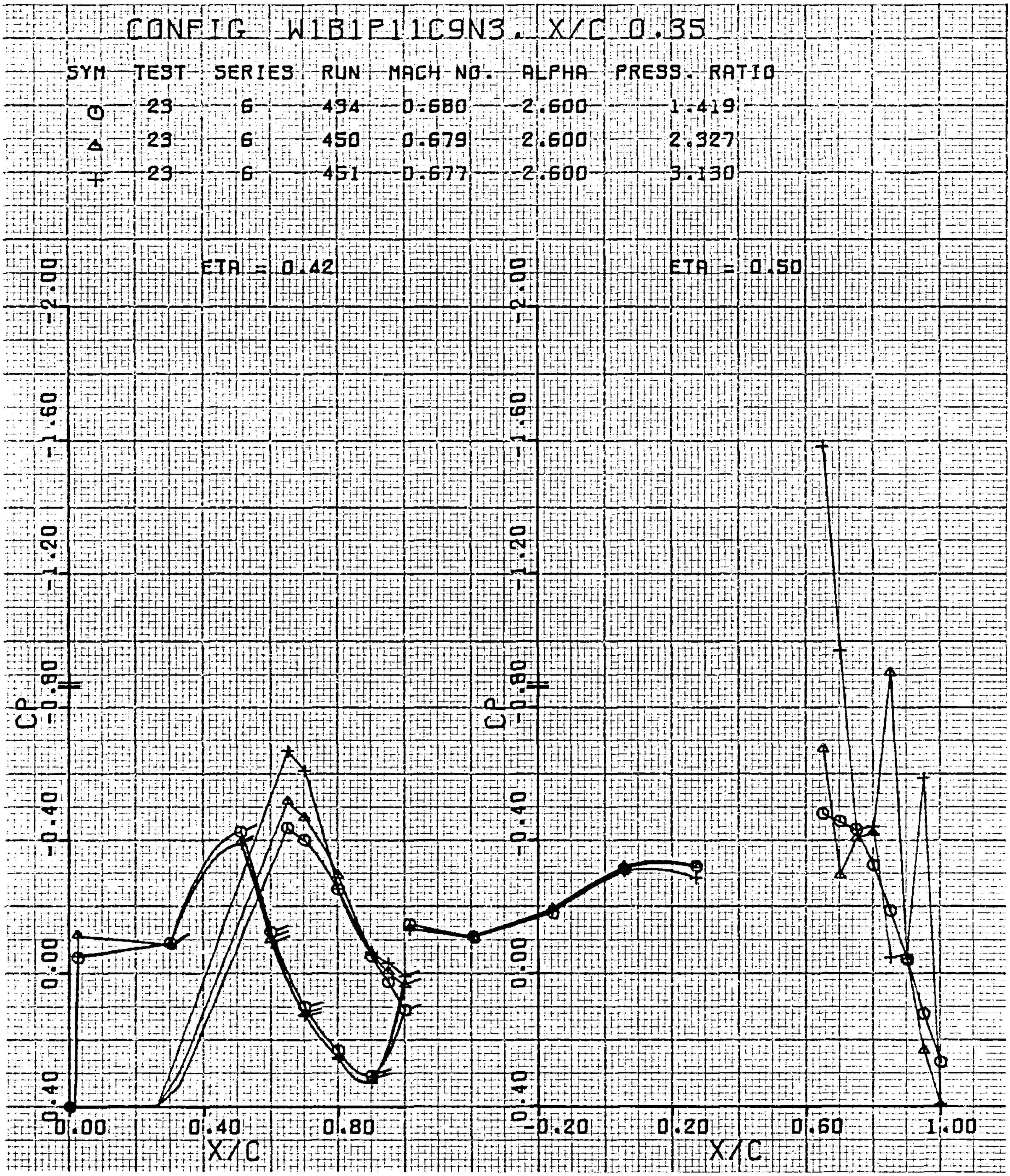

Figure 78. Wing pressure distribution, effect of nozzle pressure ratio, nozzle N_3, $x/c = 0.35$, $\eta = 0.42, 0.50$

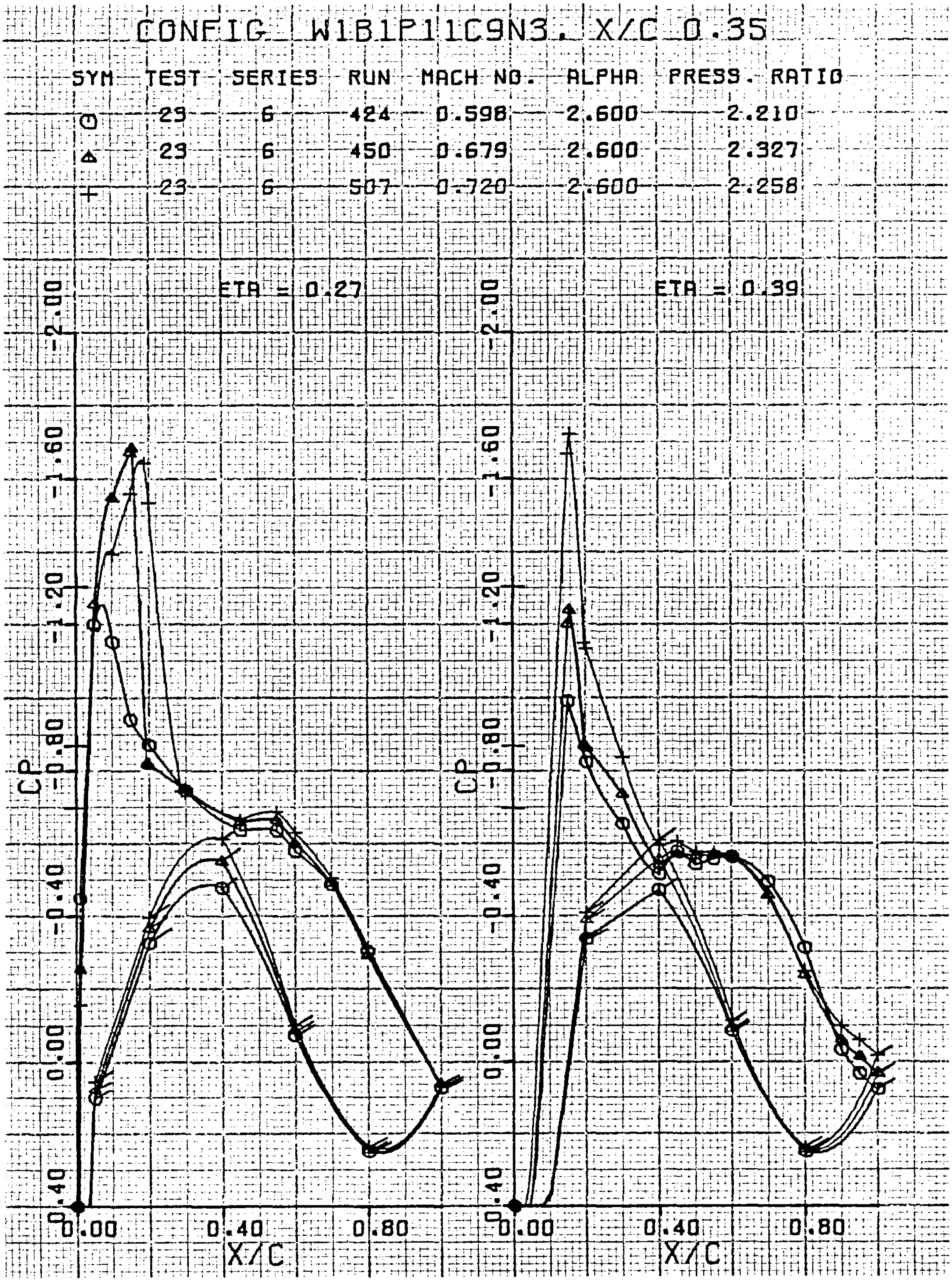

Figure 79. Wing pressure distribution, effect of Mach number, nozzle N_3, $x/c = 0.35$, $\eta = 0.27, 0.39$

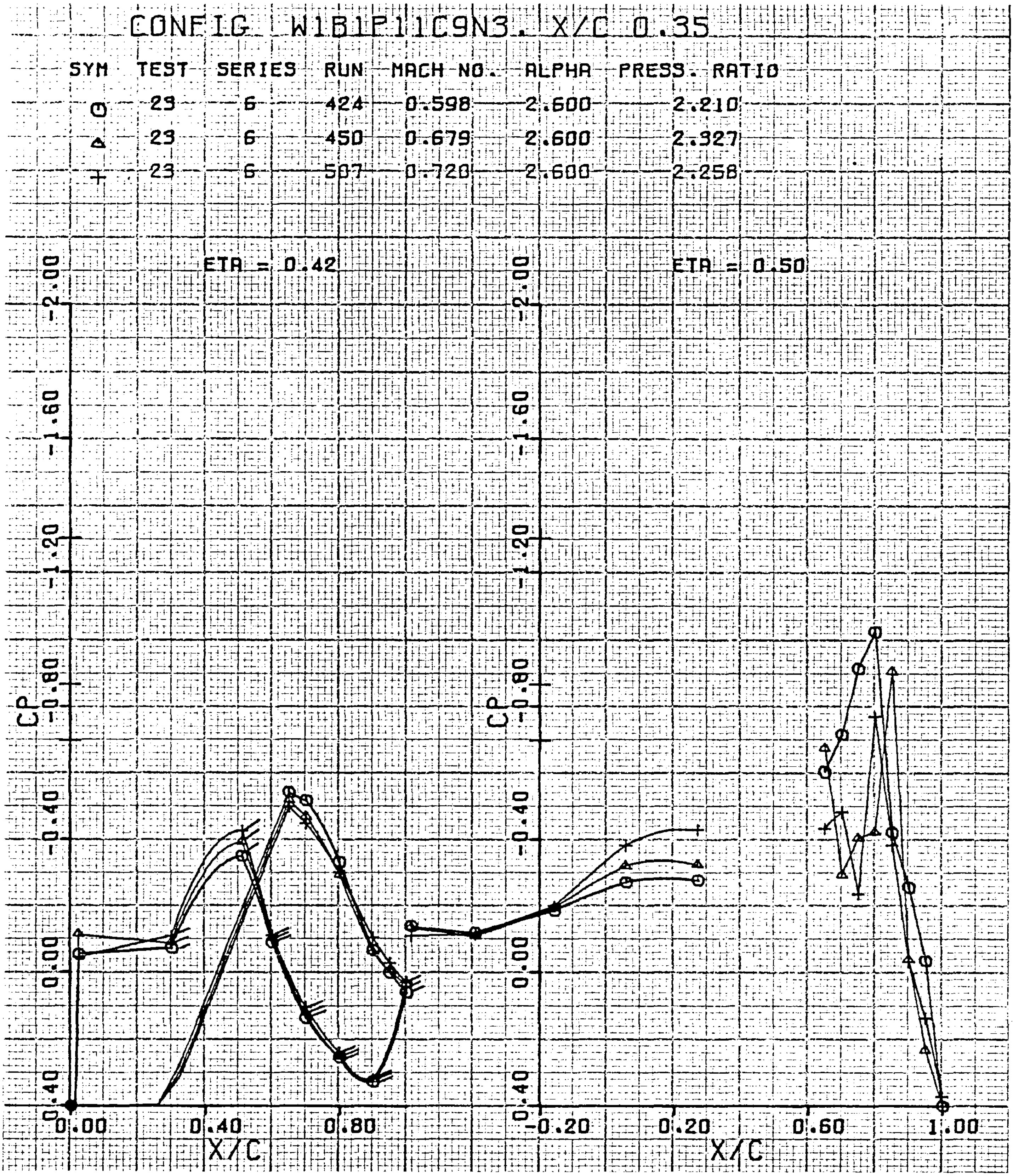

Figure 80. Wing pressure distribution, effect of Mach number, nozzle N_3, $x/c = 0.35$, $\eta = 0.42, 0.50$

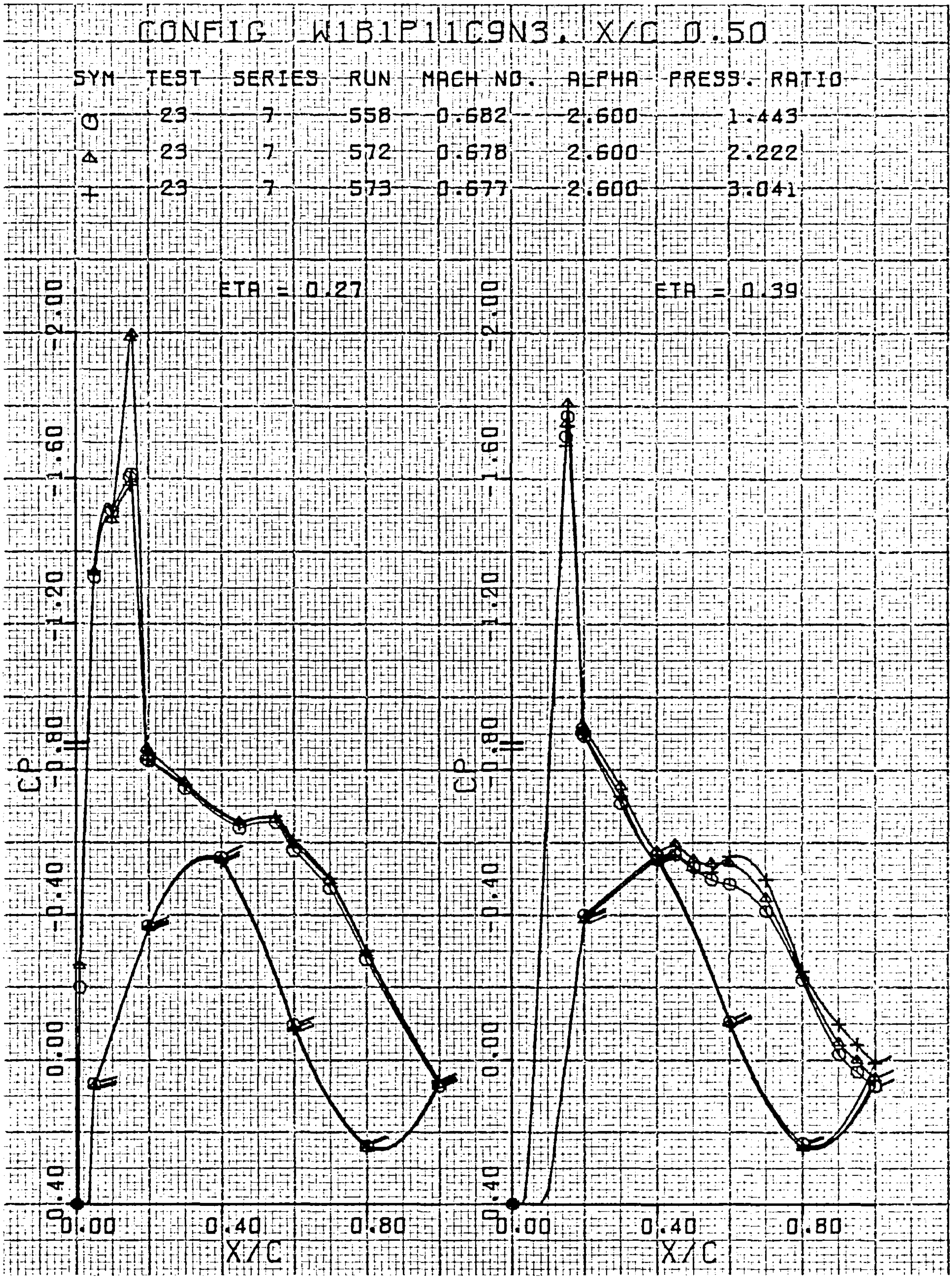

Figure 81. Wing pressure distribution, effect of nozzle pressure ratio, nozzle N_3, $x/c = 0.50$, $\eta = 0.27, 0.39$

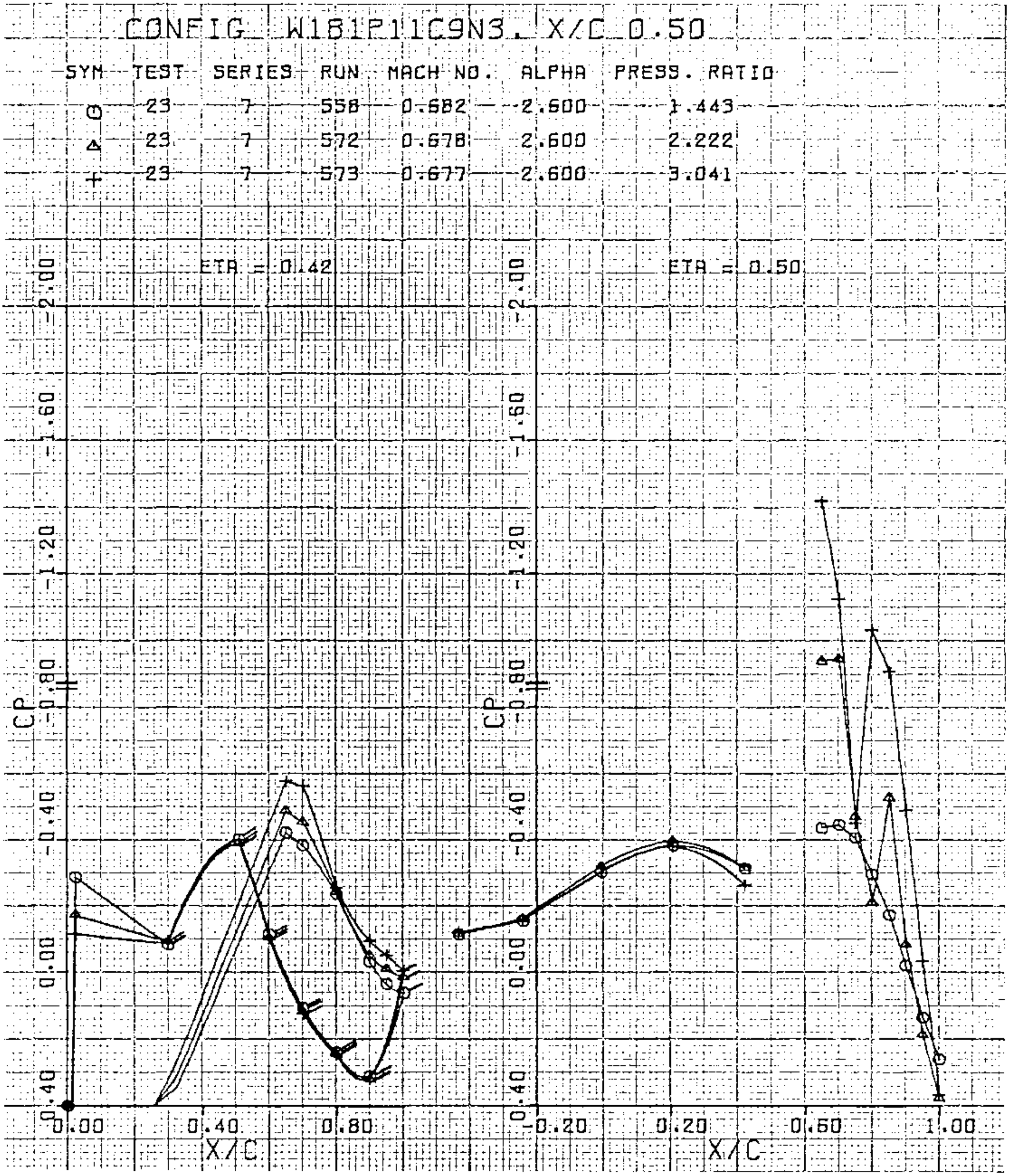

Figure 82. Wing pressure distribution, effect of nozzle pressure ratio, nozzle N_3, $x/c = 0.50$, η = 0.42, 0.50

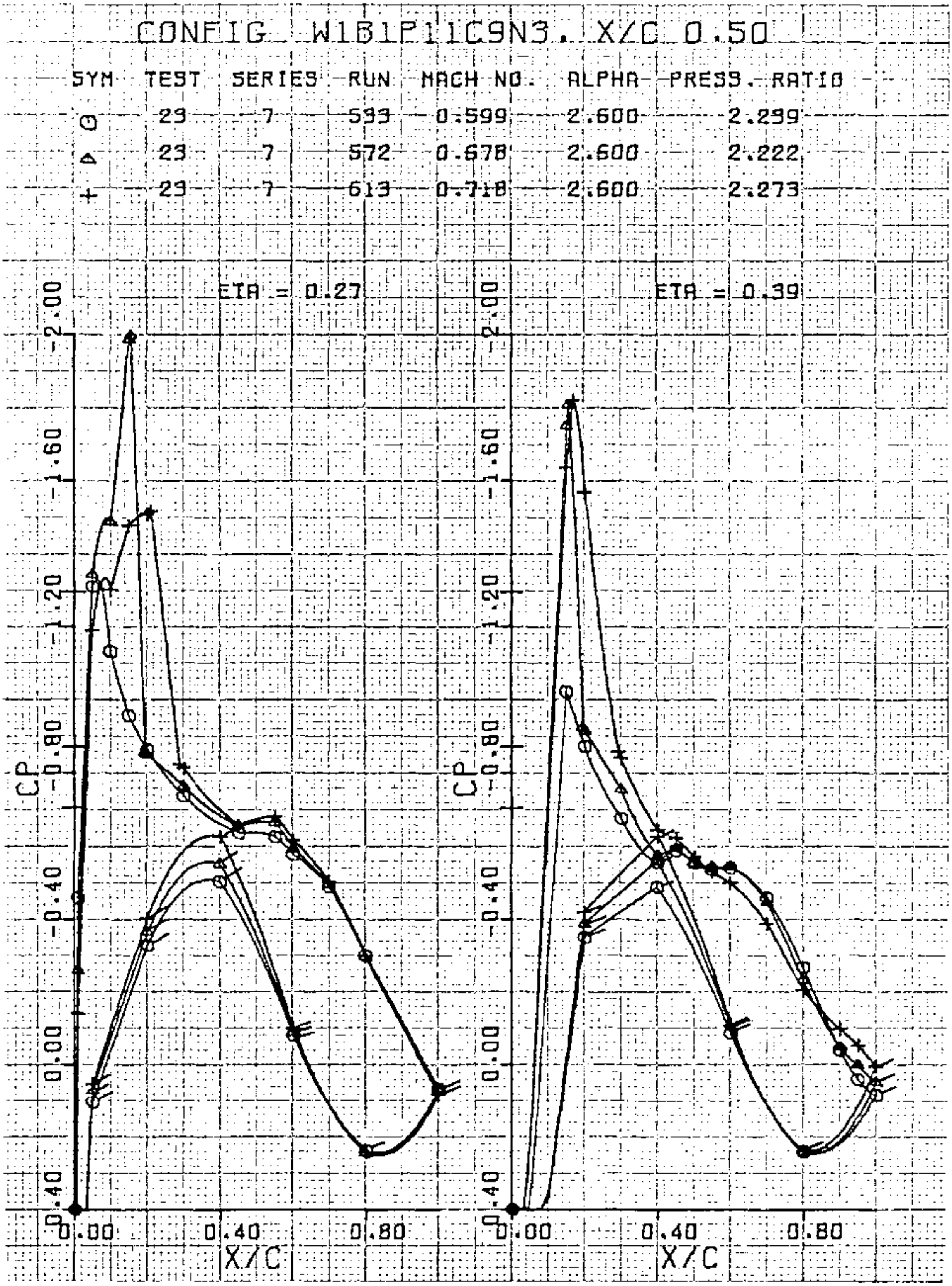

Figure 83. Wing pressure distribution, effect of Mach number, nozzle N_3, $x/c = 0.50$, $\eta = 0.27, 0.39$

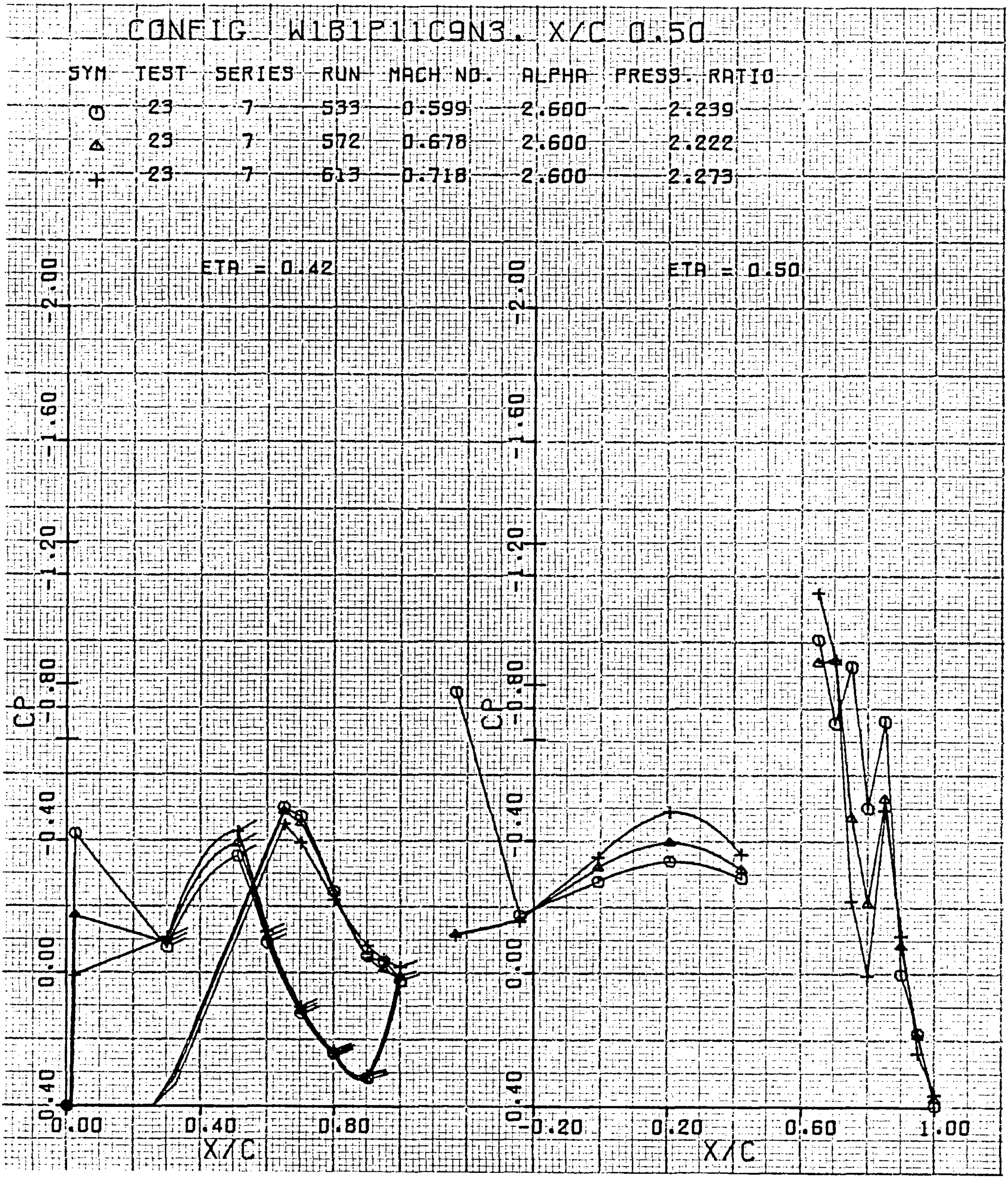

Figure 84. Wing pressure distribution, effect of Mach number, nozzle N_3, x/c = 0.50, η = 0.42, 0.50

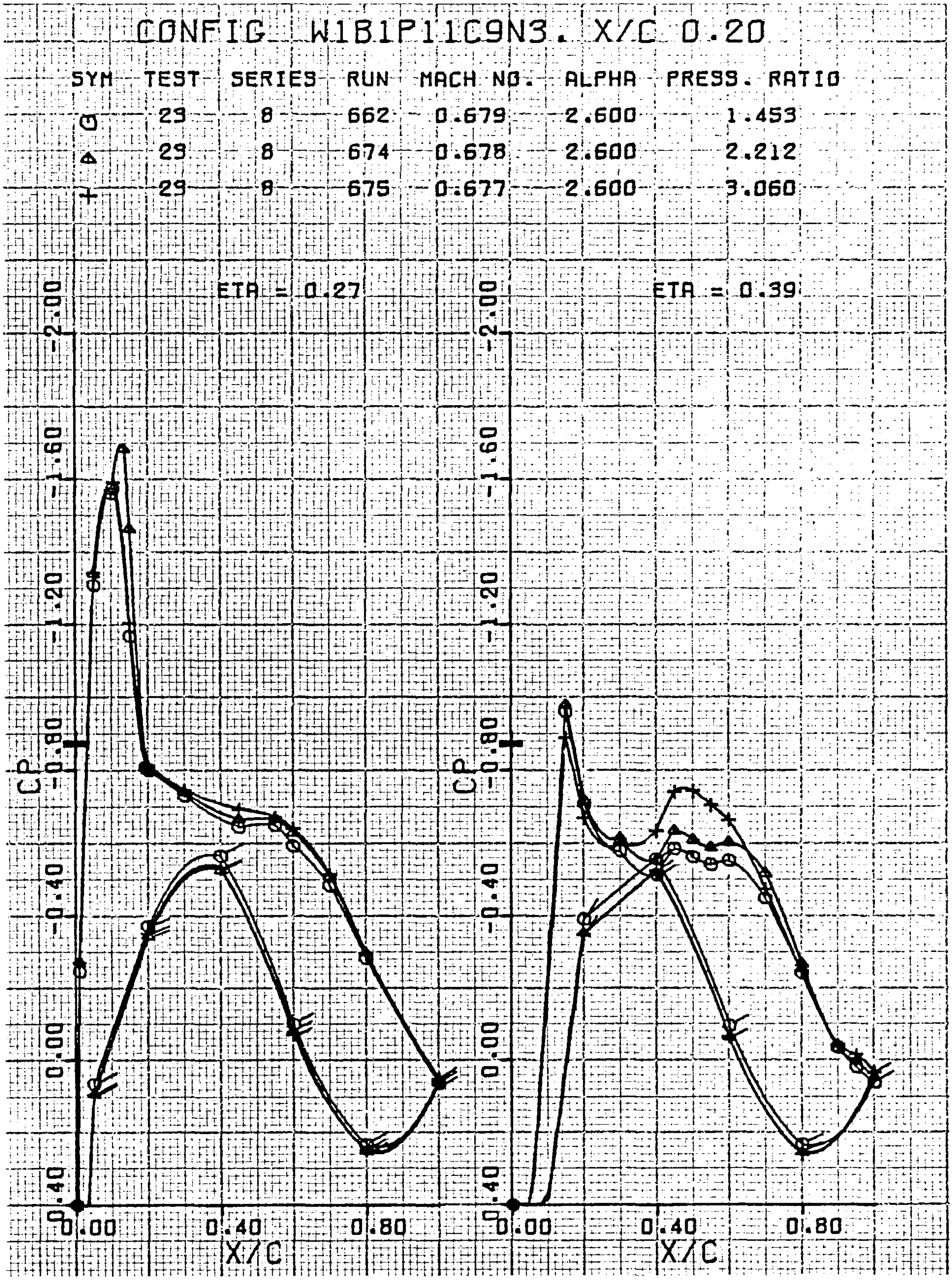

Figure 85. Wing pressure distribution, effect of nozzle pressure ratio, nozzle N_3, $x/c = 0.20$, η = 0.27, 0.39

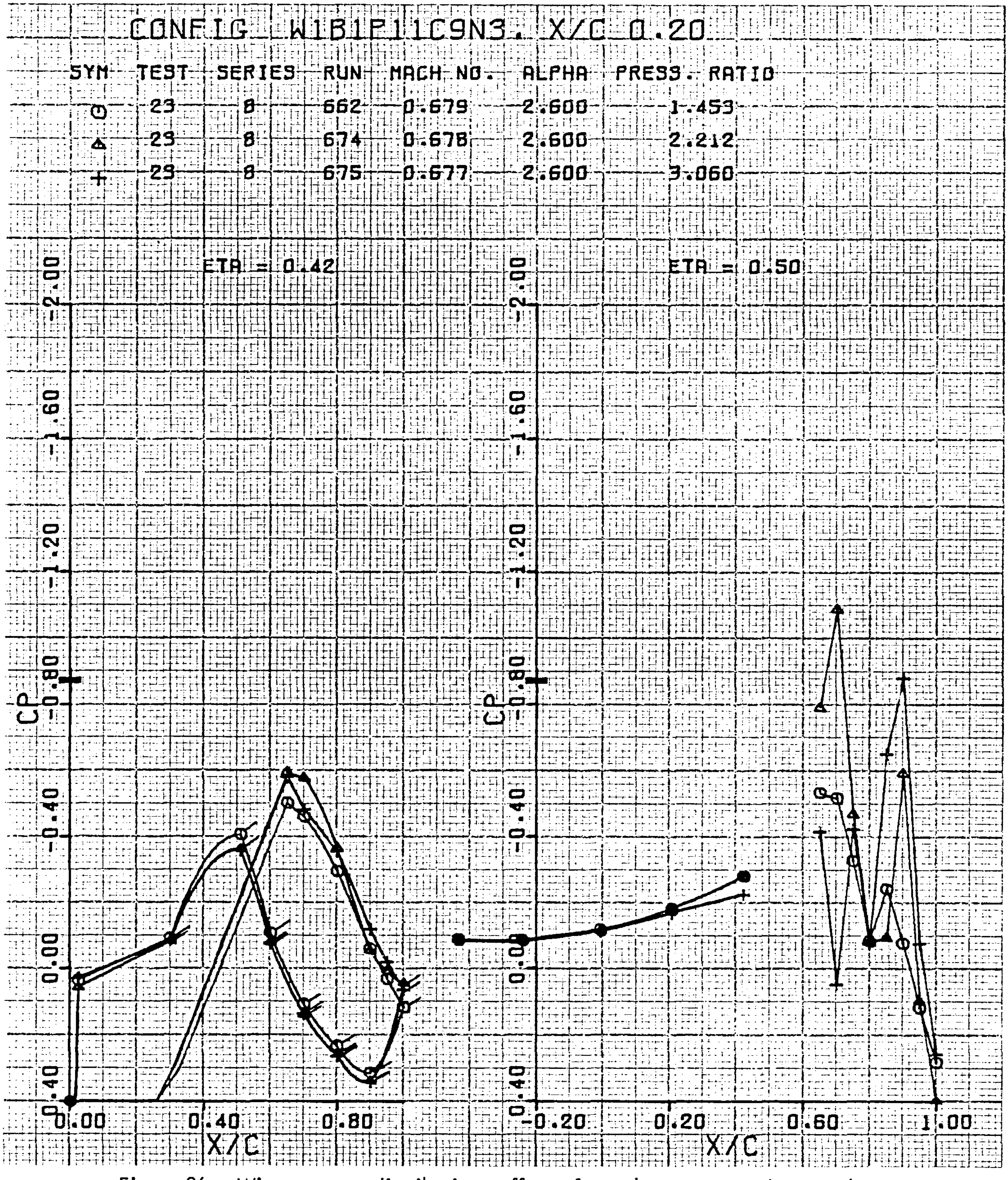

Figure 86. Wing pressure distribution, effect of nozzle pressure ratio, nozzle N_3, $x/c = 0.20$, η = 0.42, 0.50

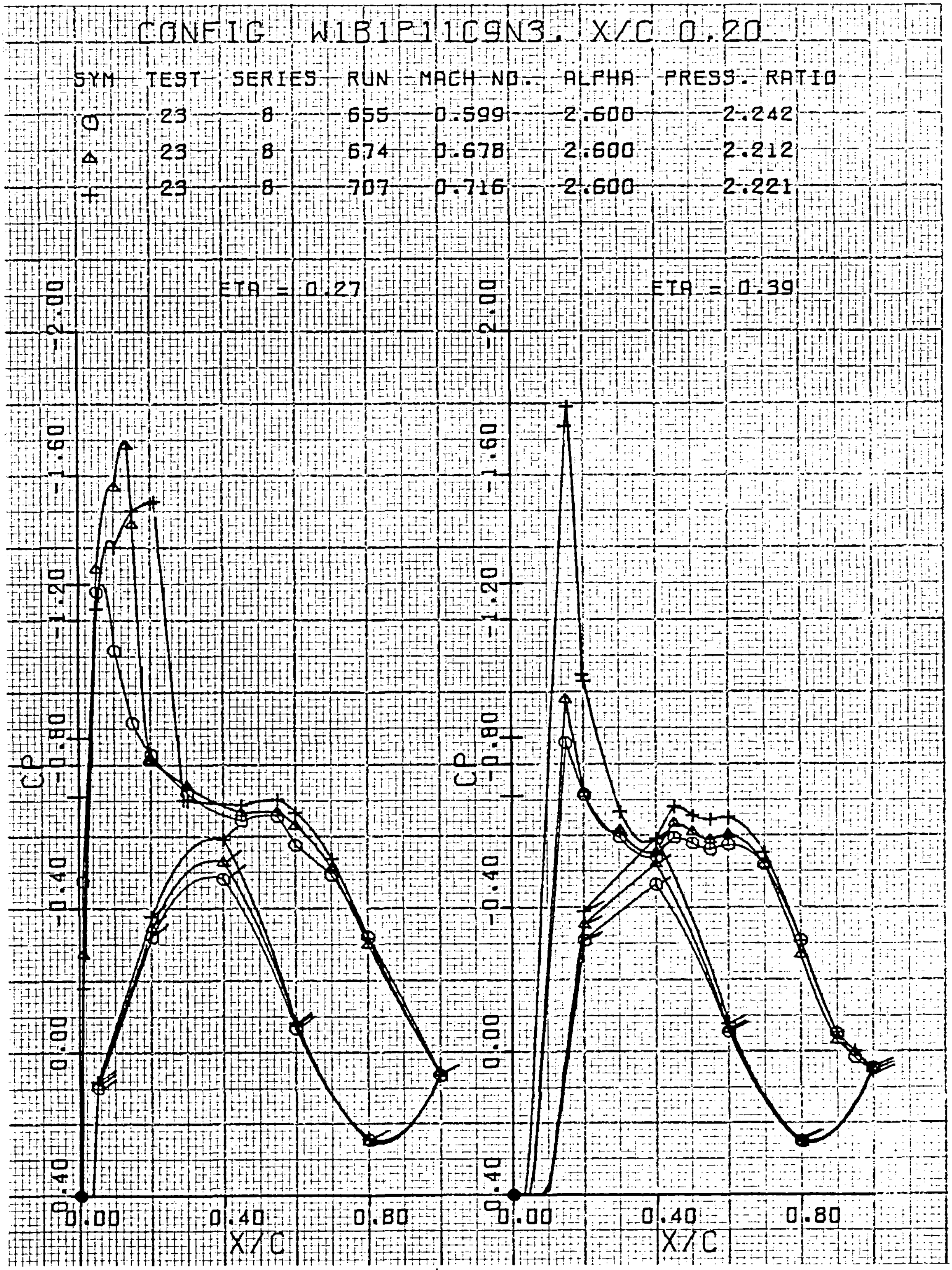

Figure 87. Wing pressure distribution, effect of Mach number, nozzle N_3, $x/c = 0.20$, $\eta = 0.27, 0.39$

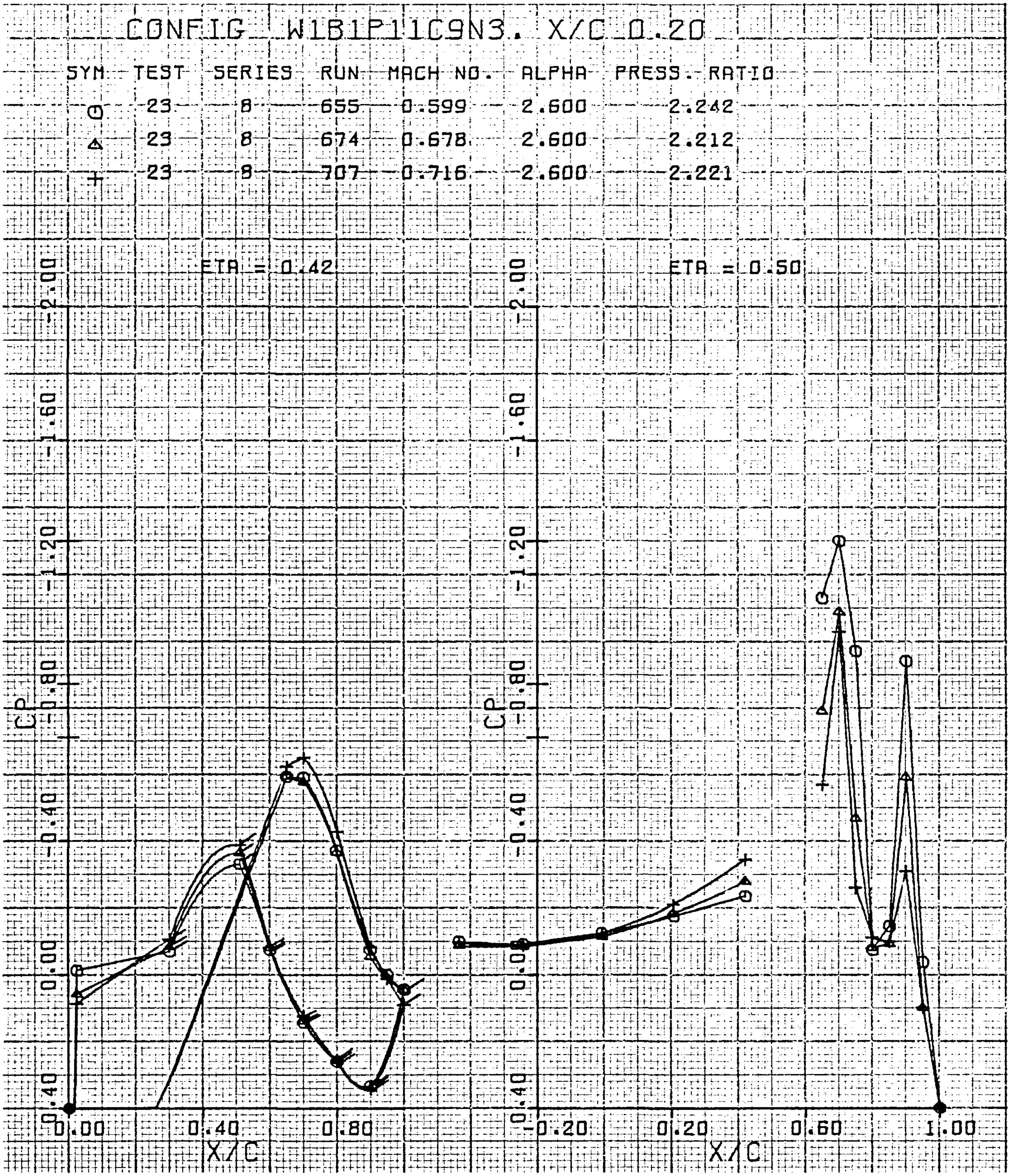

Figure 88. Wing pressure distribution, effect of Mach number, nozzle N_3, $x/c = 0.20$, η = 0.42, 0.50

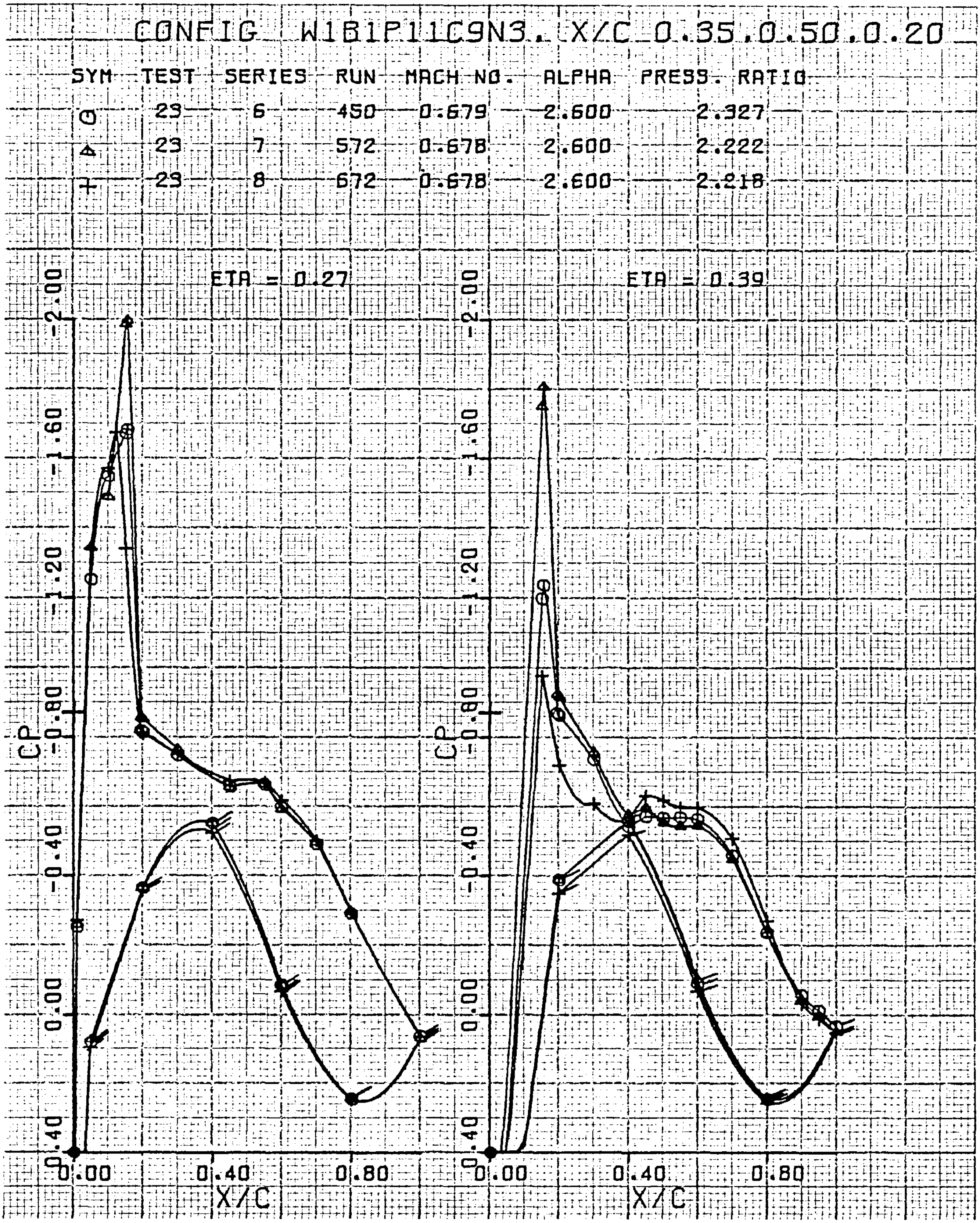

Figure 89. Wing pressure distribution, effect of x/c, nozzle N_3, η = 0.27, 0.39

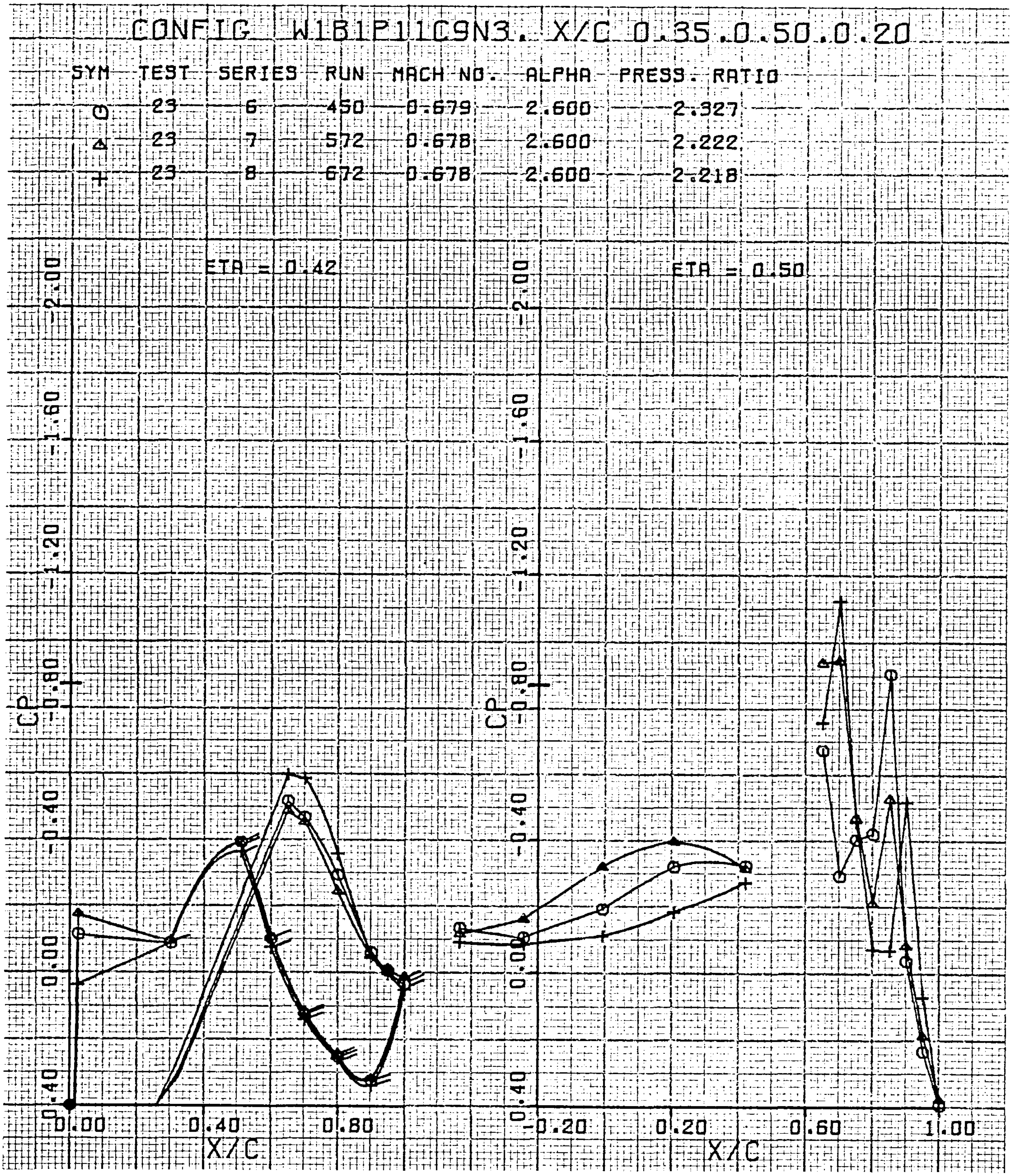

Figure 90. Wing pressure distribution, effect of x/c, nozzle N_3, $\eta = 0.42,\ 0.50$

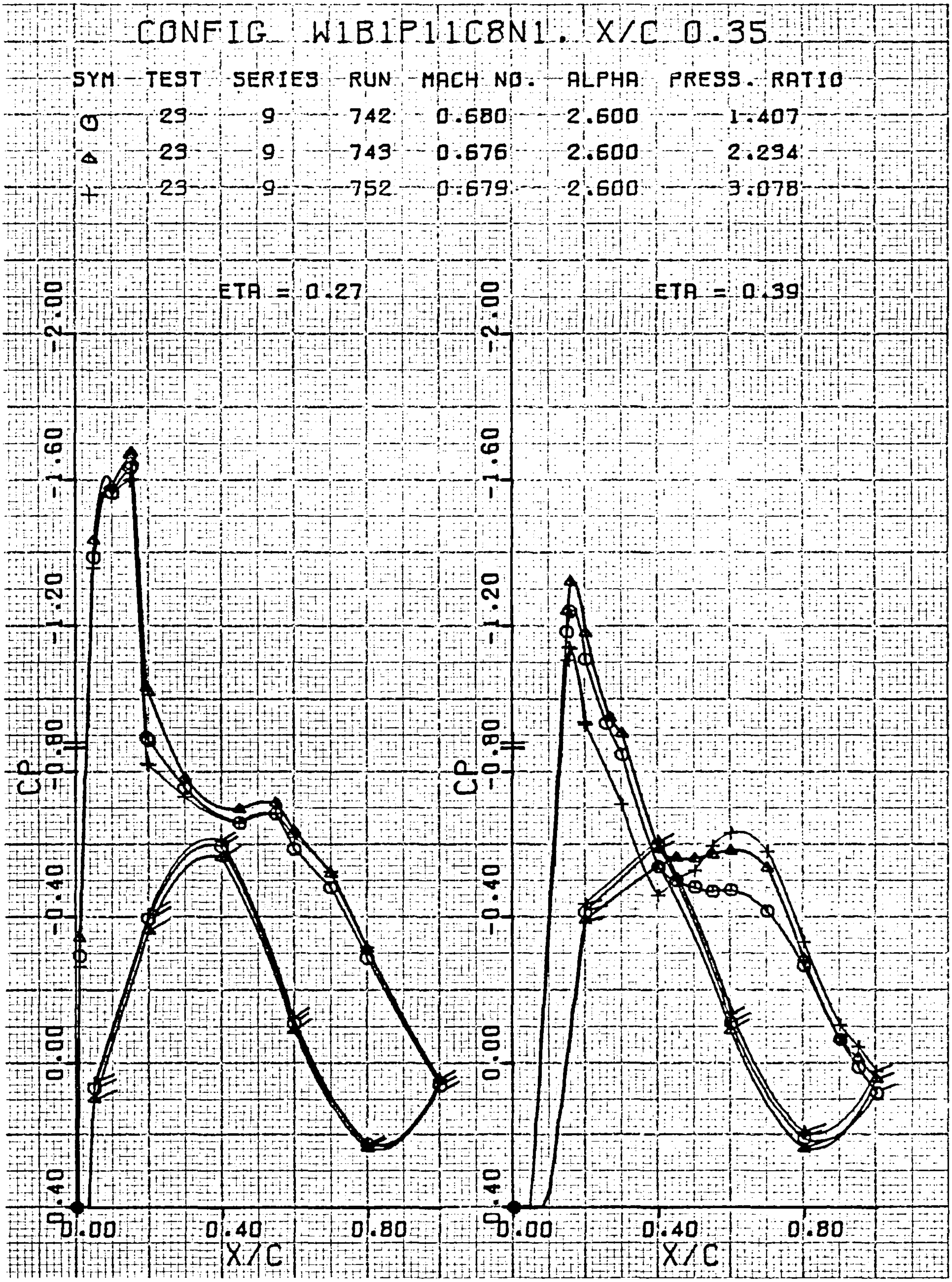

Figure 91. Wing pressure distribution, effect of nozzle pressure ratio, nozzle N_1, $x/c = 0.35$, η = 0.27, 0.39

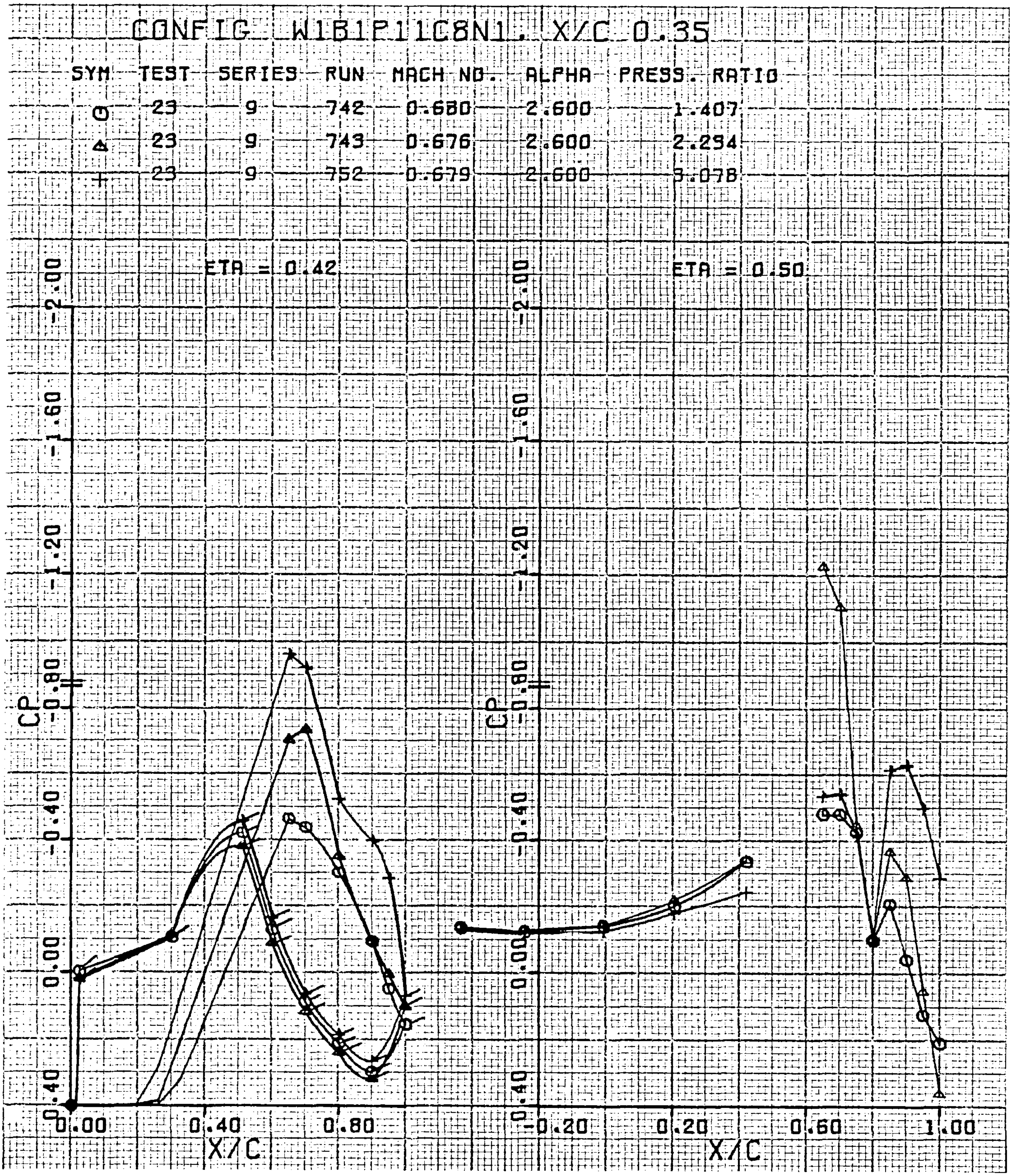

Figure 92. Wing pressure distribution, effect of nozzle pressure ratio, nozzle N_1, $x/c = 0.35$, η = 0.42, 0.50

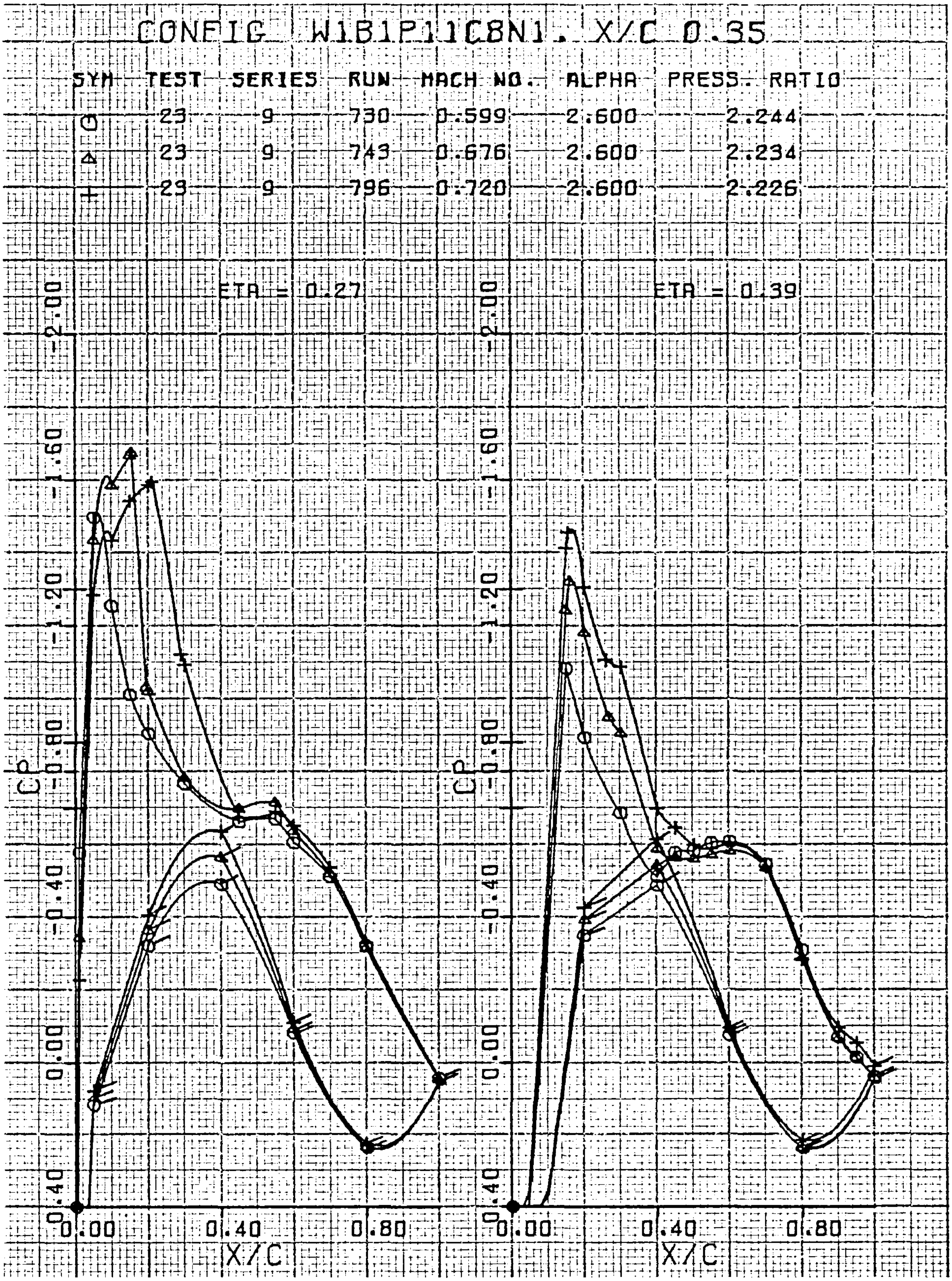

Figure 93. Wing pressure distribution, effect of Mach number, nozzle N_1, $x/c = 0.35$, $\eta = 0.27, 0.39$

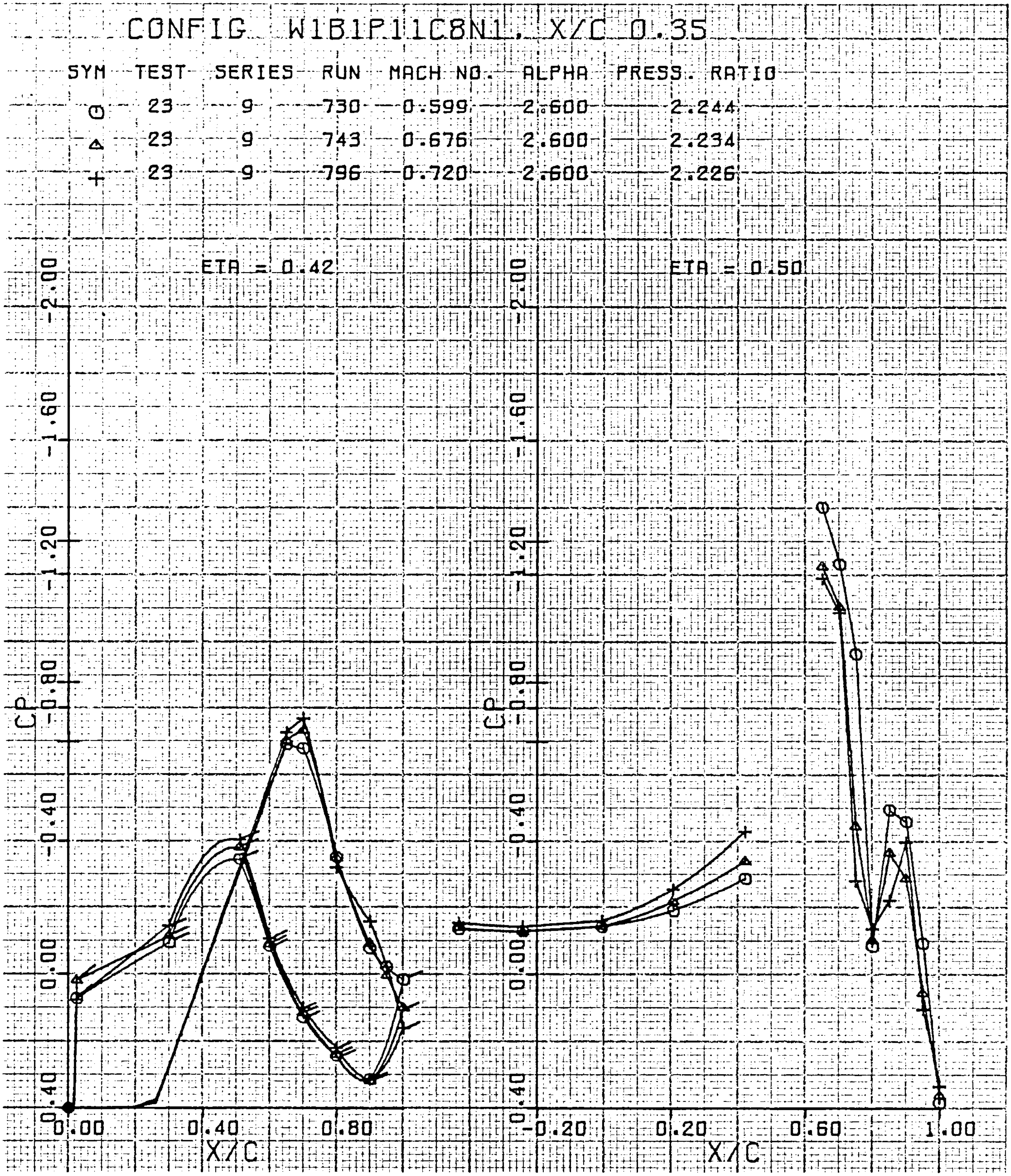

Figure 94. Wing pressure distribution, effect of Mach number, nozzle N_1, $x/c = 0.35$, $\eta = 0.42, 0.50$

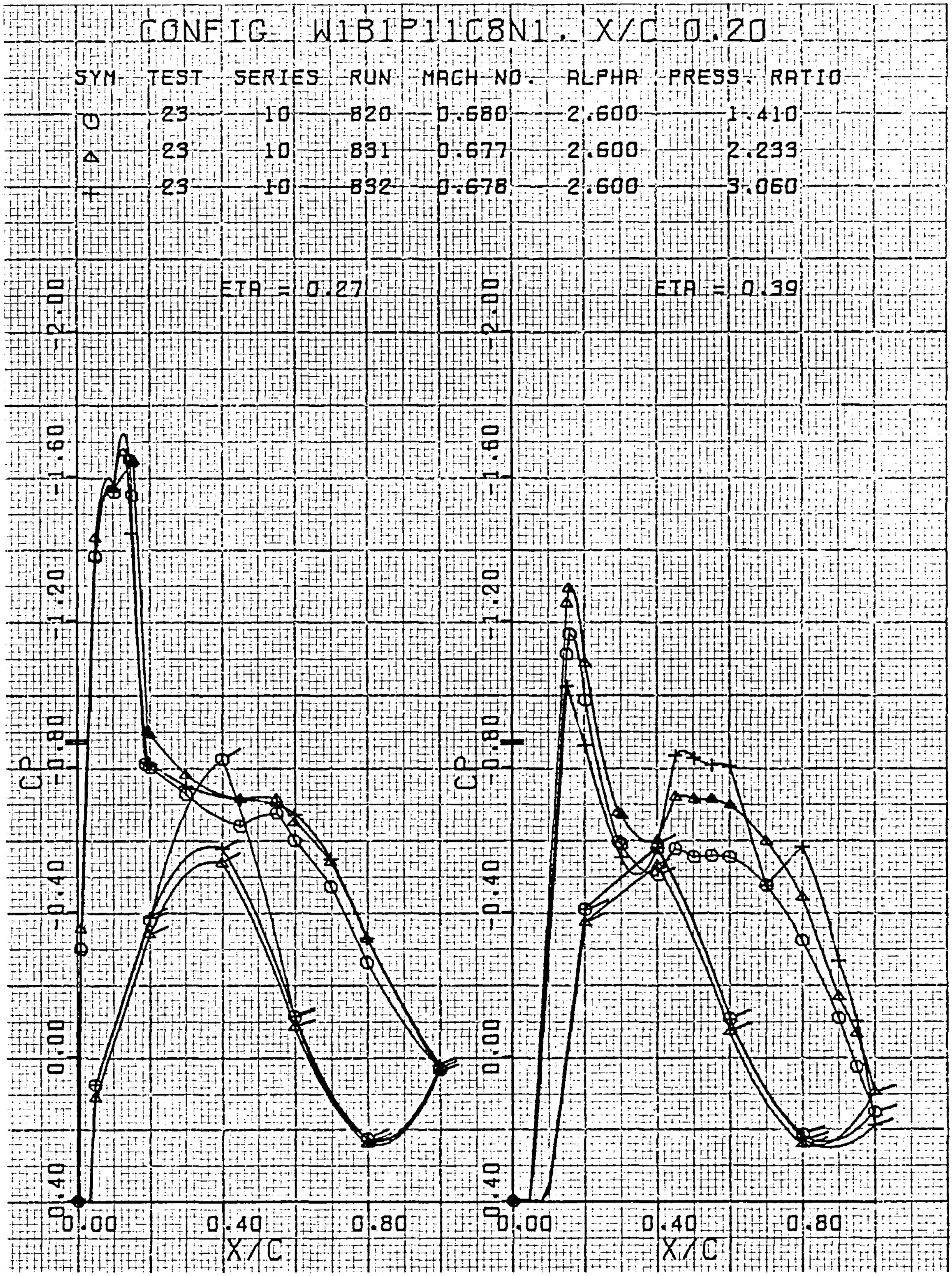

Figure 95. Wing pressure distribution, effect of nozzle pressure ratio, nozzle N_1, $x/c = 0.20$, η = 0.27, 0.39

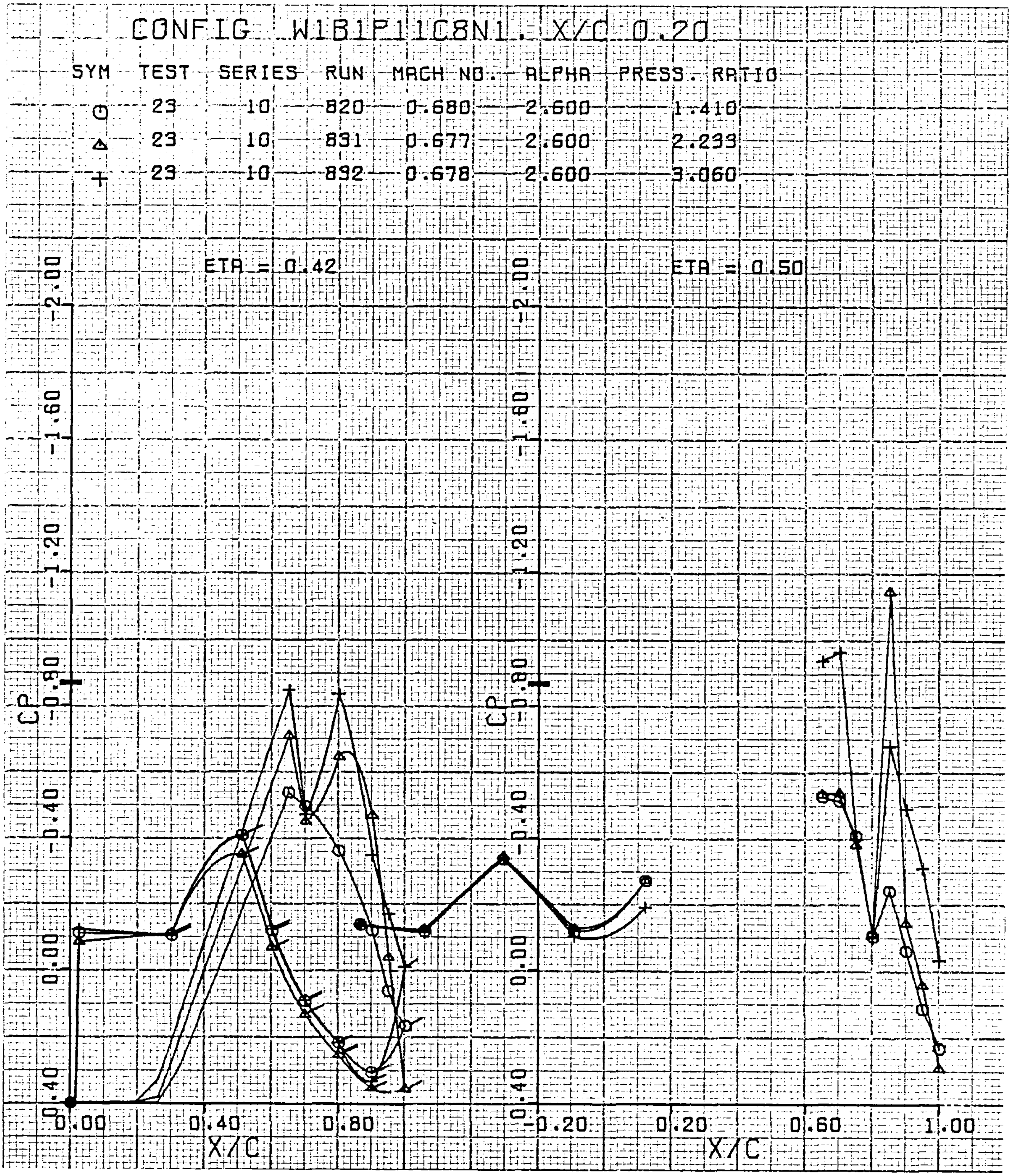

Figure 96. Wing pressure distribution, effect of nozzle pressure ratio, nozzle N_1, $x/c = 0.20$, η = 0.42, 0.50

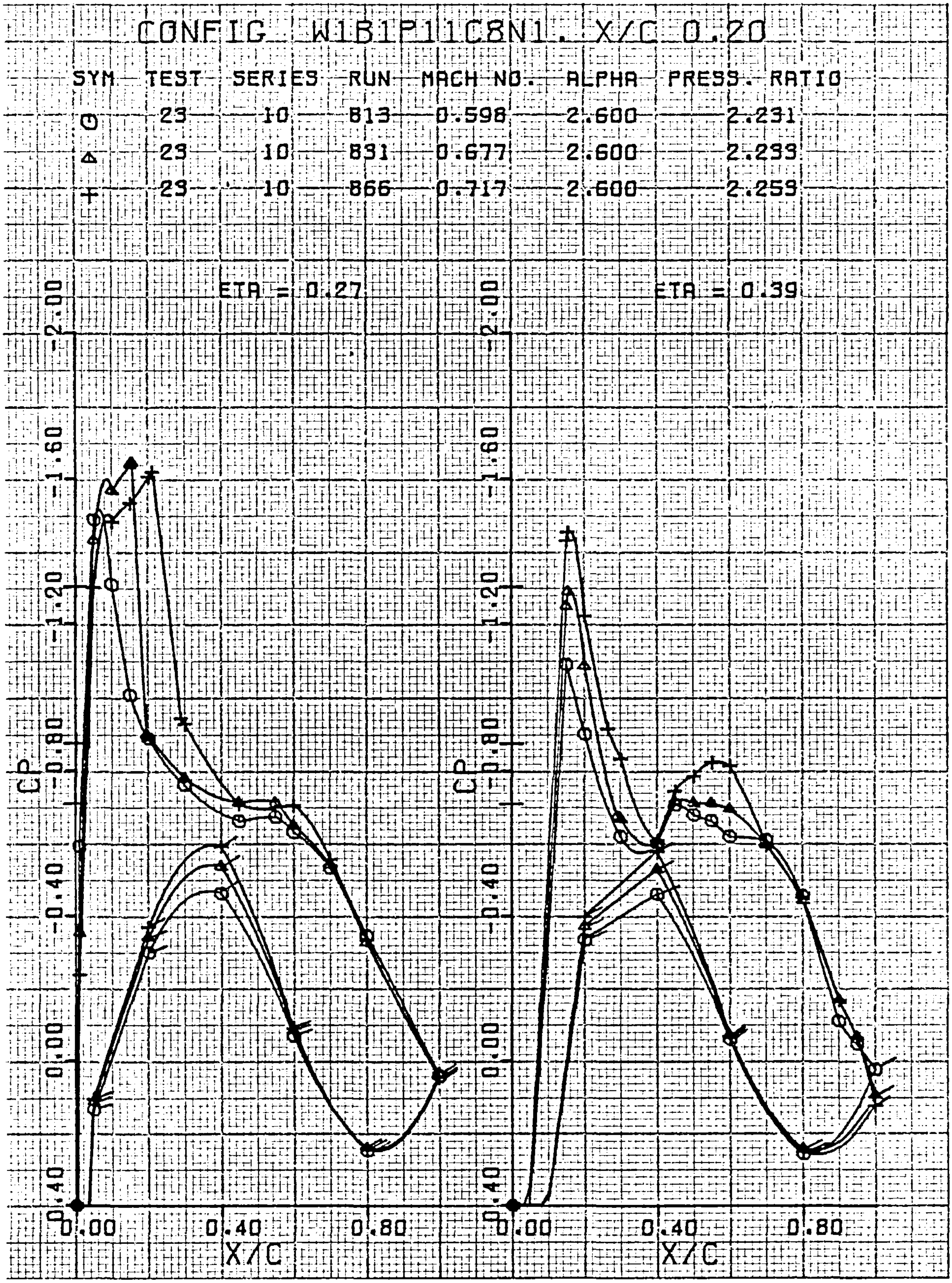

Figure 97. Wing pressure distribution, effect of Mach number, nozzle N_1, $x/c = 0.20$, $\eta = 0.27, 0.39$

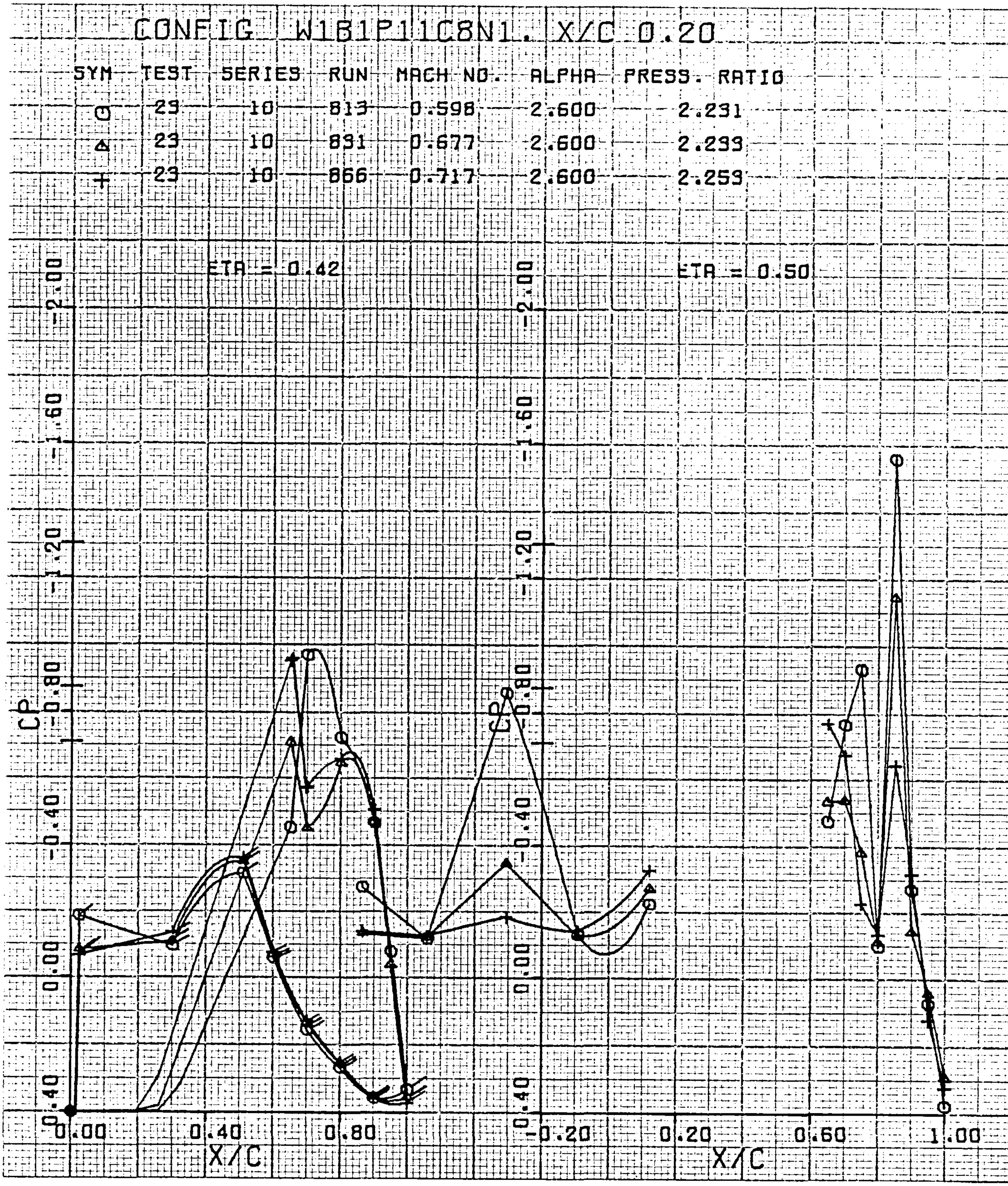

Figure 98. Wing pressure distribution, effect of Mach number, nozzle N_1, $x/c = 0.20$, $\eta = 0.42, 0.50$

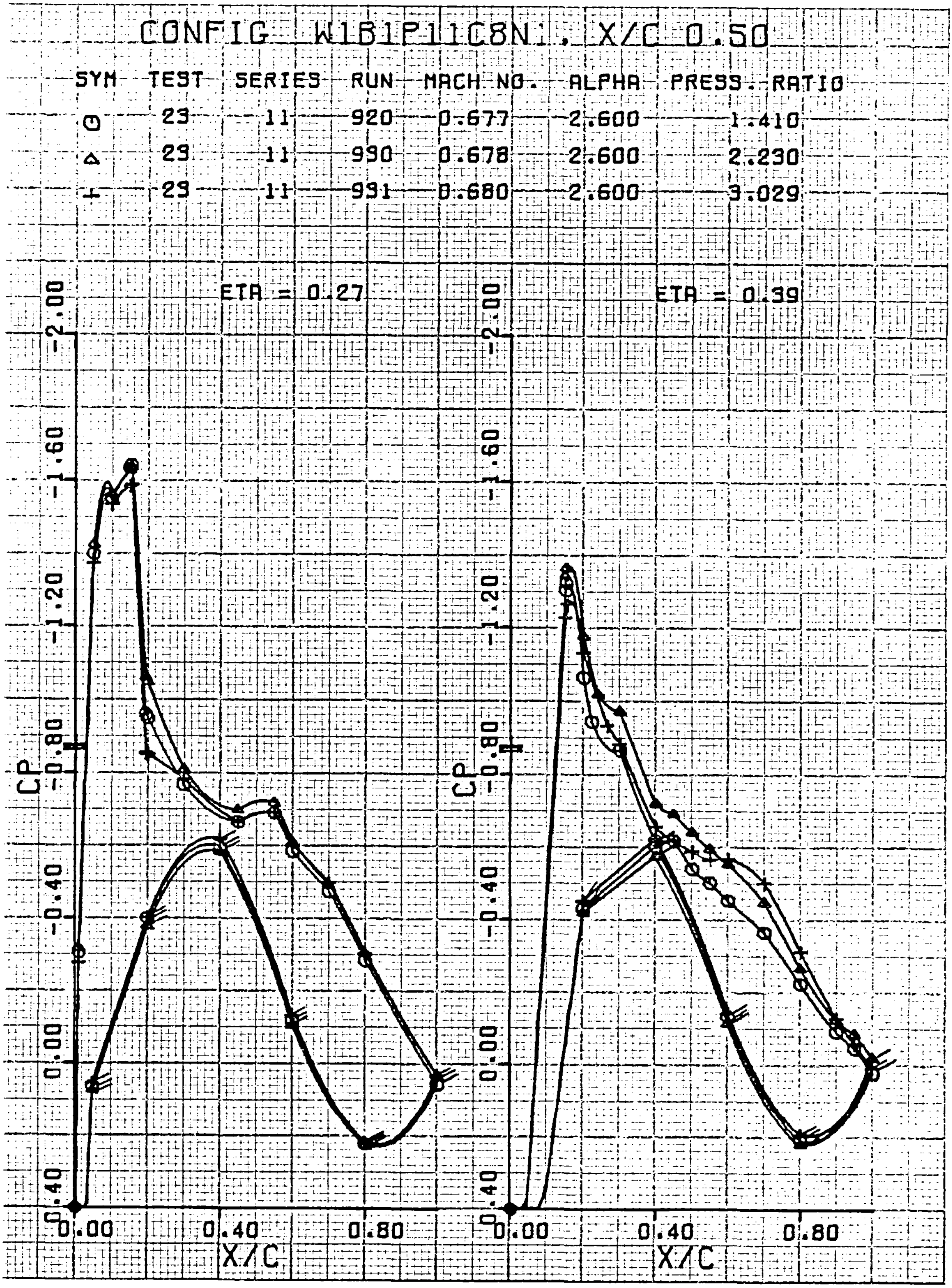

Figure 99. Wing pressure distribution, effect of nozzle pressure ratio, nozzle N_1, $x/c = 0.50$, η = 0.27, 0.39

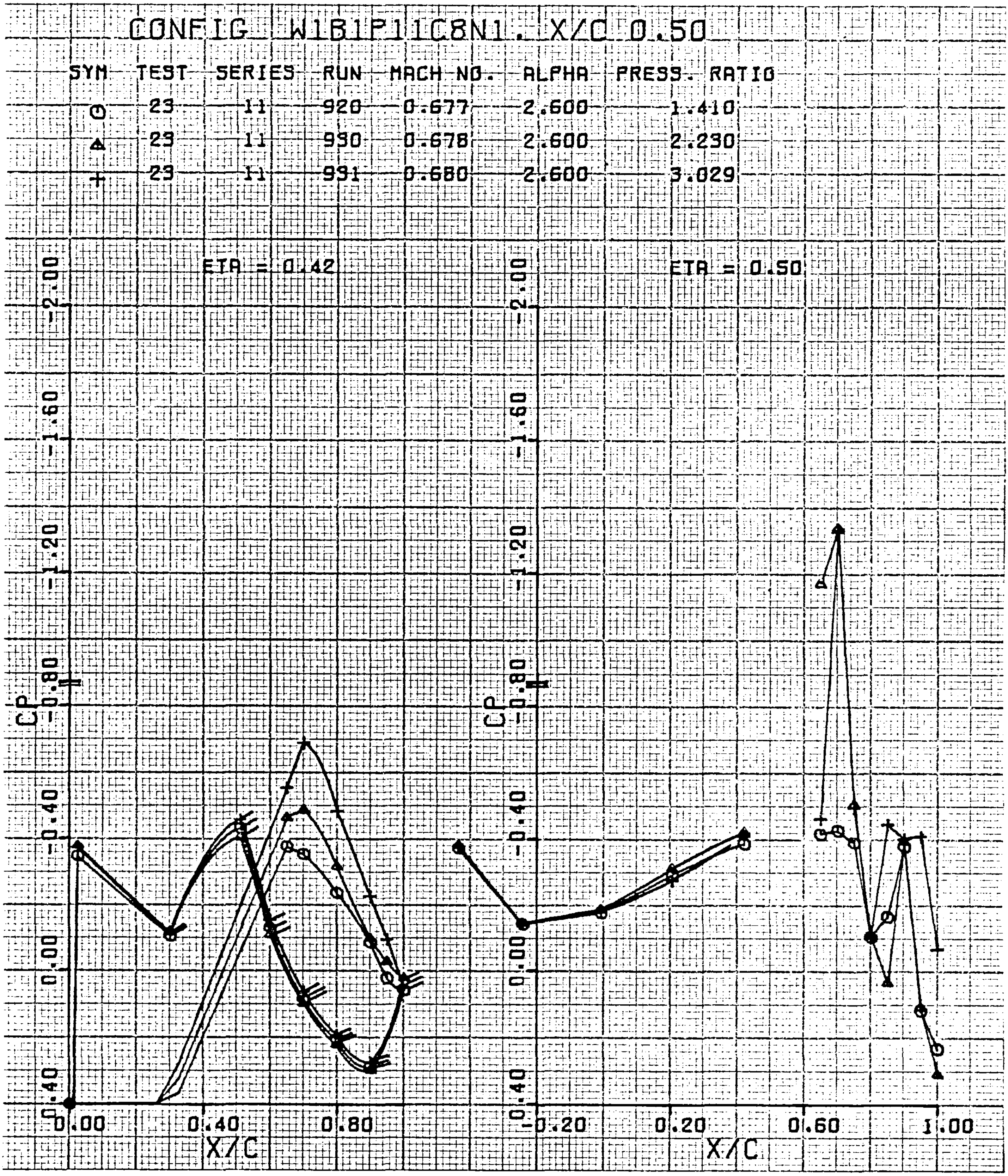

Figure 100. Wing pressure distribution, effect of nozzle pressure ratio, nozzle N_1, $x/c = 0.50$, η = 0.42, 0.50

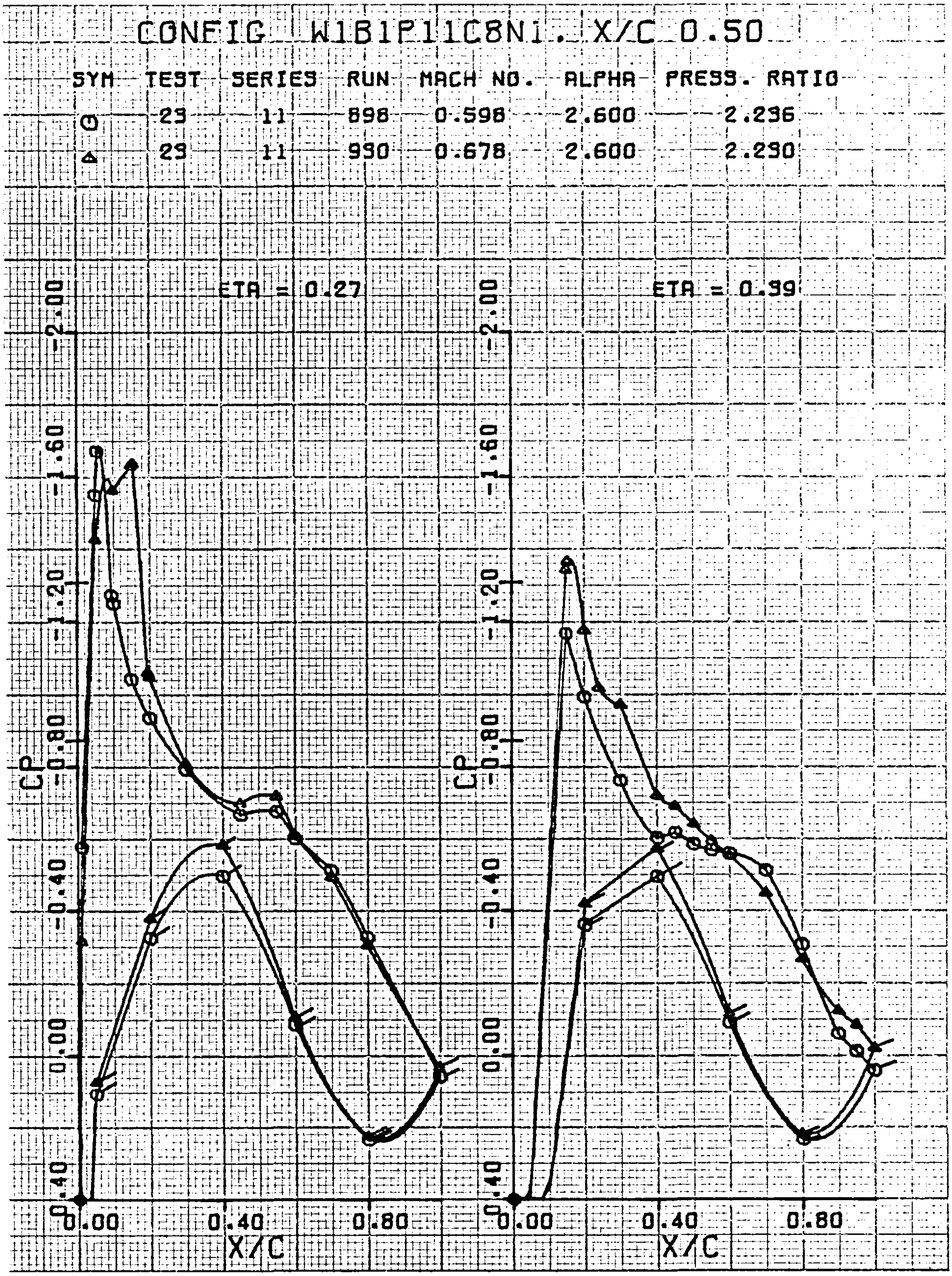

Figure 101. Wing pressure distribution, effect of Mach number, nozzle N_1, $x/c = 0.50$, η = 0.27, 0.39

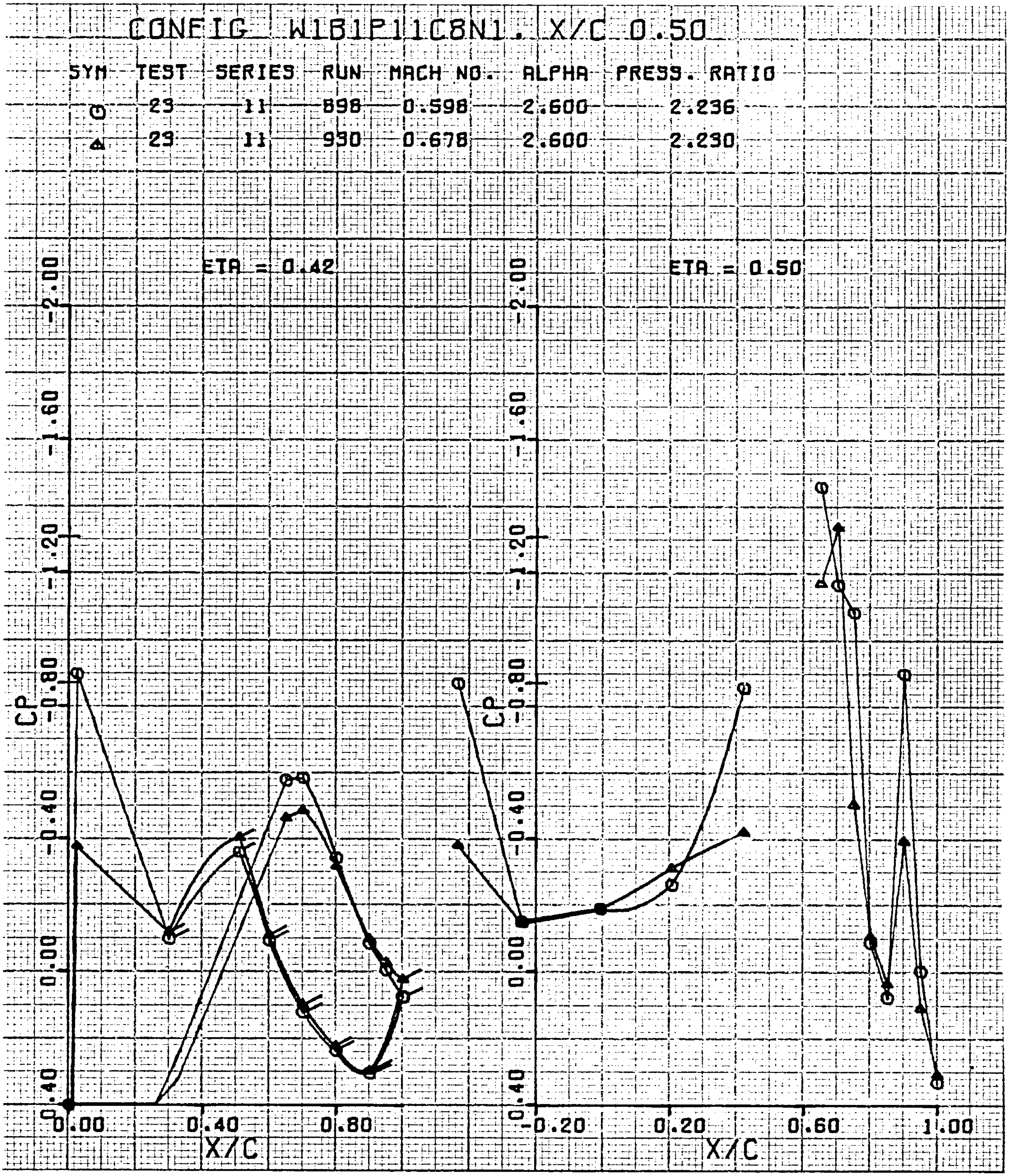

Figure 102. Wing pressure distribution, effect of Mach number, nozzle N_1, $x/c = 0.50$, $\eta = 0.42, 0.50$

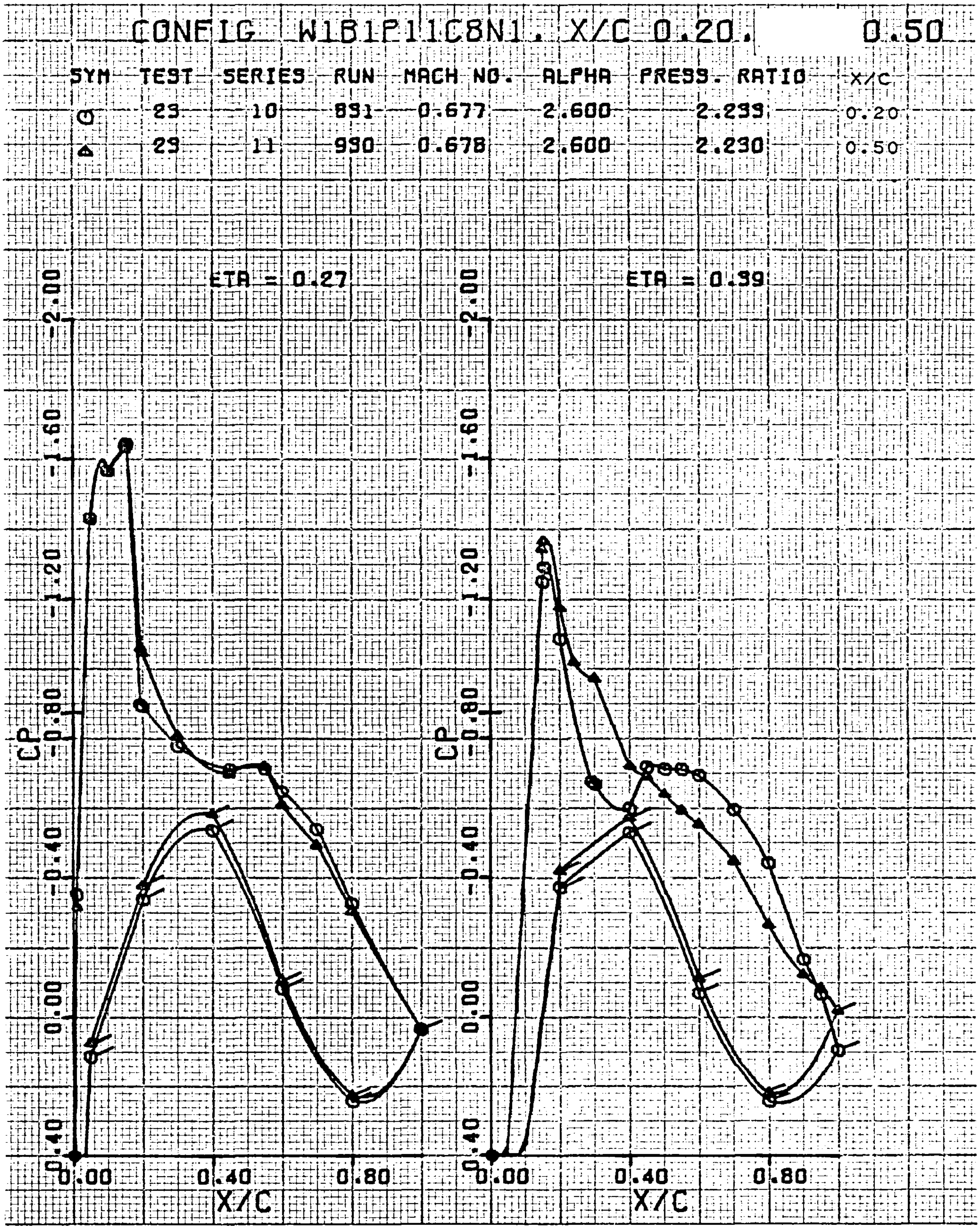

Figure 103. Wing pressure distribution, effect of x/c, nozzle N_1, η = 0.27, 0.39

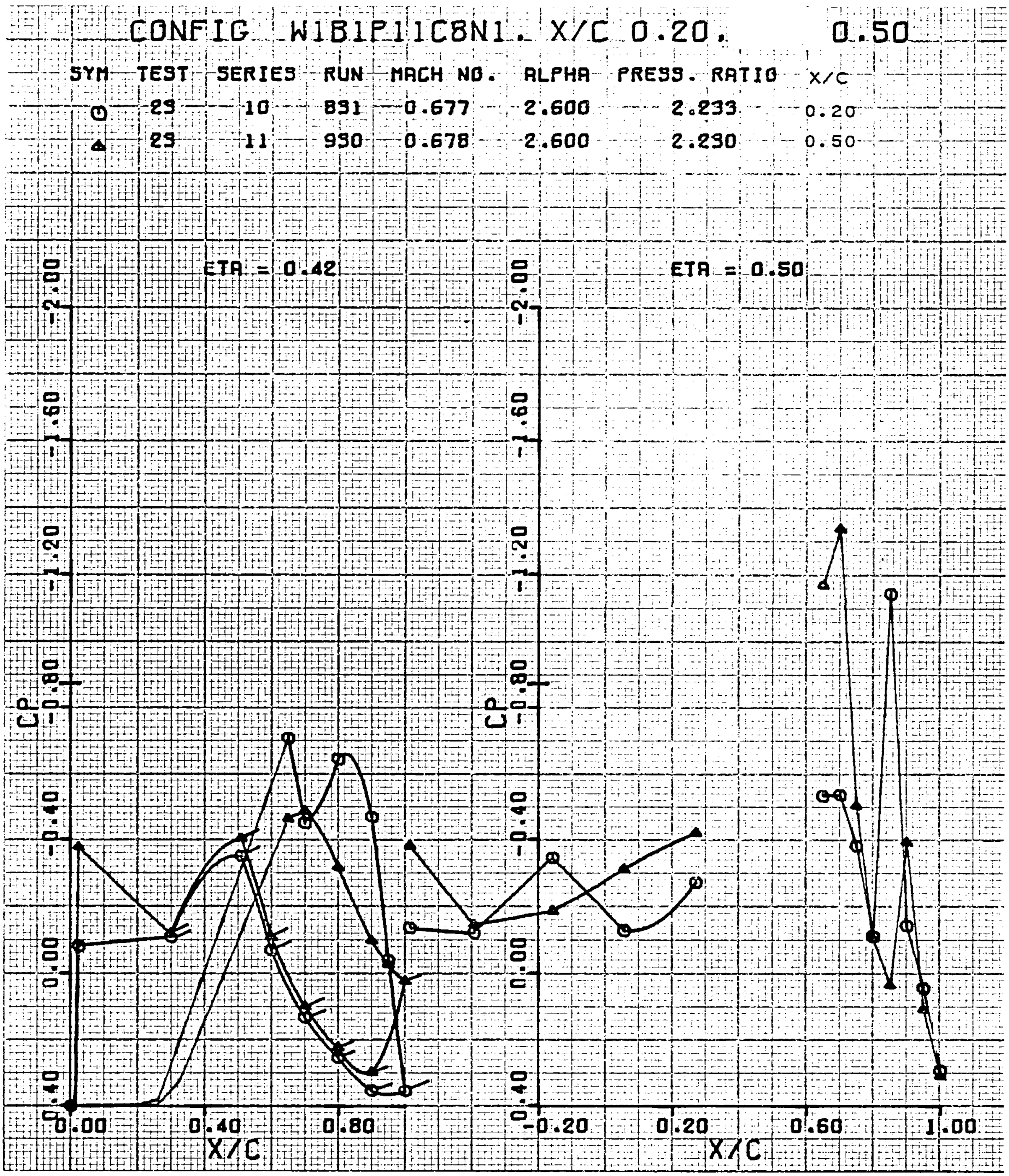

Figure 104. Wing pressure distribution, effect of x/c, nozzle N_1, η = 0.42, 0.50

5.4 Wake Pressure Patterns

Isobars in terms of local total pressure ratios measured one chord length downstream of the wing trailing edge are presented in Figures 105 through 144. Figure 105 is an illustrative example of how an axial projection of the model (nozzle, wing, and pylon fairing) is positioned relative to the coordinate system for the isobars. This relative position is maintained throughout the rest of the isobar figures, although the model projection is not shown.

Model configurations for which wake patterns are presented are selected from the preceding two groups for which pressure distributions are shown. These include N_2, pylon mounted, plus N_3, N_5, and N_6. Nozzles N_2 and N_3 are presented for both upstream pipe and standard installations.

USB CRUISE PROGRAM

CONFIG $W_1\ B_7\ P_8\ C_2\ N_3$

NOZZLE PRESSURE RATIO, H_j/p_∞ = 2.2

M_∞ = 0.70

$\alpha = 2.6^\circ$

NOTES:

(1) CHORD LENGTH, c, IS 0.1778M (7.0 INCHES)

(2) RAKE IS LOCATED ONE CHORD LENGTH BEHIND TRAILING EDGE

(3) H_l/H_∞ IS LOCAL TOTAL PRESSURE RATIO IN THE STREAM AS MEASURED BY THE RAKE

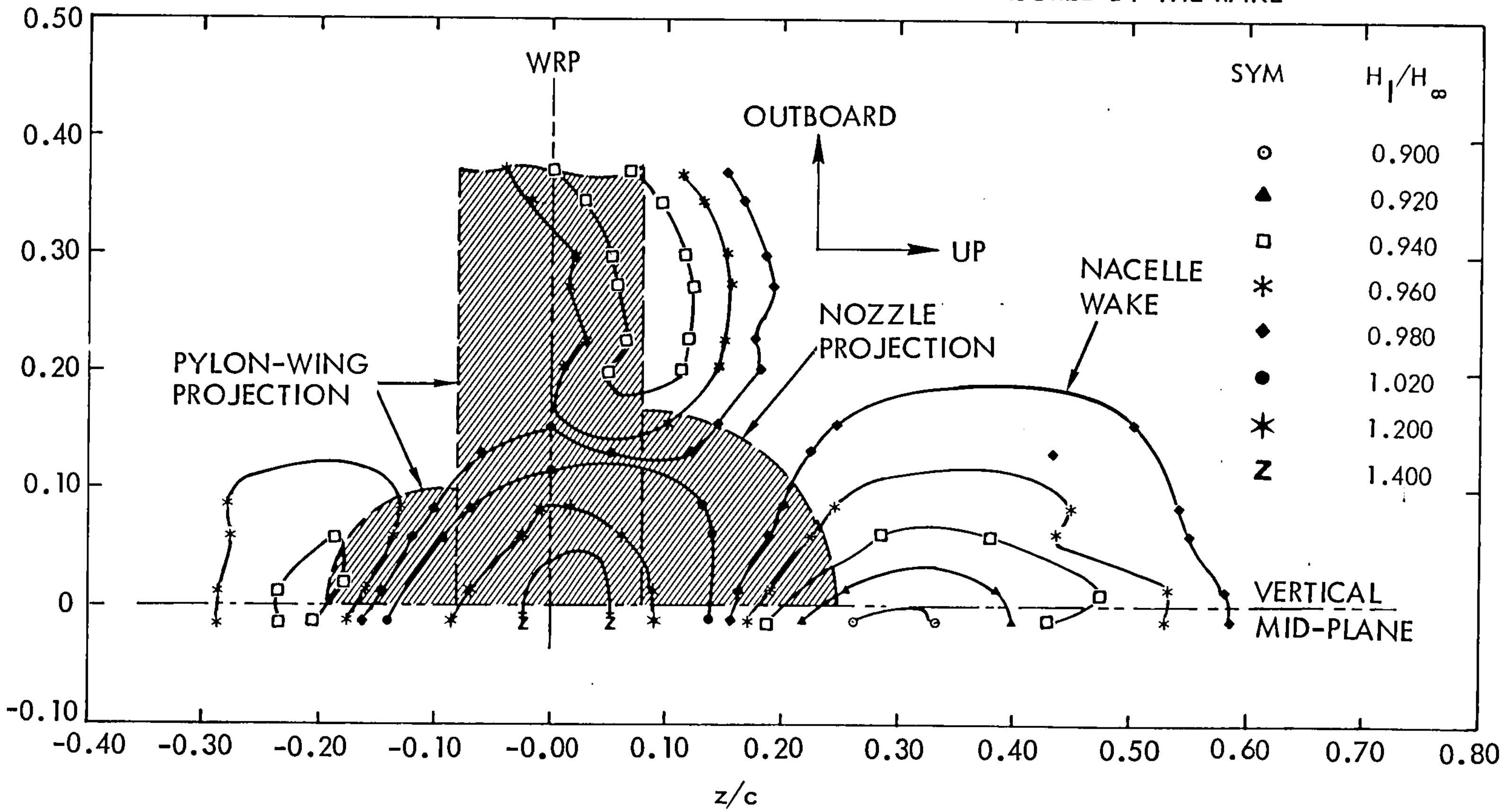

Figure 105. Wake isobar plot, illustration of how the model projection is oriented on grid

USB CRUISE PROGRAM

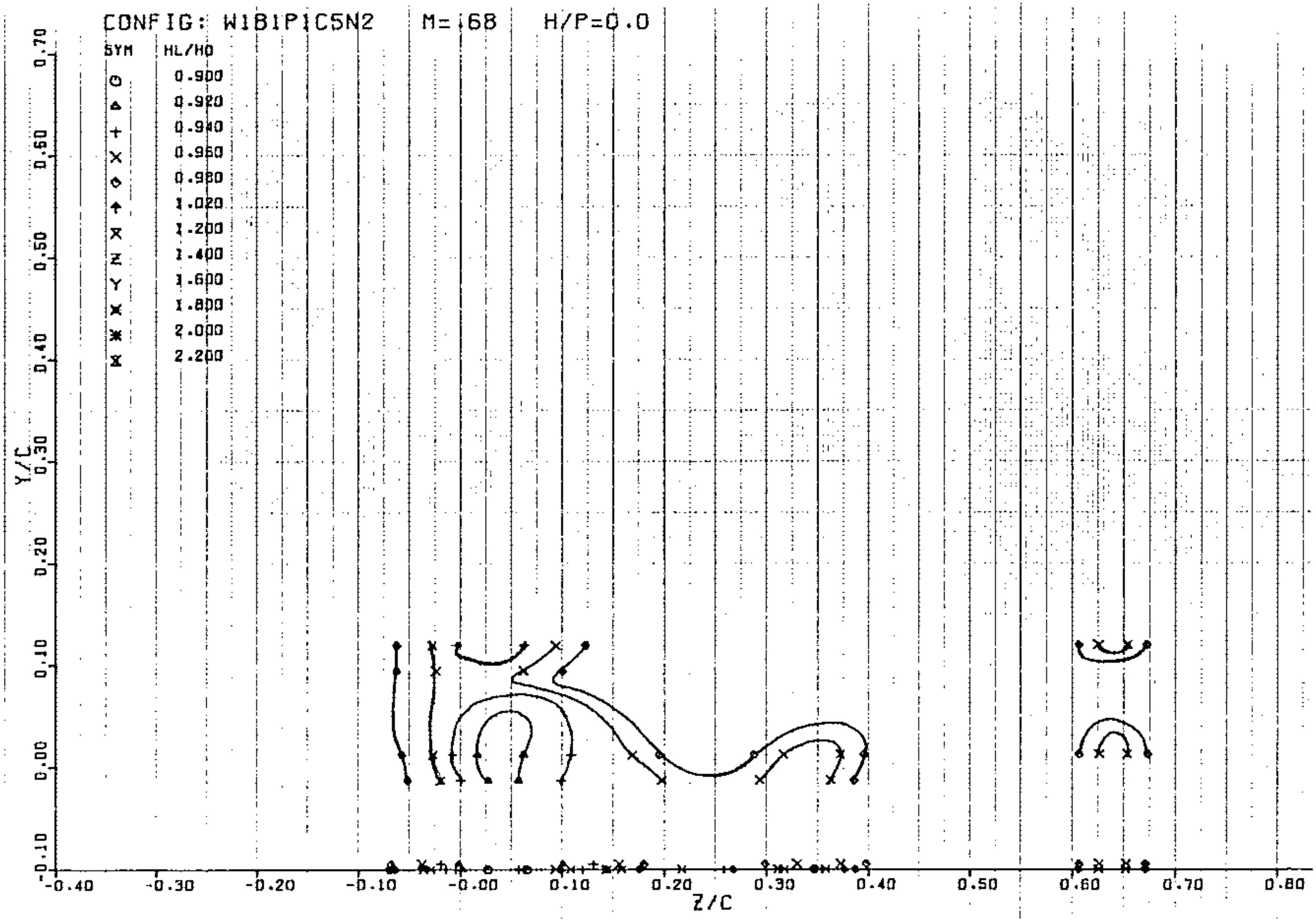

Figure 106. Isobar plot of USB nacelle-wing-jet wake pattern measured one chord length aft of trailing edge, $R_{NC} \approx 3.5 \times 10^6$ test 23, series 1, run numbers 42-45, $\alpha = 3^{\circ}$

USB CRUISE PROGRAM

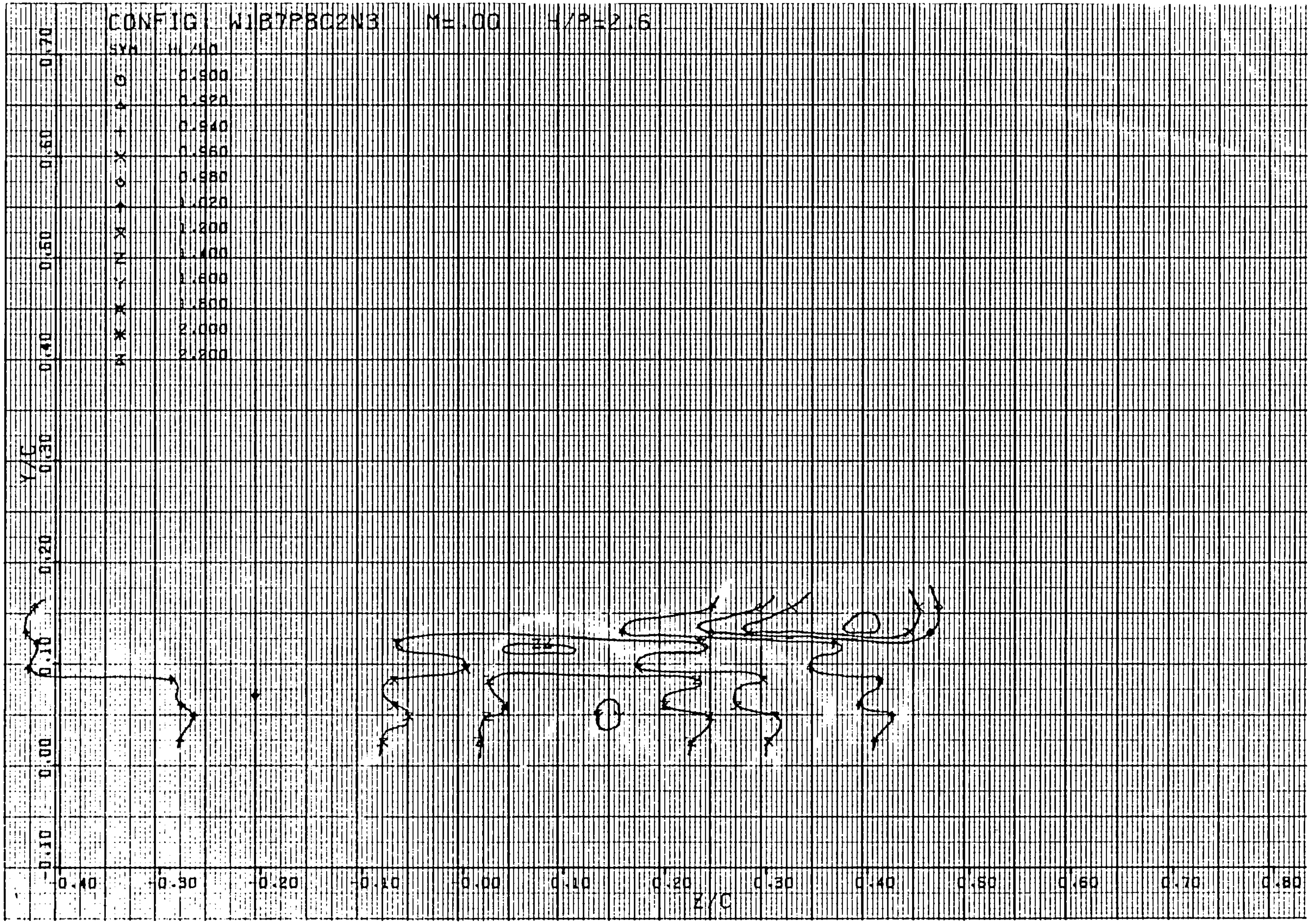

Figure 107. Isobar plot of USB nacelle-wing-jet wake pattern measured one chord length aft of trailing edge, $R_{NC} = 3.5 \times 10^6$ test 23, series 2, run numbers 101 - 104, $\alpha = 0^o$

USB CRUISE PROGRAM

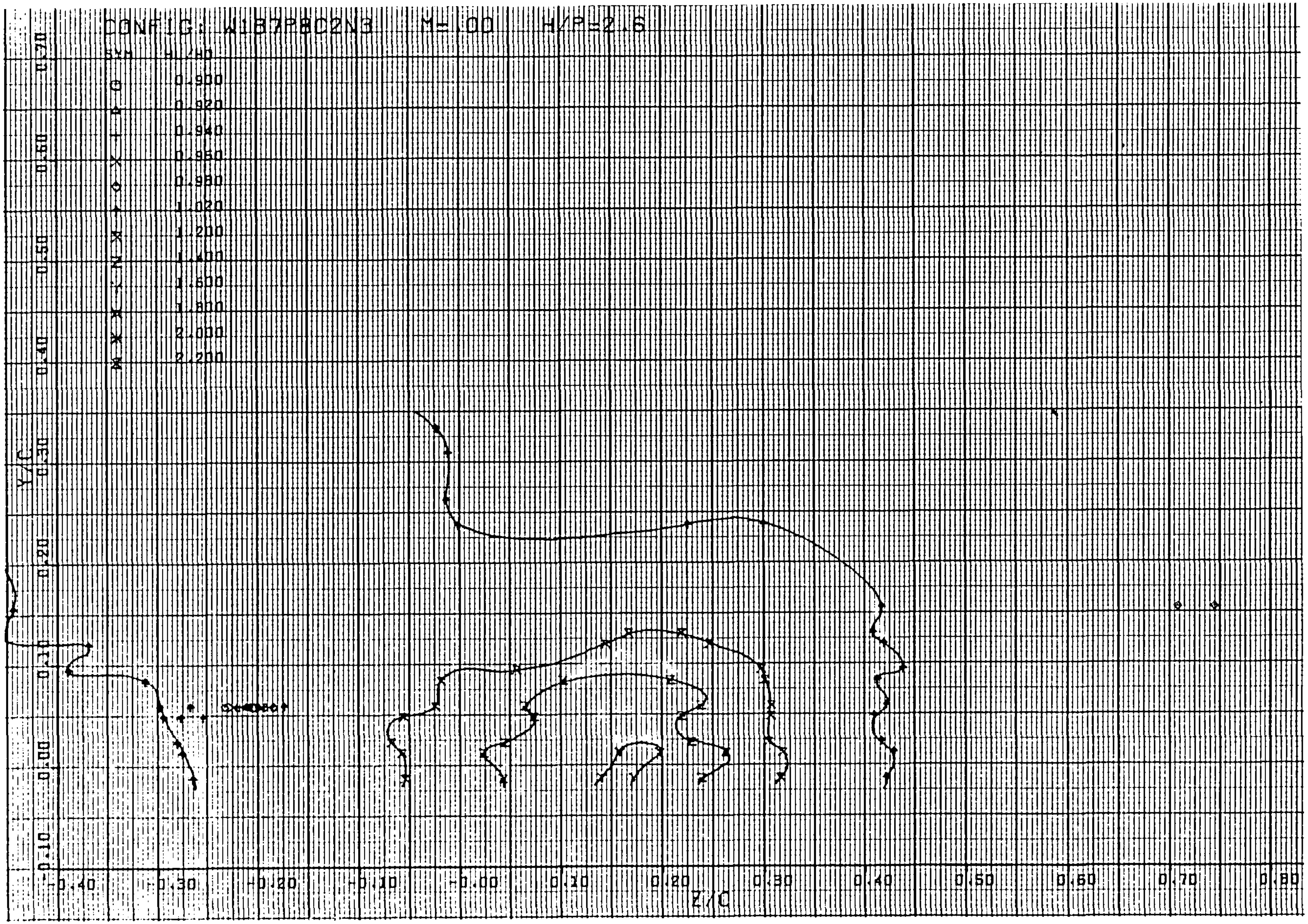

Figure 108. Isobar plot of USB nacelle-wing-jet wake pattern measured one chord length aft of trailing edge, $R_{NC} = 3.5 \times 10^6$ test 23, series 2, run numbers 105 - 111, $\alpha = 0^o$

USB CRUISE PROGRAM

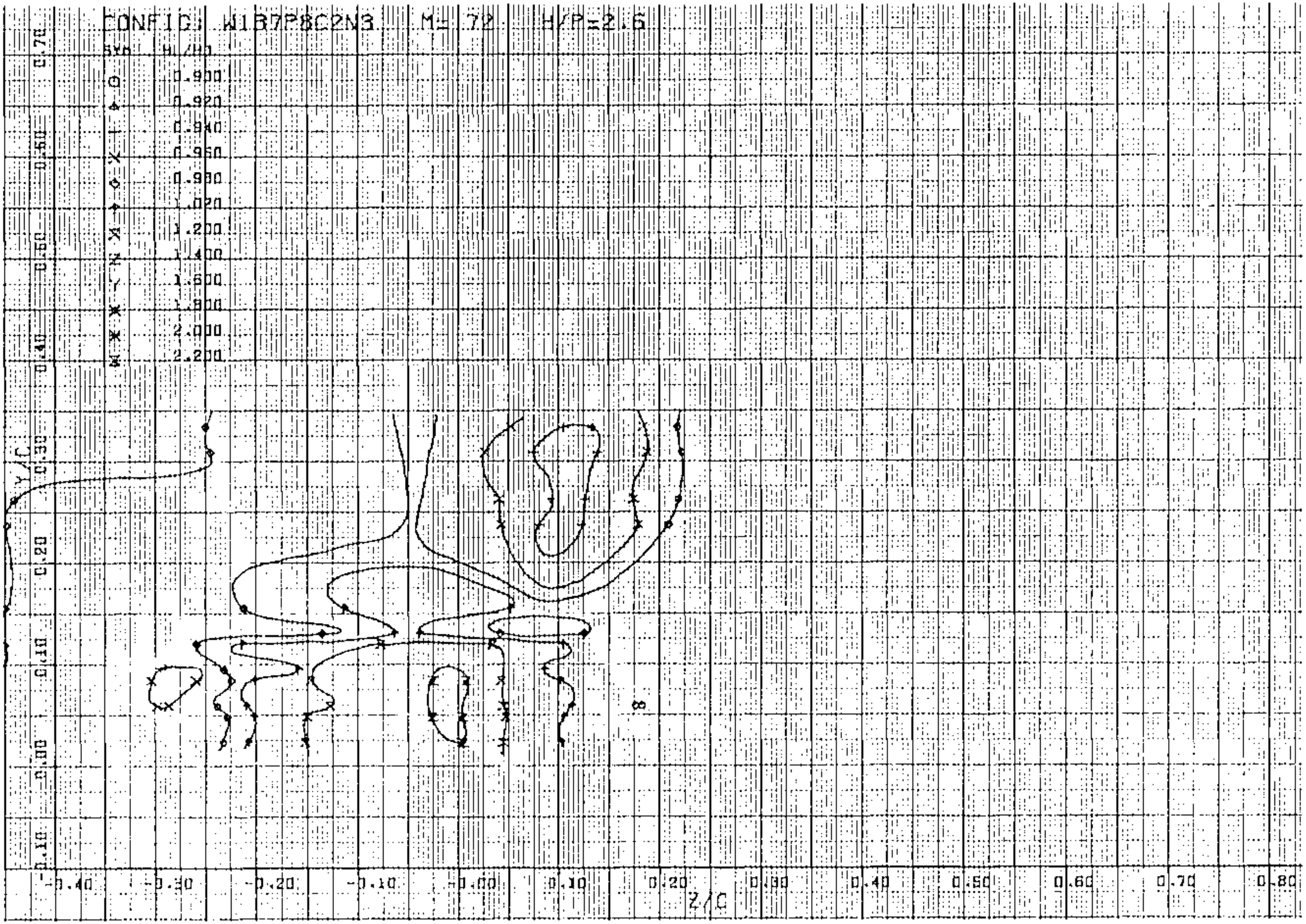

Figure 109. Isobar plot of USB nacelle-wing-jet wake pattern measured one chord length aft of trailing edge, $R_{NC} = 3.5 \times 10^6$ Test 23, series 2, run numbers 132 - 137, $\alpha = 3^o$

USB CRUISE PROGRAM

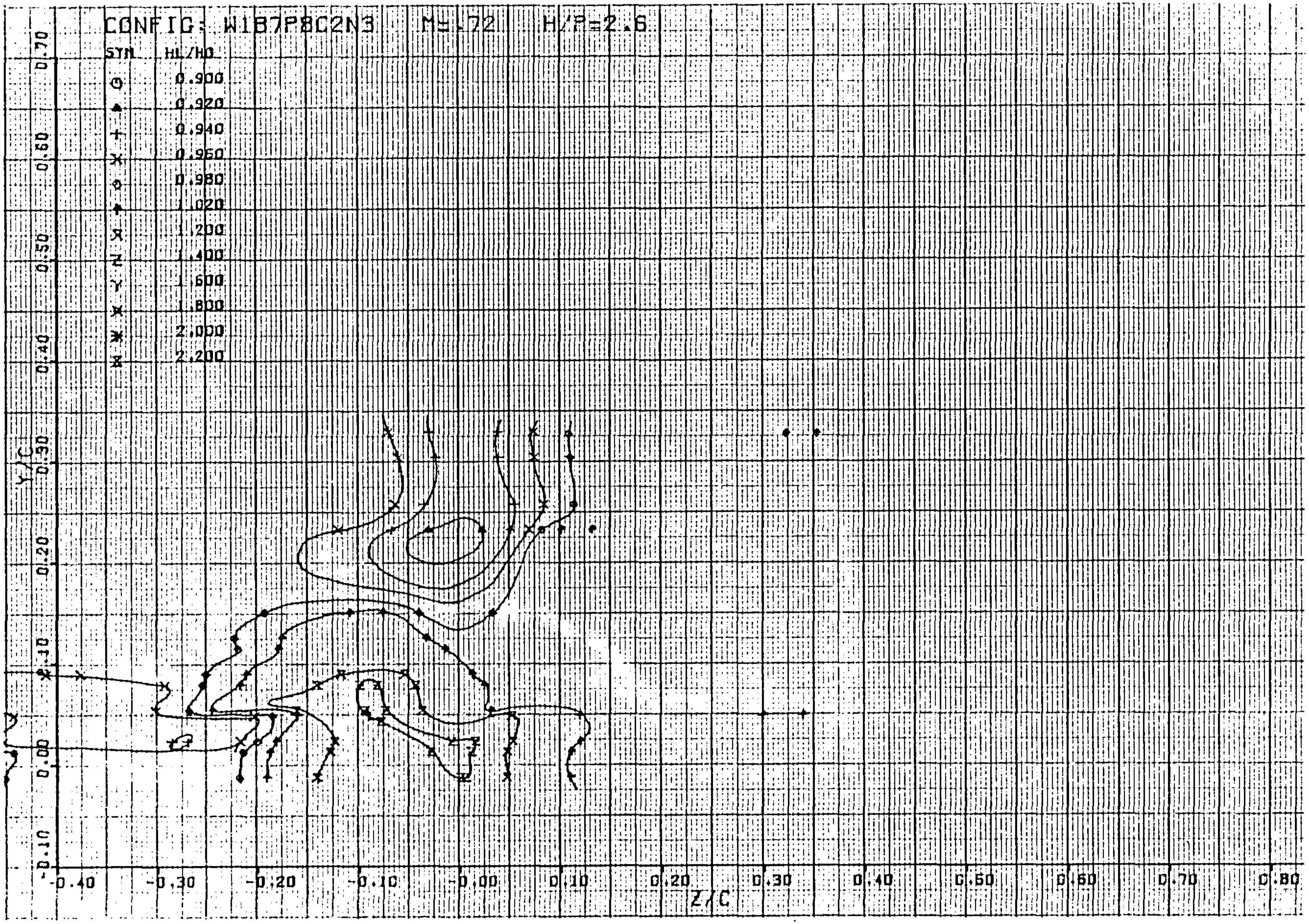

Figure 110. Isobar plot of USB nacelle-wing-jet wake pattern measured one chord length aft of trailing edge, $R_{NC} = 3.5 \times 10^6$, test 23, series 2, run numbers 138 - 144, $\alpha = 3^o$

USB CRUISE PROGRAM

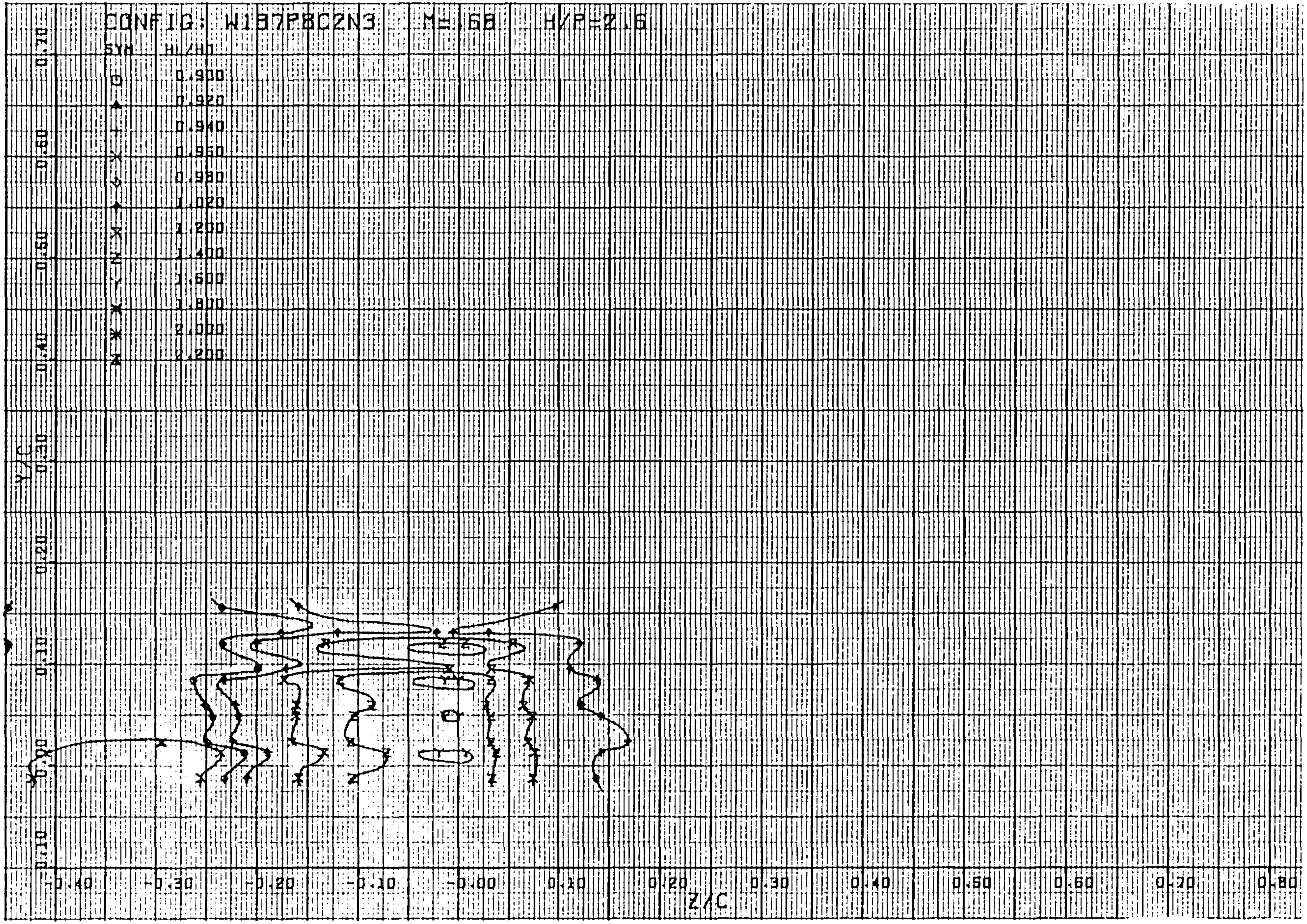

Figure 111. Isobar plot of USB nacelle-wing-jet wake pattern measured one chord length aft of trailing edge, $R_{NC} = 3.5 \times 10^6$, test 23, series 2, run numbers 145 - 149, $\alpha = 3^o$

USB CRUISE PROGRAM

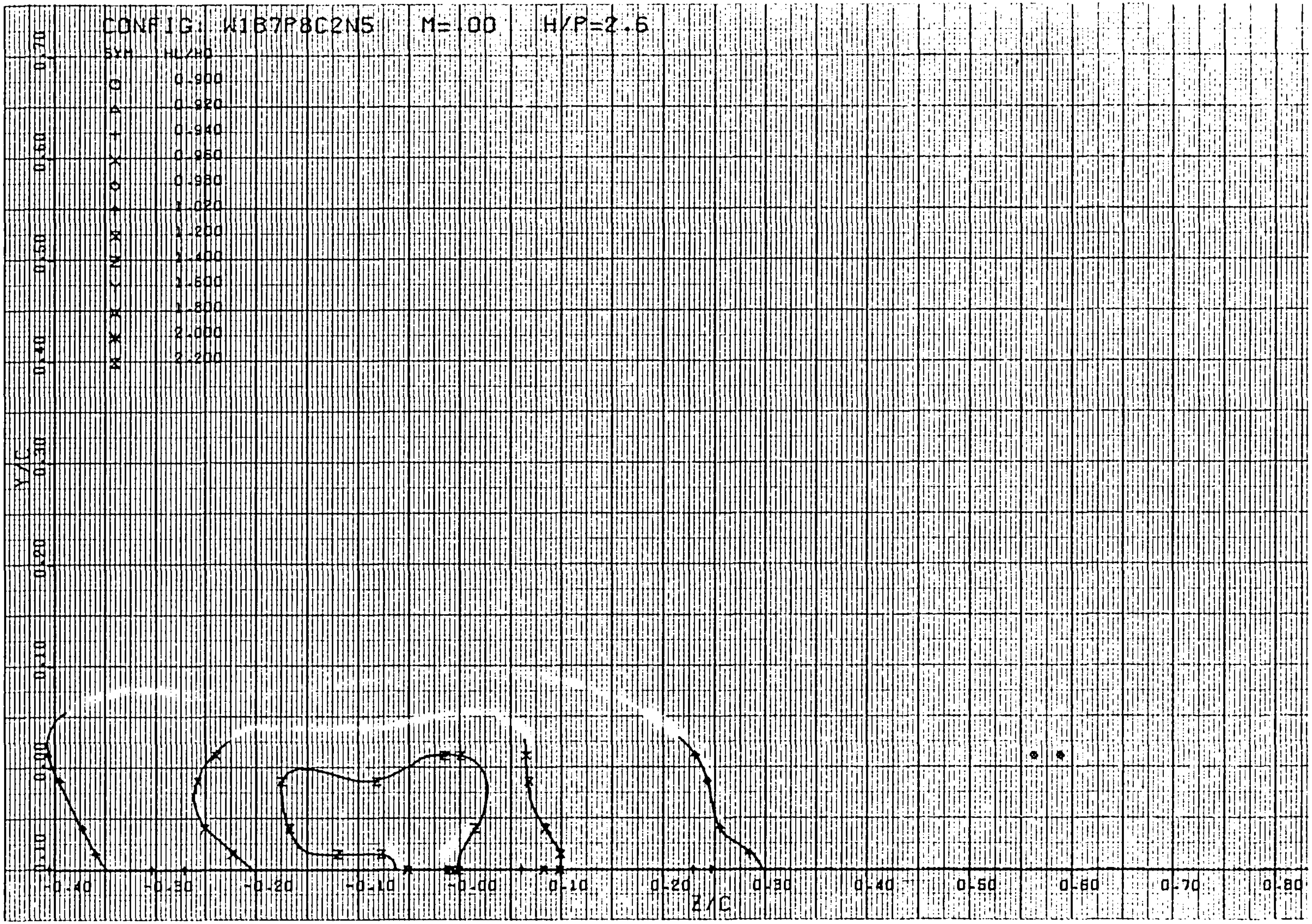

Figure 112. Isobar plot of USB nacelle-wing-jet wake pattern measured one chord length aft of trailing edge, $R_{NC} = 3.5 \times 10^6$, test 23, series 3, run numbers 210-213, $\alpha = 0^o$

USB CRUISE PROGRAM

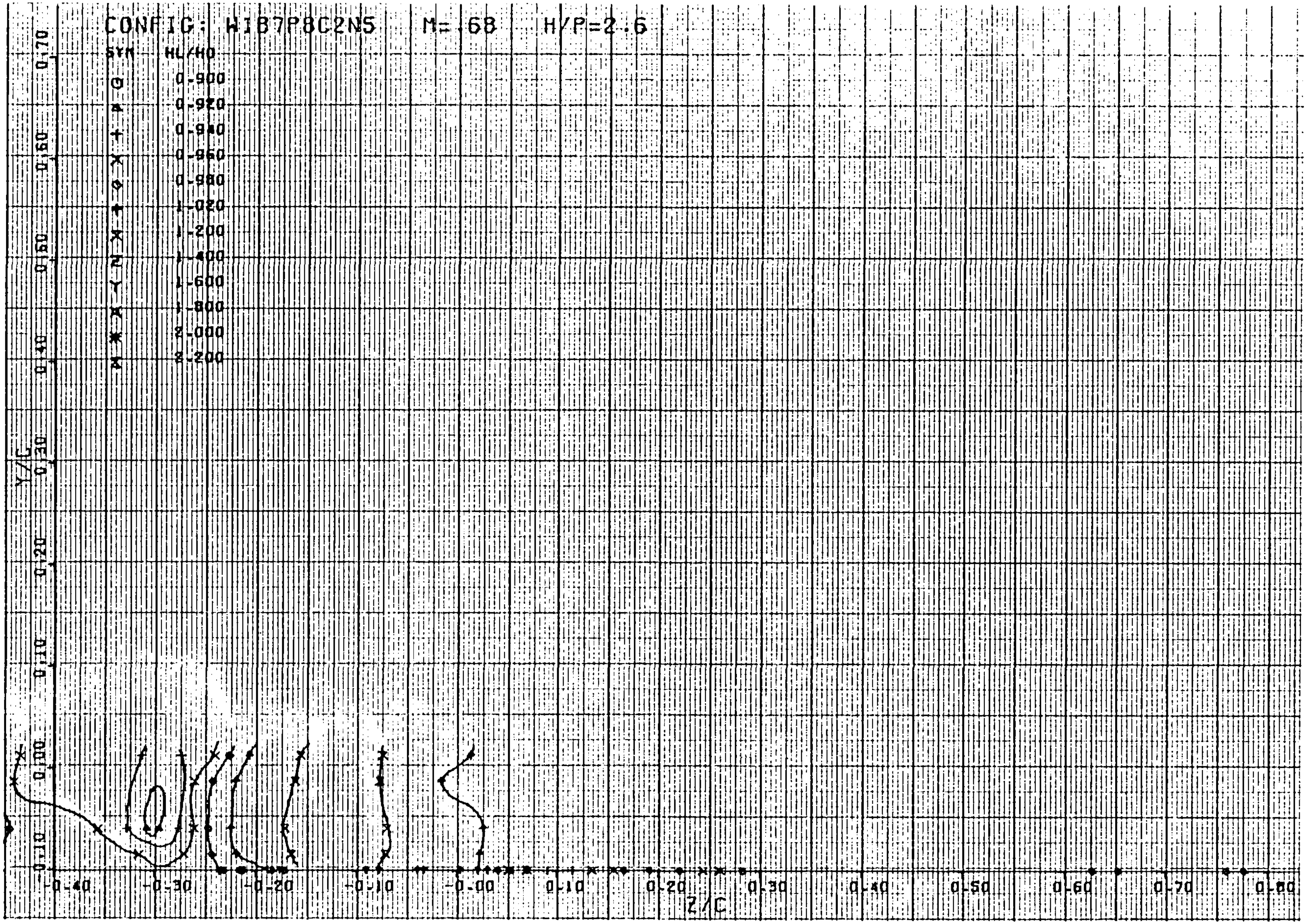

Figure 113. Isobar plot of USB nacelle-wing-jet wake pattern measured one chord length aft of trailing edge, $R_{NC} = 3.5 \times 10^6$, test 23, series 3, run numbers 206 - 209, $\alpha = 3^\circ$

USB CRUISE PROGRAM

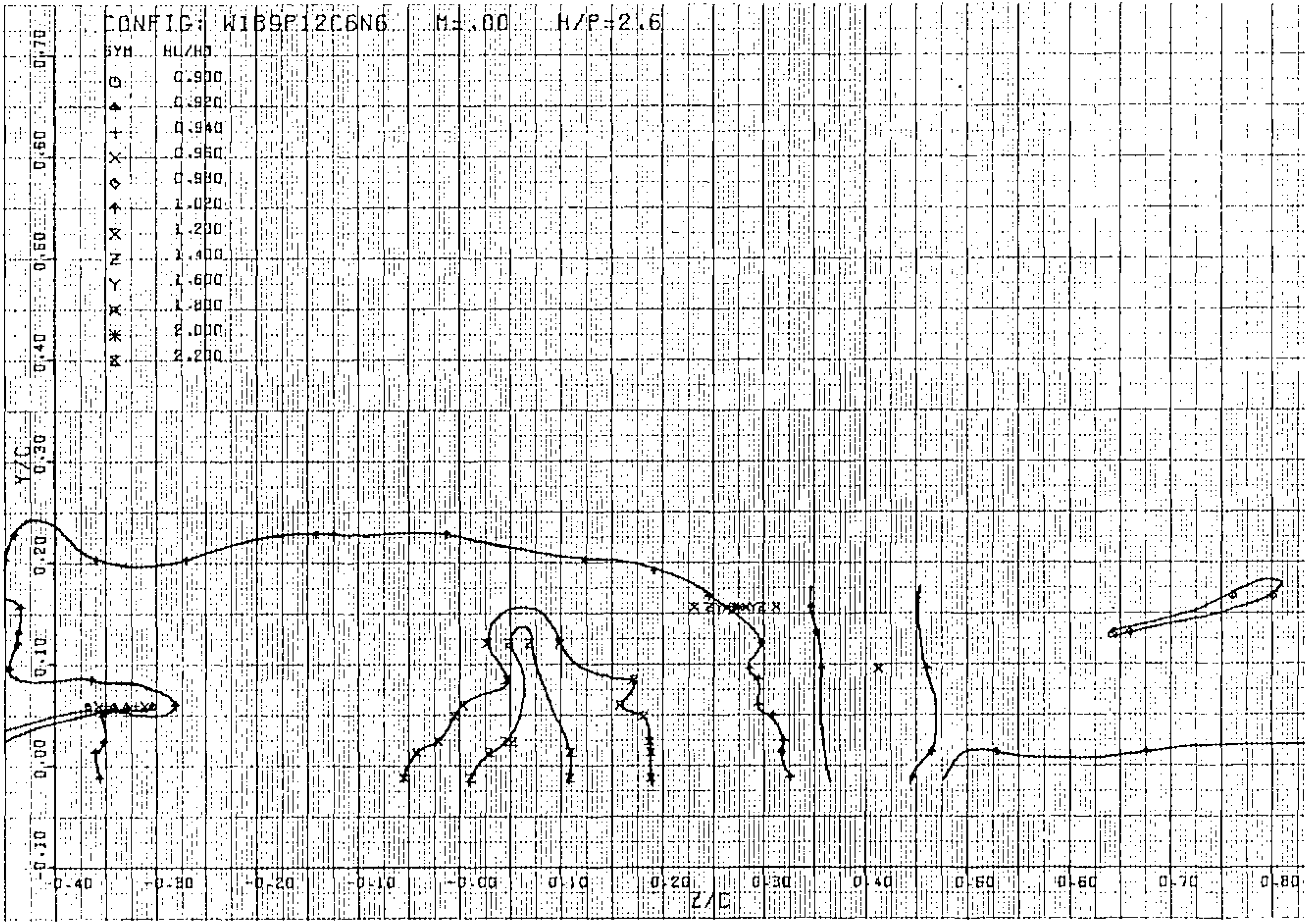

Figure 114. Isobar plot of USB nacelle-wing-jet wake pattern measured one chord length aft of trailing edge, $R_{NC} = 3.5 \times 10^6$, test 23, series 4, run numbers 270 - 276, $\alpha = 0°$

USB CRUISE PROGRAM

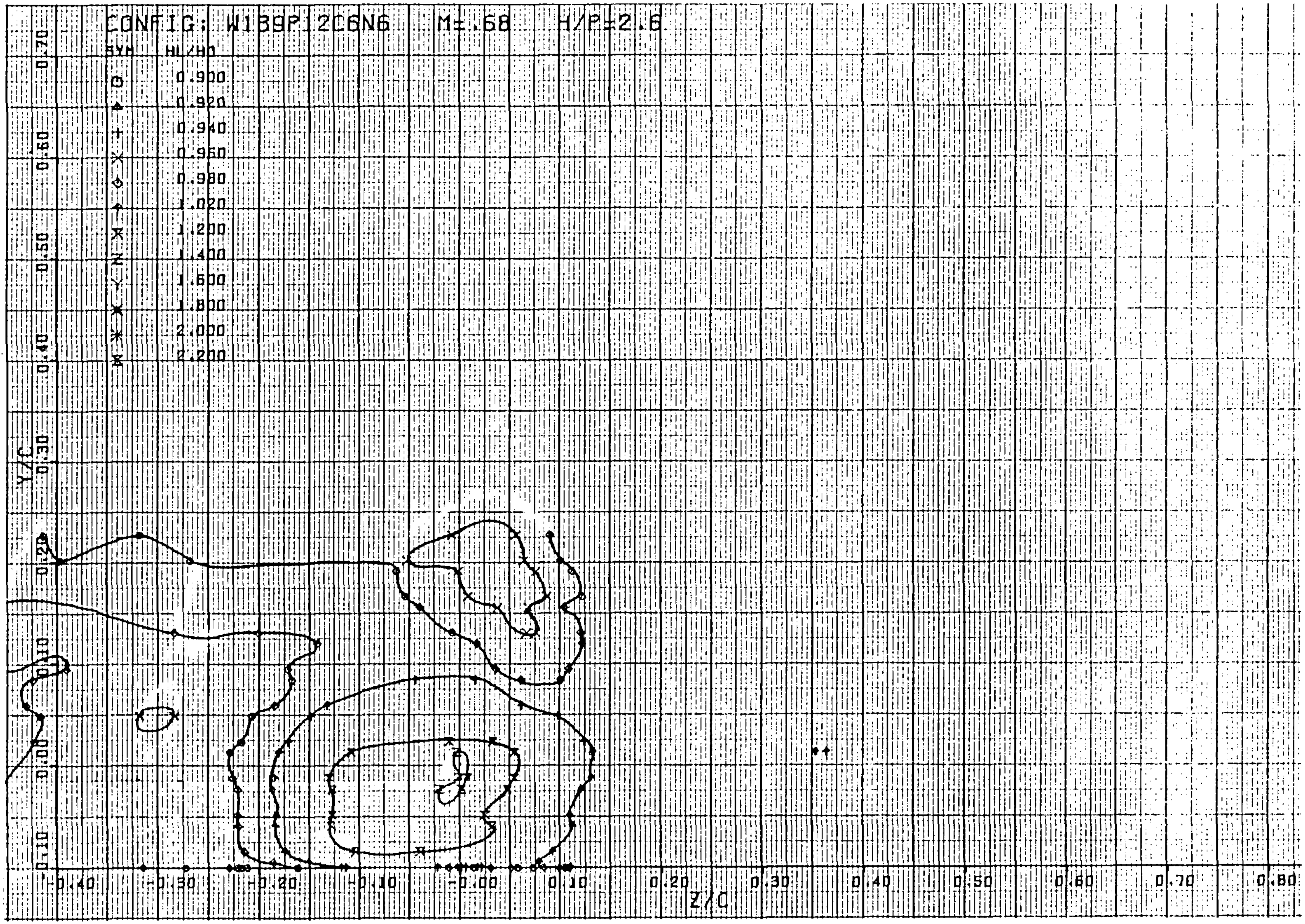

Figure 115. Isobar plot of USB nacelle-wing-jet wake pattern measured one chord length aft of trailing edge, $R_{NC} = 3.5 \times 10^6$, test 23, series 4, run numbers 290 - 302, $\alpha = 3^o$

USB CRUISE PROGRAM

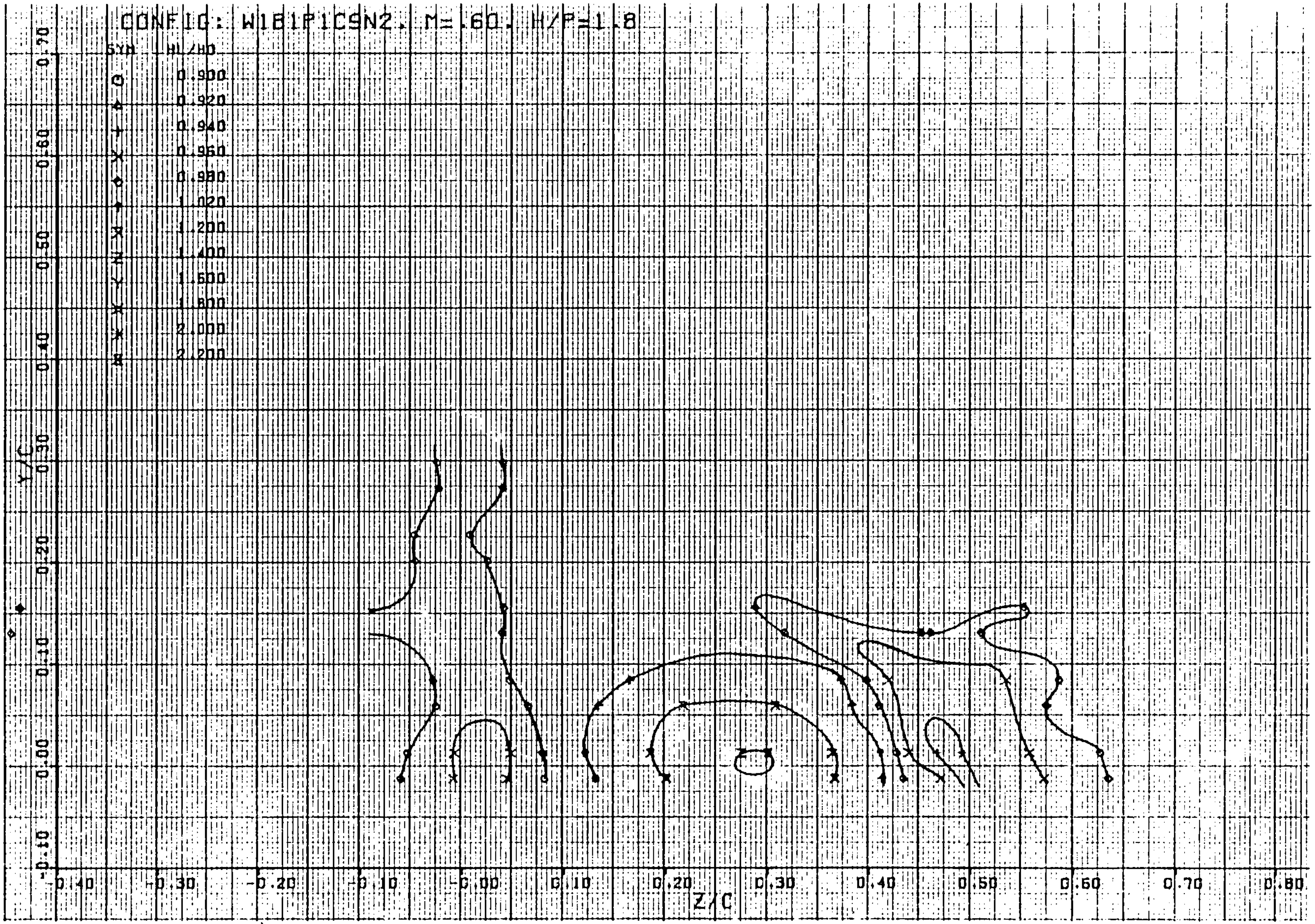

Figure 116. Isobar plot of USB nacelle-wing-jet wake pattern measured one chord length aft of trailing edge, $R_{NC} = 3.5 \times 10^6$, test 23, series 5, run numbers 307-311, $\alpha = 2.6^o$

USB CRUISE PROGRAM

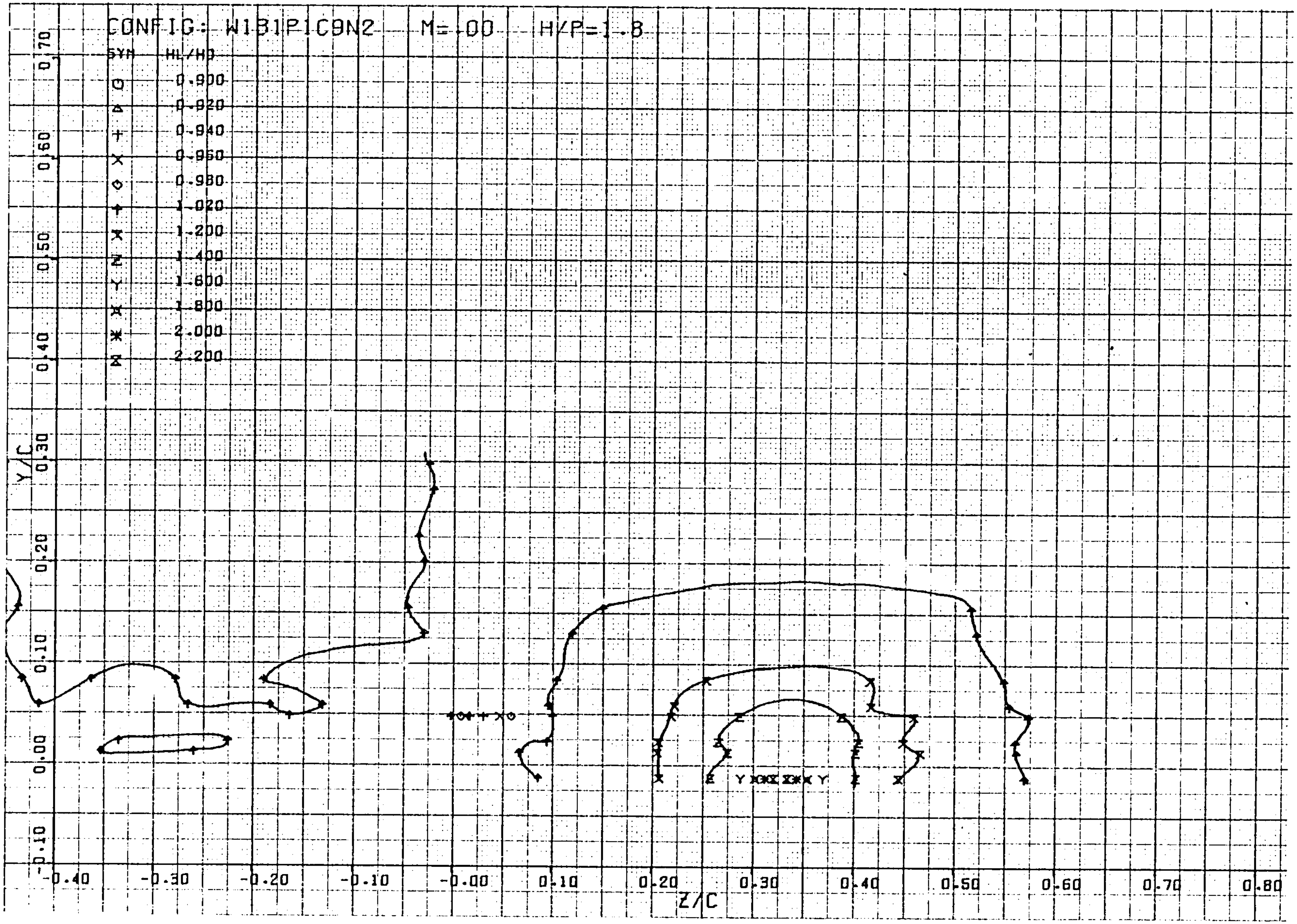

Figure 117. Isobar plot of USB nacelle-wing-jet wake pattern measured one chord length aft of trailing edge, $R_{NC} = 3.5 \times 10^6$, test 23, series 5, run numbers 323-328, $\alpha = 2.6°$

USB CRUISE PROGRAM

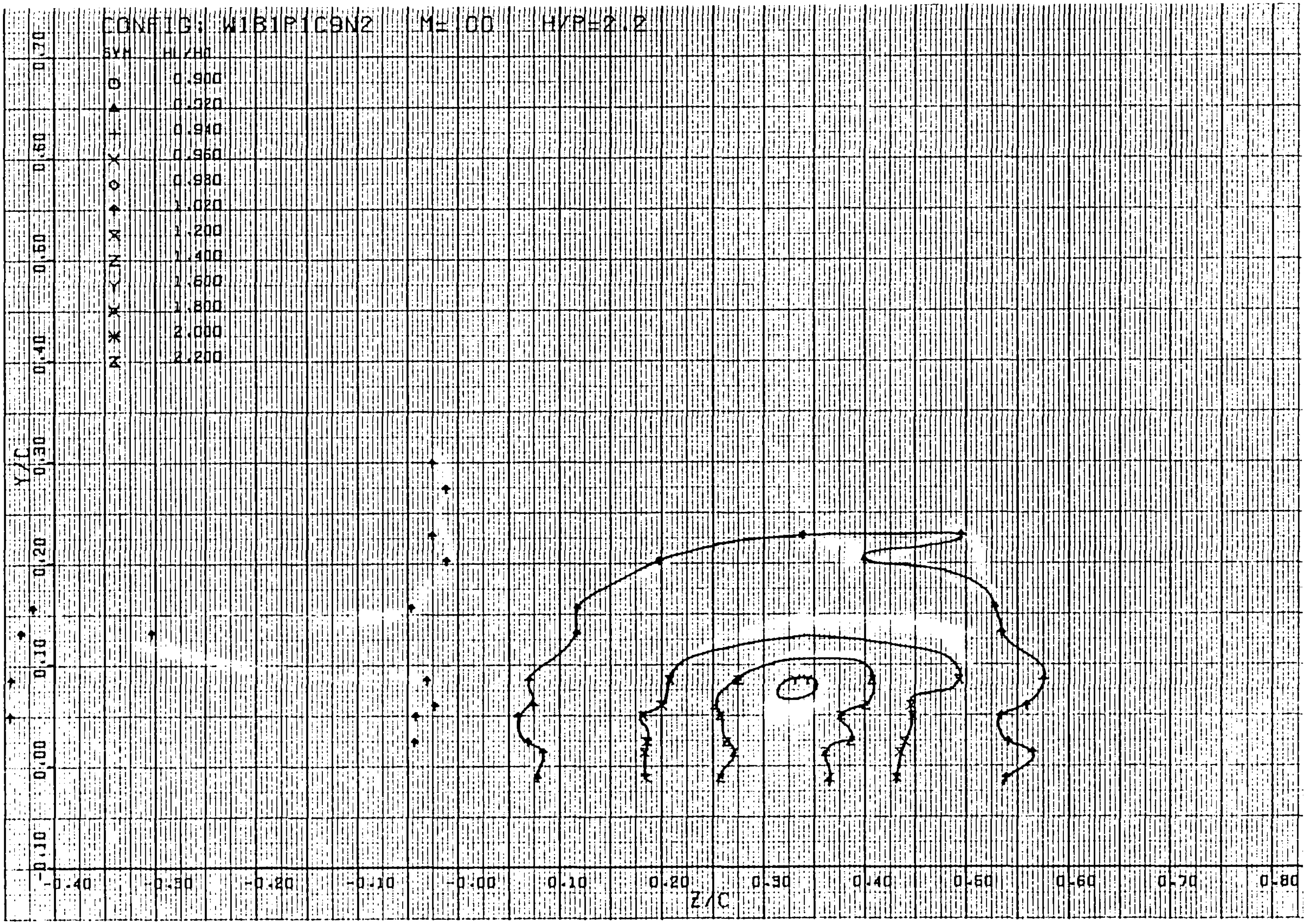

Figure 118. Isobar plot of USB nacelle-wing-jet wake pattern measured one chord length aft of trailing edge, $R_{NC} = 3.5 \times 10^6$, test 23, series 5, run numbers 329-334, $\alpha = 2.6°$

USB CRUISE PROGRAM

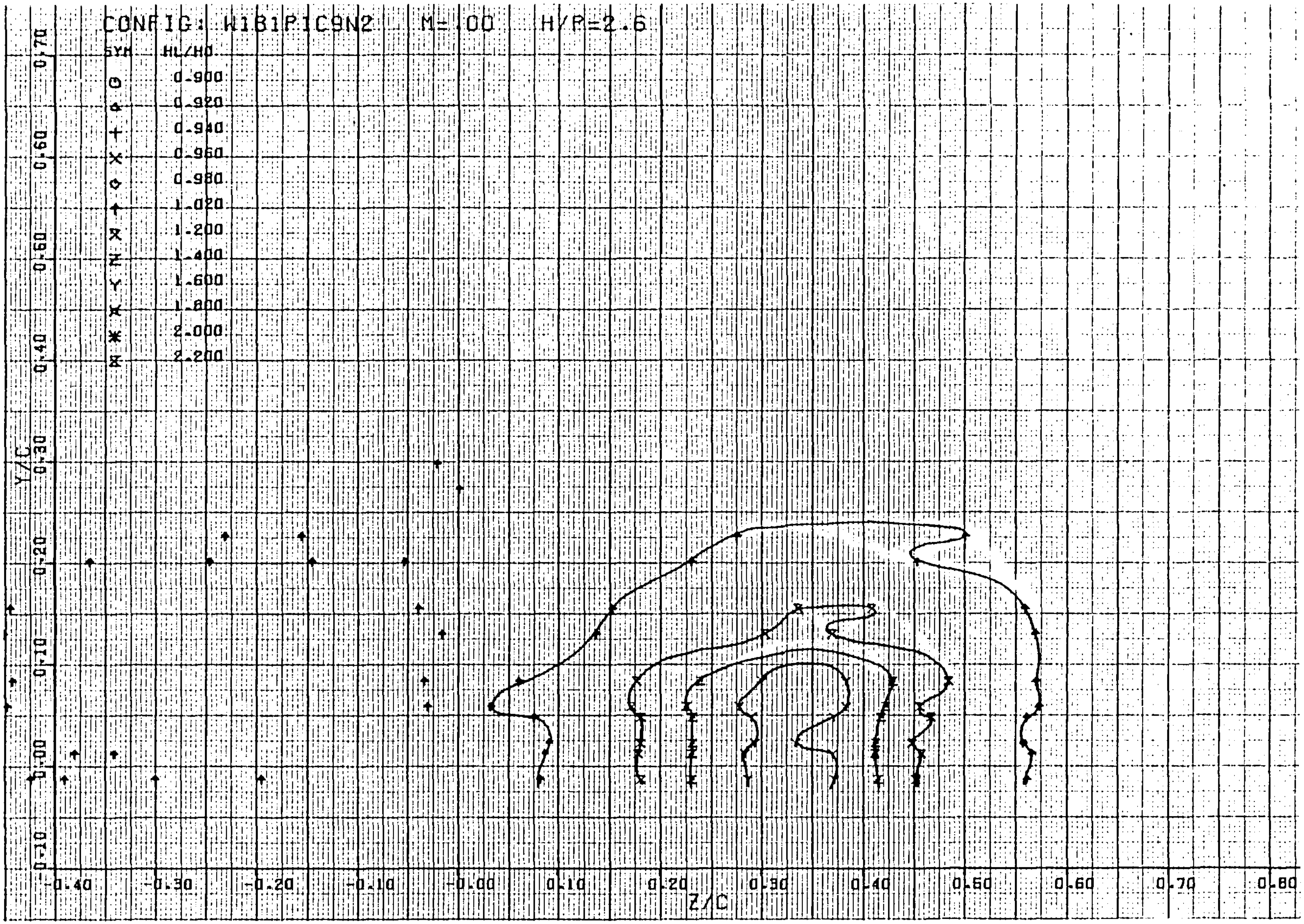

Figure 119. Isobar plot of USB nacelle-wing-jet wake pattern measured one chord length aft of trailing edge, $R_{NC} = 3.5 \times 10^6$, test 23, series 5, run numbers 335 - 340, $\alpha = 2.6^\circ$

USB CRUISE PROGRAM

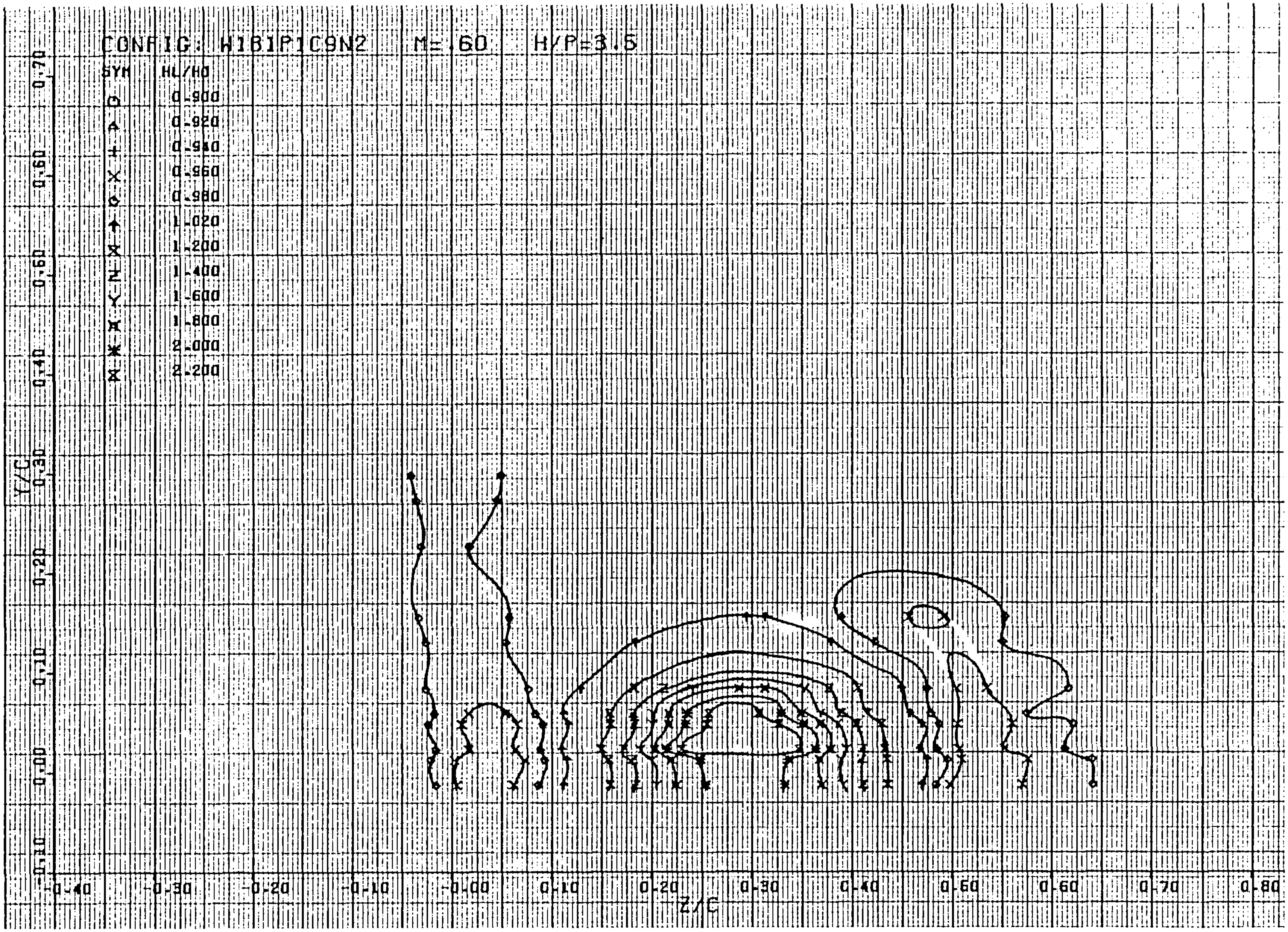

Figure 120. Isobar plot of USB nacelle-wing-jet wake pattern measured one chord length aft of trailing edge, $R_{NC} = 3.5 \times 10^6$, test 23, series 5, run numbers 341 - 346, $\alpha = 2.6°$

USB CRUISE PROGRAM

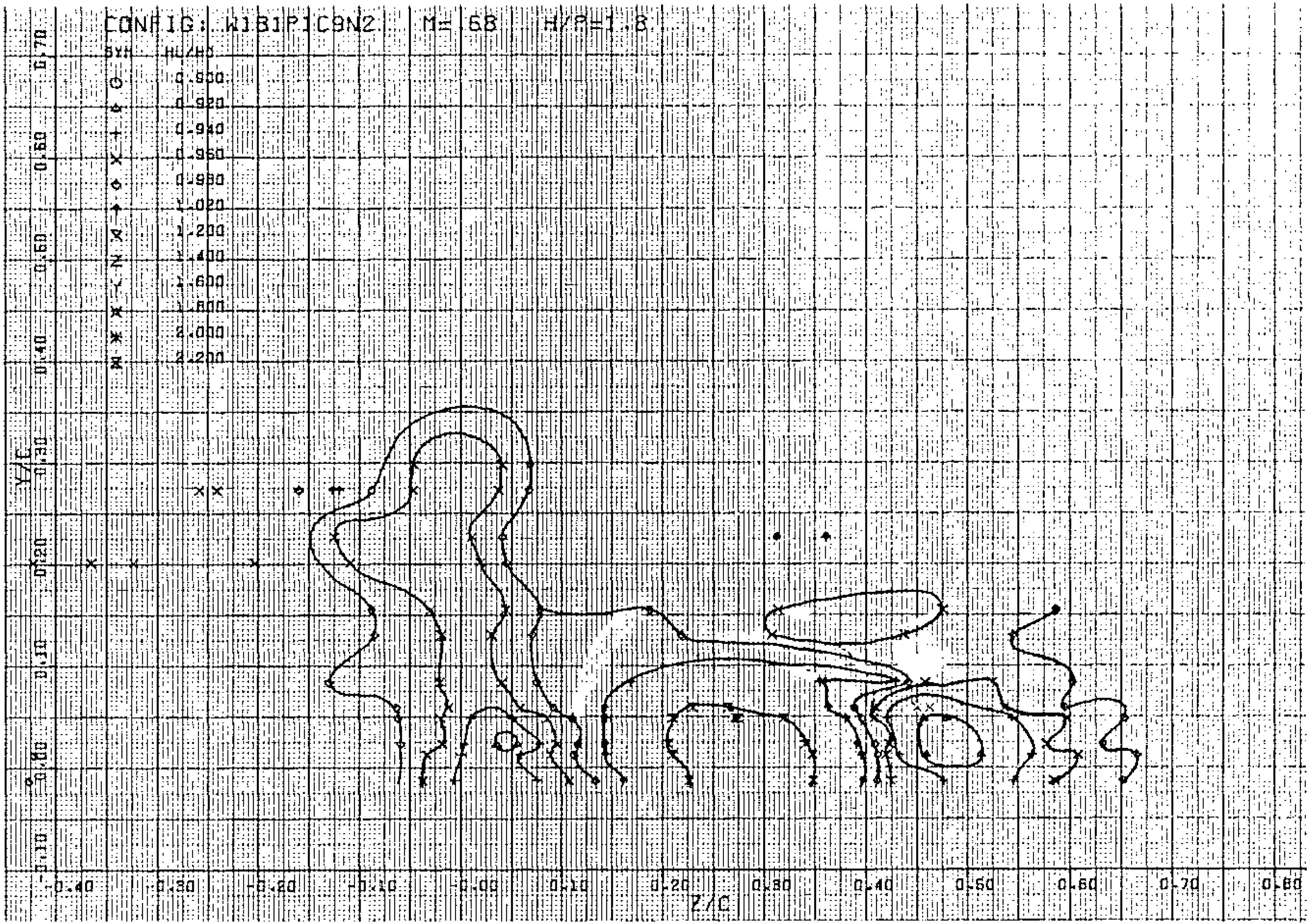

Figure 121. Isobar plot of USB nacelle-wing-jet wake pattern measured one chord length aft of trailing edge, $R_{NC} = 3.5 \times 10^6$, test 23, series 5, run numbers 349-354, $\alpha = 2.6^o$

USB CRUISE PROGRAM

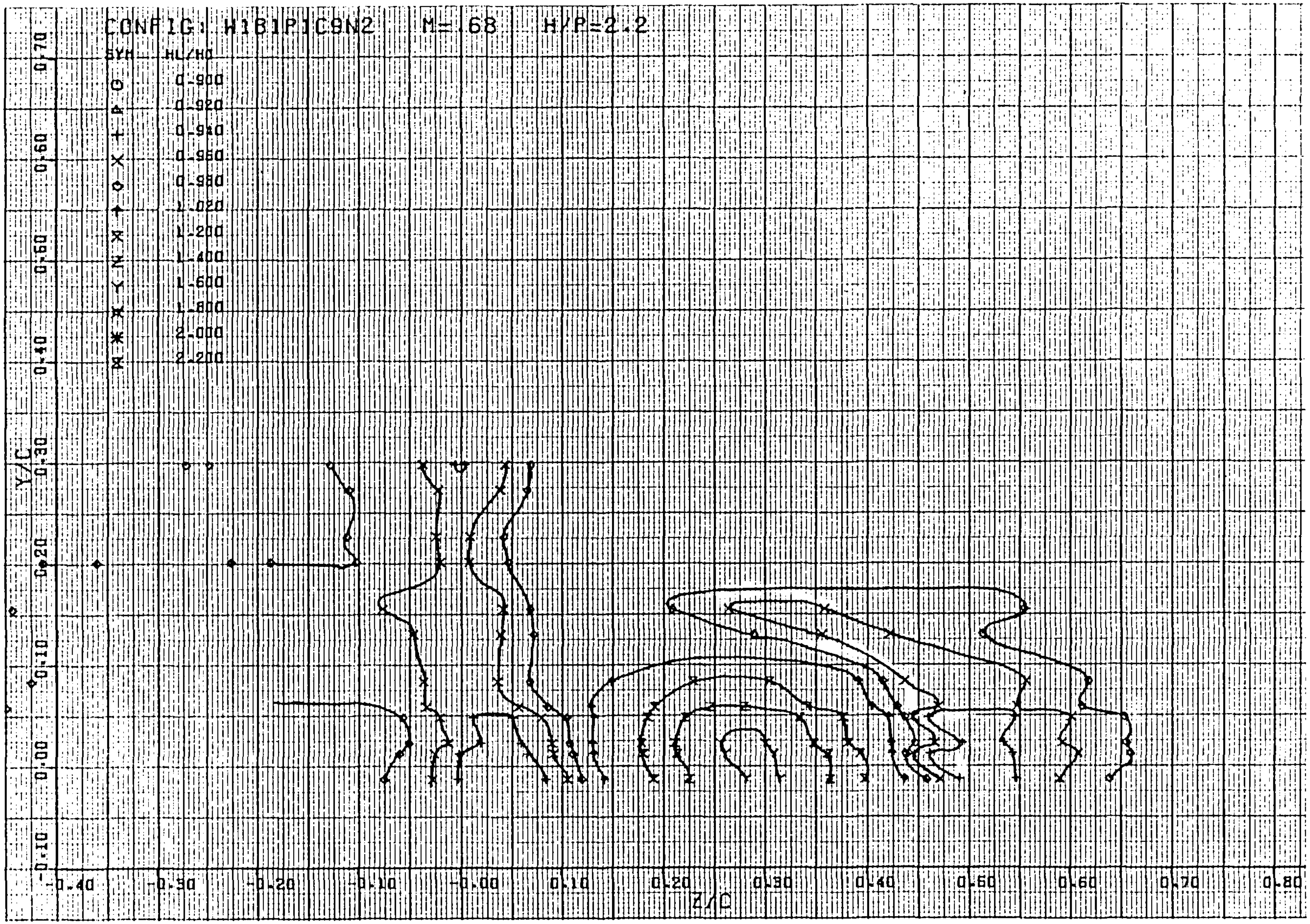

Figure 122. Isobar plot of USB nacelle-wing-jet wake pattern measured one chord length aft of trailing edge, $R_{NC} = 3.5 \times 10^6$, *test 23, series 5, run numbers 355-361*, $\alpha = 2.6^o$

USB CRUISE PROGRAM

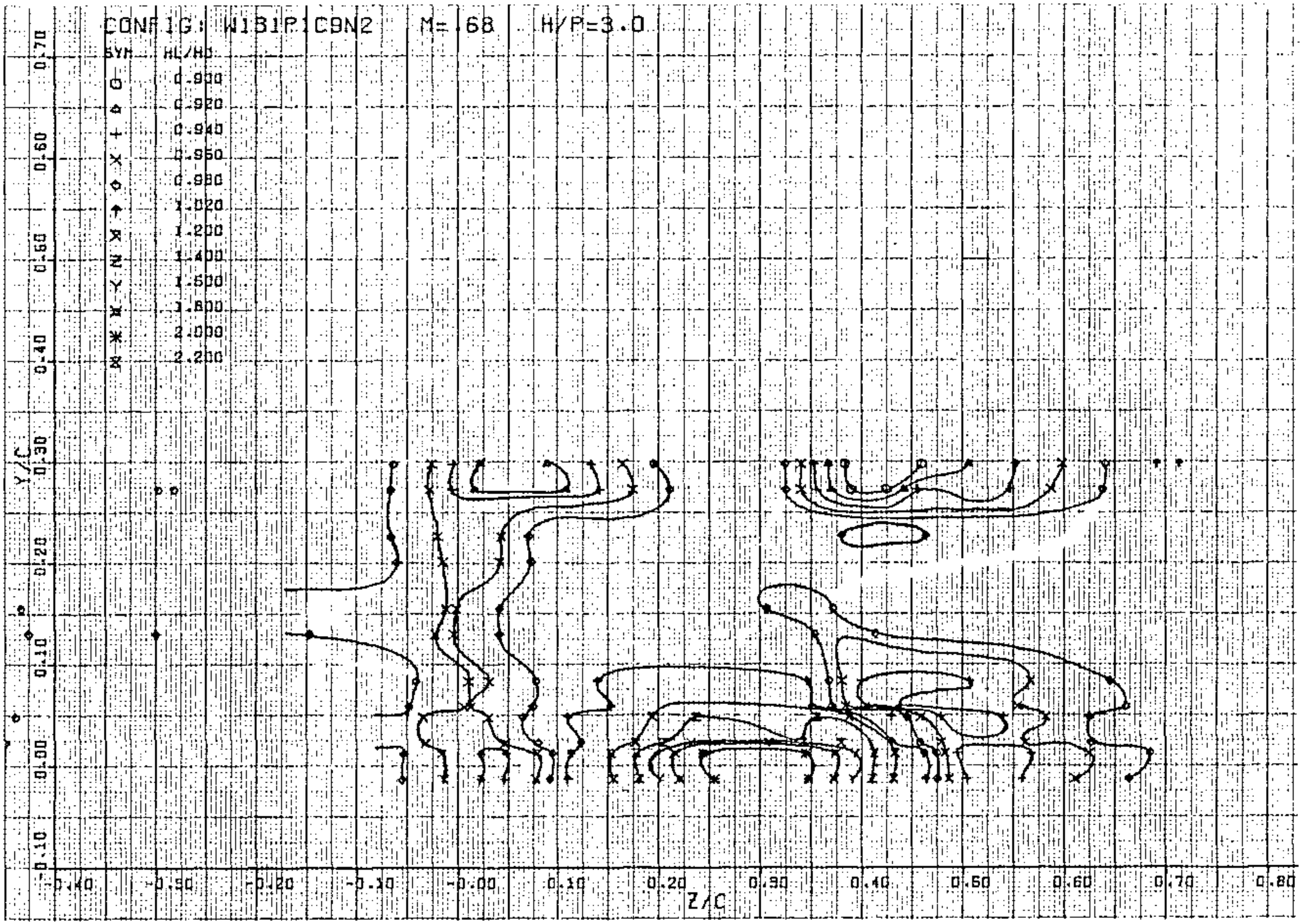

Figure 123. Isobar plot of USB nacelle-wing-jet wake pattern measured one chord length aft of trailing edge, $R_{NC} = 3.5 \times 10^6$, test 23, series 5, run numbers 362-369, $\alpha = 2.6^o$

USB CRUISE PROGRAM

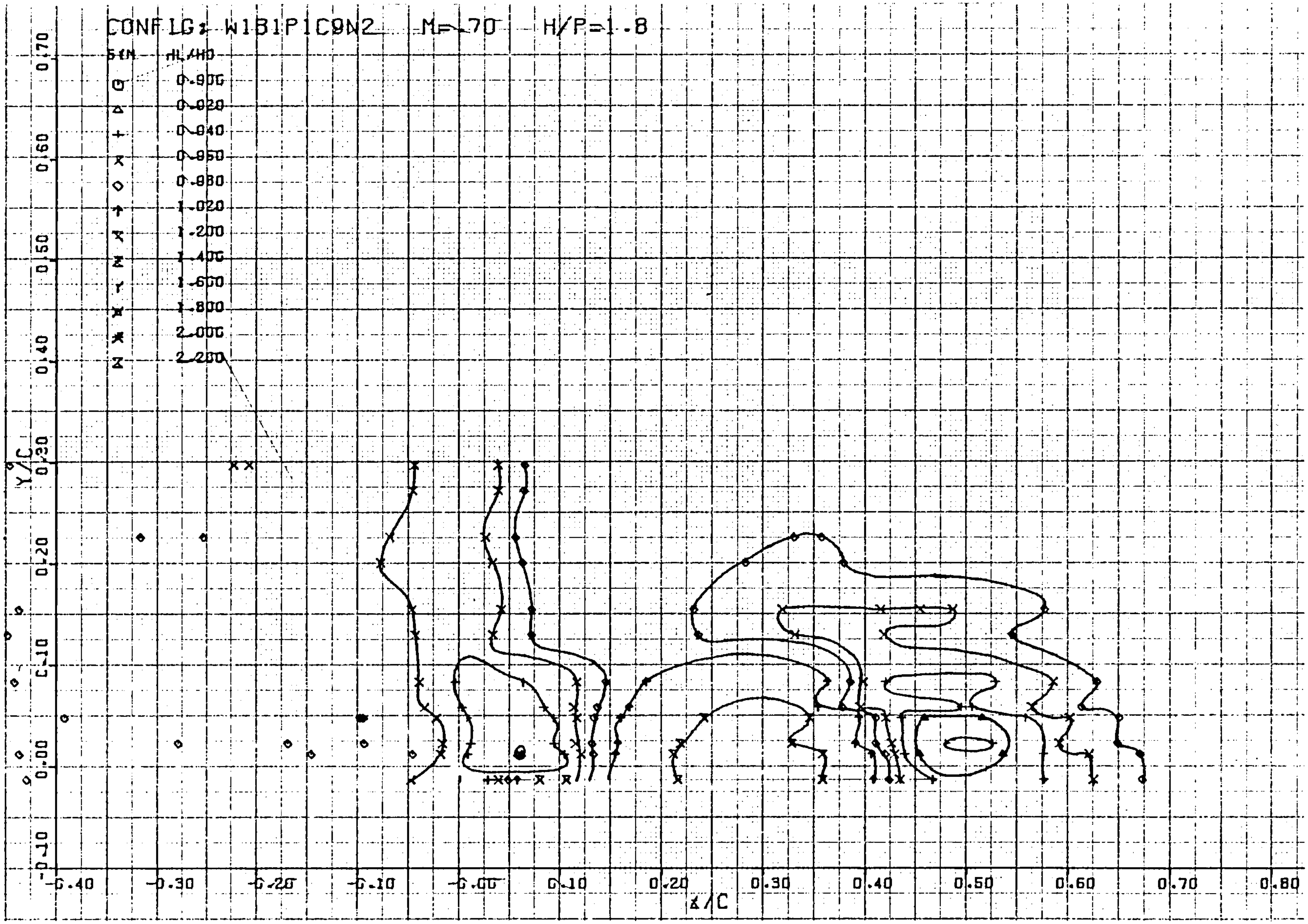

Figure 124. Isobar plot of USB nacelle-wing-jet wake pattern measured one chord length aft of trailing edge, $R_{NC} = 3.5 \times 10^6$, test 23, series 5, run numbers 371-376, $\alpha = 2.6^o$

USB CRUISE PROGRAM

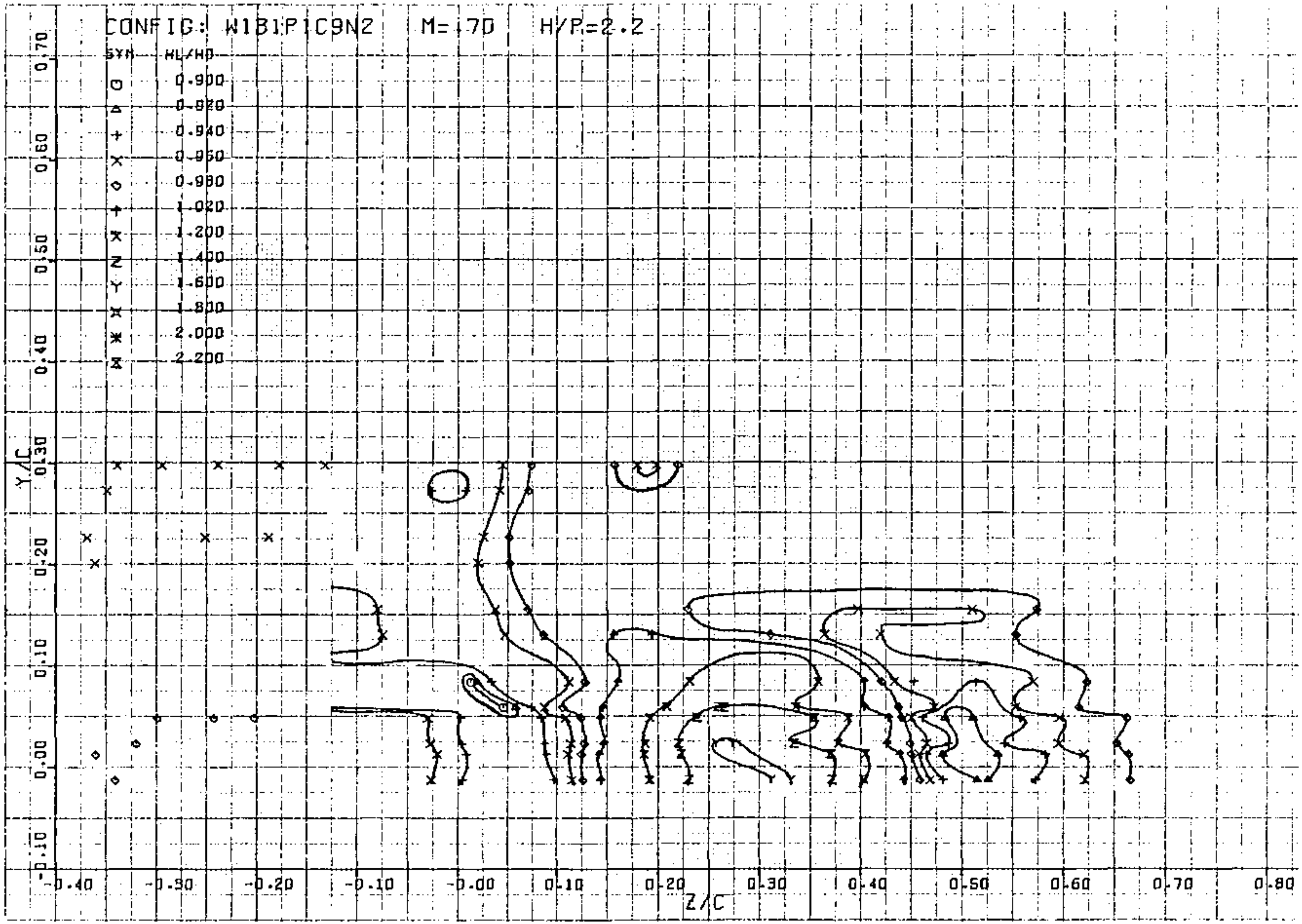

Figure 125. Isobar plot of USB nacelle-wing-jet wake pattern measured one chord length aft of trailing edge, $R_{NC} = 3.5 \times 10^6$, test 23, series 5, run numbers 377 - 382, $\alpha = 2.6^o$

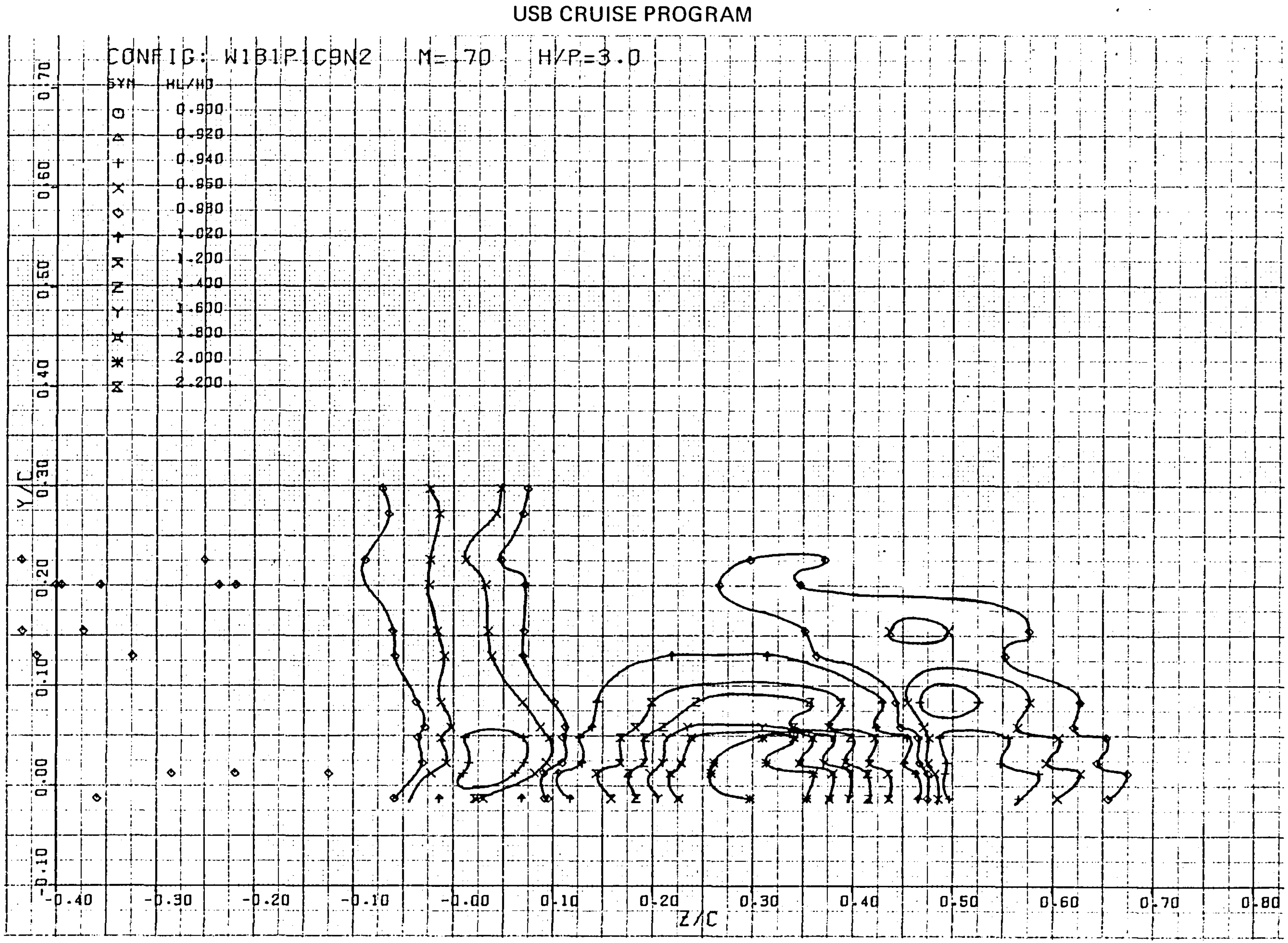

Figure 126. Isobar plot of USB nacelle-wing-jet wake pattern measured one chord length aft of trailing edge, $R_{NC} = 3.5 \times 10^6$, test 23, series 5, run numbers 383-388, $\alpha = 2.6^{\circ}$

USB CRUISE PROGRAM

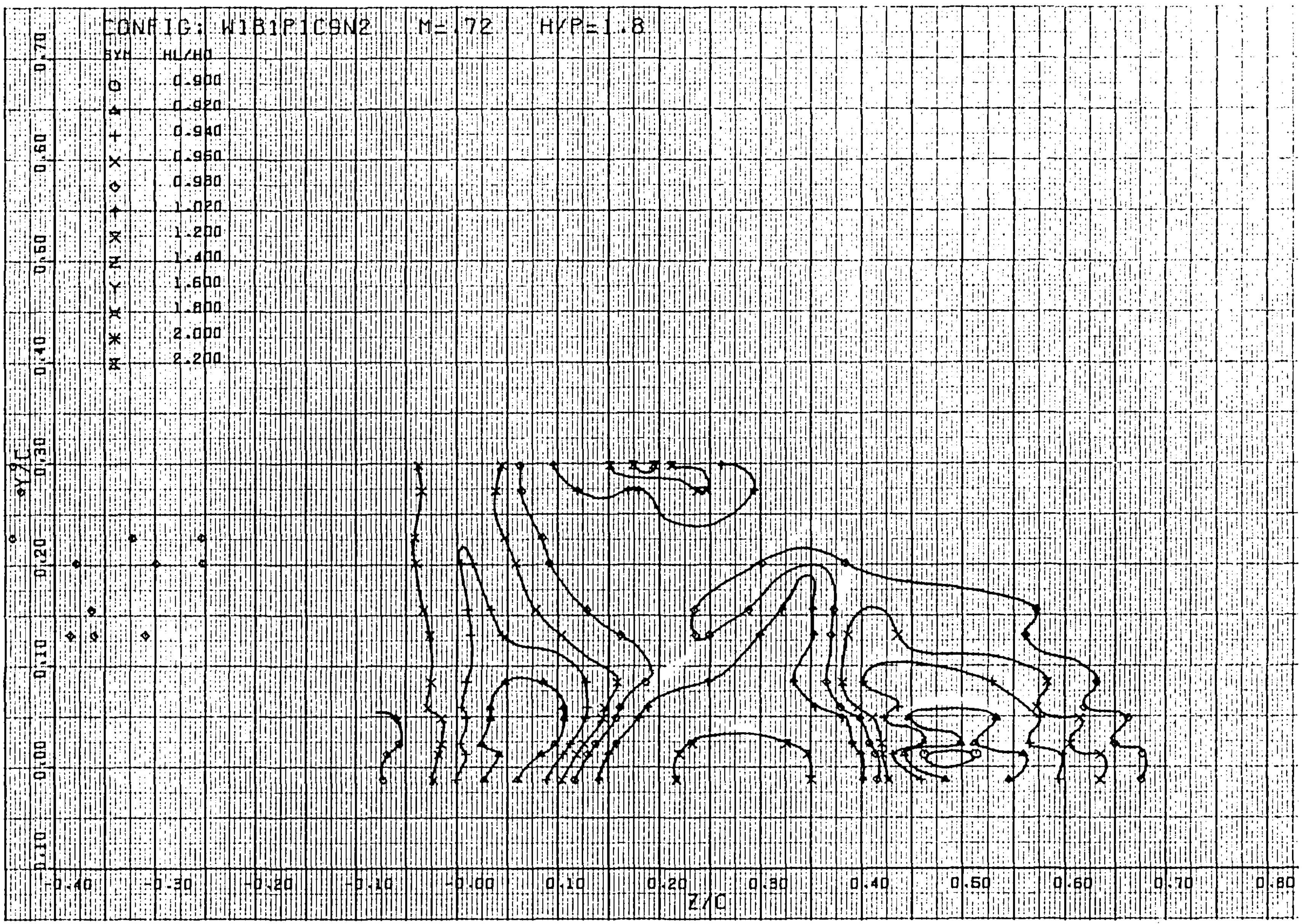

Figure 127. Isobar plot of USB nacelle-wing-jet wake pattern measured one chord length aft of trailing edge, $R_{NC} = 3.5 \times 10^6$, test 23, series 5, run numbers 392 - 397, $\alpha = 2.6^o$

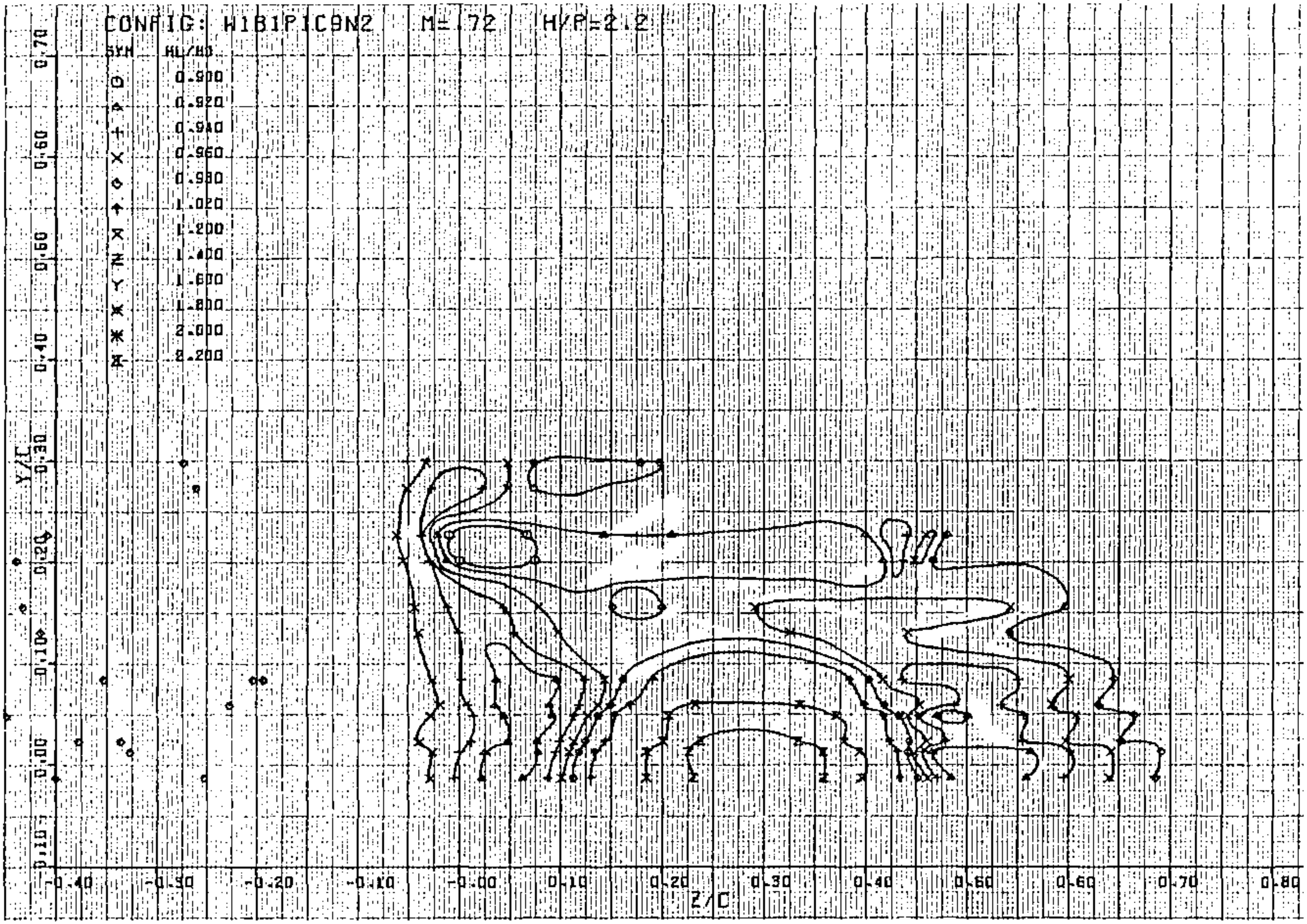

Figure 128. Isobar plot of USB nacelle-wing-jet wake pattern measured one chord length aft of trailing edge, $R_{NC} = 3.5 \times 10^6$, test 23, series 5, run numbers 398-403, $\alpha = 2.6^o$

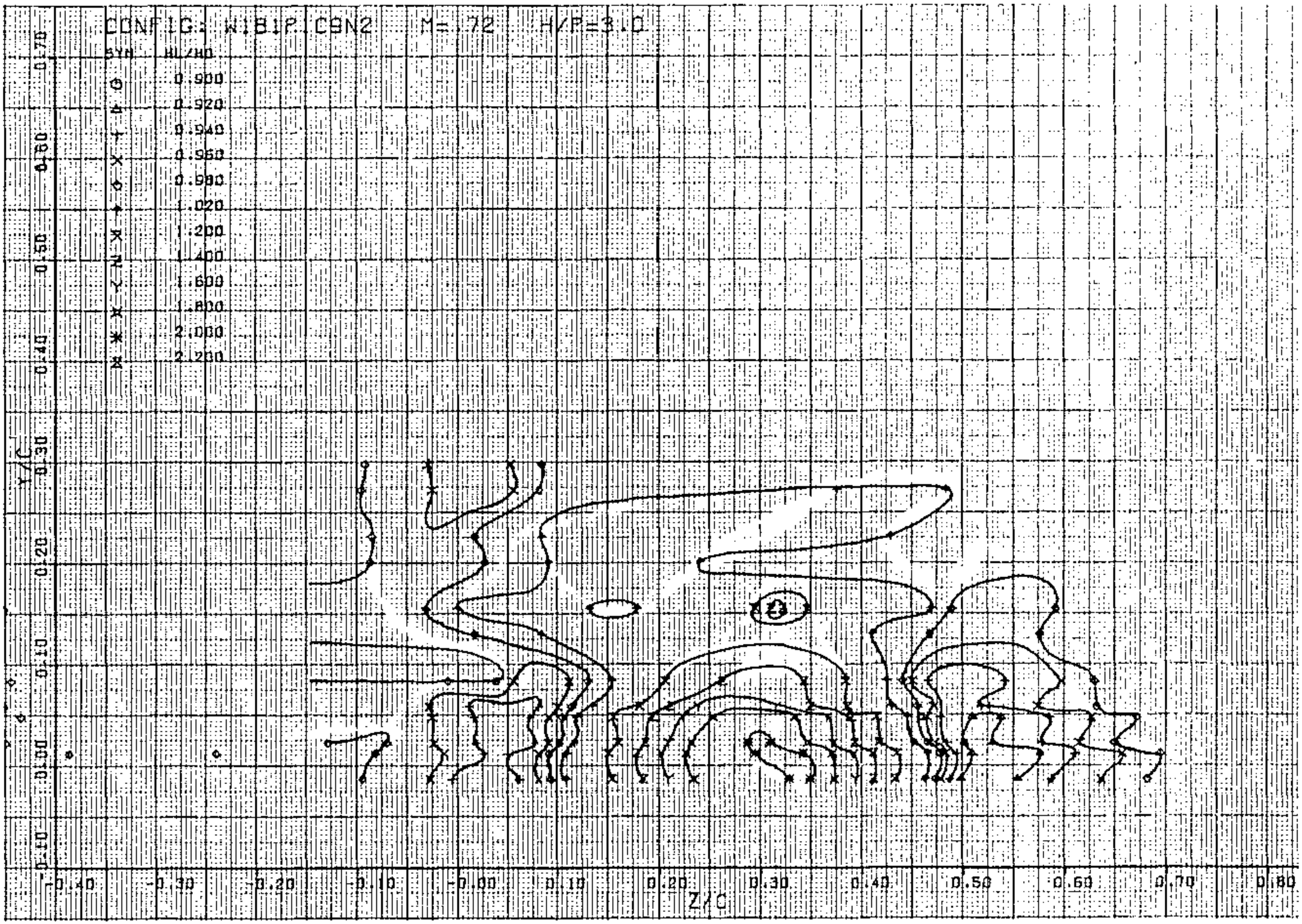

Figure 129. Isobar plot of USB nacelle-wing-jet wake pattern measured one chord length aft of trailing edge, $R_{NC} = 3.5 \times 10^6$, test 23, series 5, run numbers 404 - 409, $\alpha = 2.6^o$

USB CRUISE PROGRAM

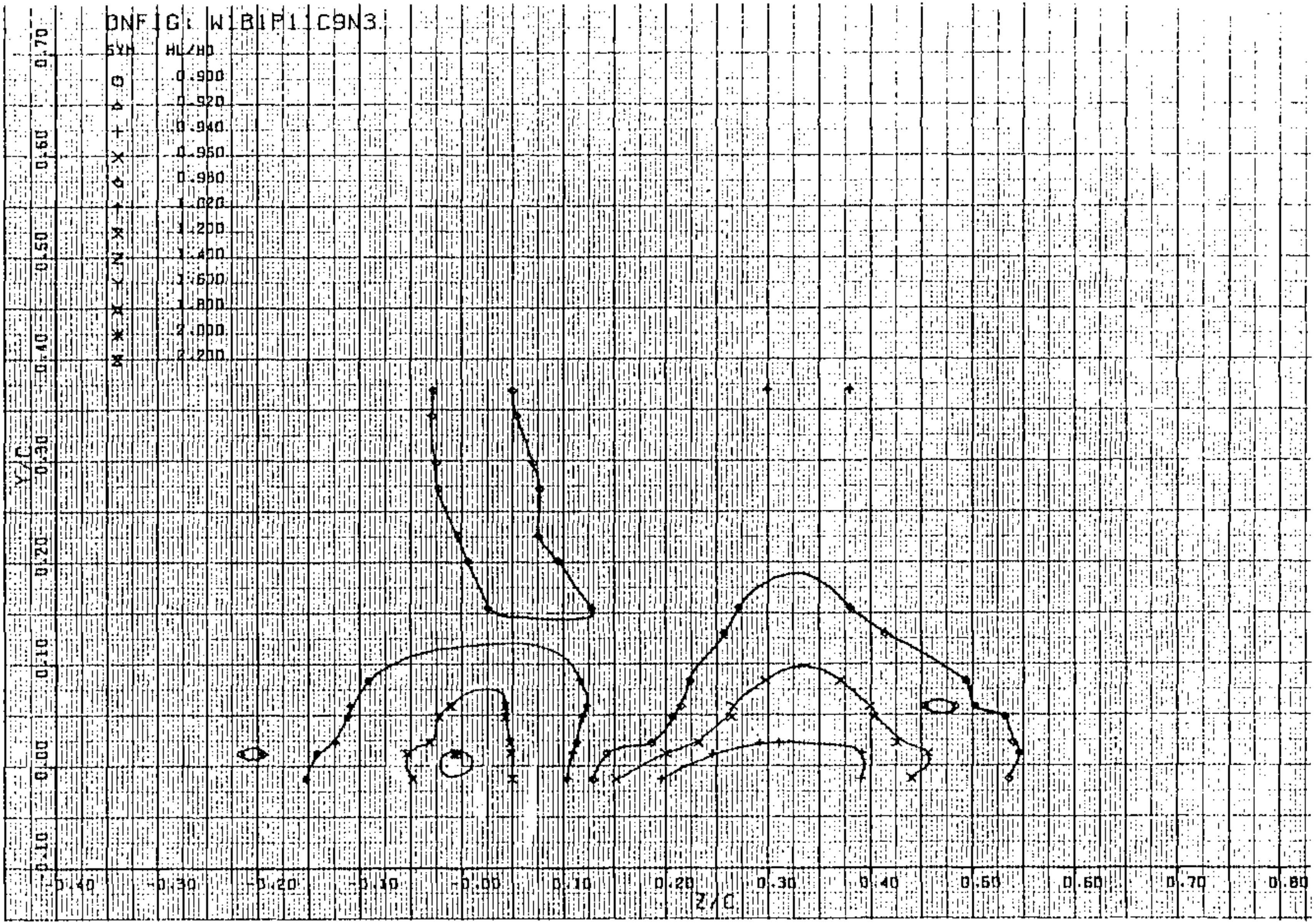

Figure 130. Isobar plot of USB nacelle-wing-jet wake pattern measured one chord length aft of trailing edge, $R_{NC} = 3.5 \times 10^6$, test 23, series 5, run numbers 412 - 418, $\alpha = 2.6^\circ$

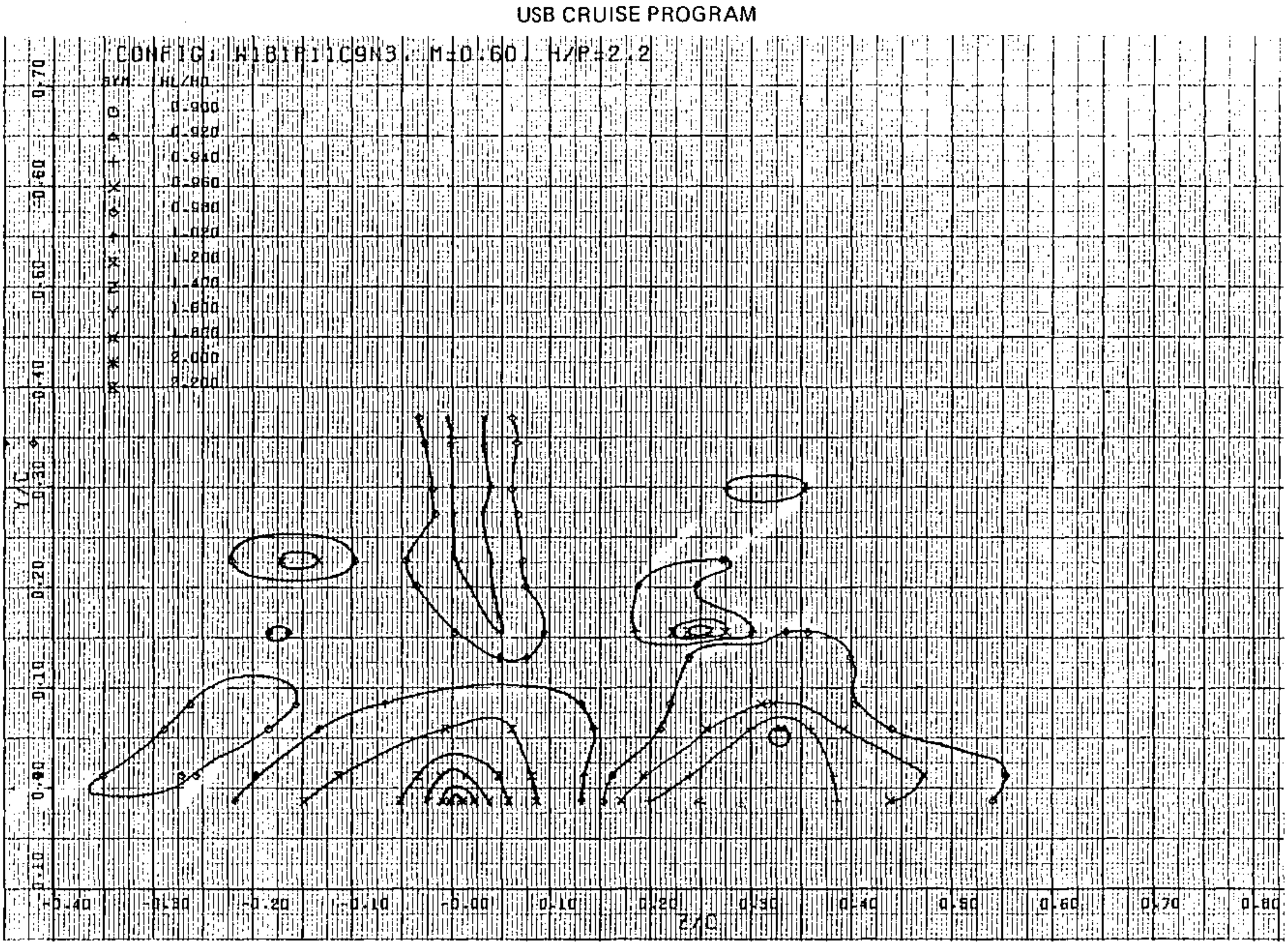

Figure 131. Isobar plot of USB nacelle-wing-jet wake pattern measured one chord length aft of trailing edge, $R_{NC} = 3.5 \times 10^6$, test 23, series 6, run numbers 419-424, $\alpha = 2.6°$

USB CRUISE PROGRAM

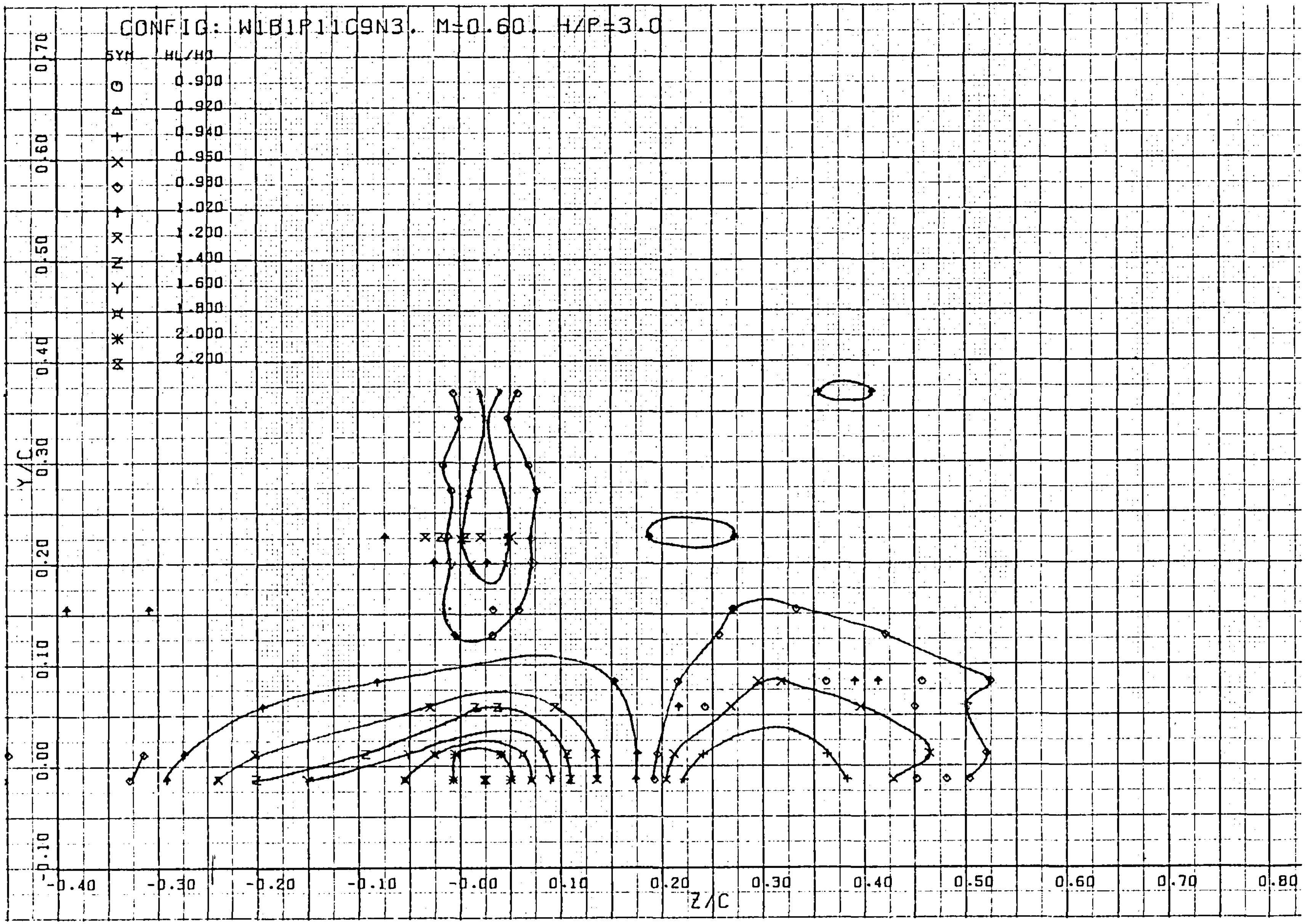

Figure 132. Isobar plot of USB nacelle-wing-jet wake pattern measured one chord length aft of trailing edge, $R_{NC} = 3.5 \times 10^6$, test 23, series 6, run numbers 425-433, $\alpha = 2.6°$

USB CRUISE PROGRAM

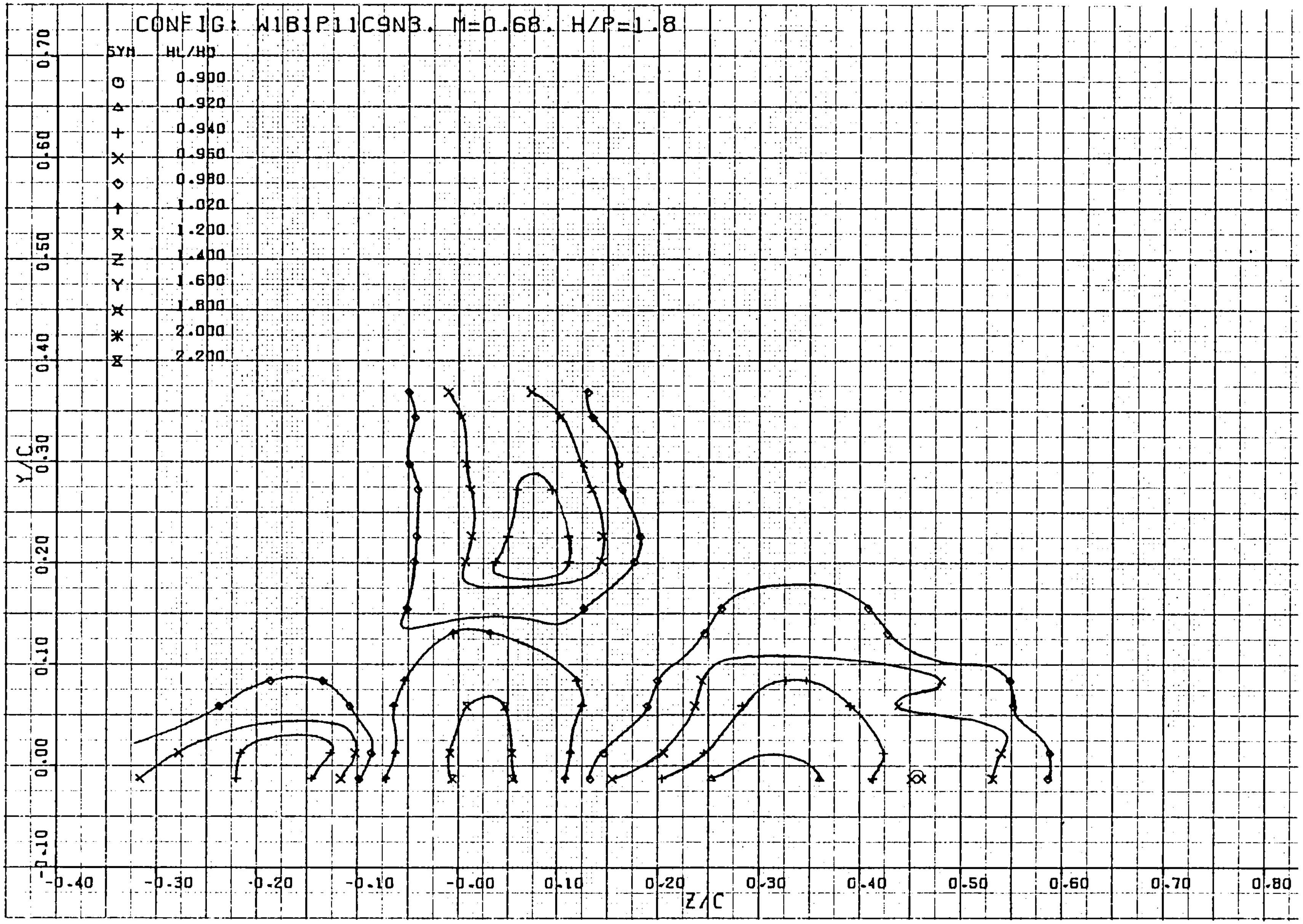

Figure 133. Isobar plot of USB nacelle-wing-jet wake pattern measured one chord length aft of trailing edge, $R_{NC} = 3.5 \times 10^6$, test 23, series 6, run numbers 435 - 444, $\alpha = 2.6^o$

USB CRUISE PROGRAM

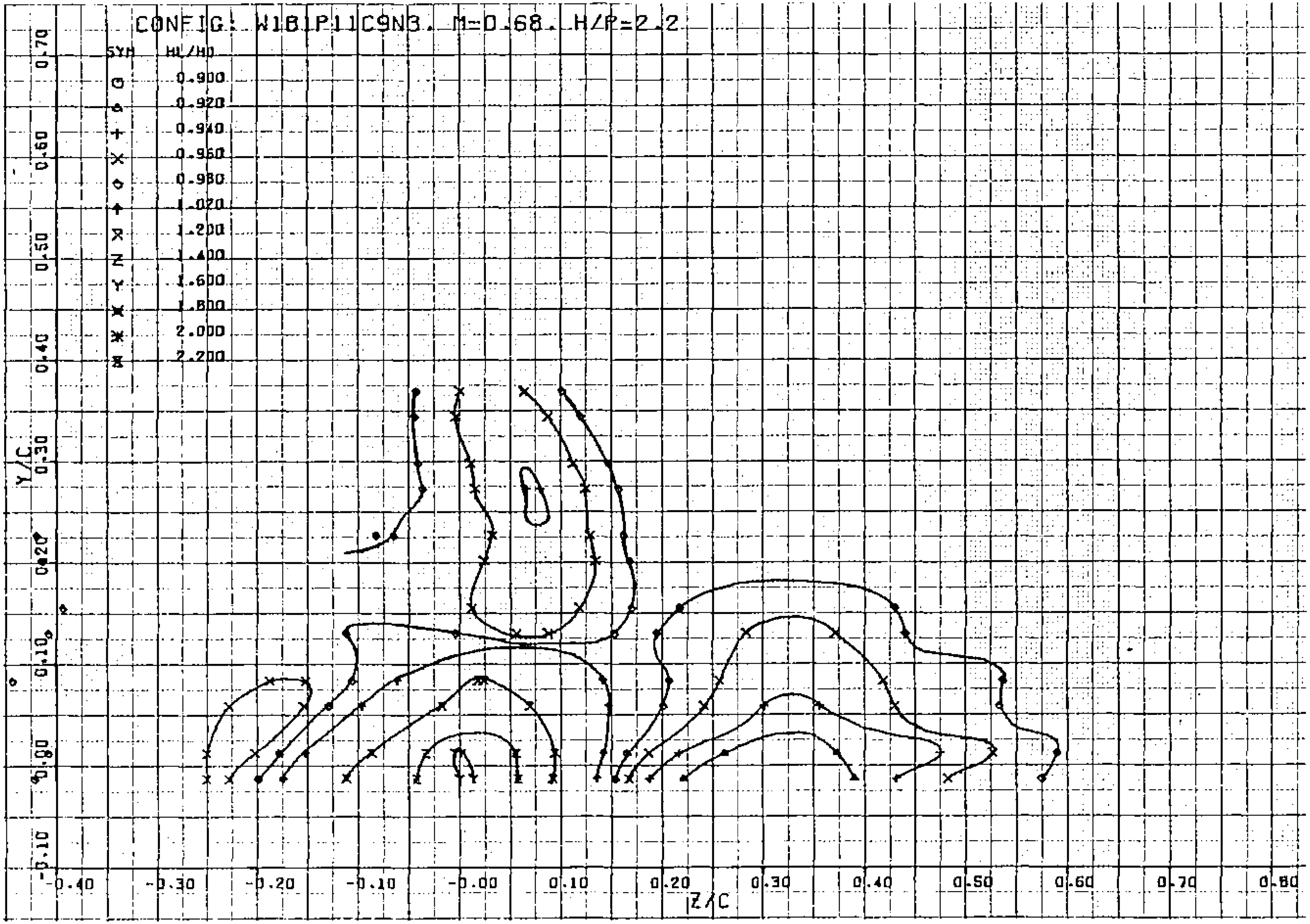

Figure 134. Isobar plot of USB nacelle-wing-jet wake pattern measured one chord length aft of trailing edge, $R_{NC} = 3.5 \times 10^6$, test 23, series 6, run numbers 445 - 450, $\alpha = 2.6^\circ$

USB CRUISE PROGRAM

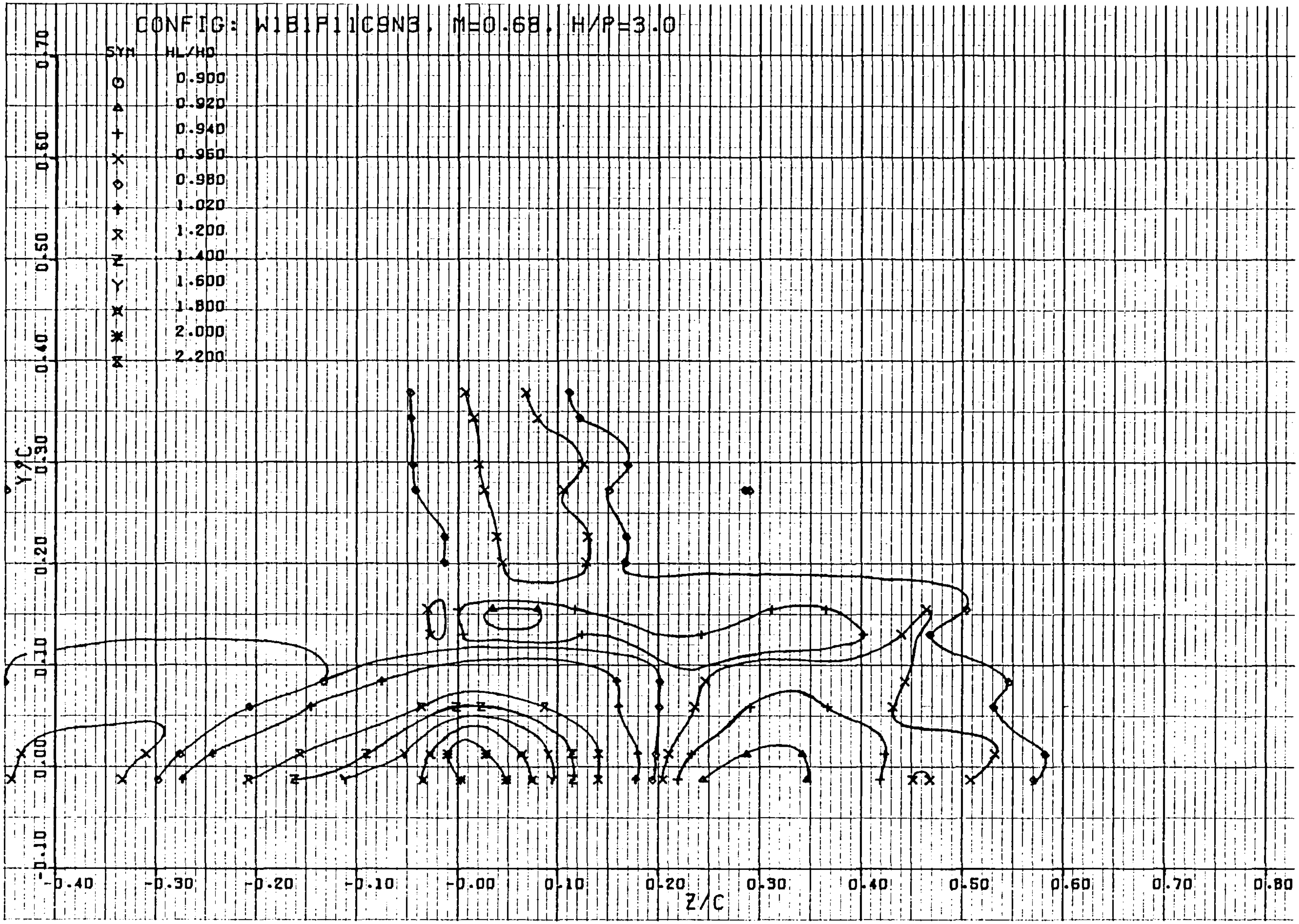

Figure 135. Isobar plot of USB nacelle-wing-jet wake pattern measured one chord length aft of trailing edge, $R_{NC} = 3.5 \times 10^6$, test 23, series 6, run numbers 451 - 456, $\alpha = 2.6^\circ$

USB CRUISE PROGRAM

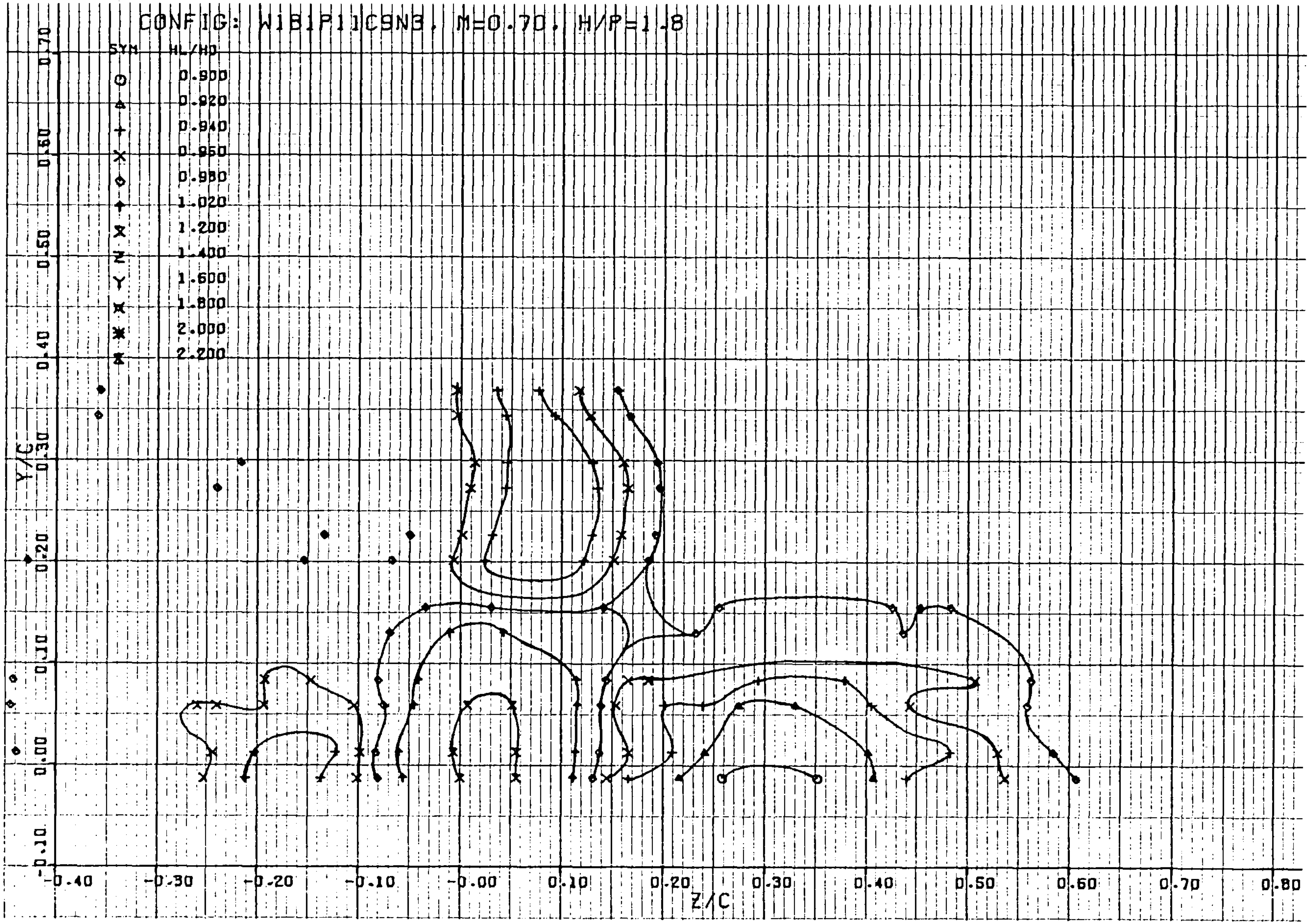

Figure 136. Isobar plot of USB nacelle-wing-jet wake pattern measured one chord length aft of trailing edge, $R_{NC} = 3.5 \times 10^6$, test 23, series 6, run numbers 457 - 462, $\alpha = 2.6^o$

USB CRUISE PROGRAM

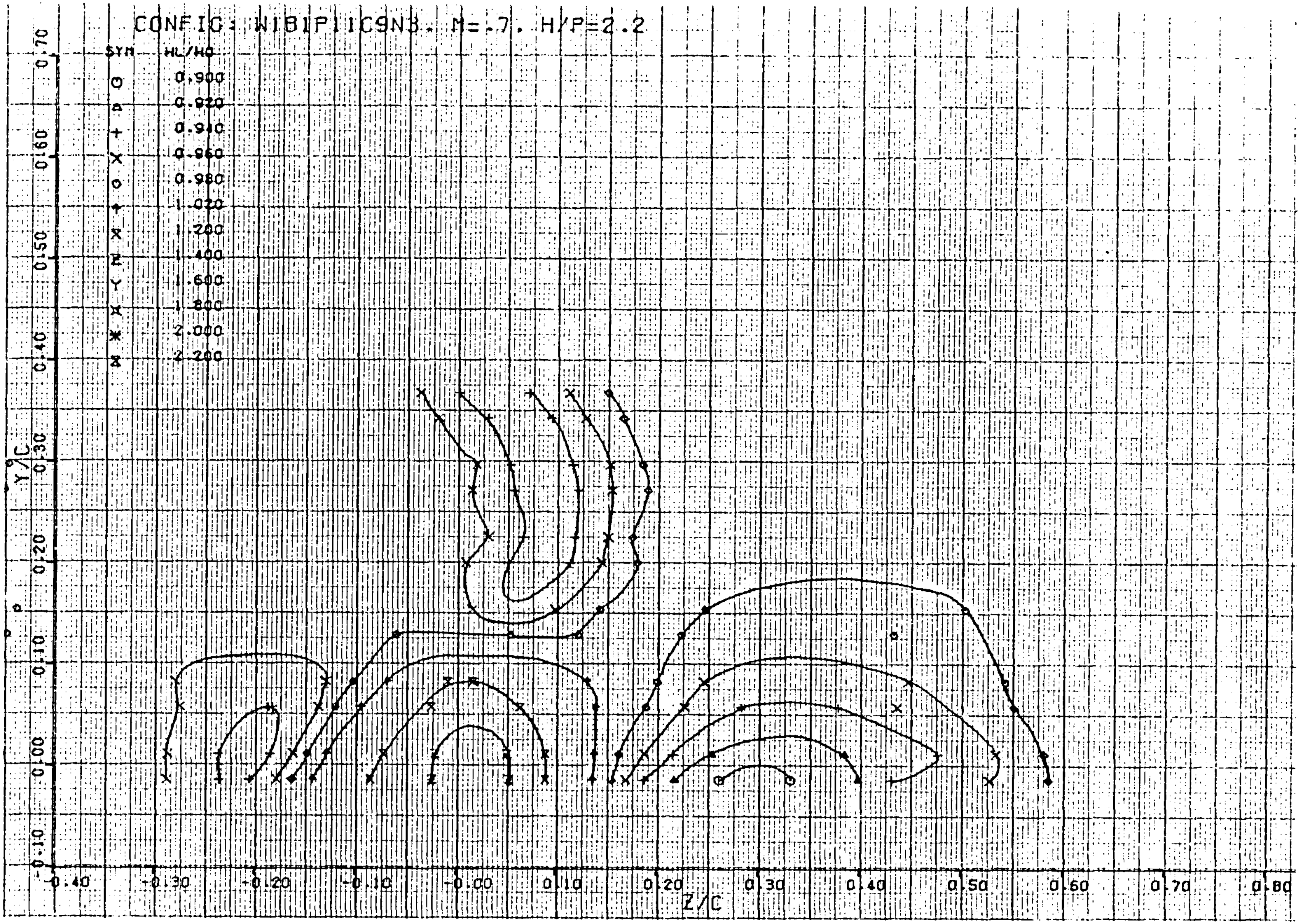

Figure 137. Isobar plot of USB nacelle-wing-jet wake pattern measured one chord length aft of trailing edge, R_{NC} - 3.5×10^6, test 23, series 6, run numbers 464 - 469, α = 2.6°

USB CRUISE PROGRAM

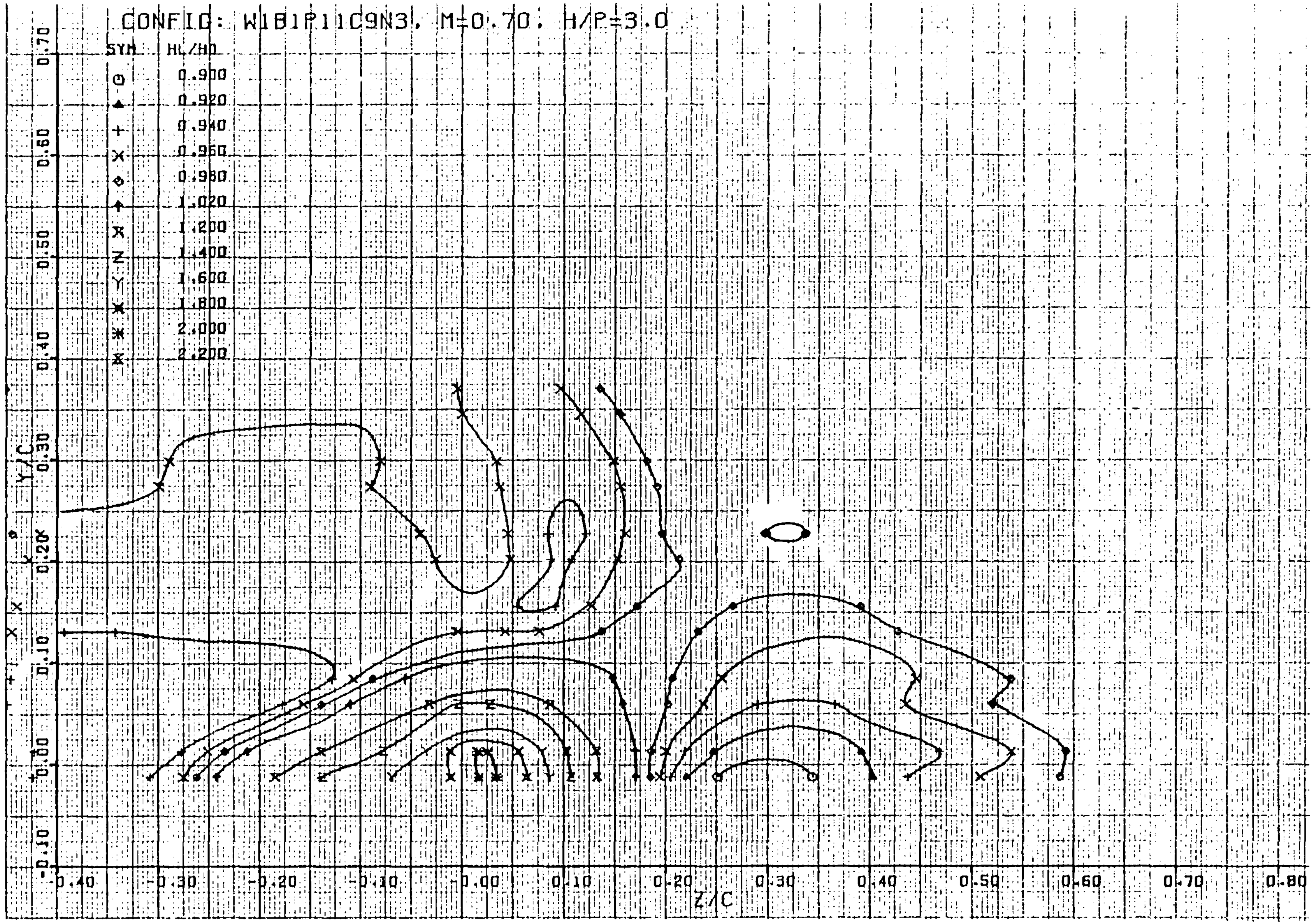

Figure 138. Isobar plot of USB nacelle-wing-jet wake pattern measured one chord length aft of trailing edge, $R_{NC} = 3.5 \times 10^6$, test 23, series 6, run numbers 470 - 475, $\alpha = 2.6^o$

USB CRUISE PROGRAM

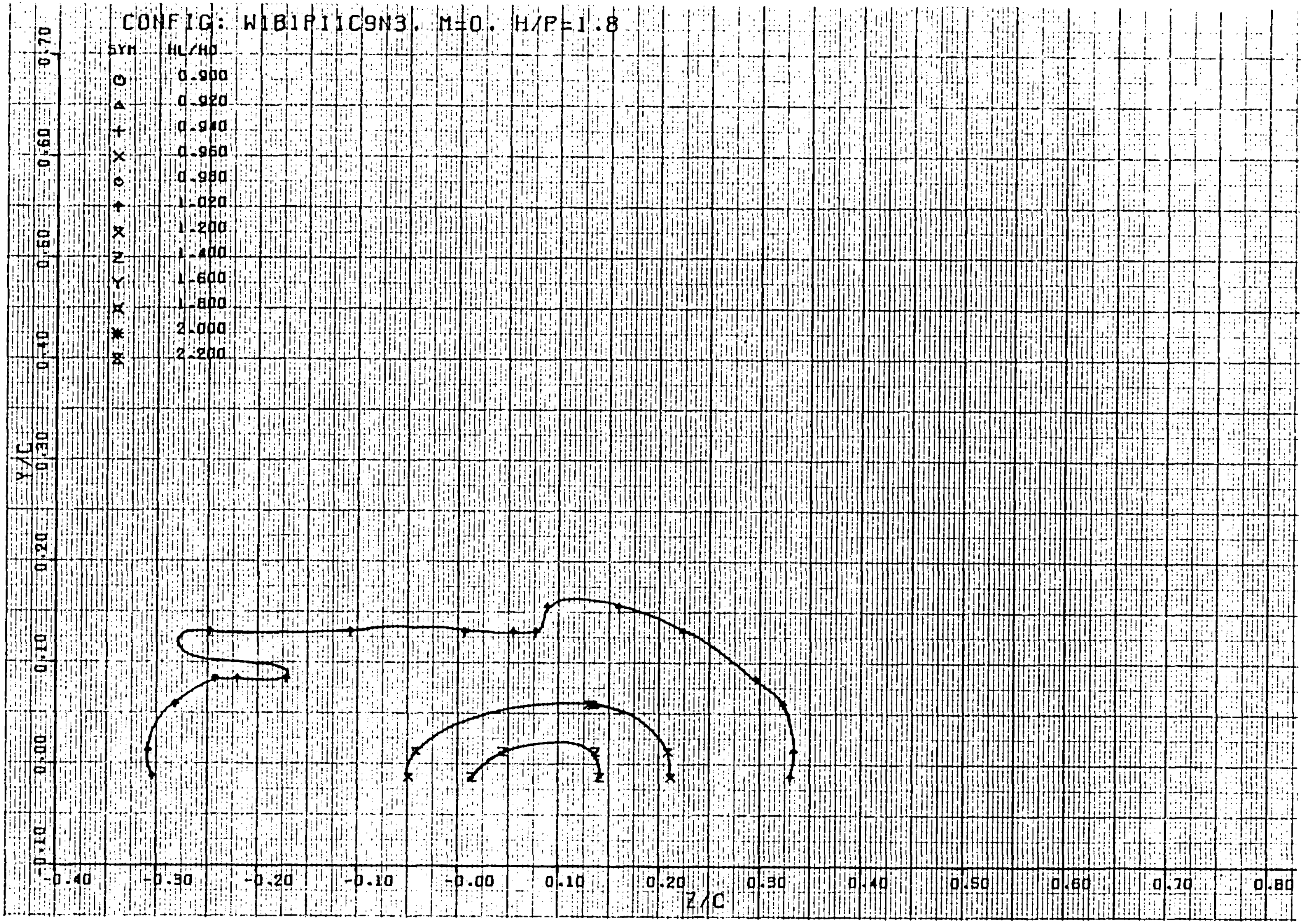

Figure 139. Isobar plot of USB nacelle-wing-jet wake pattern measured one chord length aft of trailing edge, $R_{NC} = 3.5 \times 10^6$, test 23, series 6, run numbers 476 - 481, $\alpha = 2.6^{\circ}$

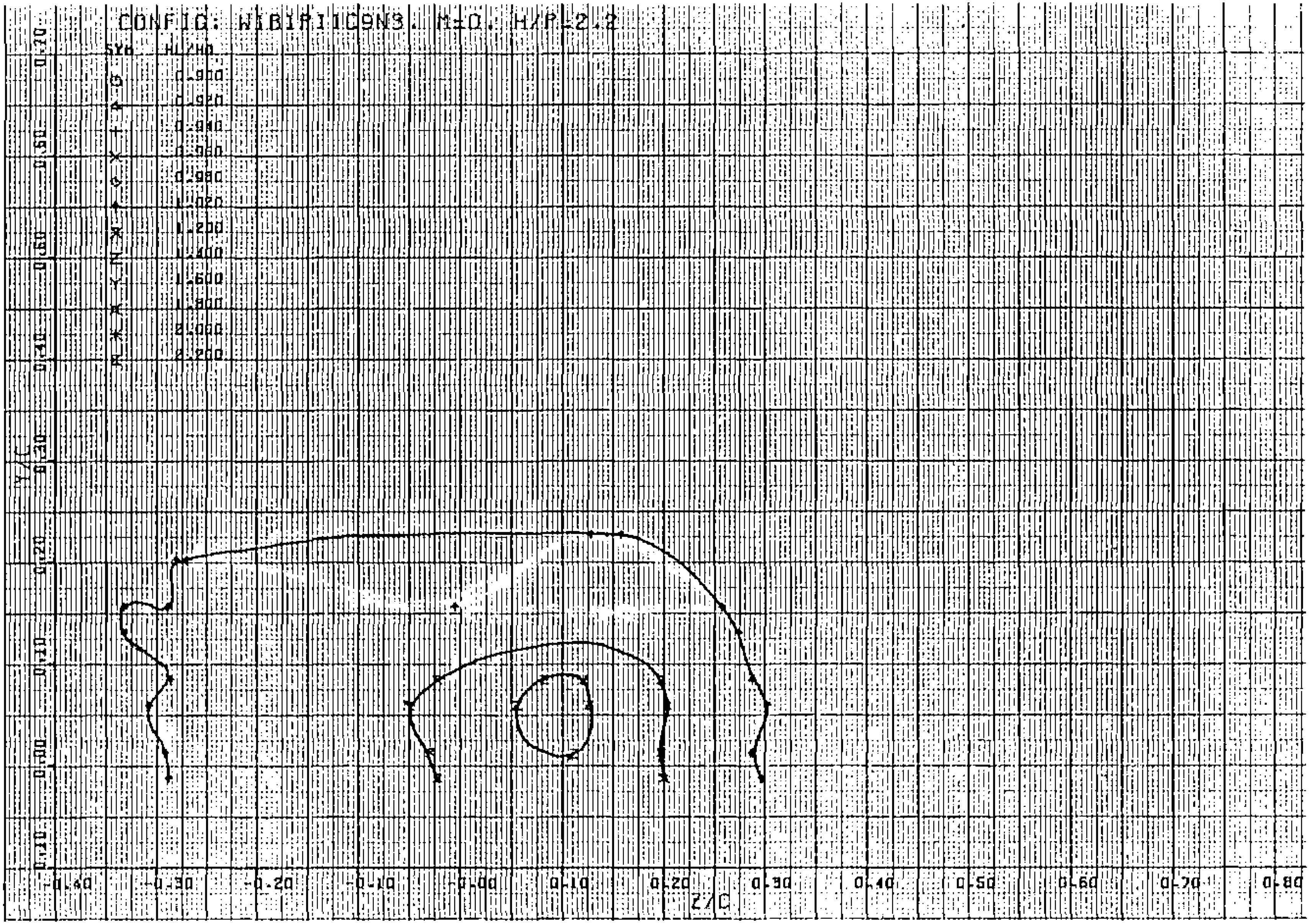

Figure 140. Isobar plot of USB nacelle-wing-jet wake pattern measured one chord length aft of trailing edge, $R_{NC} = 3.5 \times 10^6$, test 23, series 6, run numbers 482 - 487, $\alpha = 2.6^\circ$

USB CRUISE PROGRAM

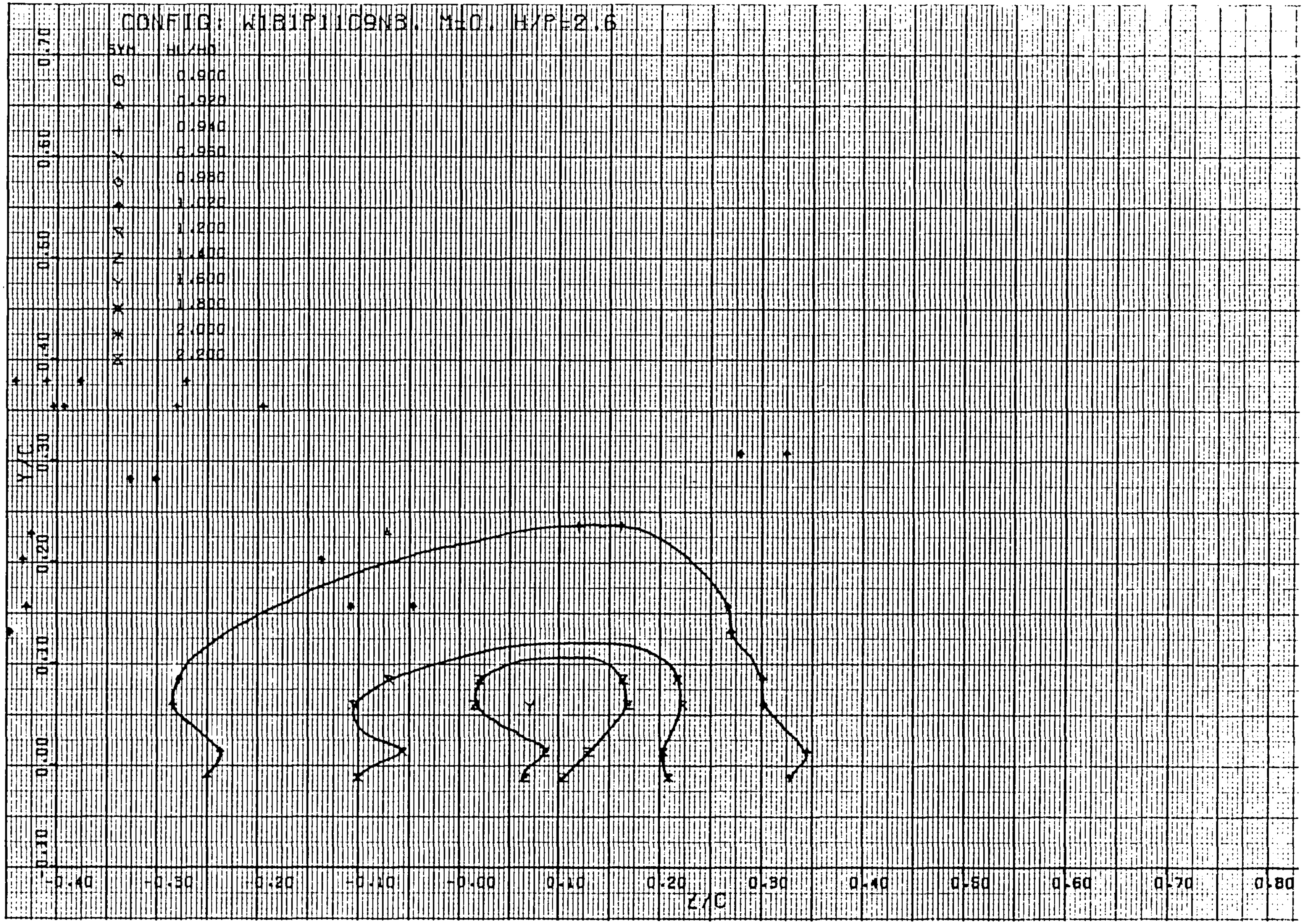

Figure 141. Isobar plot of USB nacelle-wing-jet wake pattern measured one chord length aft of trailing edge, $R_{NC} = 3.5 \times 10^6$, test 23, series 6, run numbers 488 - 493, $\alpha = 2.6^\circ$

USB CRUISE PROGRAM

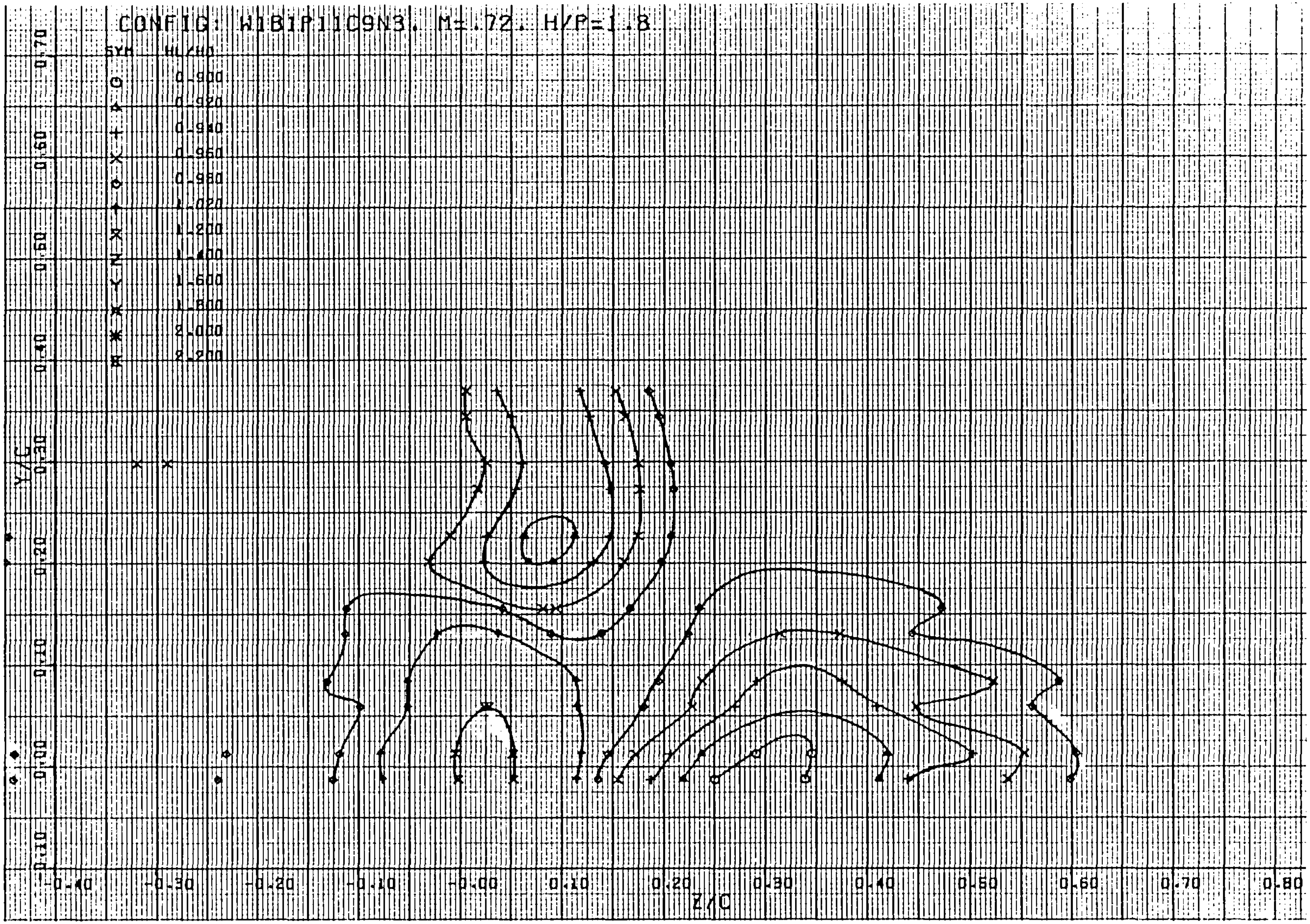

Figure 142. Isobar plot of USB nacelle-wing-jet wake pattern measured one chord length aft of trailing edge, $R_{NC} = 3.5 \times 10^6$, test 23, series 6, run numbers 495 - 501, $\alpha = 2.6^{\circ}$

USB CRUISE PROGRAM

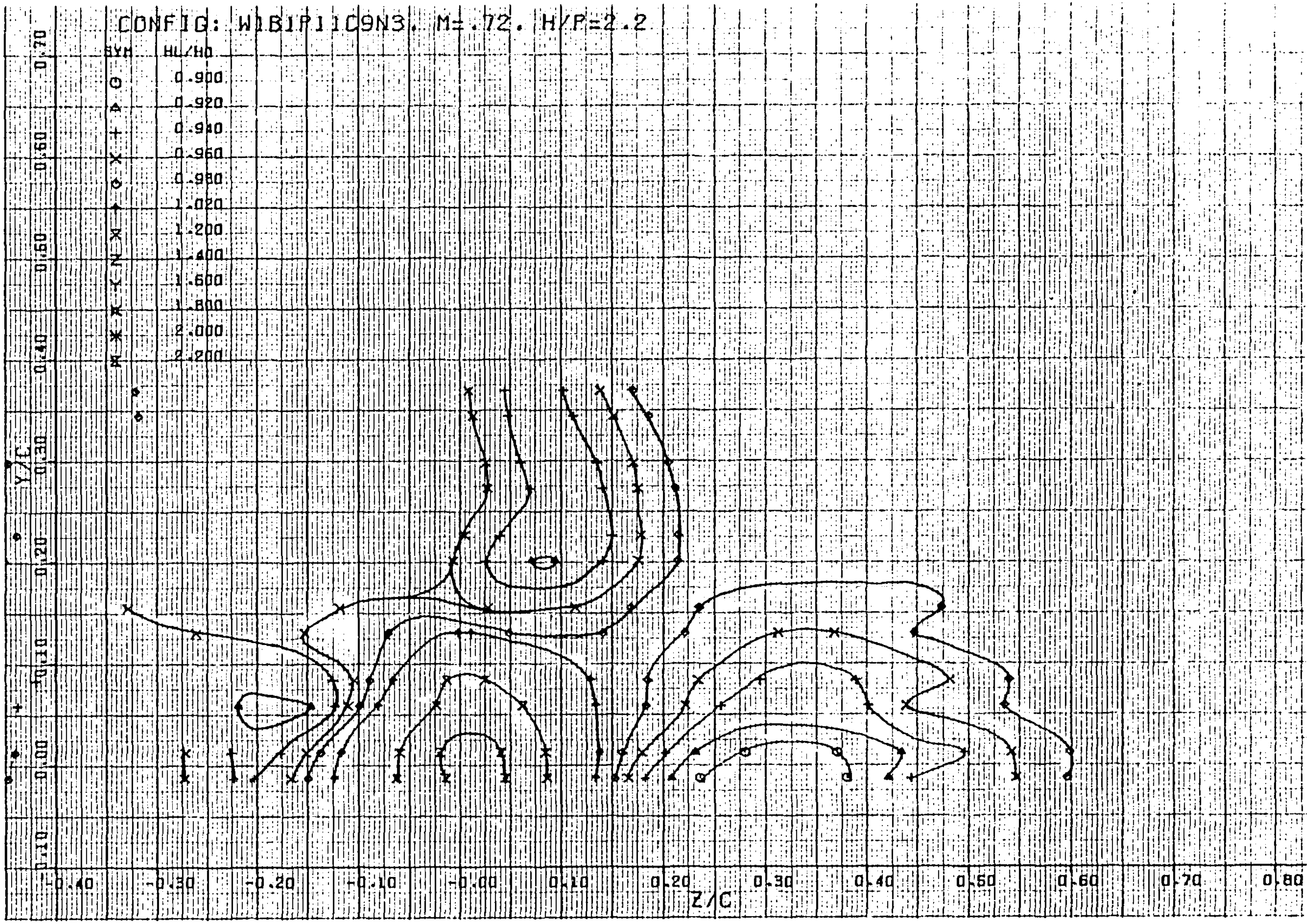

Figure 143. Isobar plot of USB nacelle-wing-jet wake pattern measured one chord length aft of trailing edge, $R_{NC} = 3.5 \times 10^6$, test 23, series 6, run numbers 502 - 507, $\alpha = 2.6^\circ$

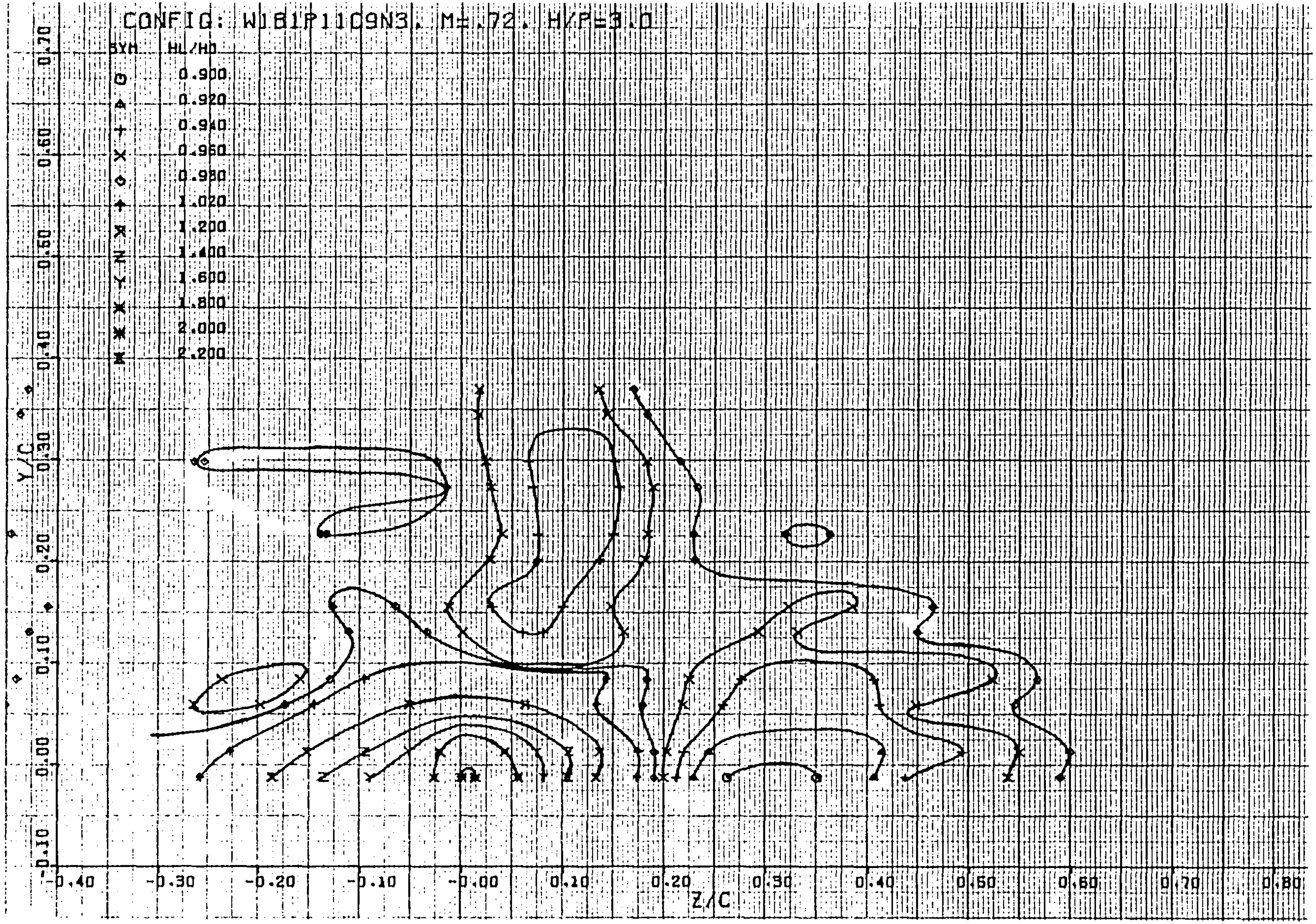

Figure 144. Isobar plot of USB nacelle-wing-jet wake pattern measured one chord length aft of trailing edge, $R_{NC} = 3.5 \times 10^6$, test 23, series 6, run numbers 508 - 517, $\alpha = 2.6°$

6.0 SWEPT WING TEST RESULTS

The presentation of the swept wing pressure test results is divided into two parts. These are the model pressure distributions and the wake pressure patterns; they are described separately in the following two sub-sections.

6.1 Model Pressure Distributions

Surface static pressure data for each of the configurations that were ran in the swept wing pressure tests are presented in Figures 145 through 188. The format is the same as was employed for Figures 45 through 104 in Section 5. The data begin with the clean, swept wing, which is followed by a pylon-mounted flow-through nacelle with the circular nozzle N_2. Single and dual versions of $N_8{}^1$ and $N_8{}^2$ are then presented. Finally, data for the AR = 6 nozzle, N_{13}, are shown. All data in this series are presented at a Reynolds' number of 3.5 million based on wing chord.

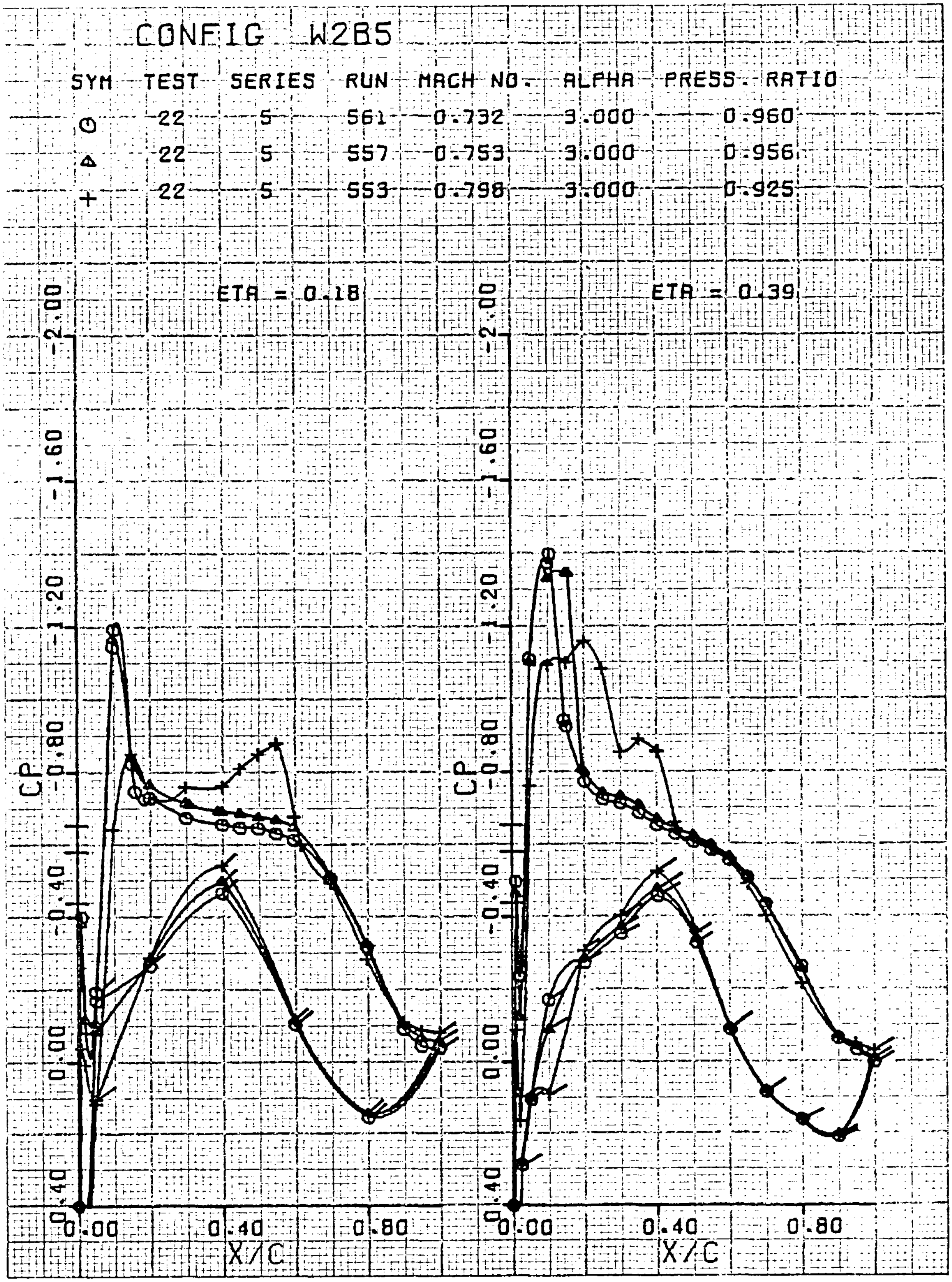

Figure 145. Clean, swept wing pressure distribution, effect of M_∞, η = 0.18, 0.39

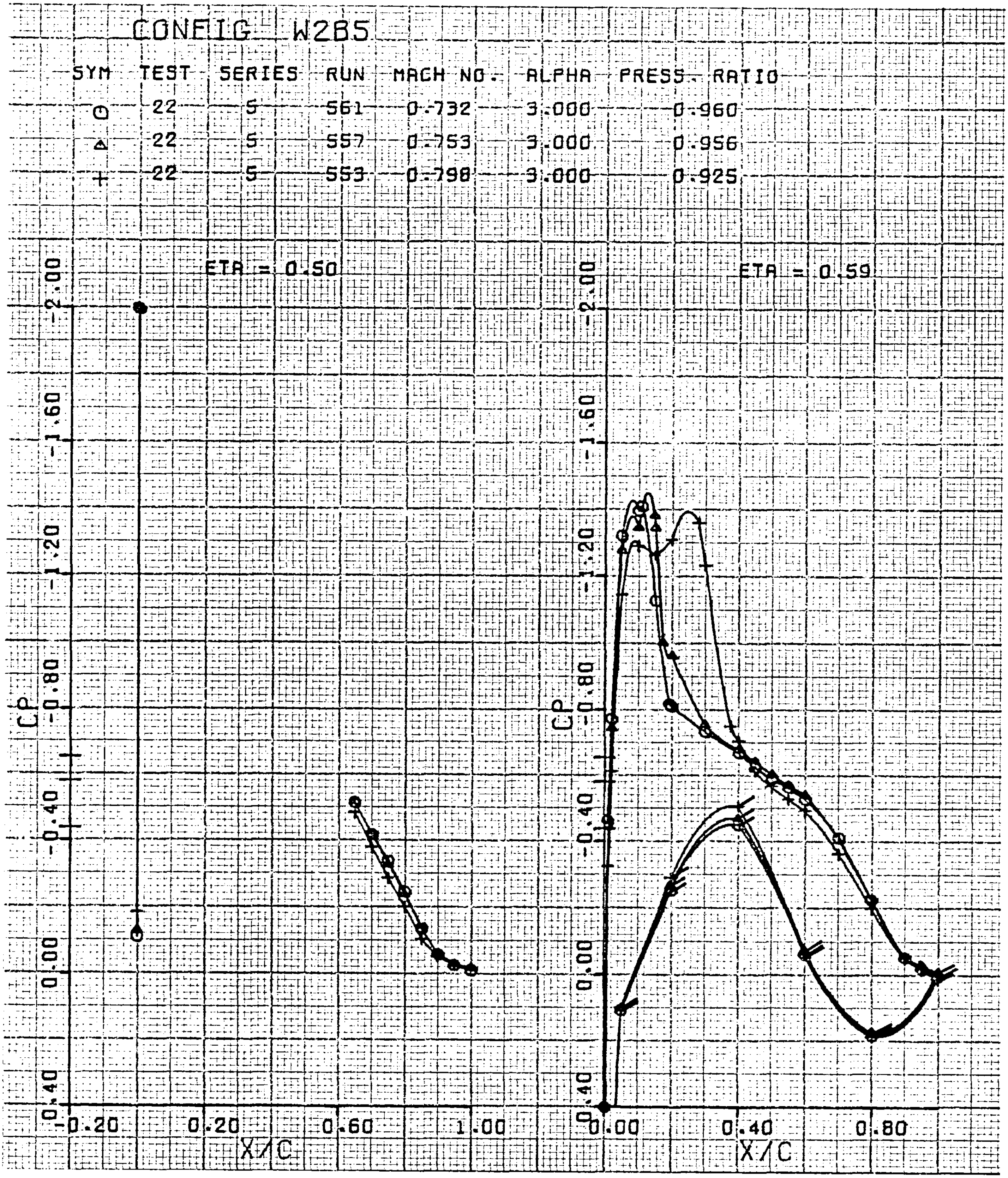

Figure 146. Clean, swept wing pressure distribution, effect of M_∞, η = 0.50, 0.59

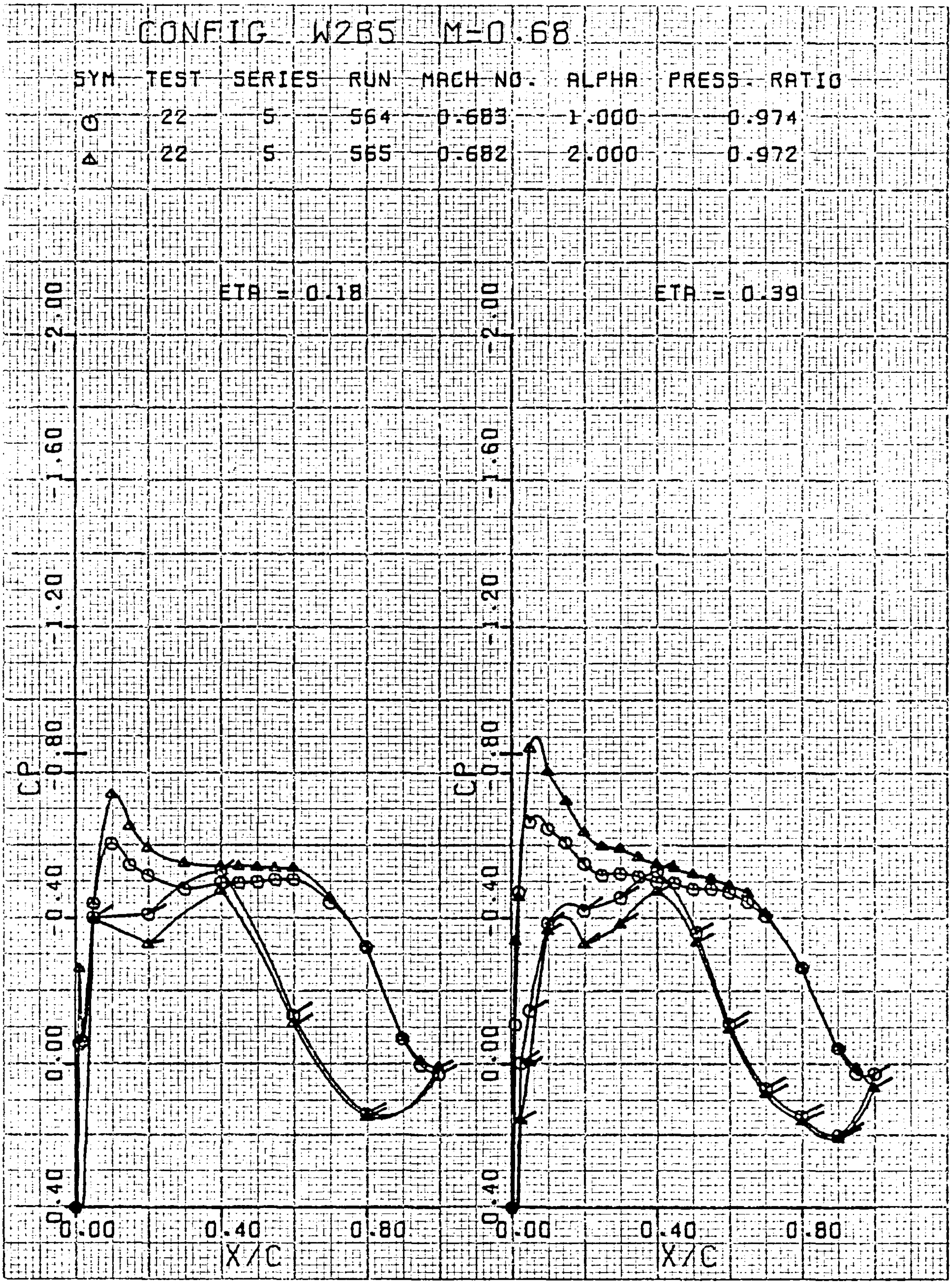

Figure 147. Clean, swept wing pressure distribution, effect of α, $M_\infty = 0.68$, $\eta = 0.18, 0.39$

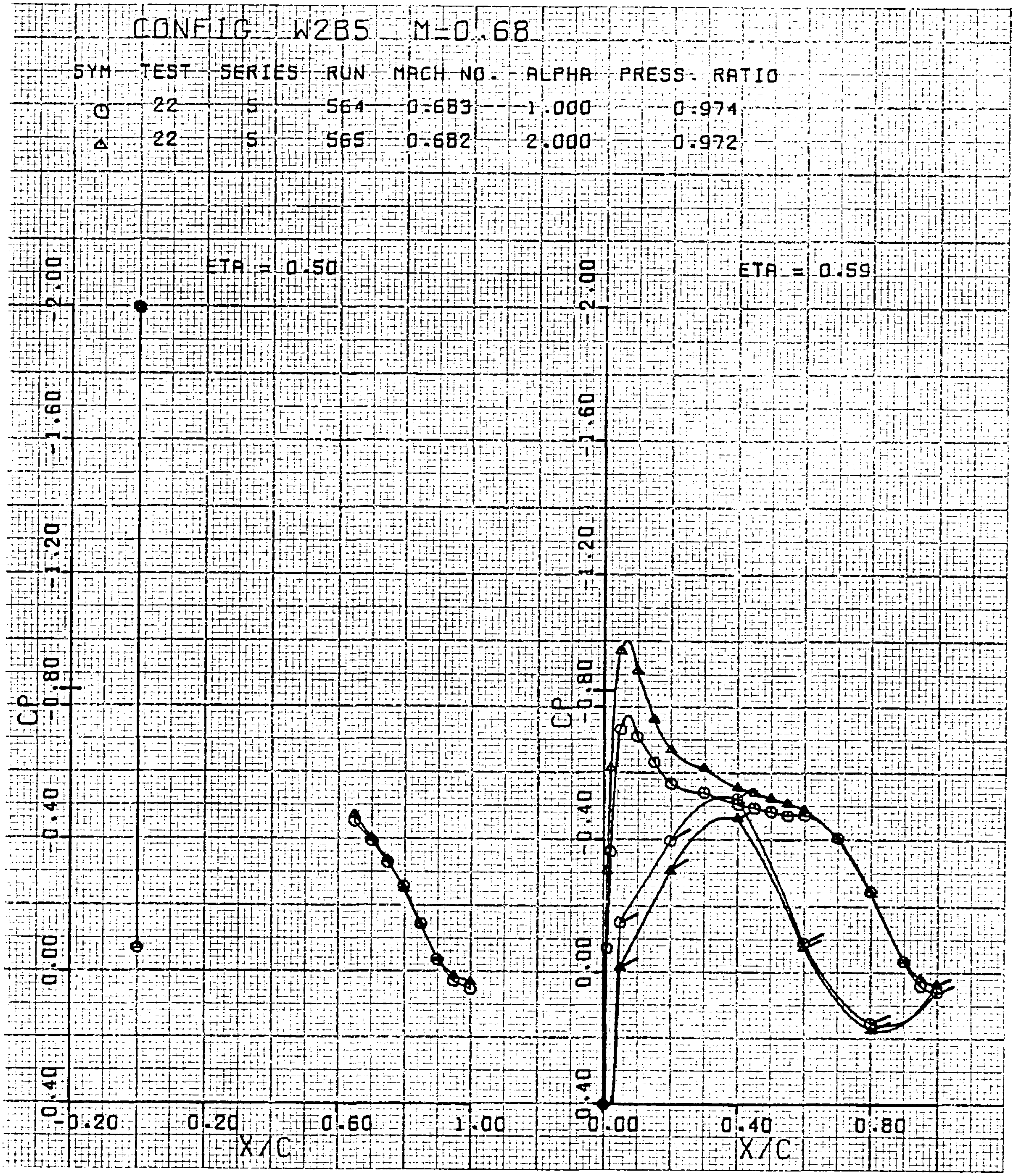

Figure 148. Clean, swept wing pressure distribution, effect of α, $M_\infty = 0.68$, $\eta = 0.50,\ 0.59$

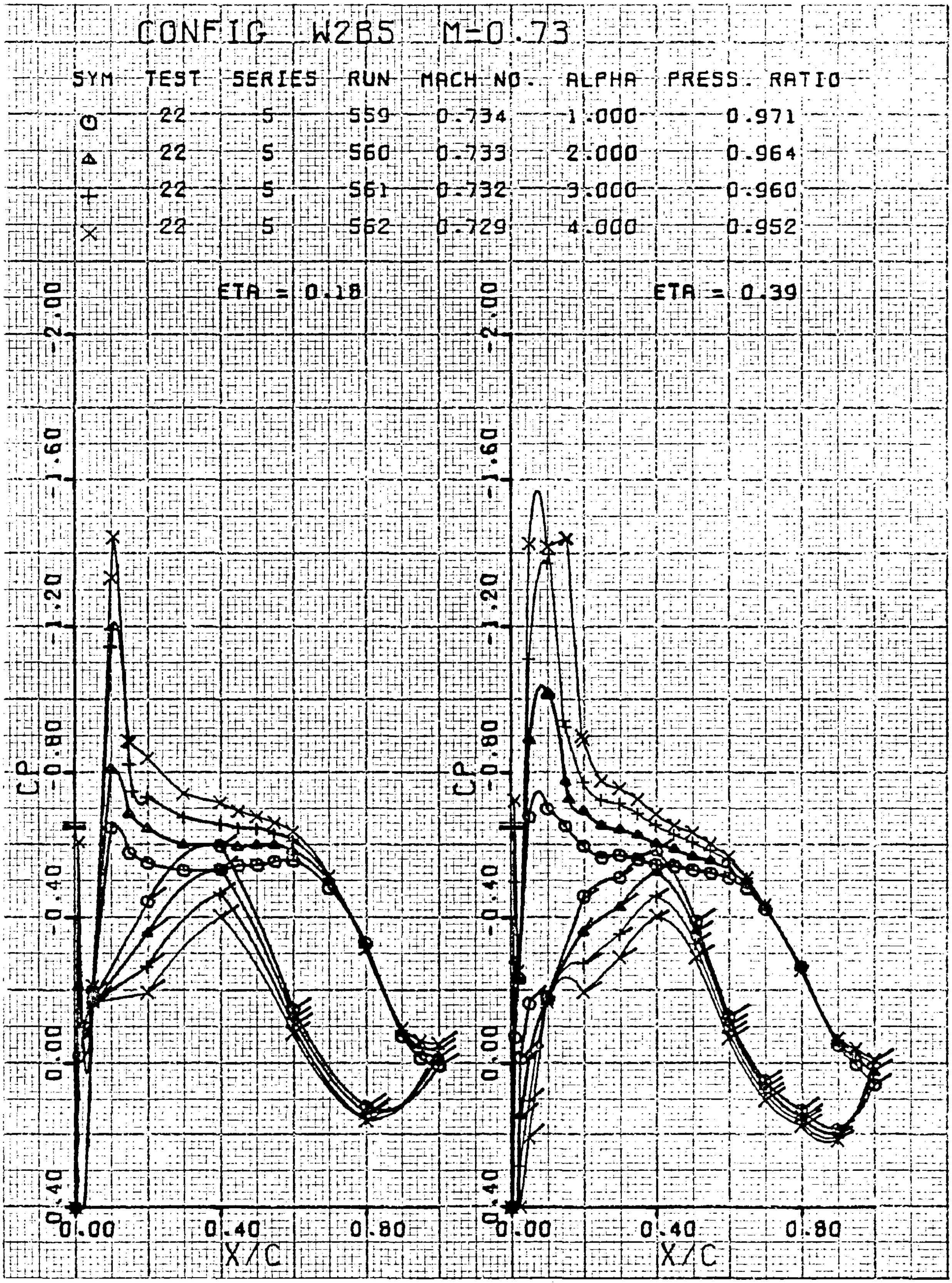

Figure 149. Clean, swept wing pressure distribution, effect of α, M_∞ = 0.73, η = 0.18, 0.39

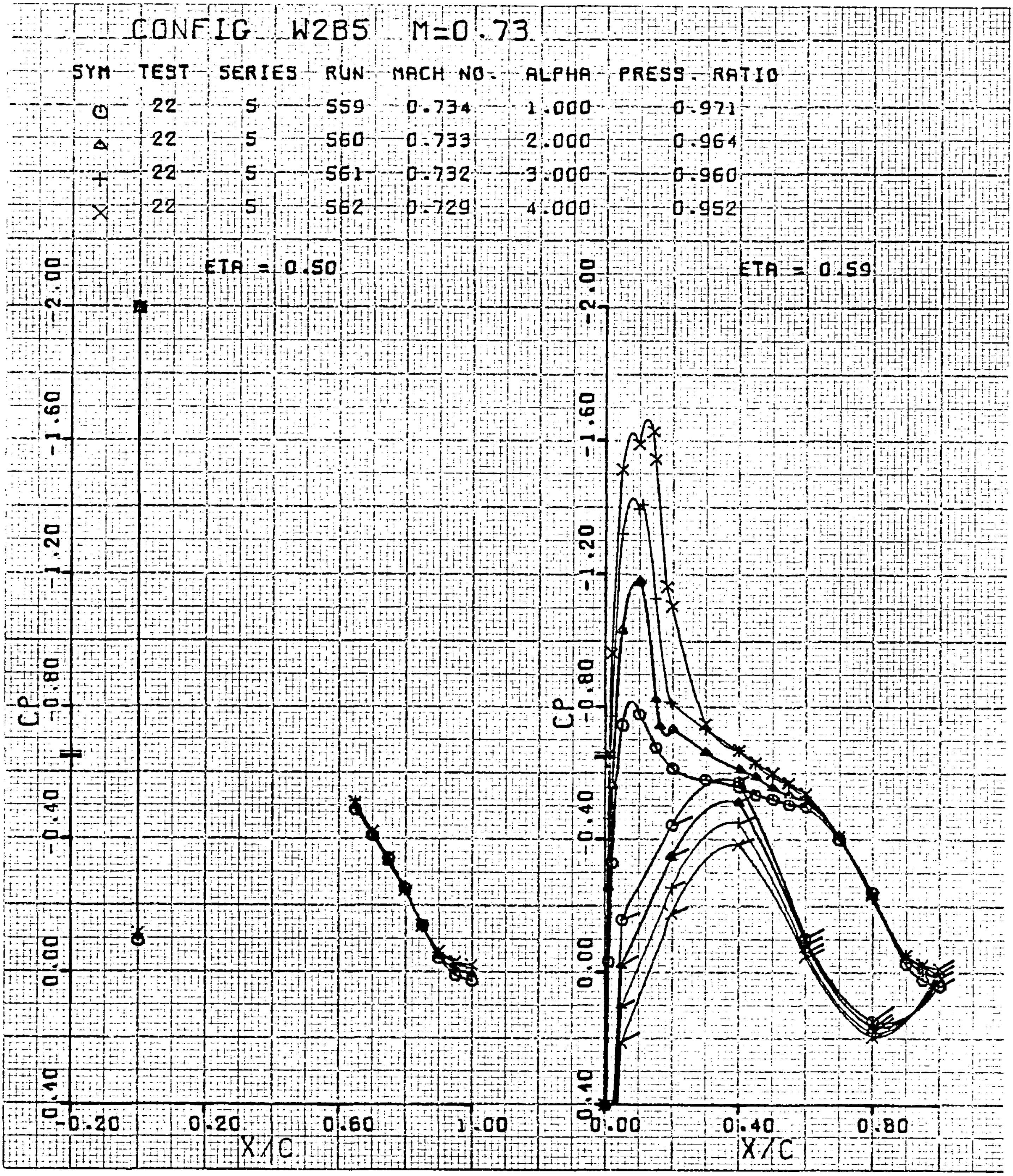

Figure 150. Clean, swept wing pressure distribution, effect of α, M_∞ = 0.73, η = 0.50, 0.59

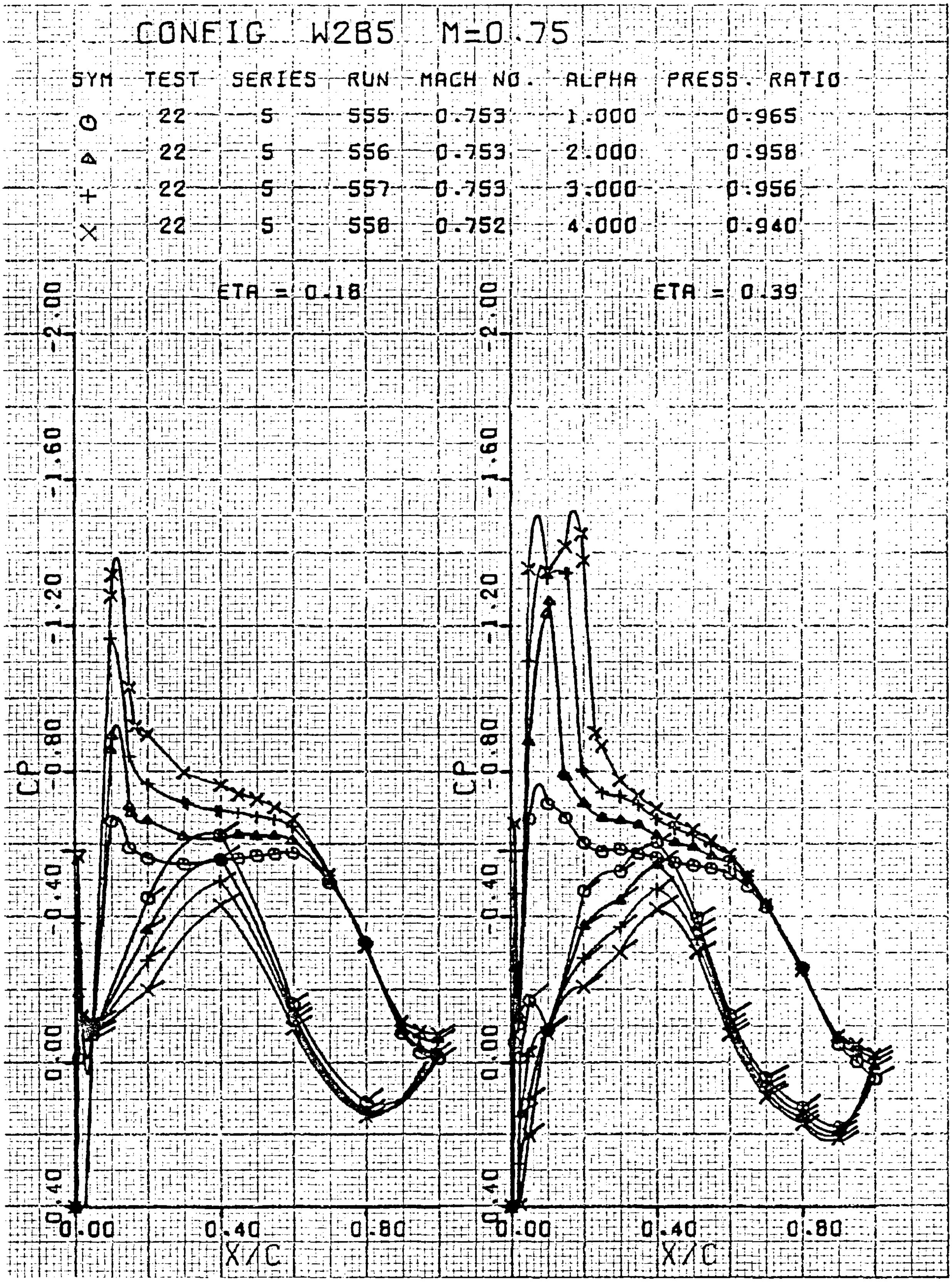

Figure 151. Clean, swept wing pressure distribution, effect of α, $M_\infty = 0.75$, $\eta = 0.18, 0.39$

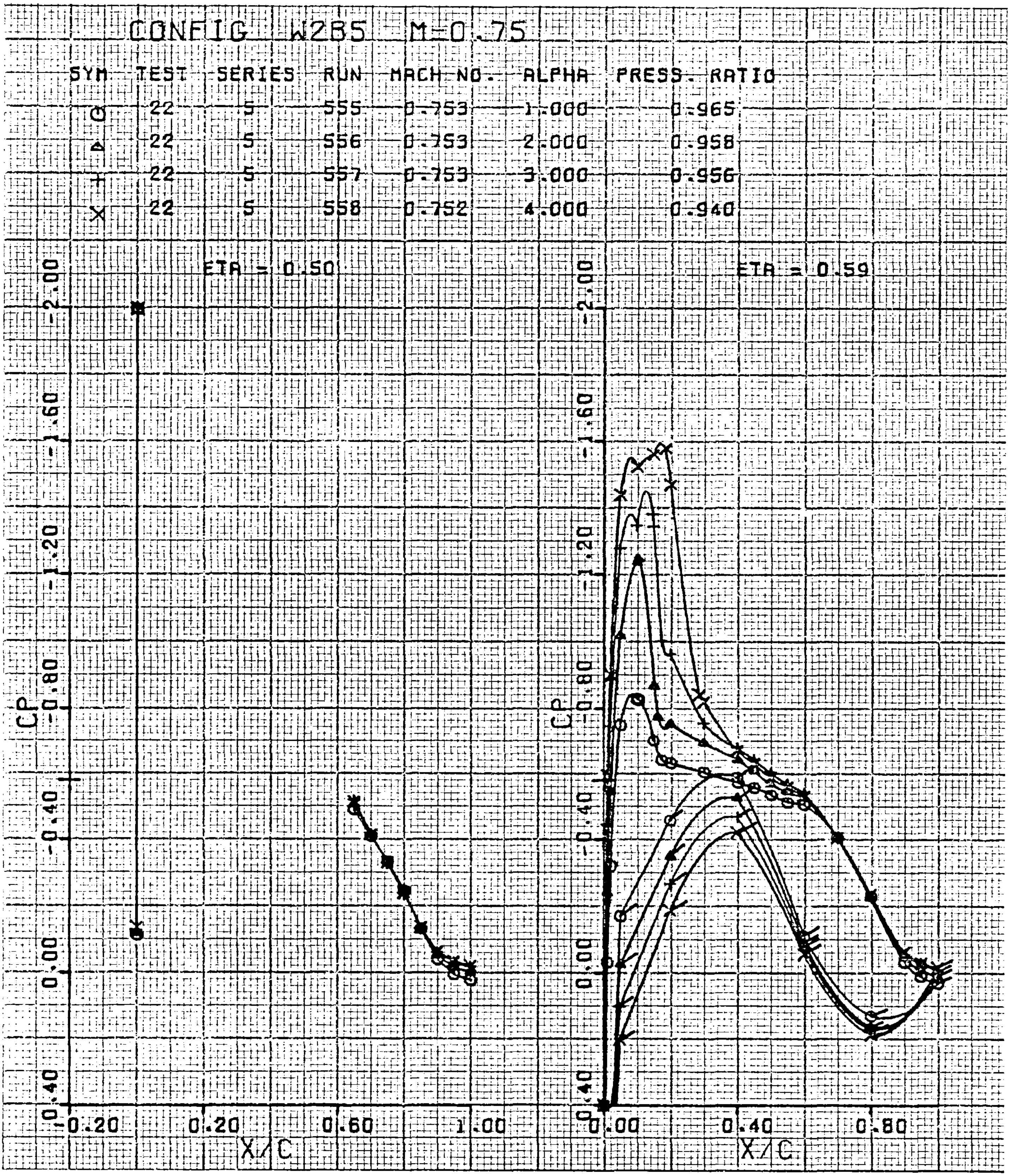

Figure 152. Clean, swept wing pressure distribution, effect of α, M_∞ = 0.75, η = 0.50, 0.59

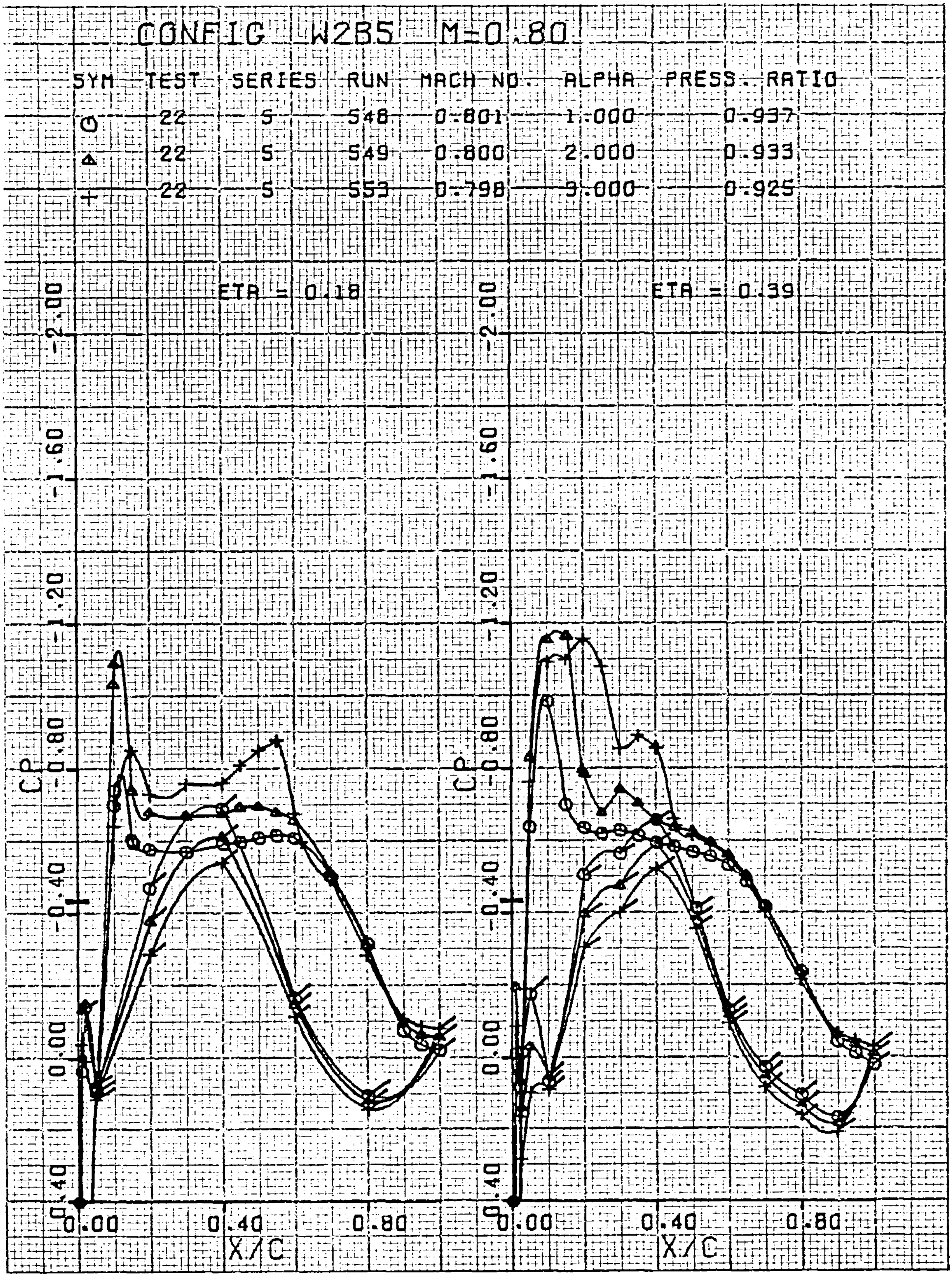

Figure 153. Clean, swept wing pressure distribution, effect of α, $M_\infty = 0.80$, $\eta = 0.18, 0.39$

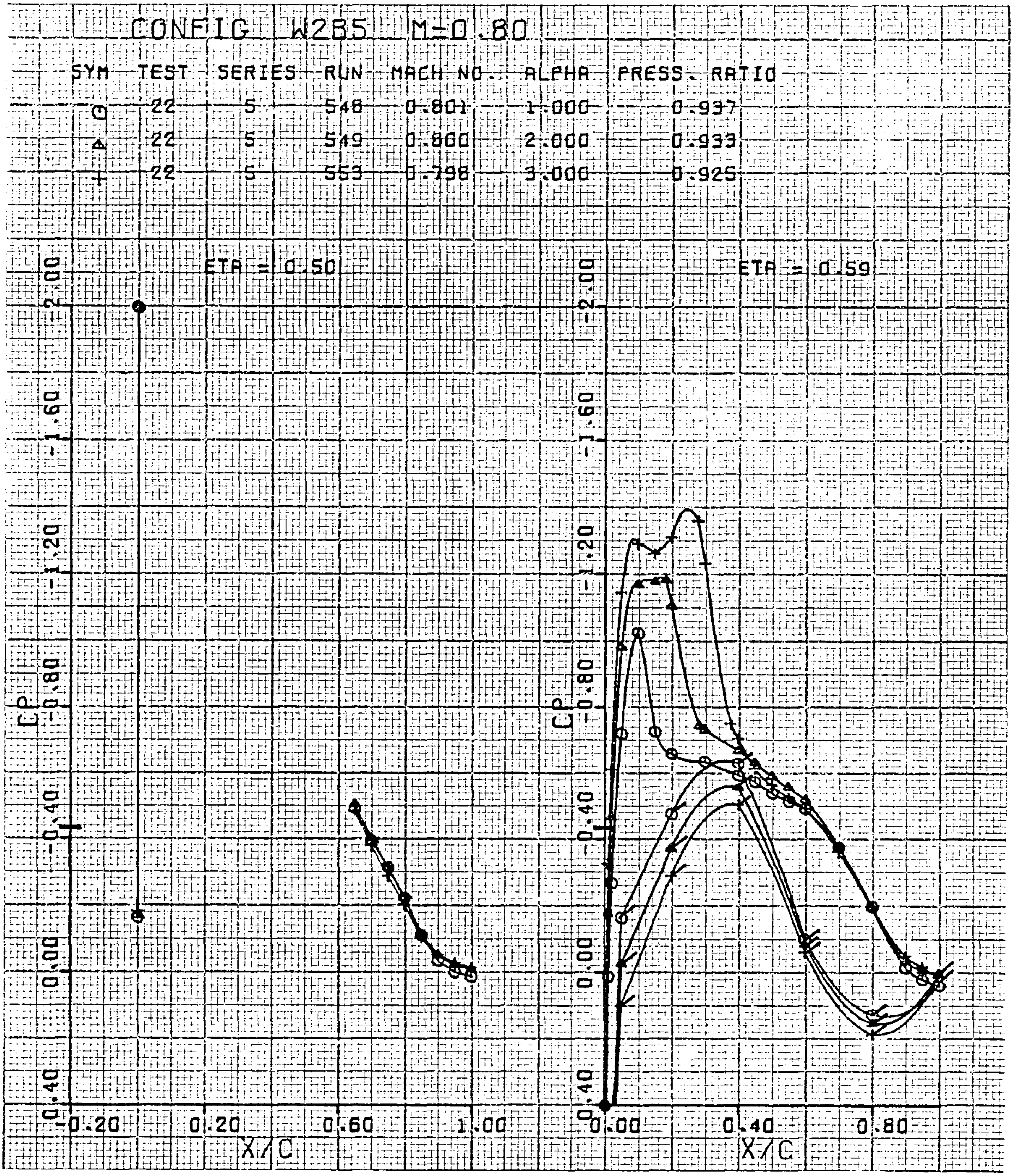

Figure 154. Clean, swept wing pressure distribution, effect of α, M_∞ = 0.80, η = 0.50, 0.59

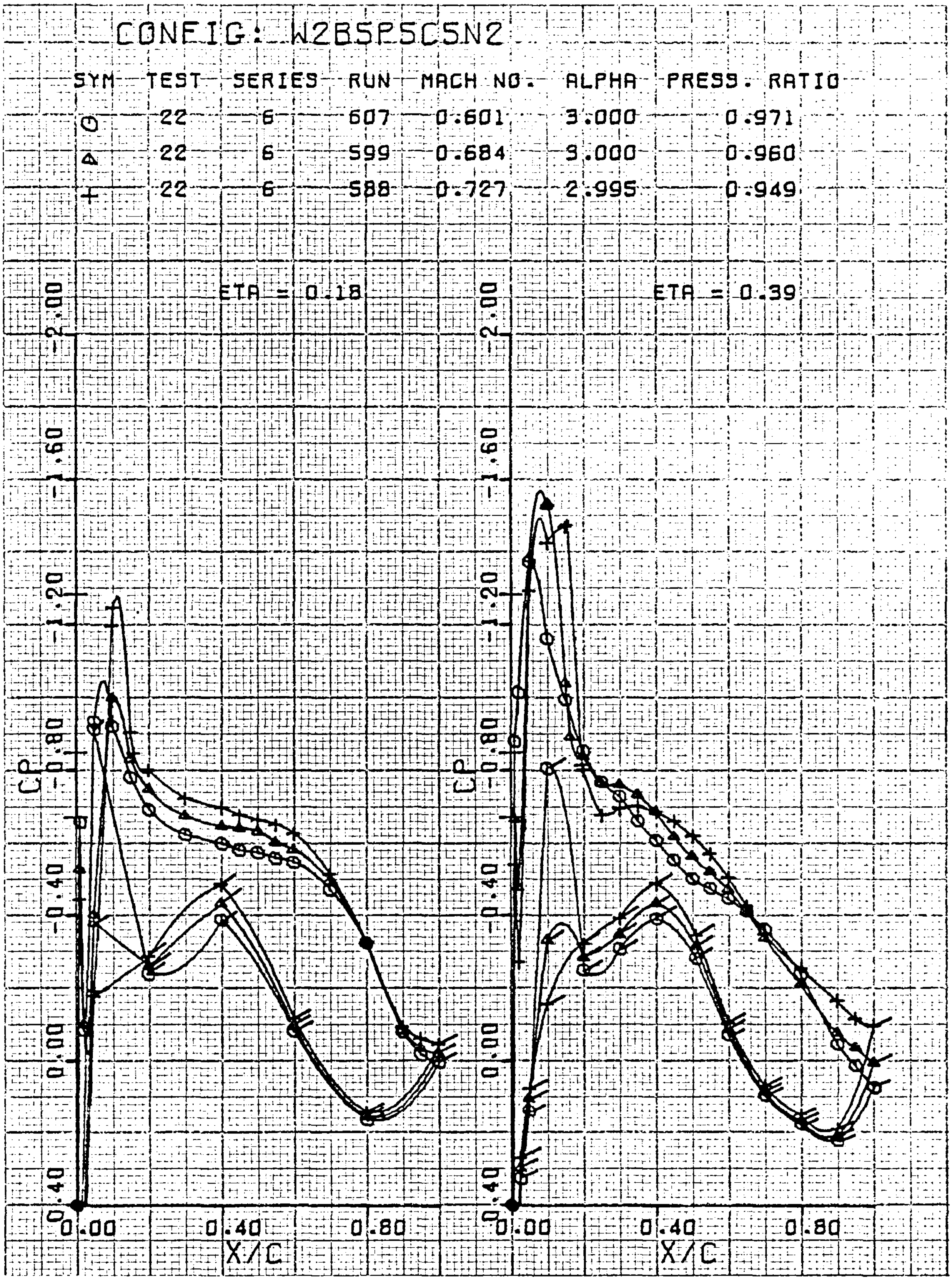

Figure 155. Wing pressure distribution, effect of Mach number, nozzle N_2, η = 0.18, 0.39

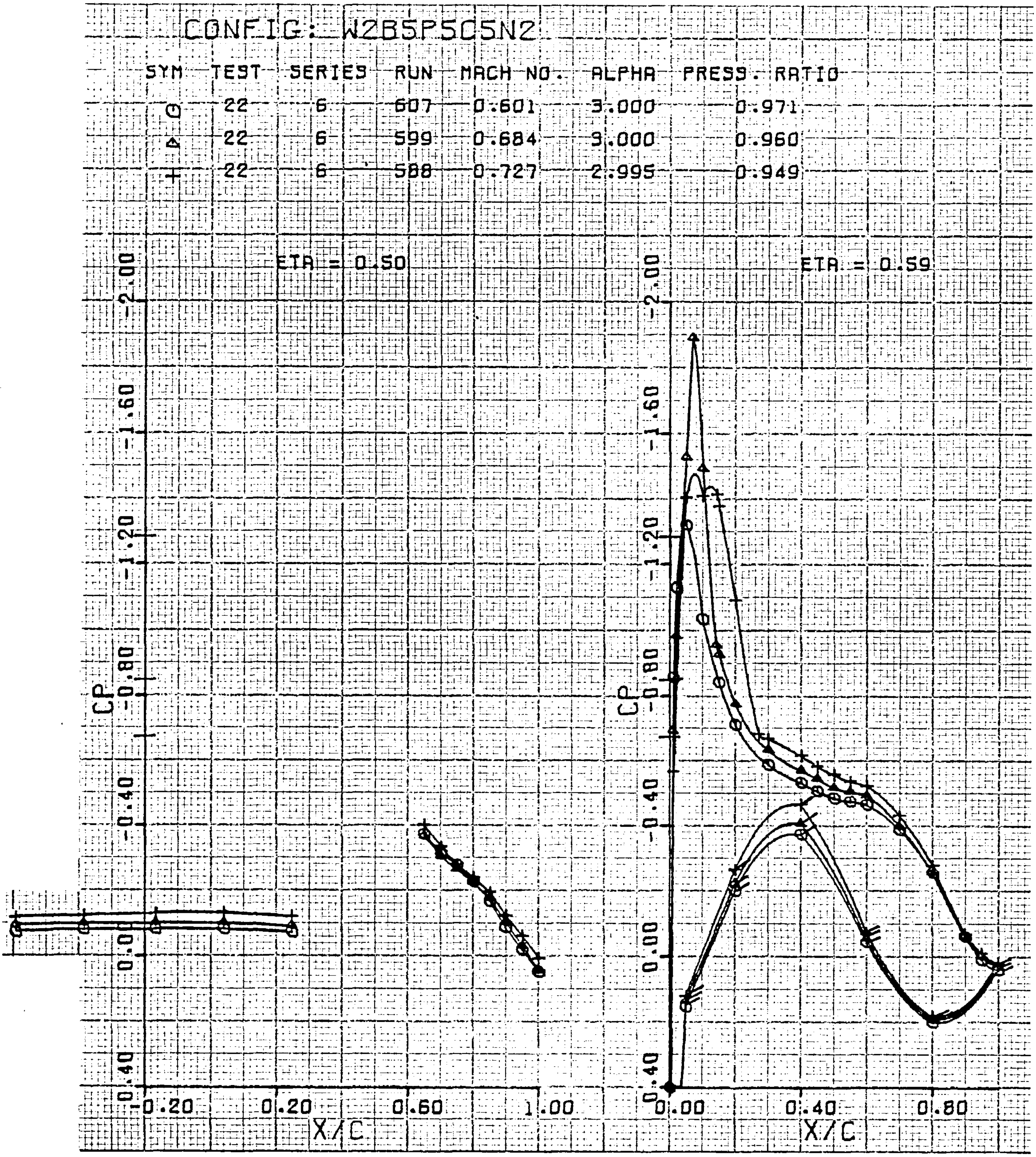

Figure 156. Wing pressure distribution, effect of Mach number, nozzle N_2, η = 0.50, 0.59

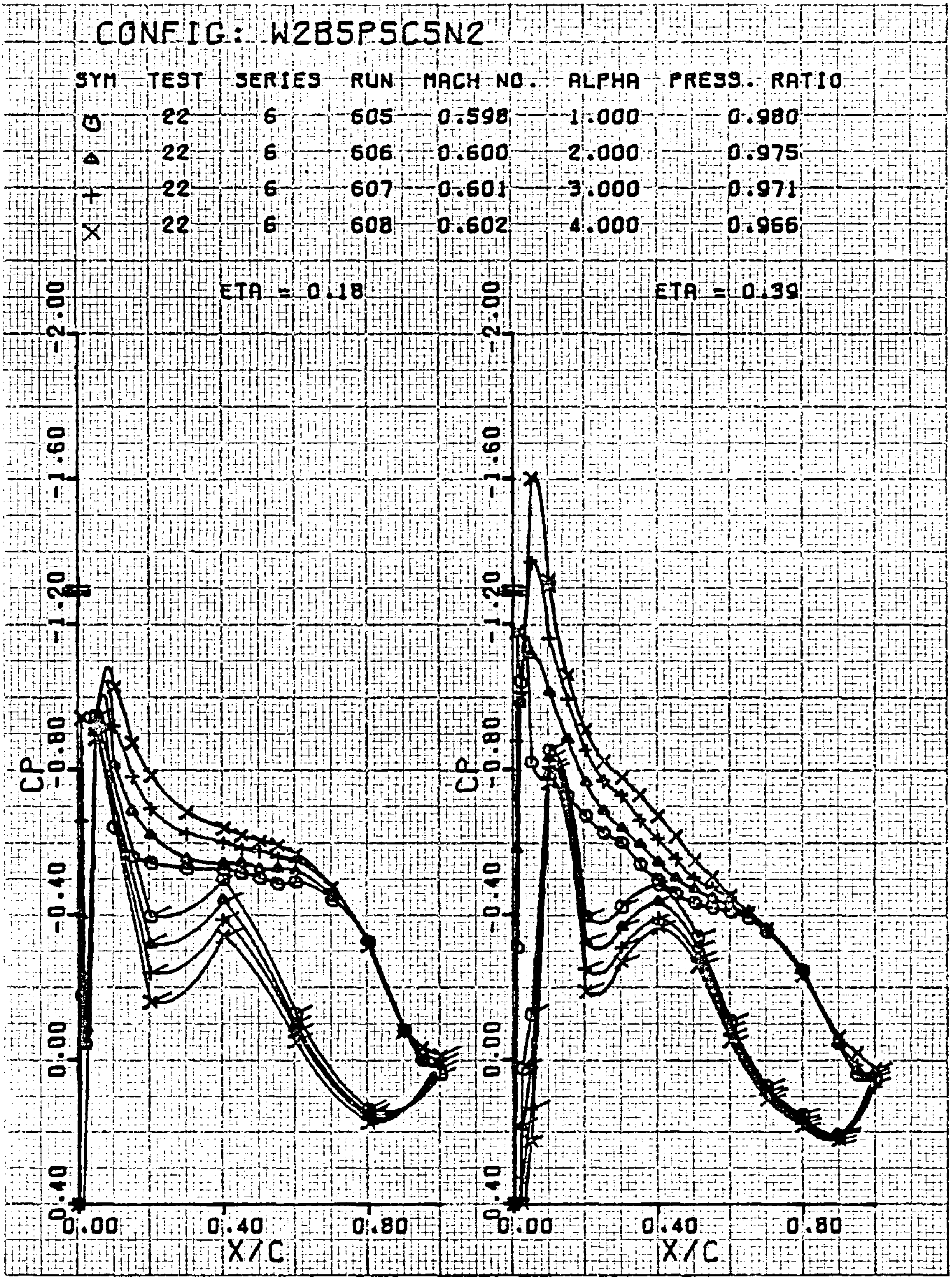

Figure 157. Wing pressure distribution, effect of α, nozzle N_2, $M_\infty = 0.60$, $\eta = 0.18, 0.39$

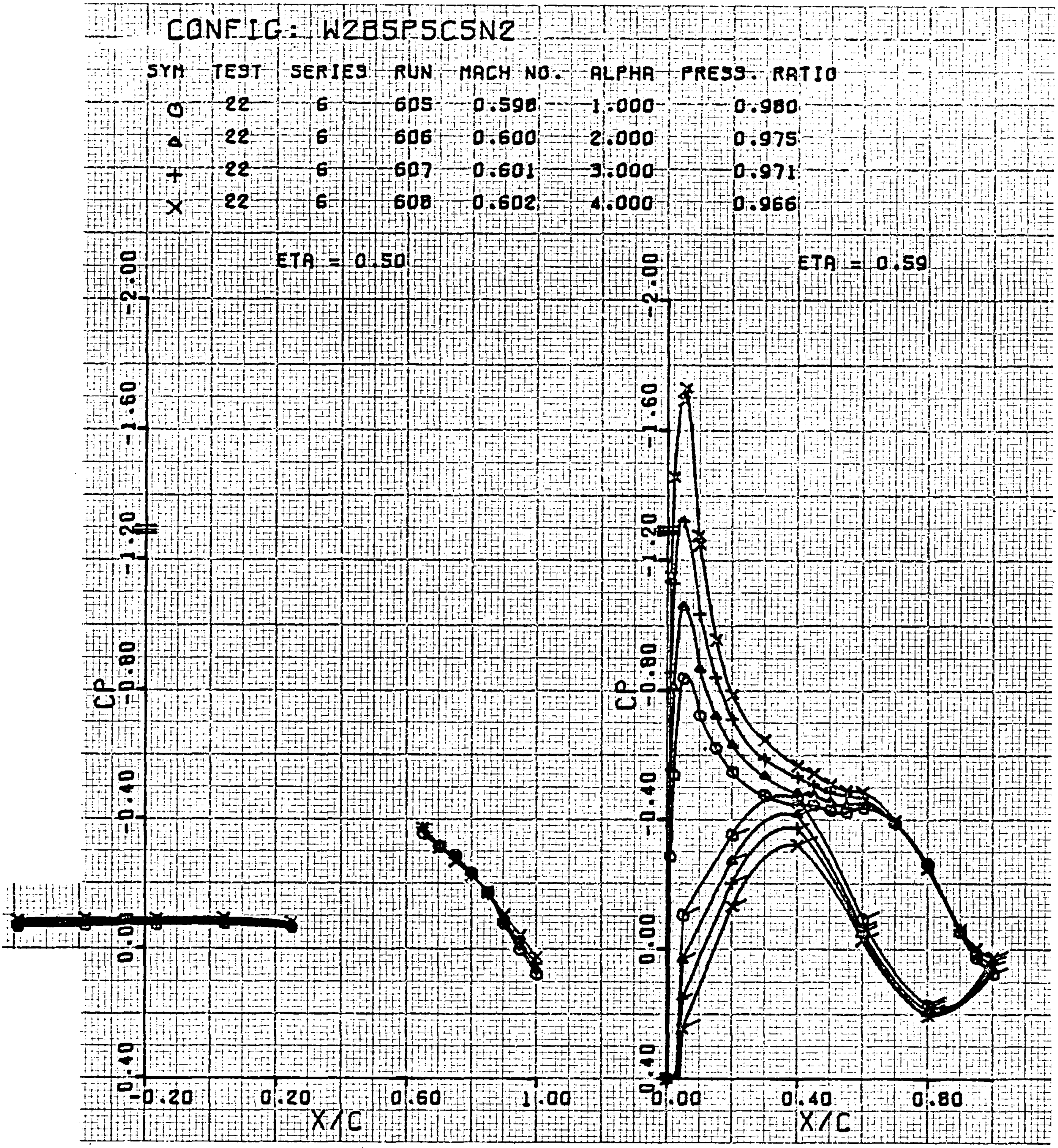

Figure 158. Wing pressure distribution, effect of α, nozzle N_2, $M_\infty = 0.60$, $\eta = 0.50, 0.59$

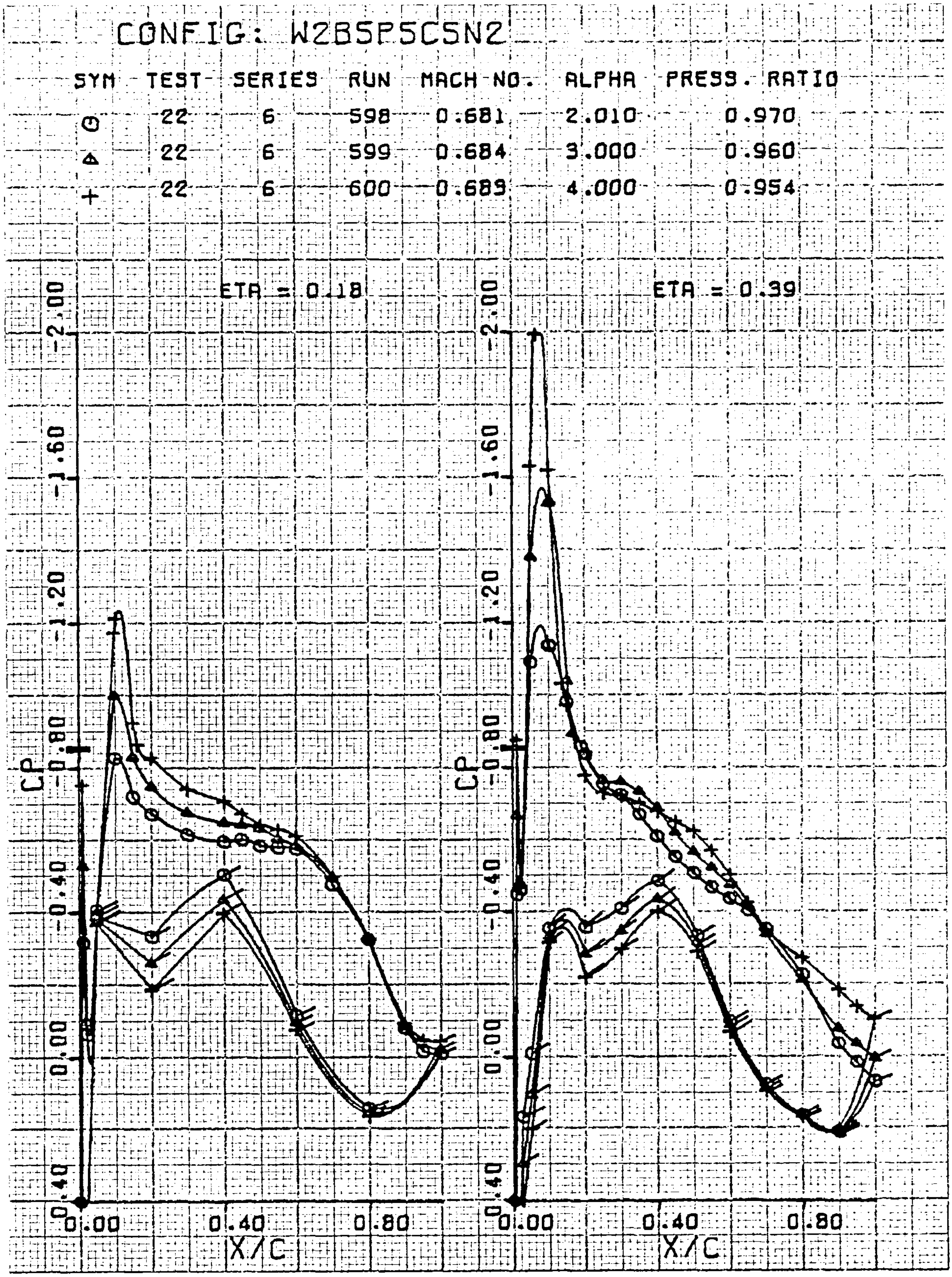

Figure 159. Wing pressure distribution, effect of α, nozzle N_2, $M_\infty = 0.68$, $\eta = 0.18, 0.39$

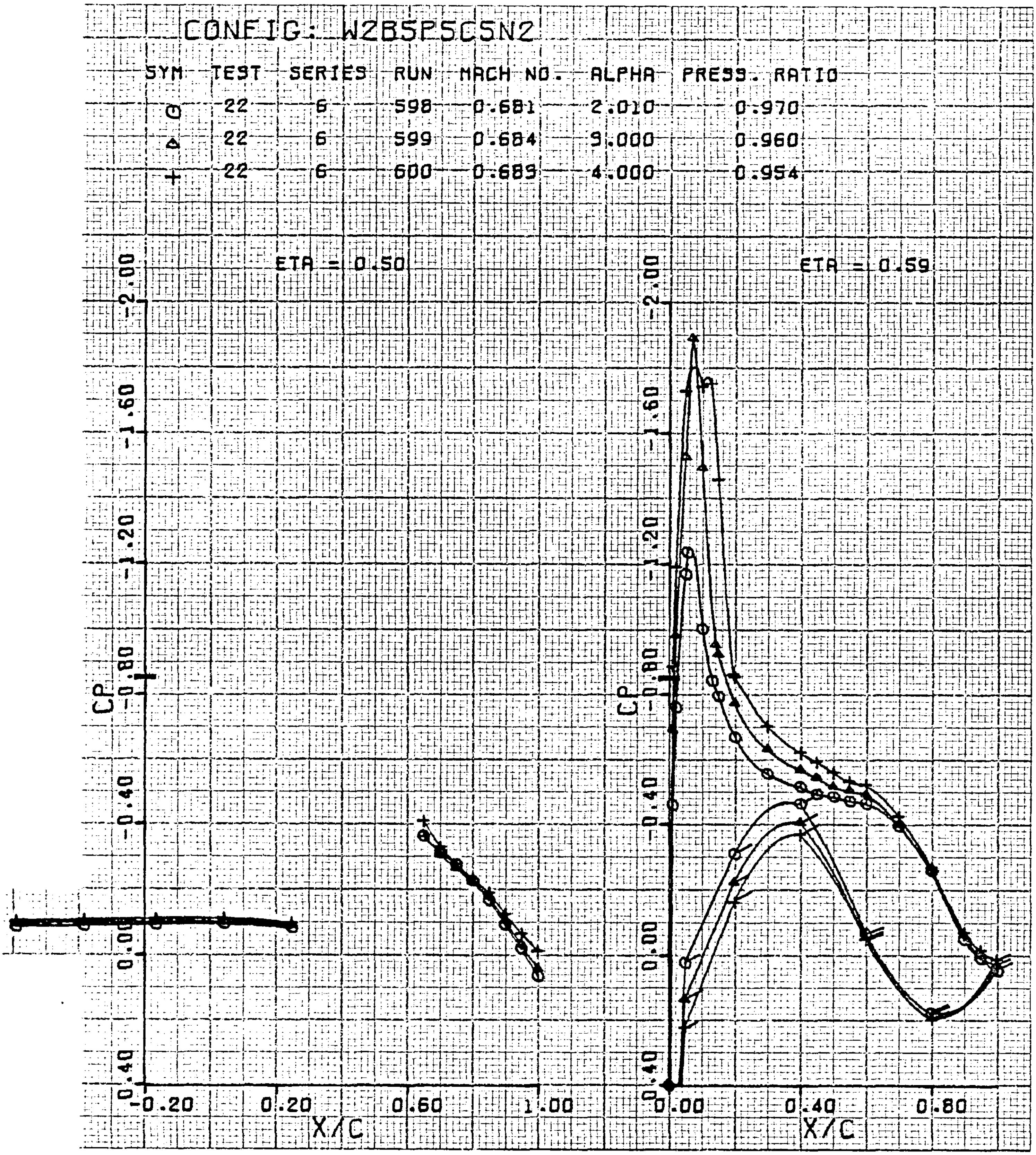

Figure 160. Wing pressure distribution, effect of α, nozzle N_2, $M_\infty = 0.68$, $\eta = 0.50, 0.59$

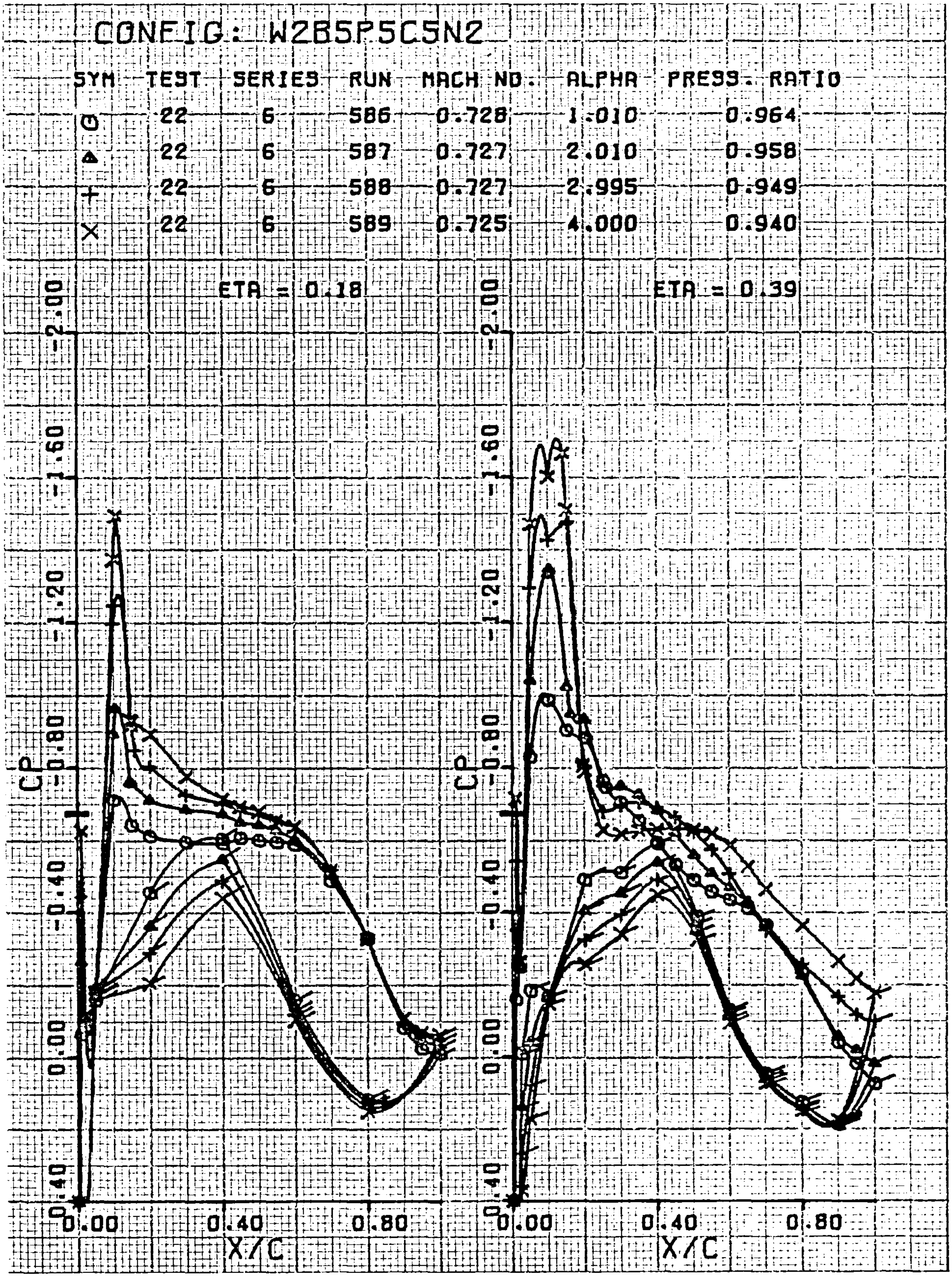

Figure 161. Wing pressure distribution, effect of α, nozzle N_2, $M_\infty = 0.73$, $\eta = 0.18, 0.39$

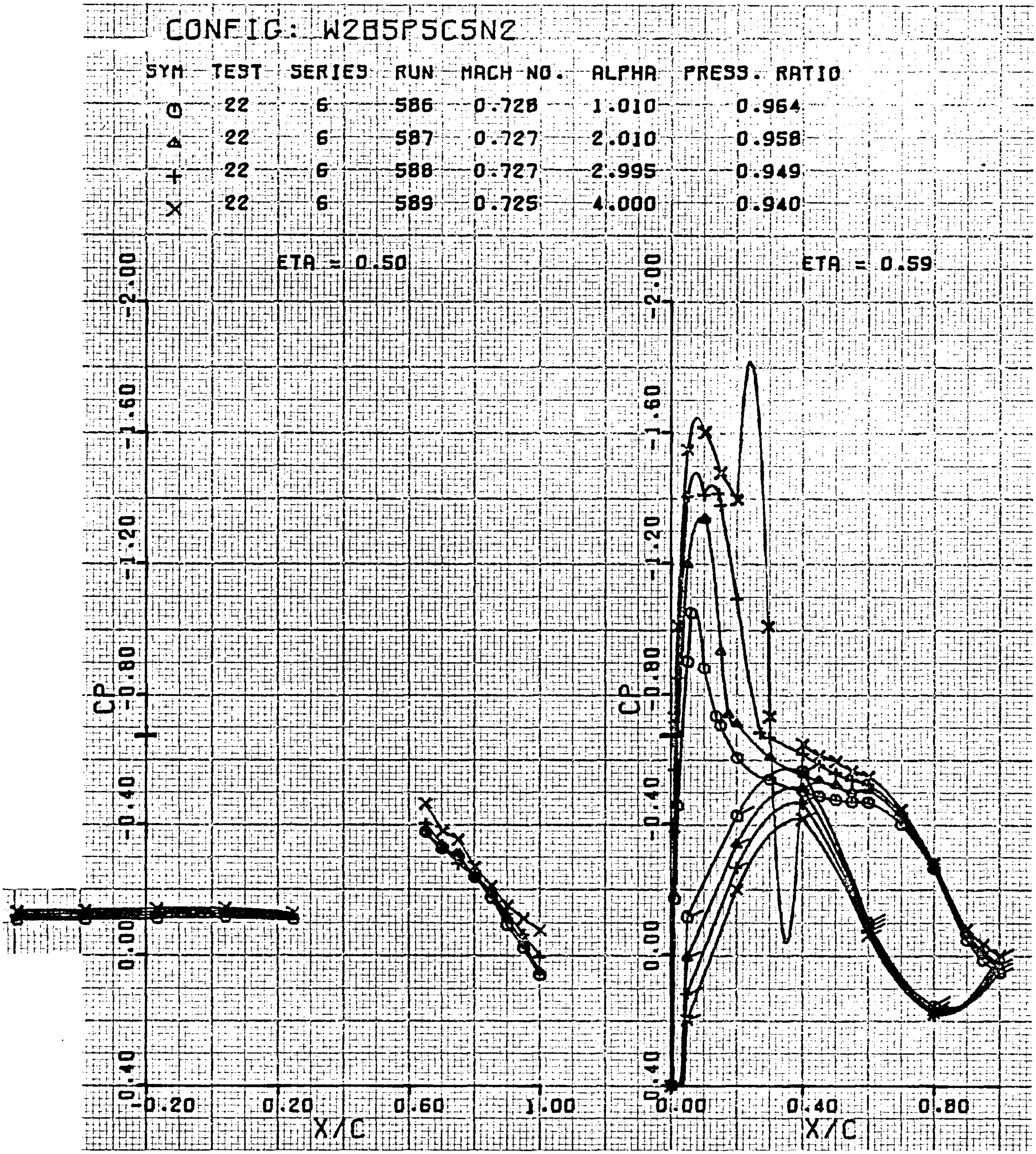

Figure 162. Wing pressure distribution, effect of α, nozzle N_2, $M_\infty = 0.73$, $\eta = 0.50, 0.59$

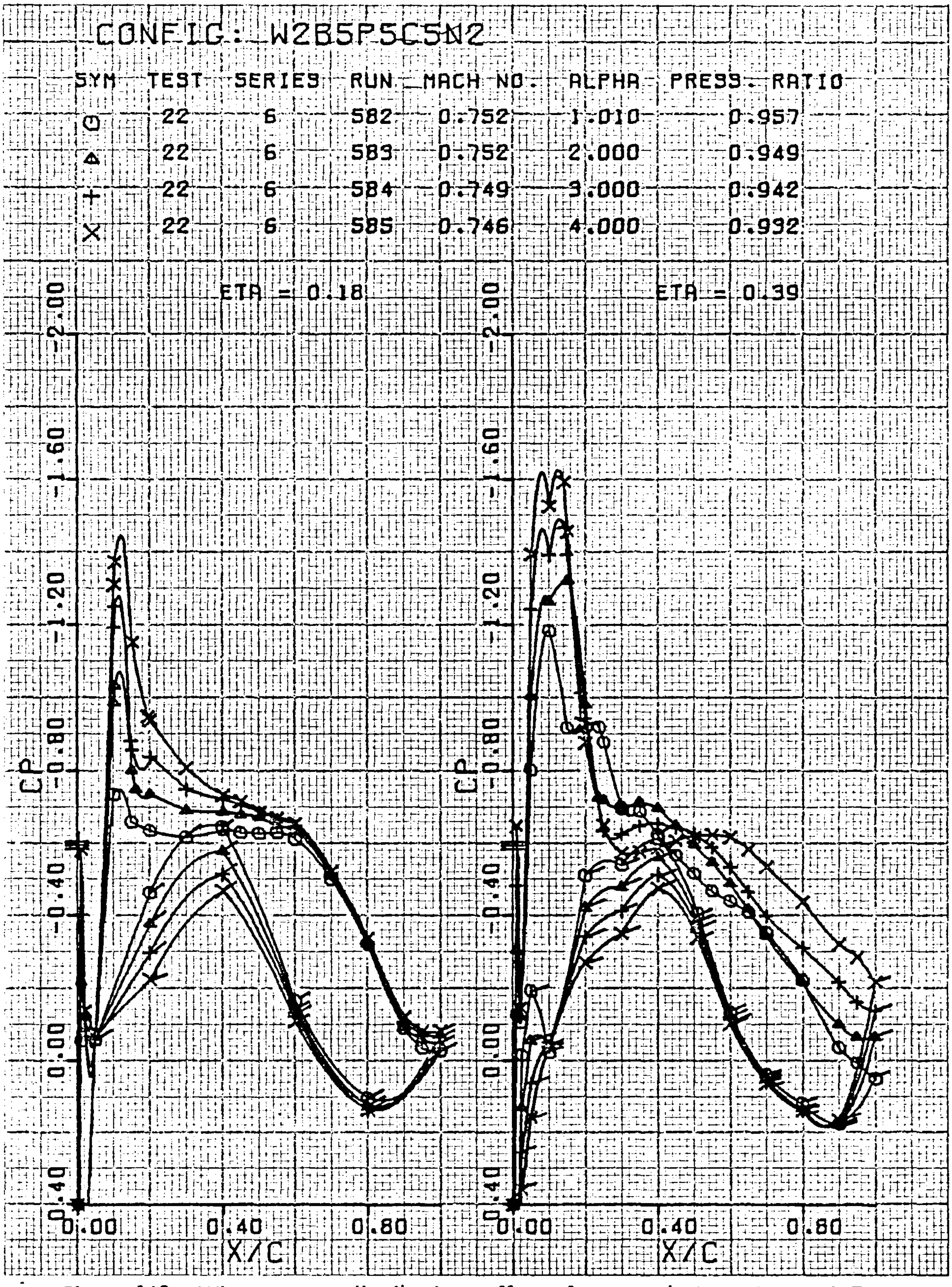

Figure 163. Wing pressure distribution, effect of α, nozzle N_2, $M_\infty = 0.75$, $\eta = 0.18, 0.39$

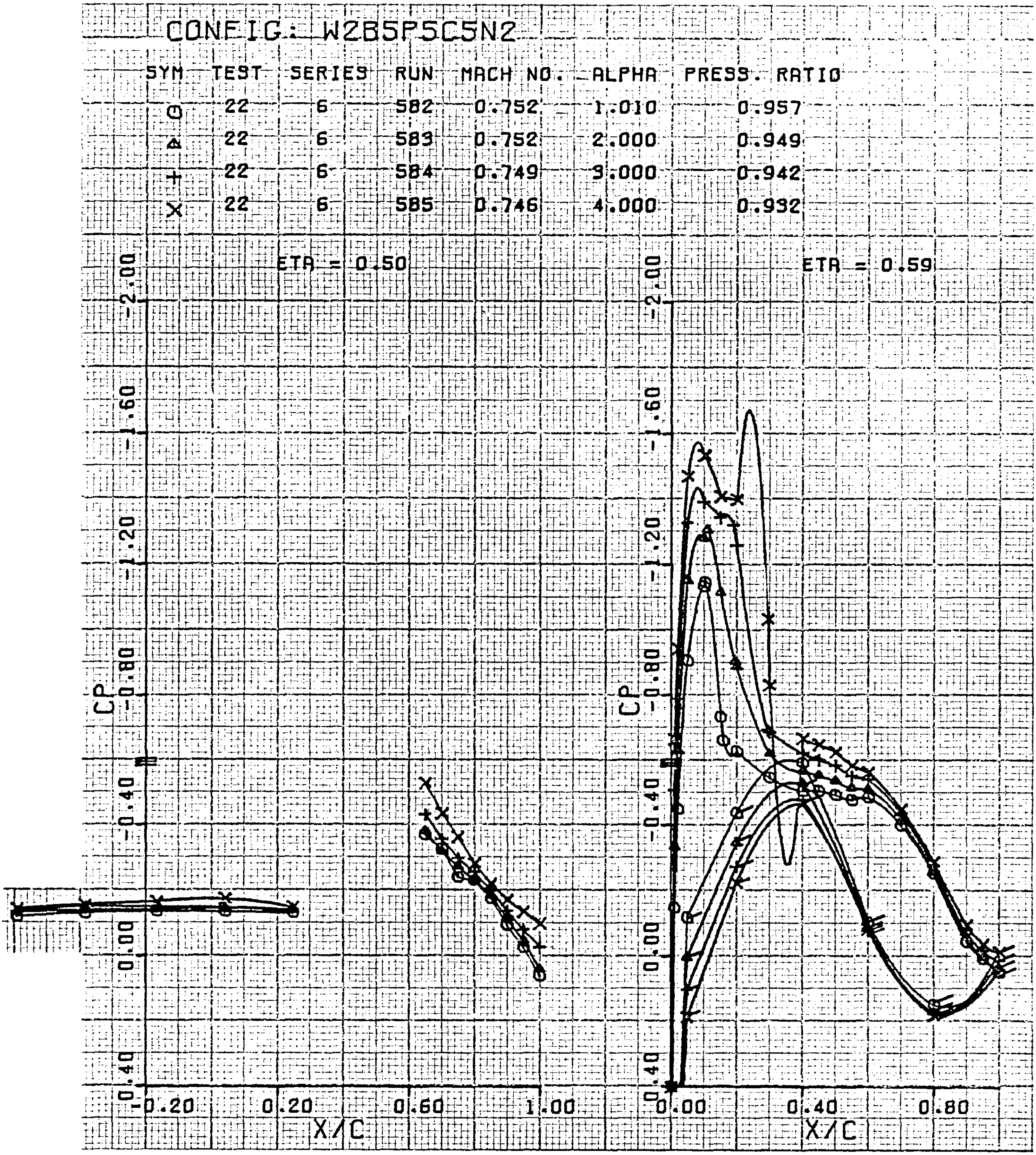

Figure 164. Wing pressure distribution, effect of α, nozzle N_2, M_∞ = 0.75, η = 0.50, 0.59

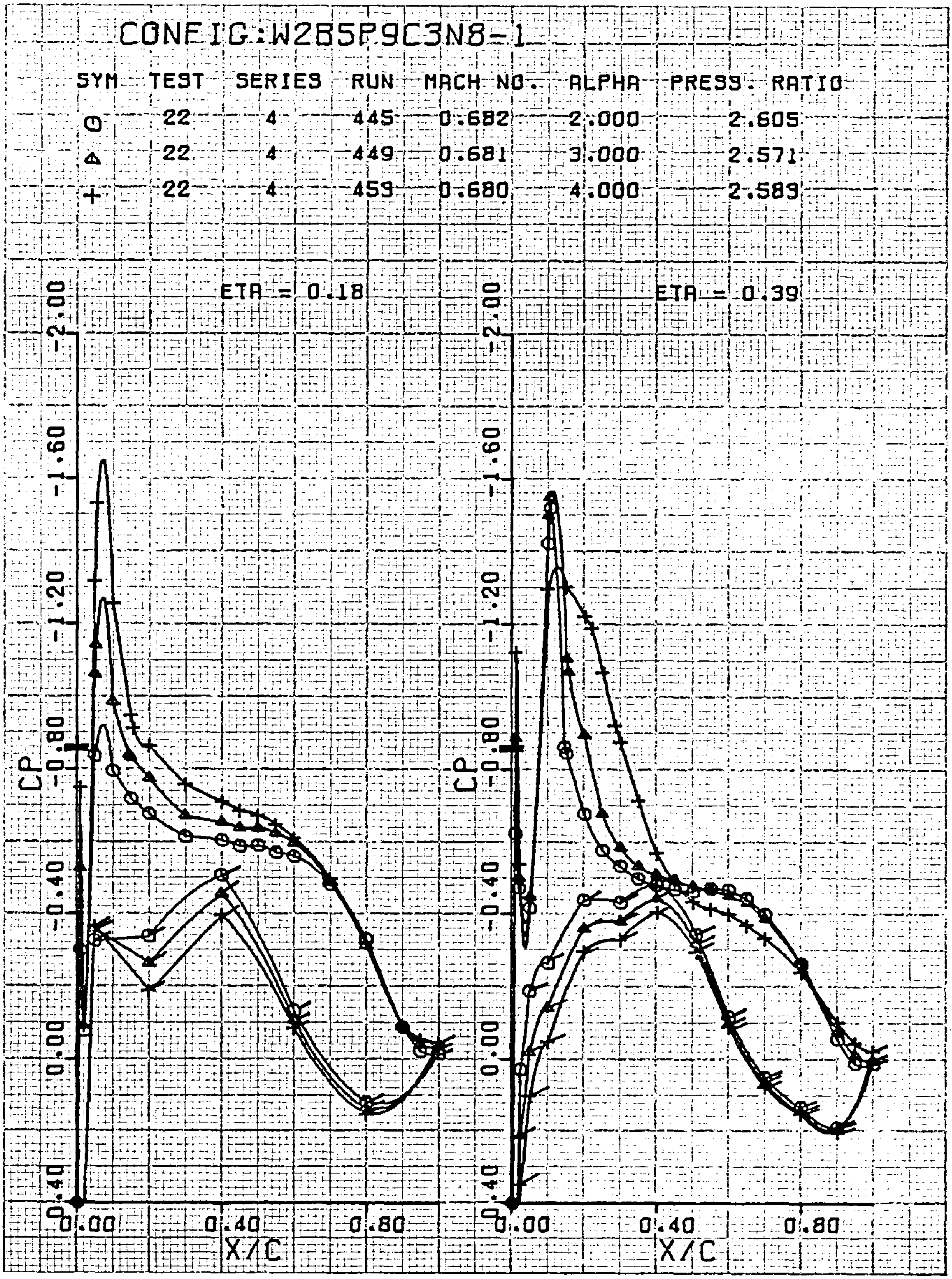

Figure 165. Wing pressure distribution, effect of α, nozzle N_8^1, $M_\infty = 0.68$, $\eta = 0.18, 0.39$

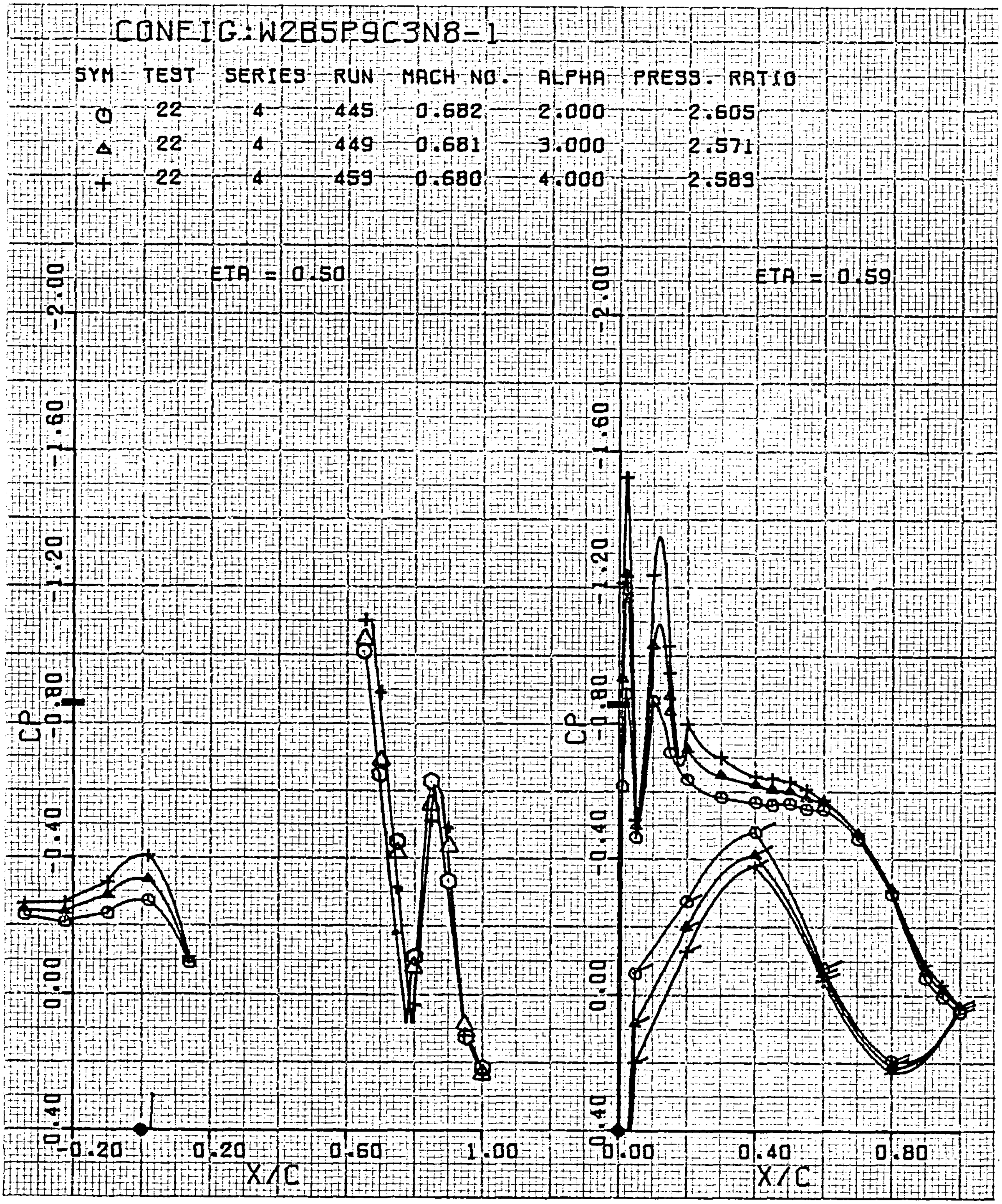

Figure 166. Wing pressure distribution, effect of α, nozzle $N_8^{\ 1}$, $M_\infty = 0.68$, $\eta = 0.50, 0.59$

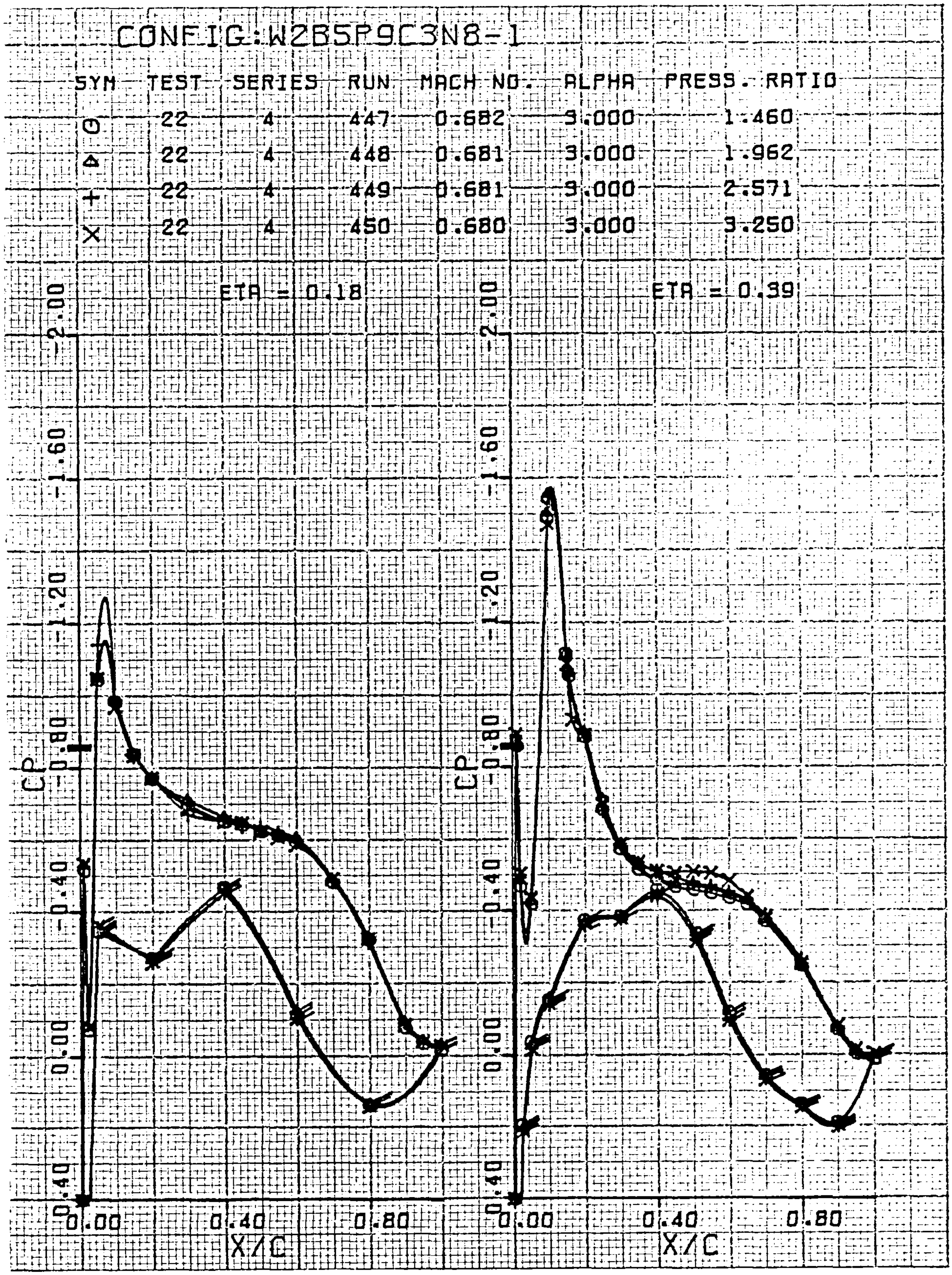

Figure 167. Wing pressure distribution, effect of nozzle pressure ratio, nozzle N_8^1, $M_\infty = 0.68$, $\eta = 0.18, 0.39$

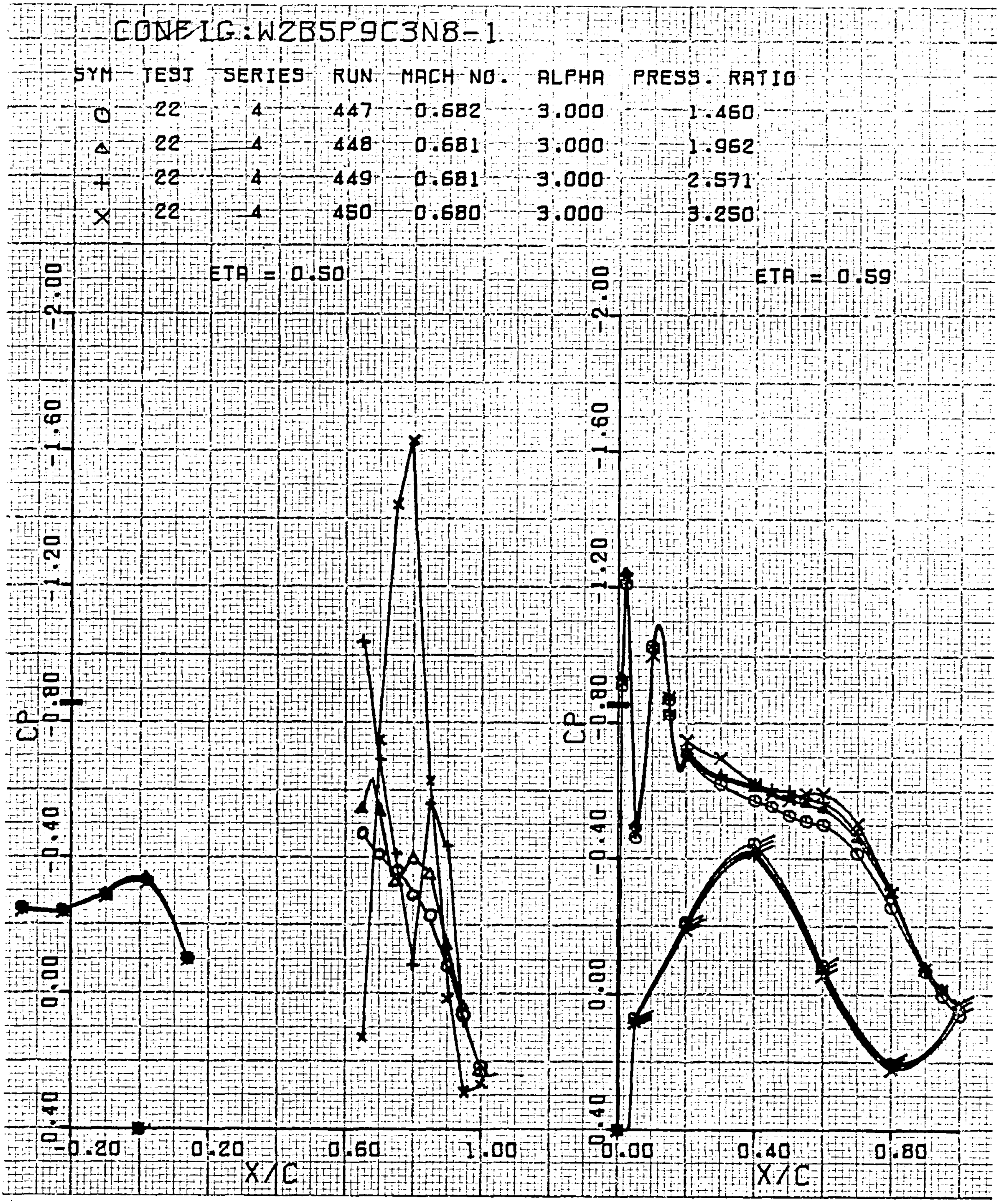

Figure 168. Wing pressure distribution, effect of nozzle pressure ratio, nozzle N_8^{1}, $M_\infty = 0.68$, $\eta = 0.50, 0.59$

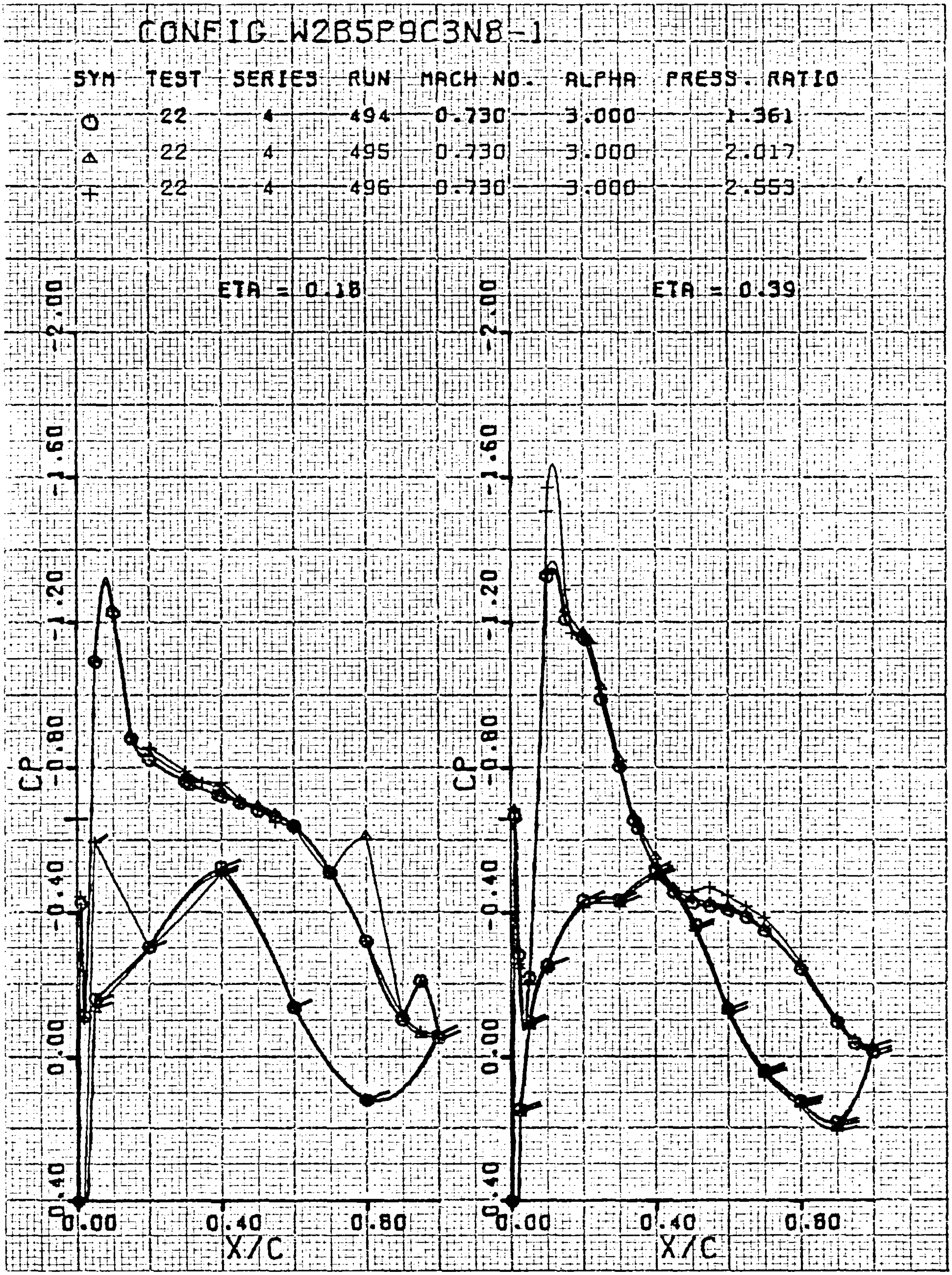

Figure 169. Wing pressure distribution, effect of nozzle pressure ratio, nozzle $N_8^{\,1}$, $M_\infty = 0.73$, $\eta = 0.18, 0.39$

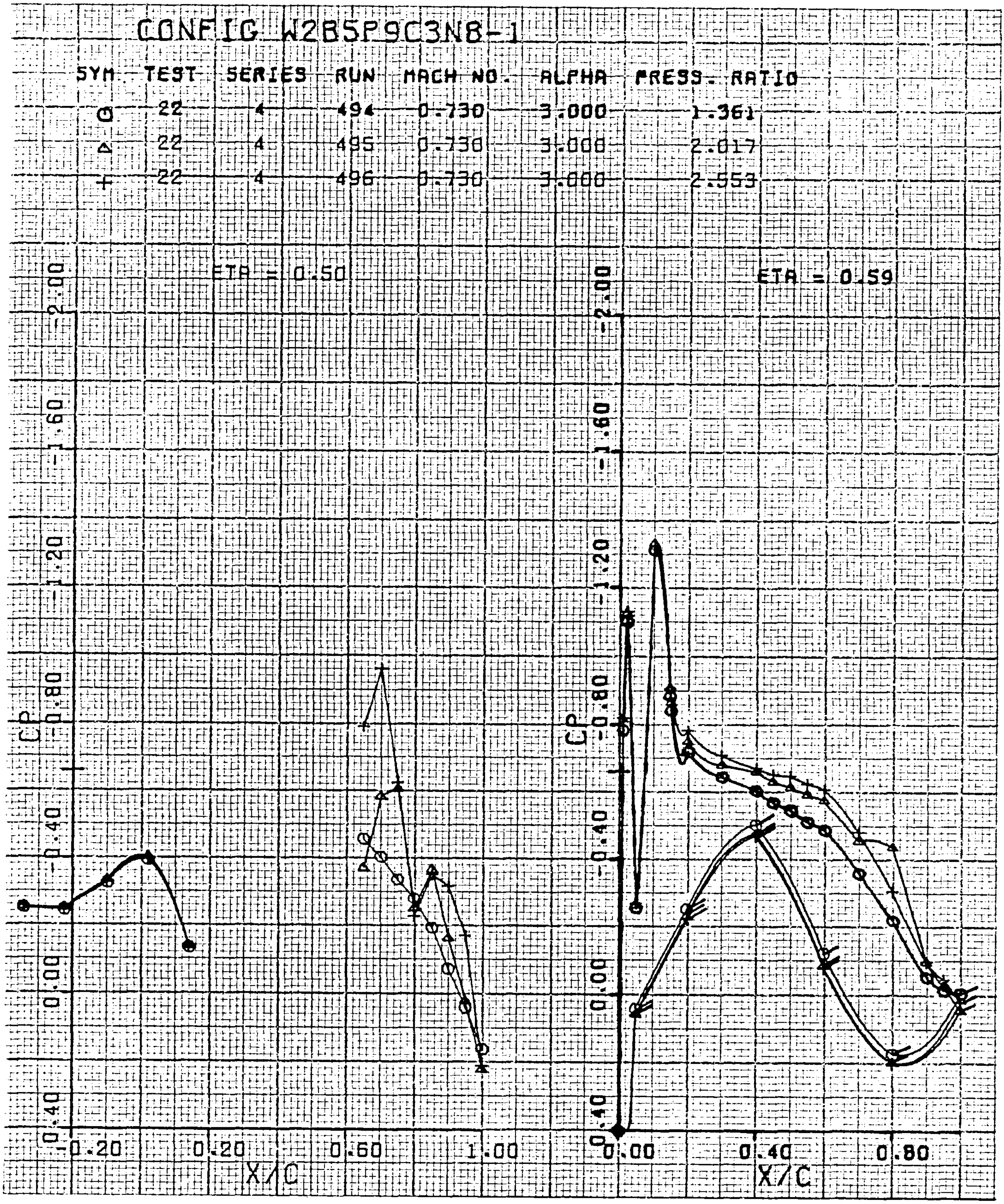

Figure 170. Wing pressure distribution, effect of nozzle pressure ratio, nozzle N_8^{1}, $M_\infty = 0.73$, $\eta = 0.50, 0.59$

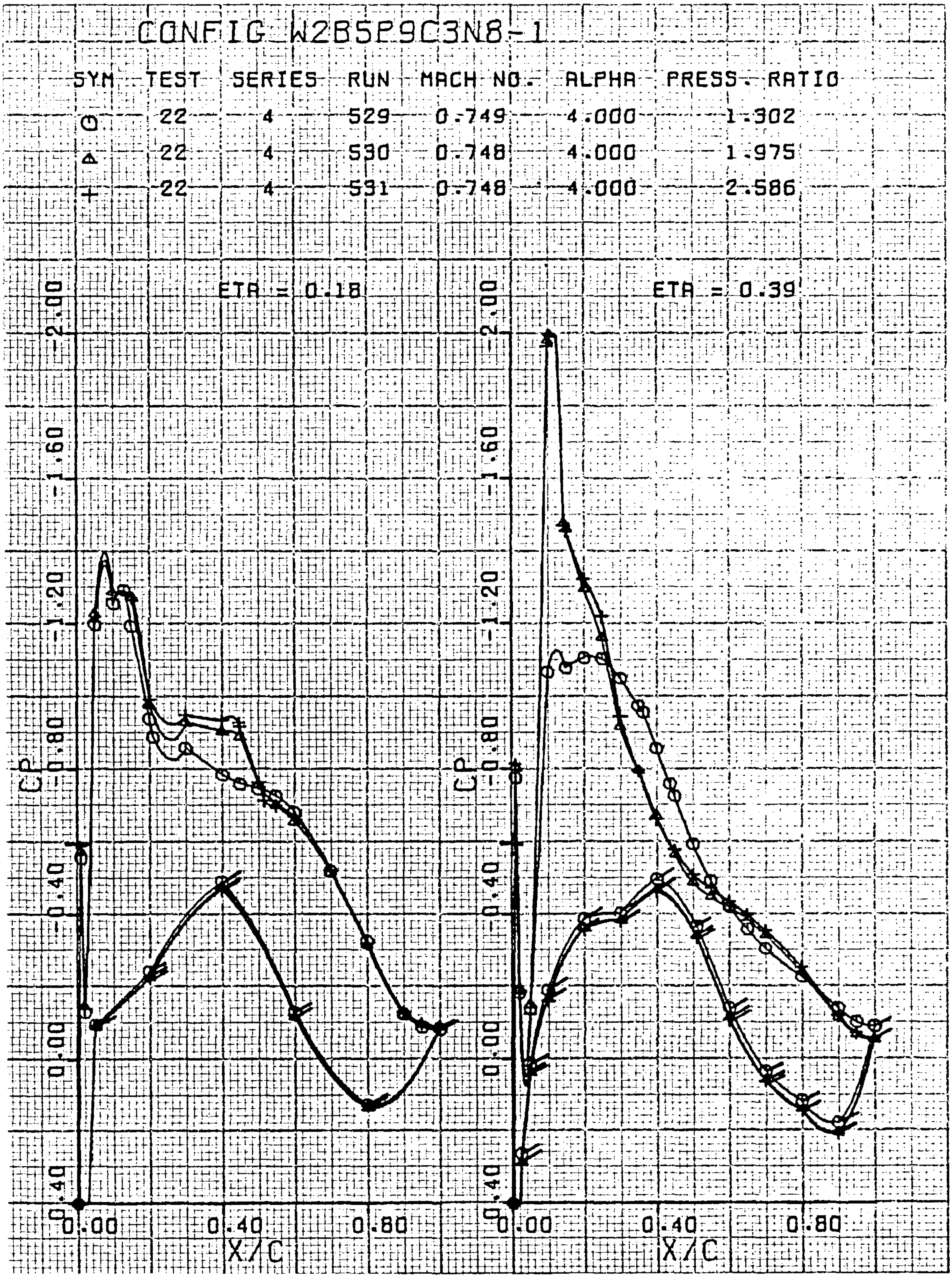

Figure 171. Wing pressure distribution, effect of nozzle pressure ratio, nozzle $N_8^{\,1}$, $M_\infty = 0.75$, $\eta = 0.18, 0.39$

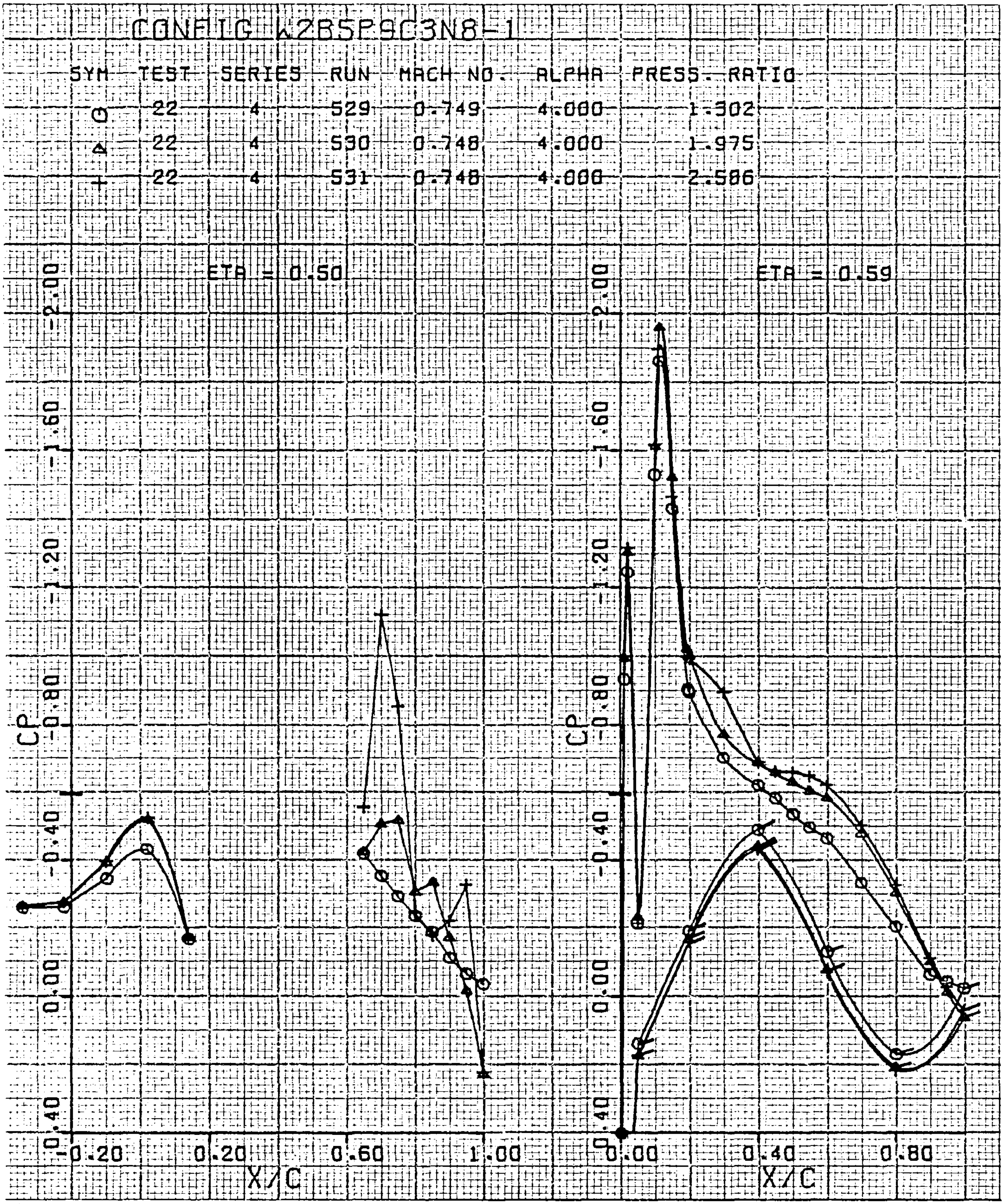

Figure 172. Wing pressure distribution, effect of nozzle pressure ratio, nozzle $N_8^{\ 1}$, $M_\infty = 0.75$, $\eta = 0.50, 0.59$

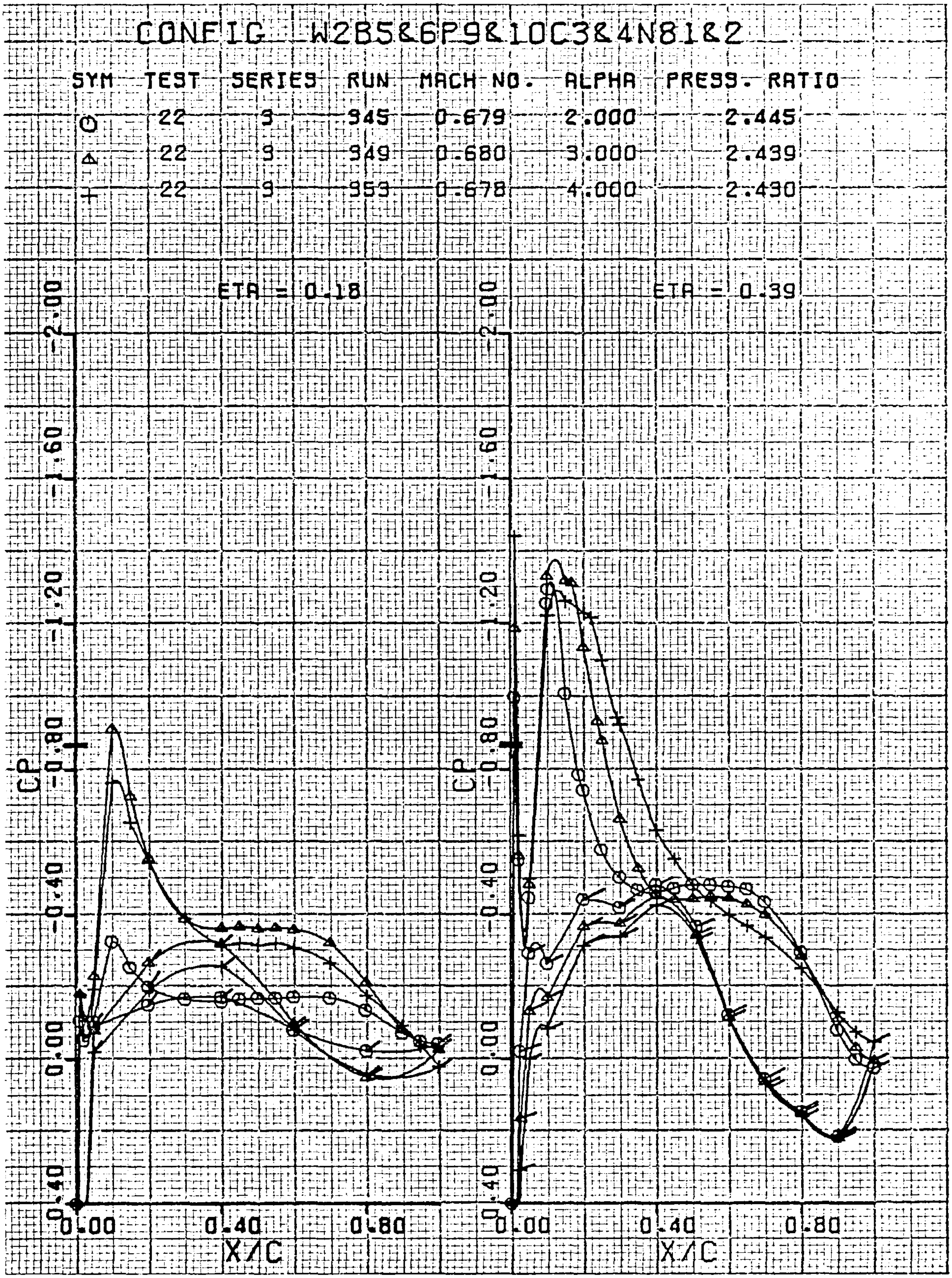

Figure 173. Wing pressure distribution, effect of α, nozzles N_8^{1} and N_8^{2}, $M_\infty = 0.68$, $\eta = 0.18, 0.39$

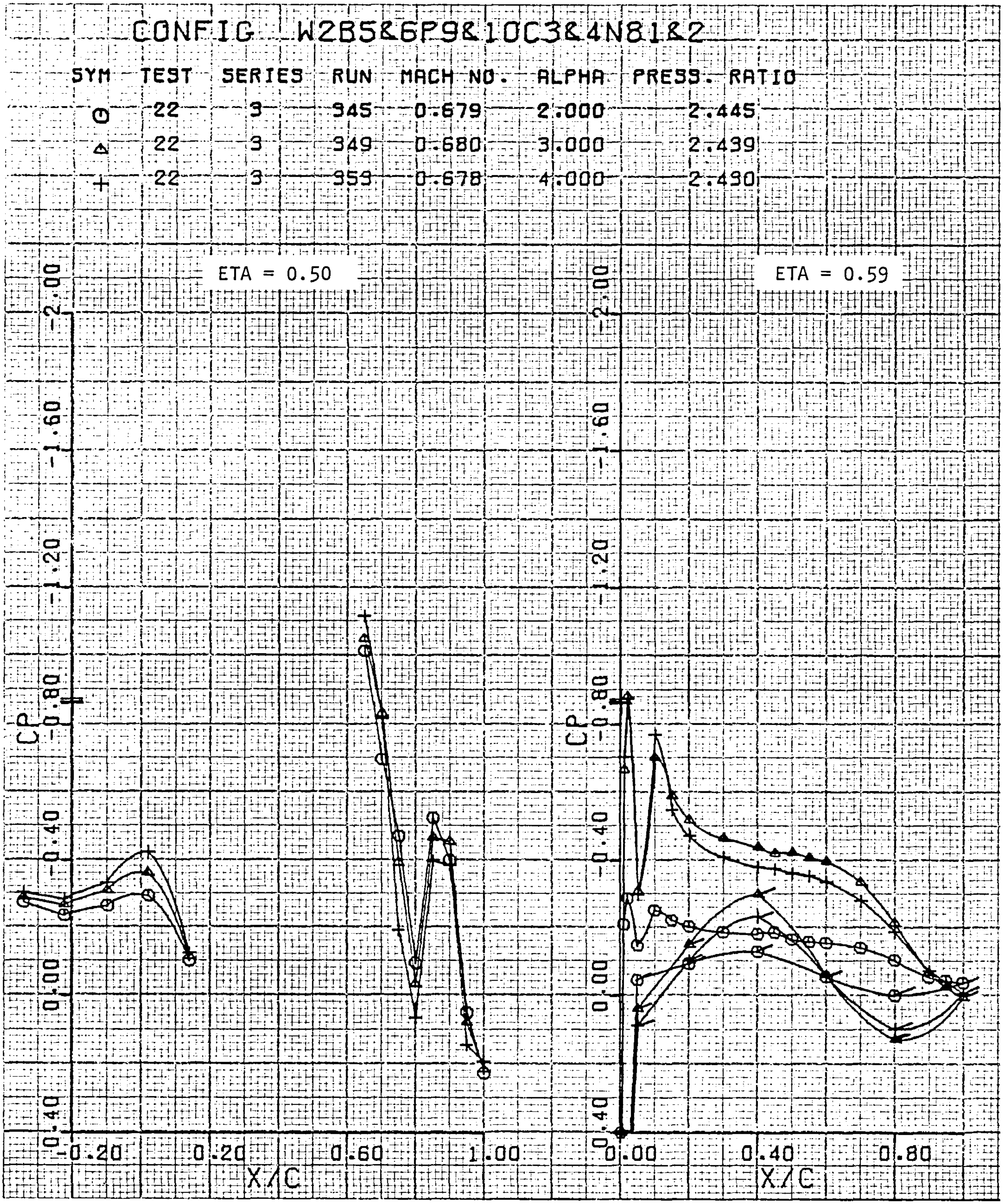

Figure 174. Wing pressure distribution, effect of α, nozzles N_8^1 and N_8^2, $M_\infty = 0.68$, $\eta = 0.50, 0.59$

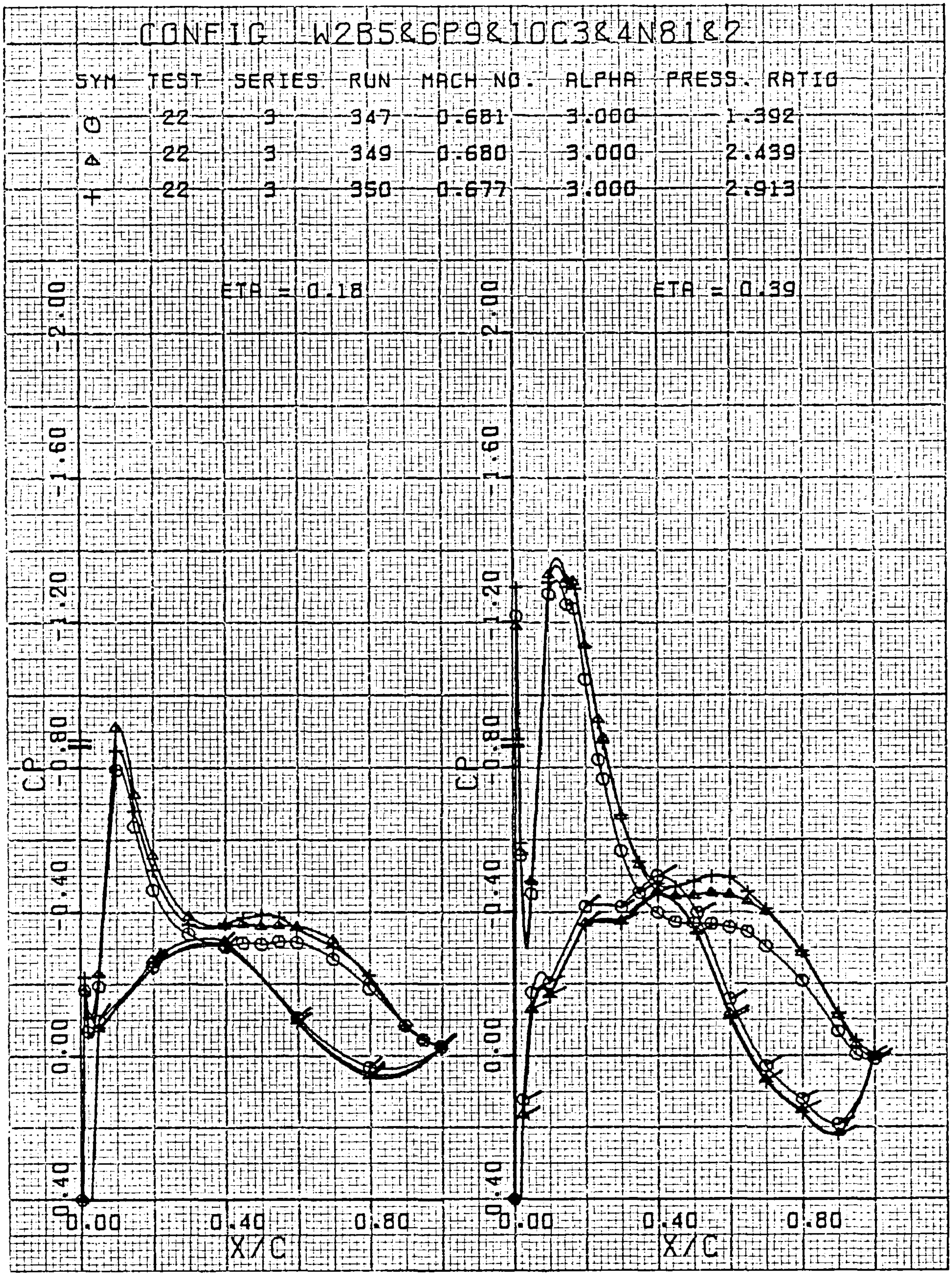

Figure 175. Wing pressure distribution, effect of nozzle pressure ratio, nozzles N_8^{1} and N_8^{2}, $M_\infty = 0.68$, $\eta = 0.18, 0.39$

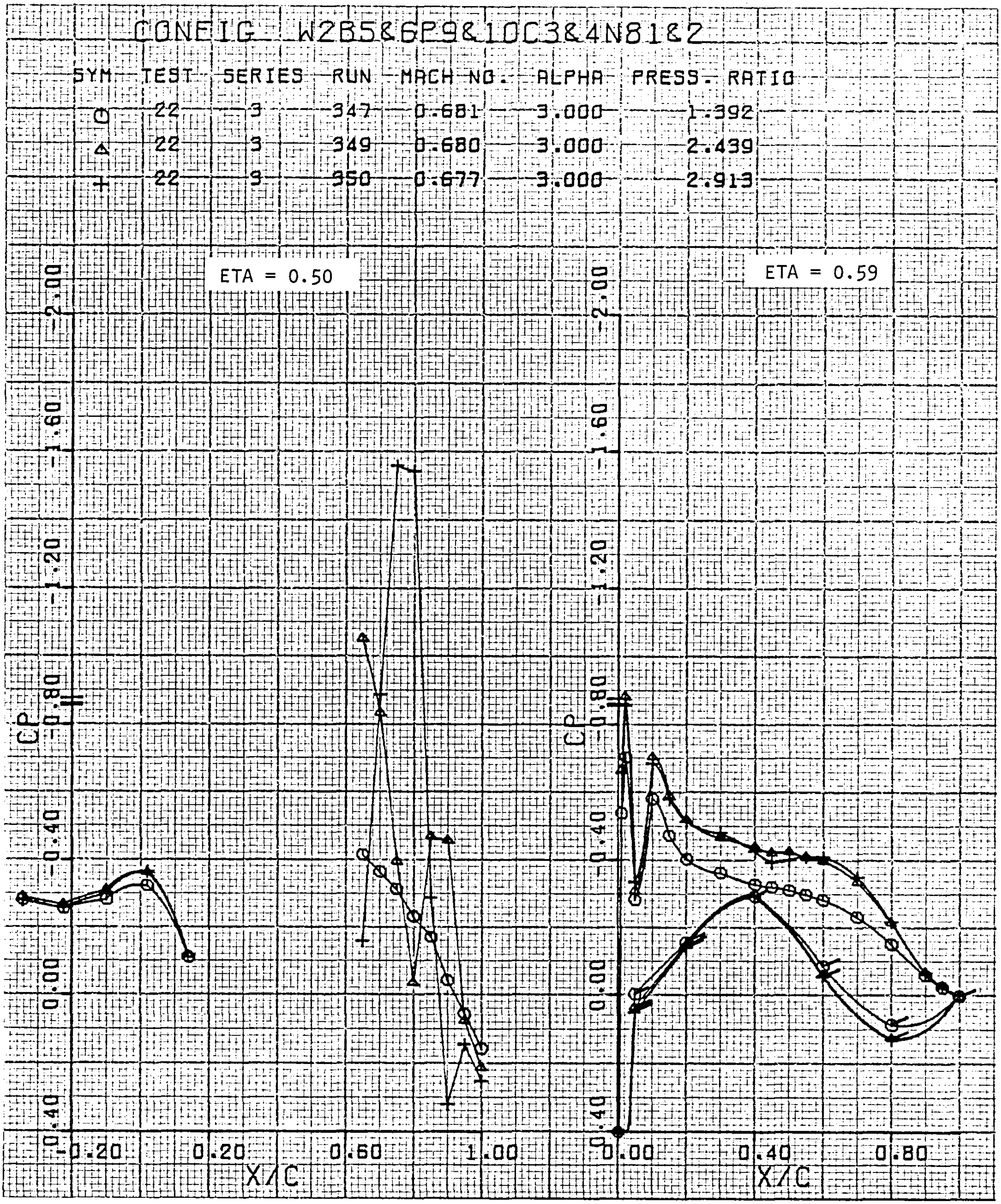

Figure 176. Wing pressure distribution, effect of nozzle pressure ratio, nozzles N_8^1 and N_8^2, $M_\infty = 0.68$, $\eta = 0.50, 0.59$

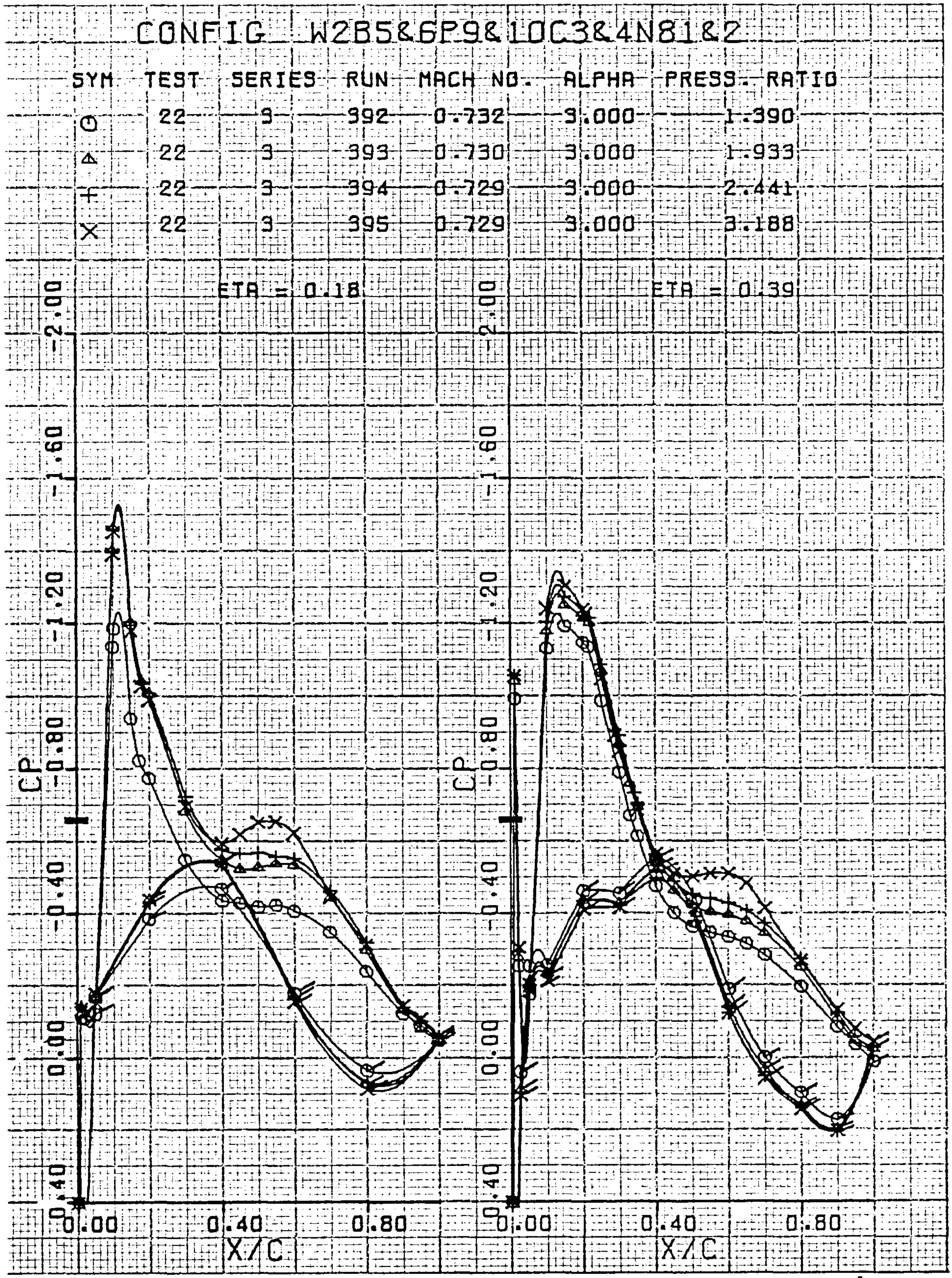

Figure 177. Wing pressure distribution, effect of nozzle pressure ratio, nozzles N_8^{1} and N_8^{2}, $M_\infty = 0.73$, $\eta = 0.18, 0.39$

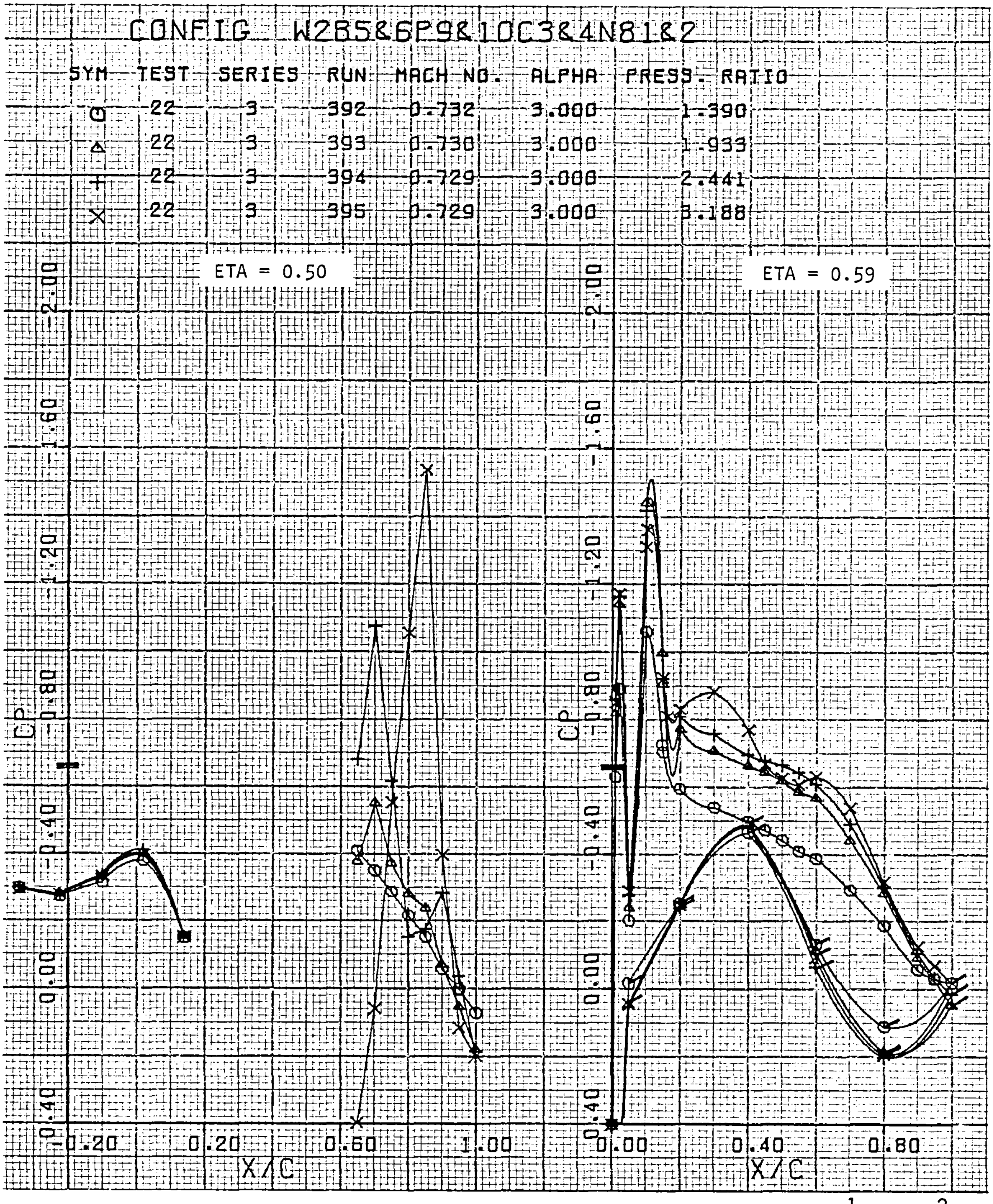

Figure 178. Wing pressure distribution, effect of nozzle pressure ratio, nozzles $N_8^{\ 1}$ and $N_8^{\ 2}$, $M_\infty = 0.73$, $\eta = 0.50, 0.59$

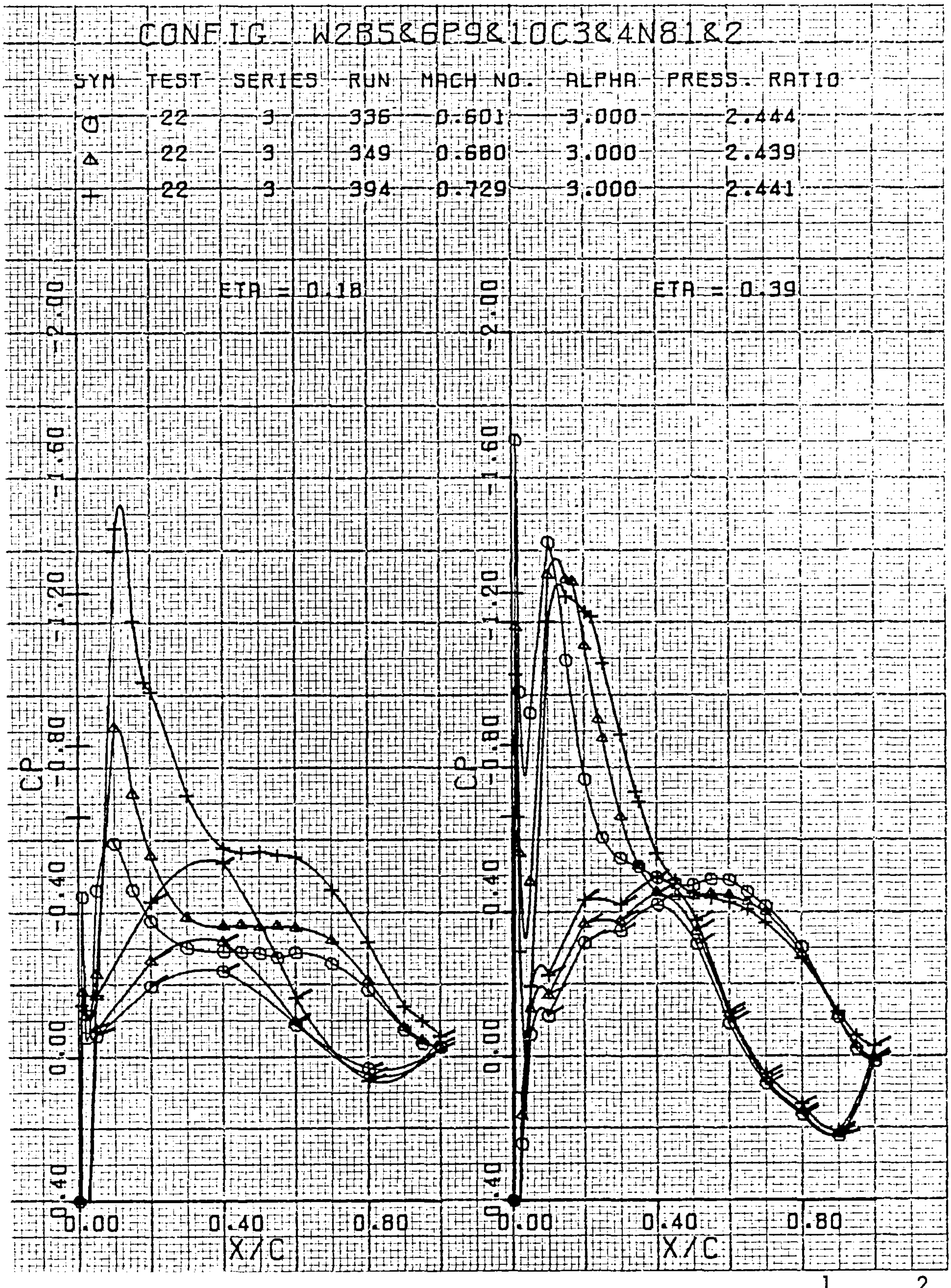

Figure 179. Wing pressure distribution, effect of Mach number, nozzles N_8^1 and N_8^2, η = 0.18, 0.39

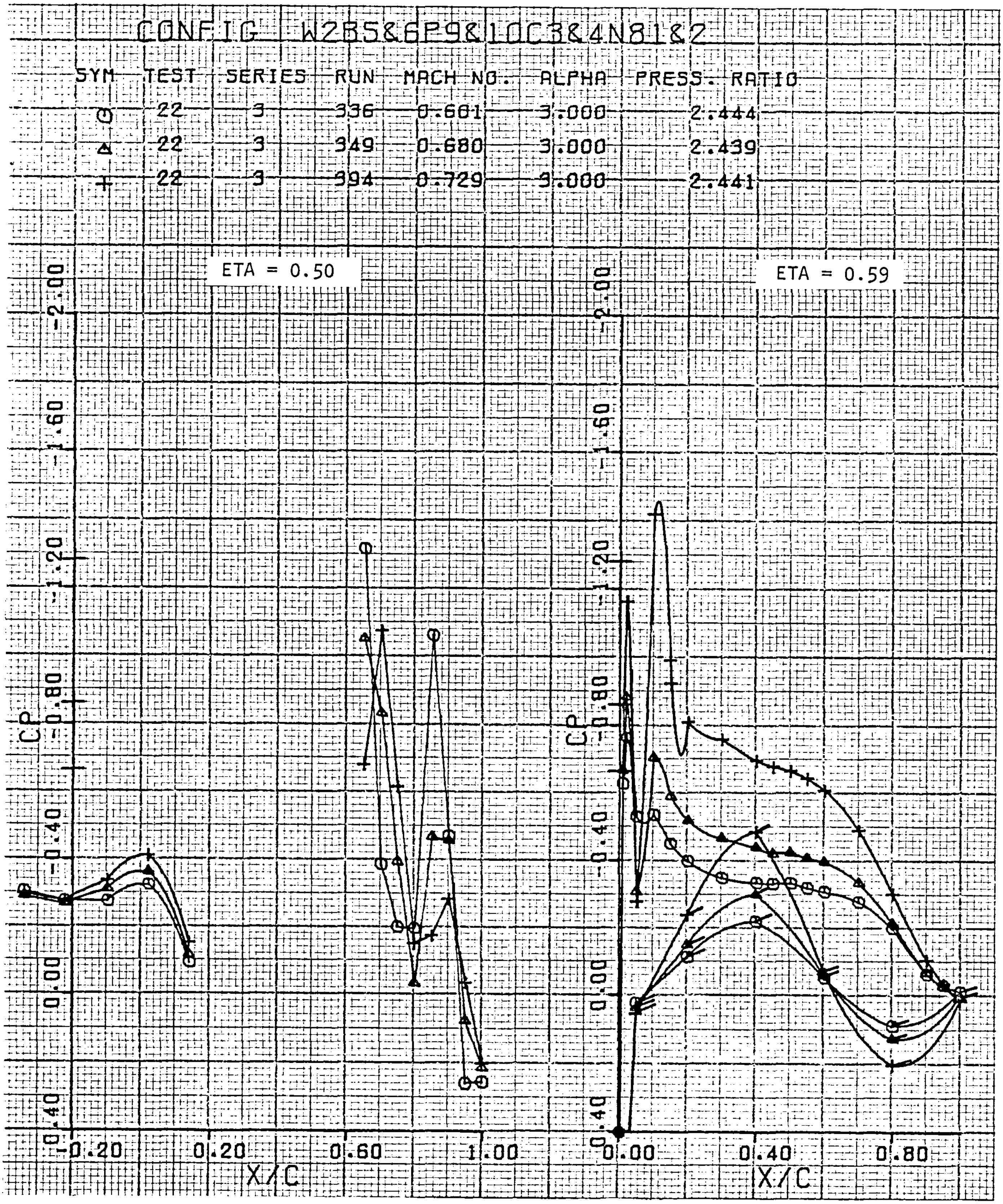

Figure 180. Wing pressure distribution, effect of Mach number, nozzles N_8^{1} and N_8^{2}, η = 0.50, 0.59

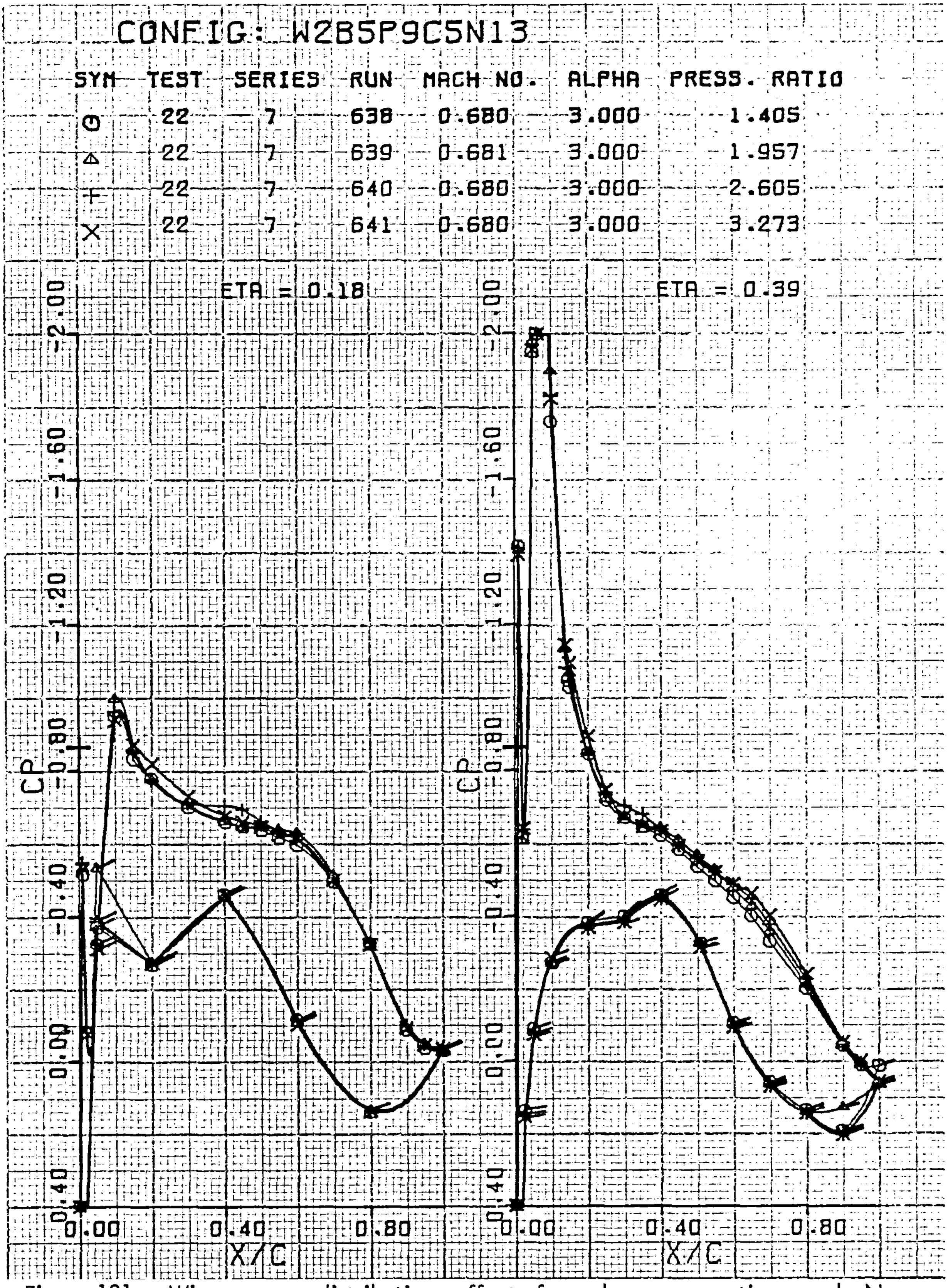

Figure 181. Wing pressure distribution, effect of nozzle pressure ratio, nozzle N_{13}, $M_\infty = 0.68$, $\eta = 0.18, 0.39$

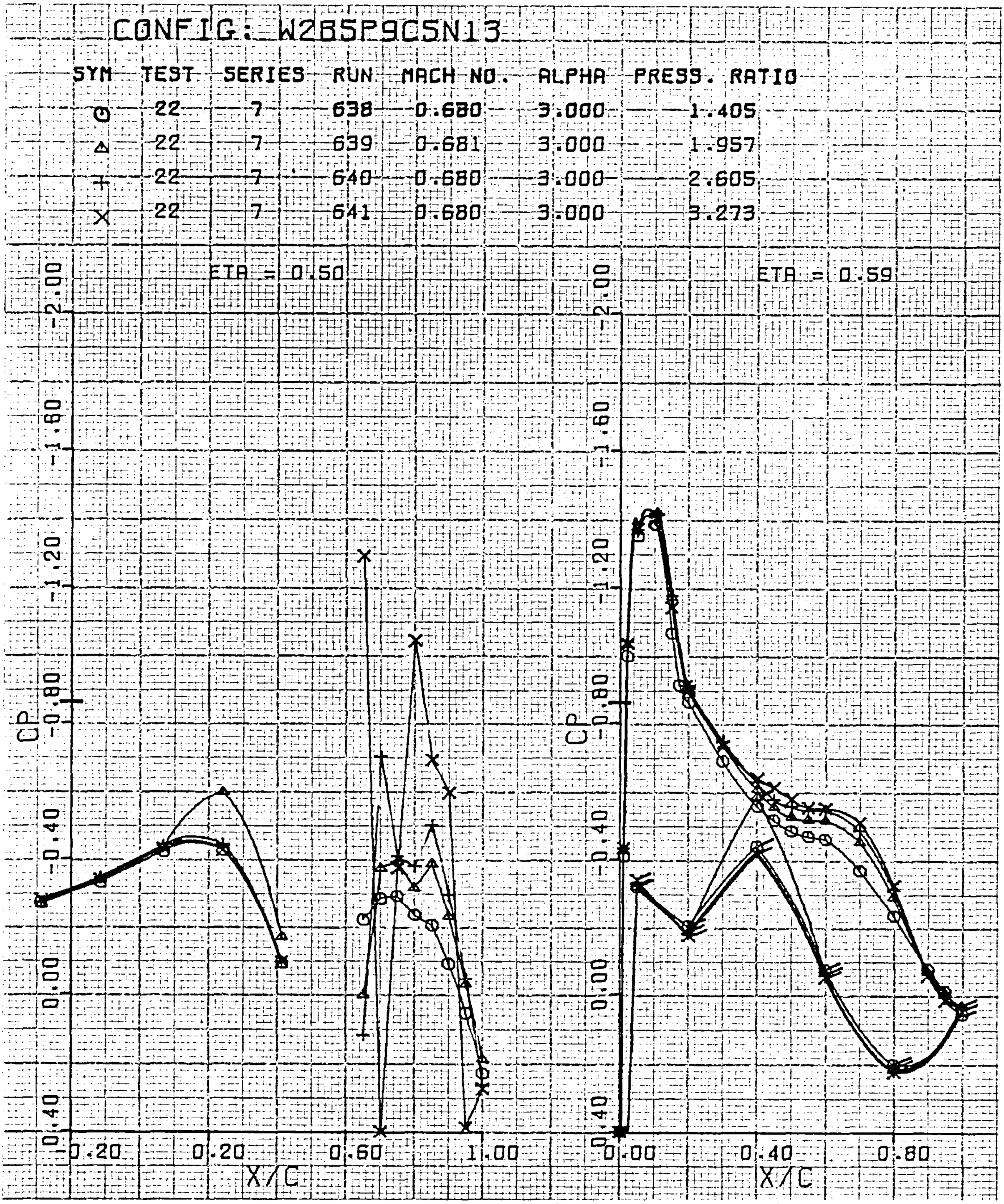

Figure 182. Wing pressure distribution, effect of nozzle pressure ratio, nozzle N_{13}, $M_\infty = 0.68$, $\eta = 0.50, 0.59$

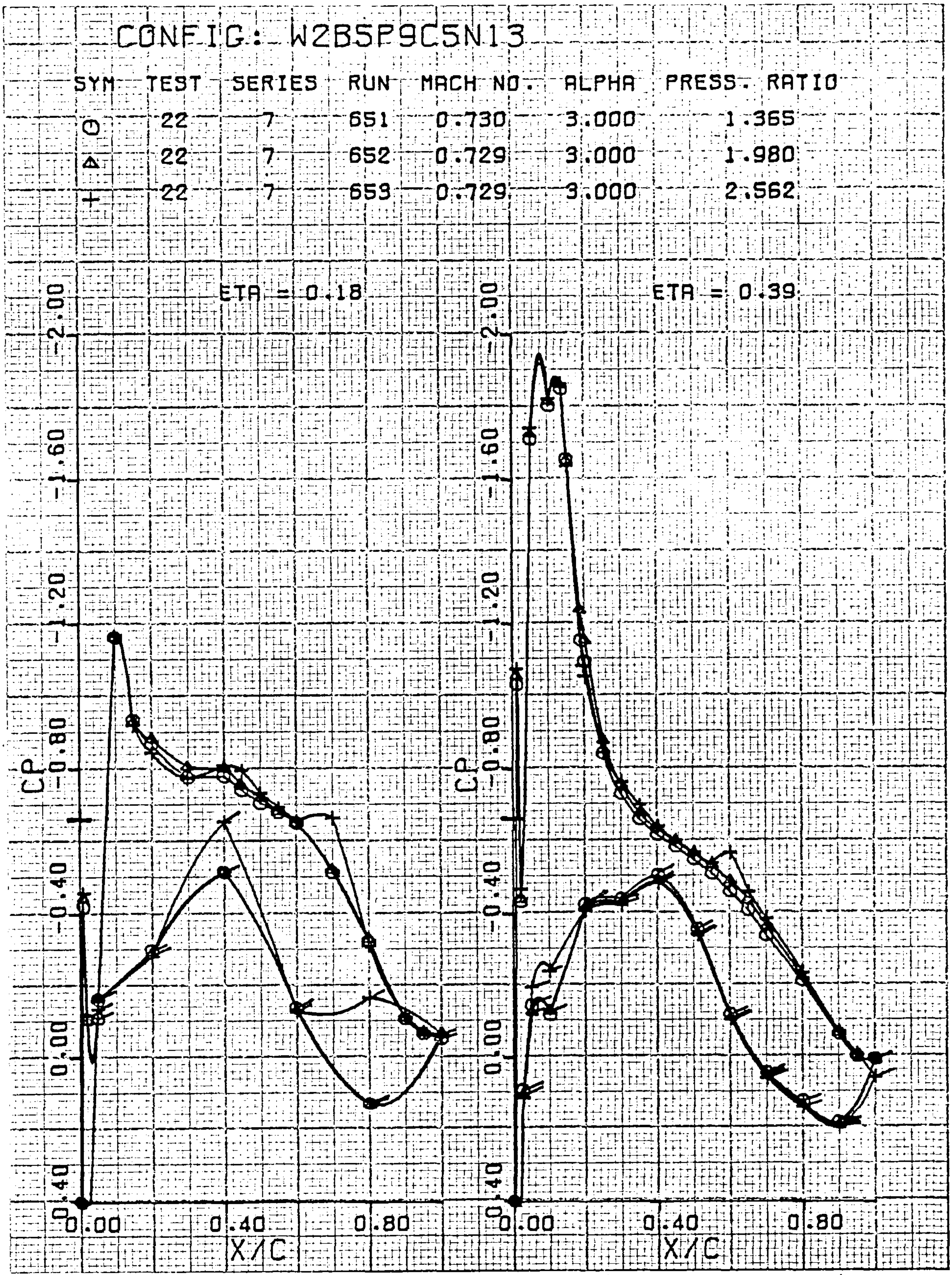

Figure 183. Wing pressure distribution, effect of nozzle pressure ratio, nozzle N_{13}, $M_\infty = 0.73$, $\bar{\eta} = 0.18, 0.39$

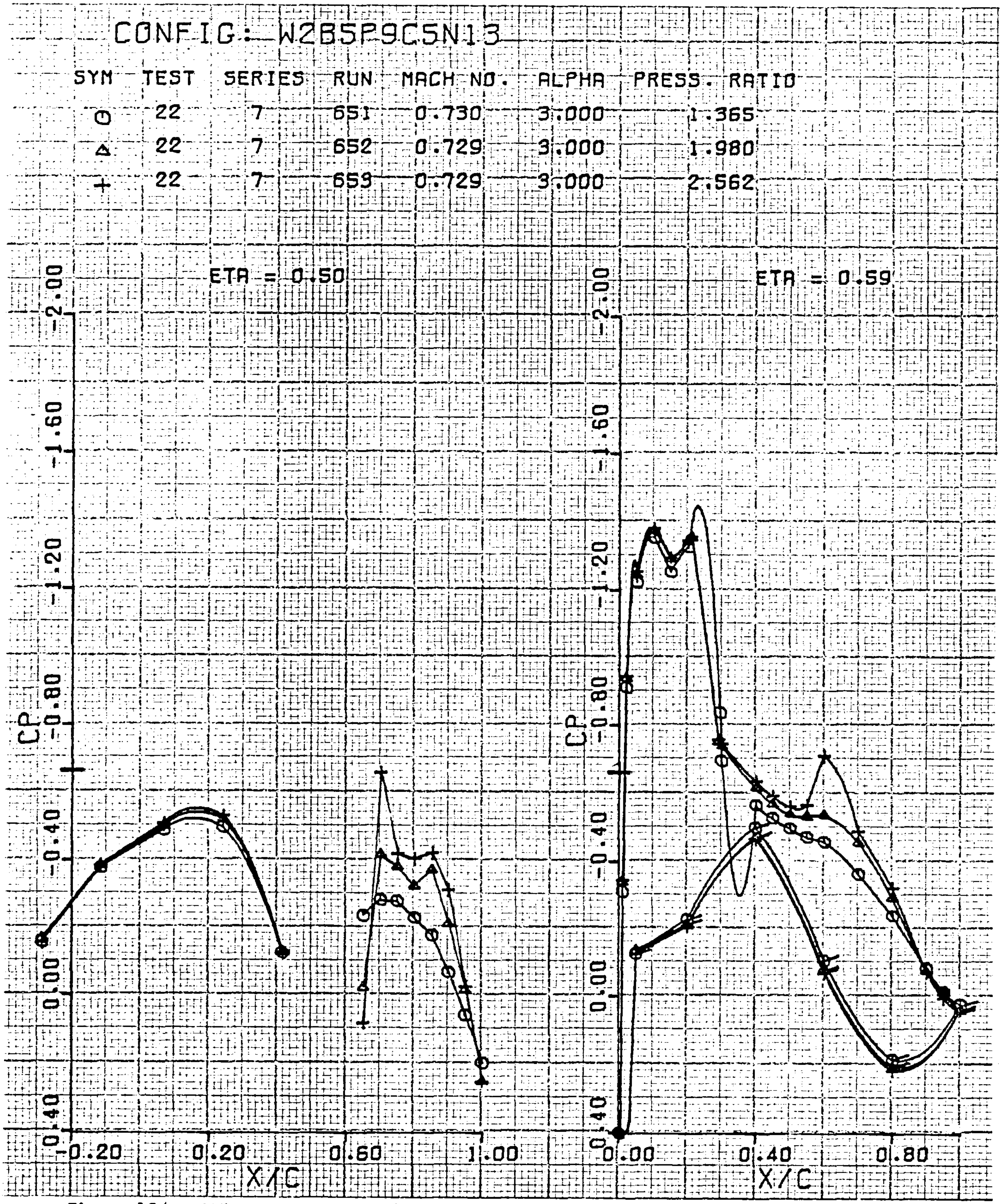

Figure 184. Wing pressure distribution, effect of nozzle pressure ratio, nozzle N_{13}, $M_\infty = 0.73$, $\eta = 0.50, 0.59$

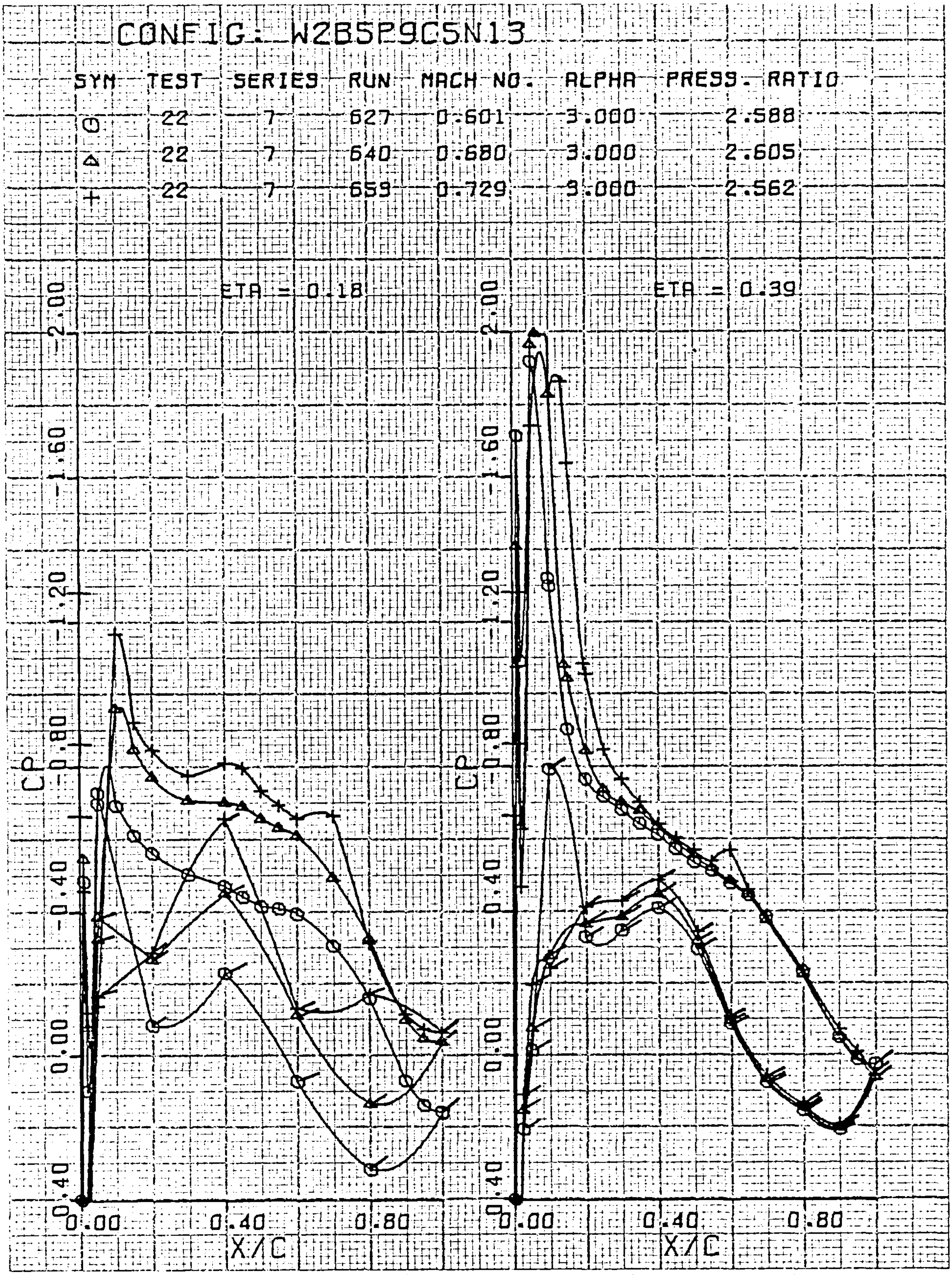

Figure 185. Wing pressure distribution, effect of Mach number, nozzle N_{13}, $\eta = 0.18, 0.39$

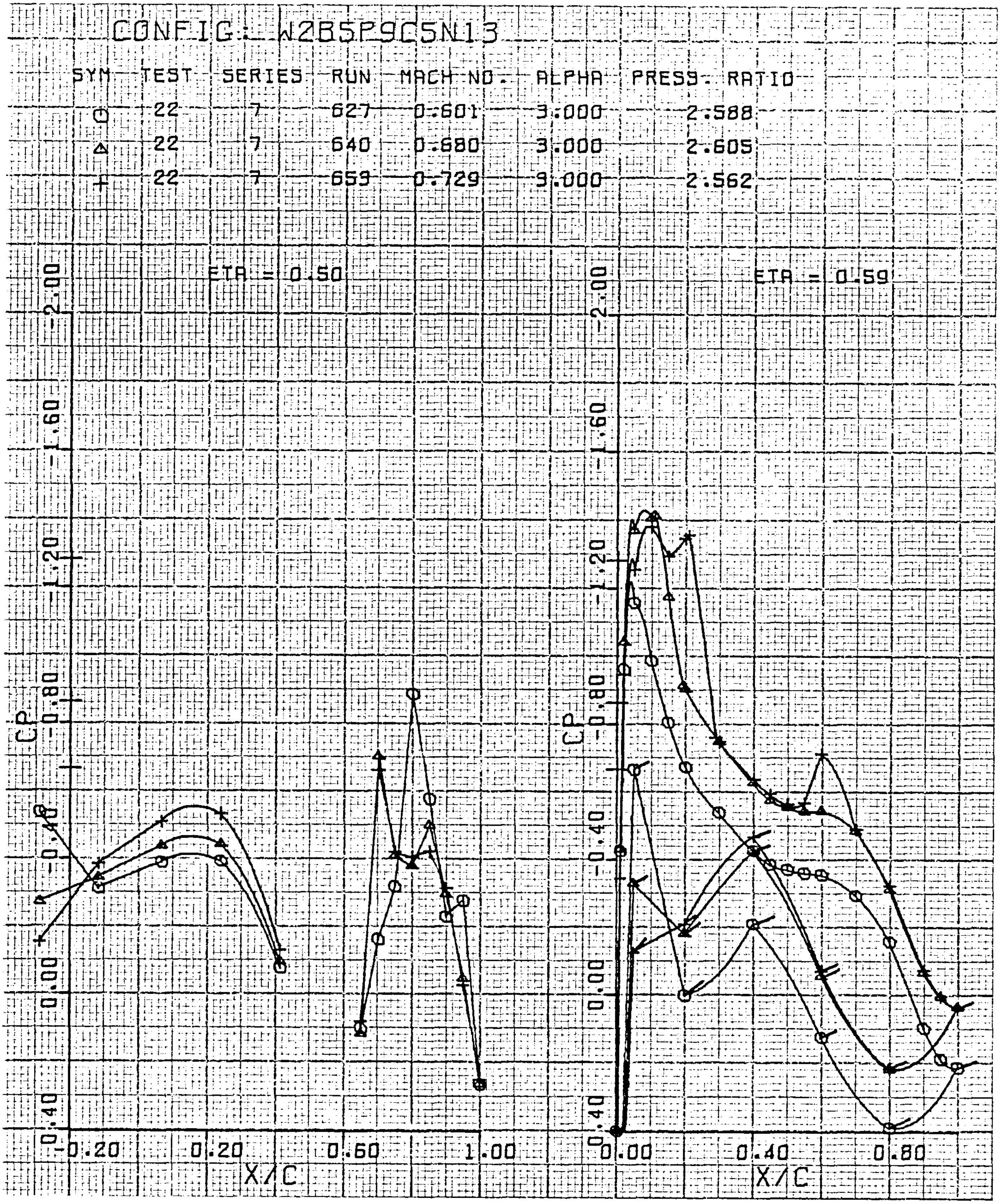

Figure 186. Wing pressure distribution, effect of Mach number, nozzle N_{13}, η = 0.50, 0.59

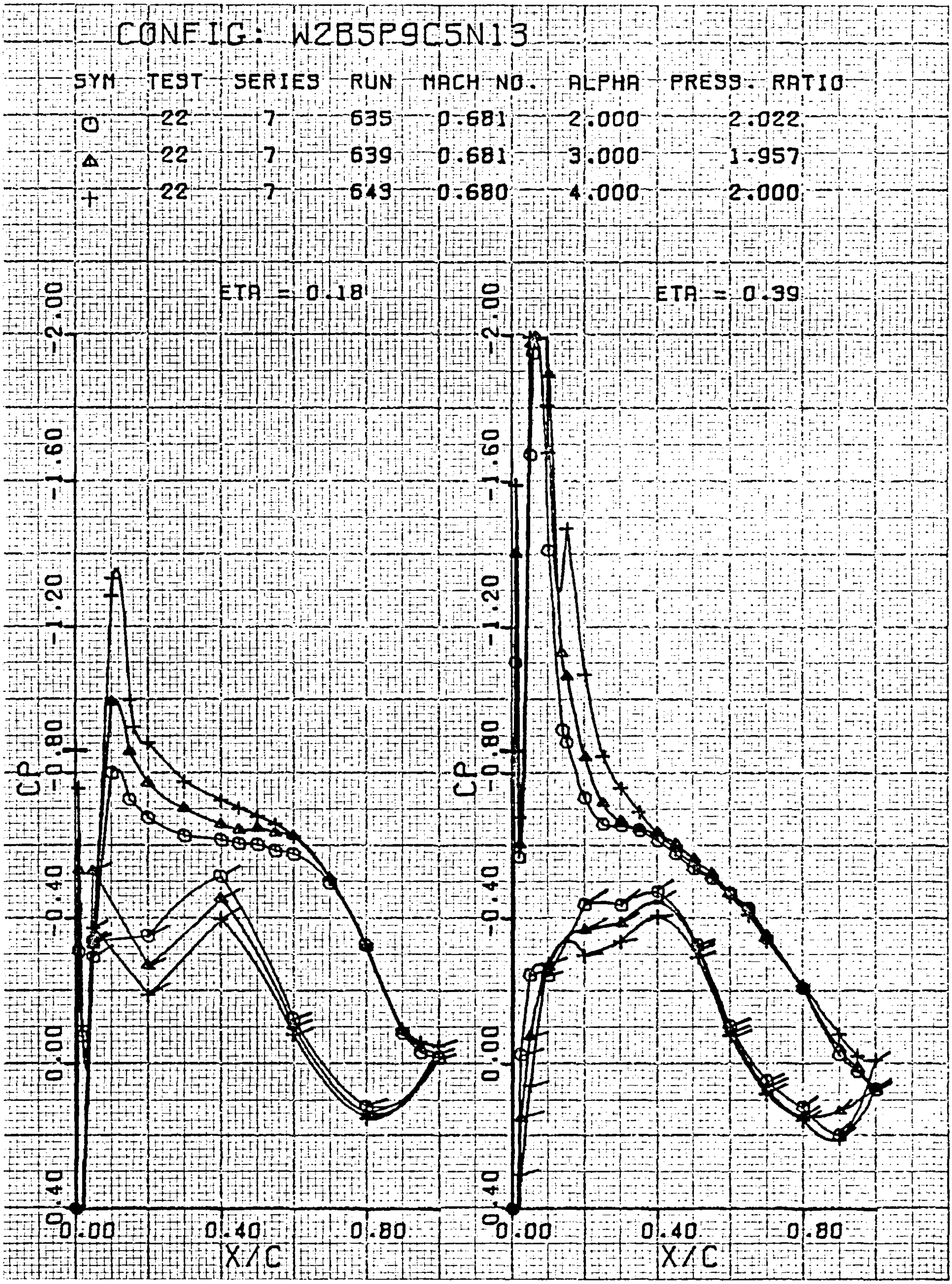

Figure 187. Wing pressure distribution, effect of α, nozzle N_{13}, M_∞ = 0.68, η = 0.18, 0.39

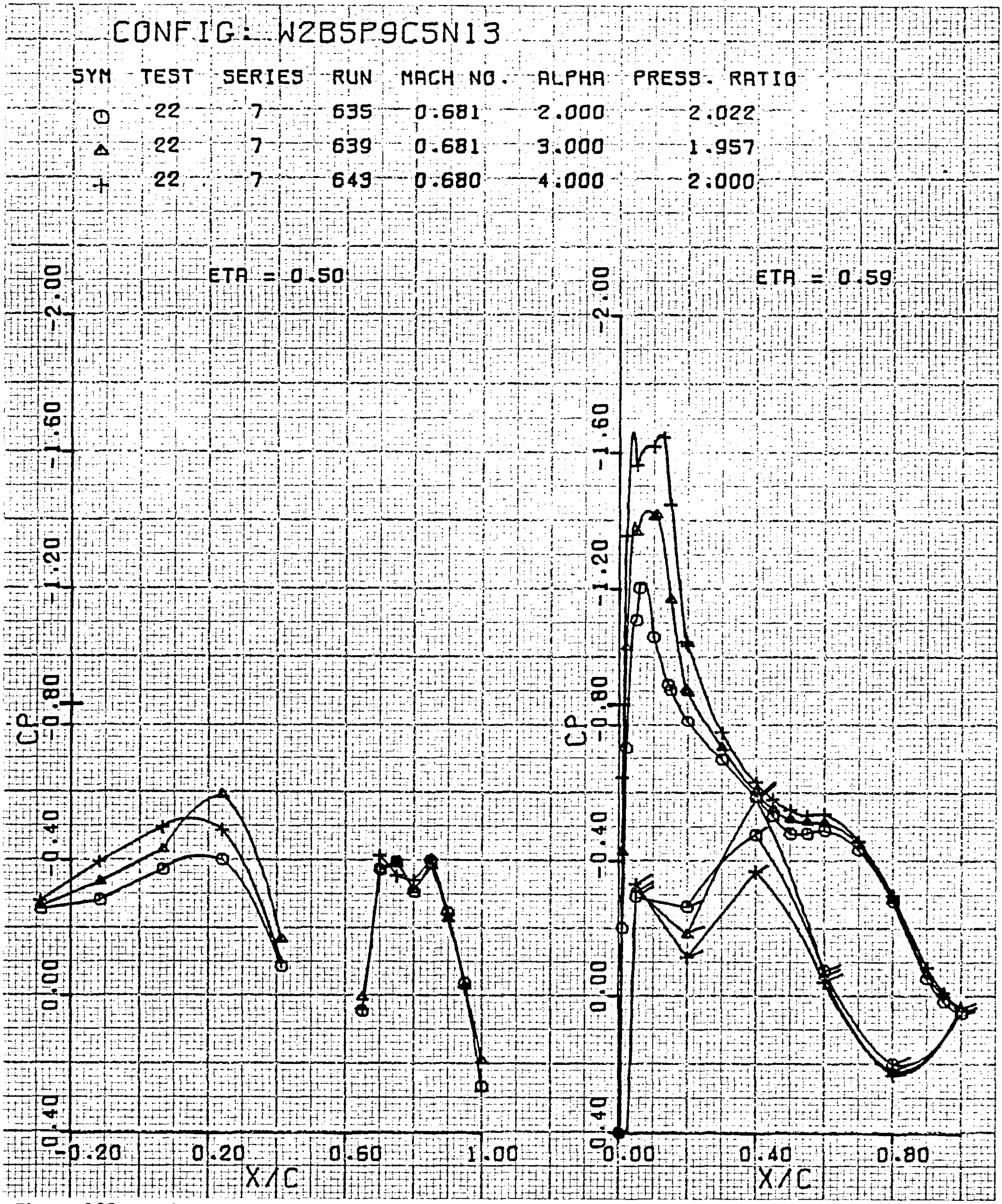

Figure 188. Wing pressure distribution, effect of α, nozzle N_{13}, M_∞ = 0.68, η = 0.50, 0.59

6.2 Wake Pressure Patterns

Isobars for selected swept wing configurations are presented in Figures 189 through 199. The format is identical to that employed for the straight wing isobars and the illustrative figure, 105, applies to this section also.

Model configurations for which wake patterns are presented are N_8^1, N_8^2, and N_{13}.

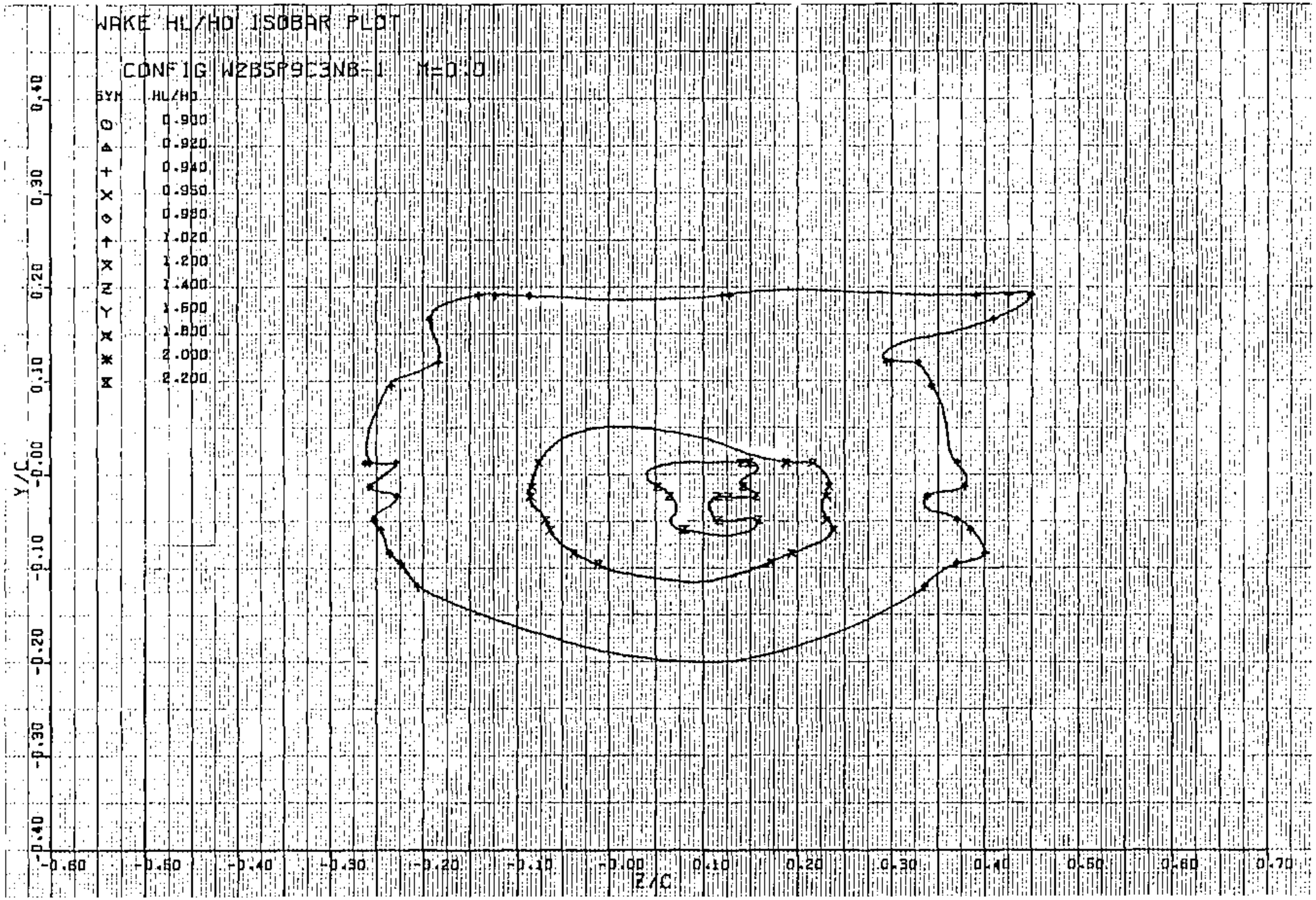

Figure 189. Isobar plot of USB nacelle-wing-jet wake pattern measured one chord length aft of trailing edge, $R_{NC} = 3.5 \times 10^6$, test 22, series 4, run numbers 465 - 470, $\alpha = 3^o$

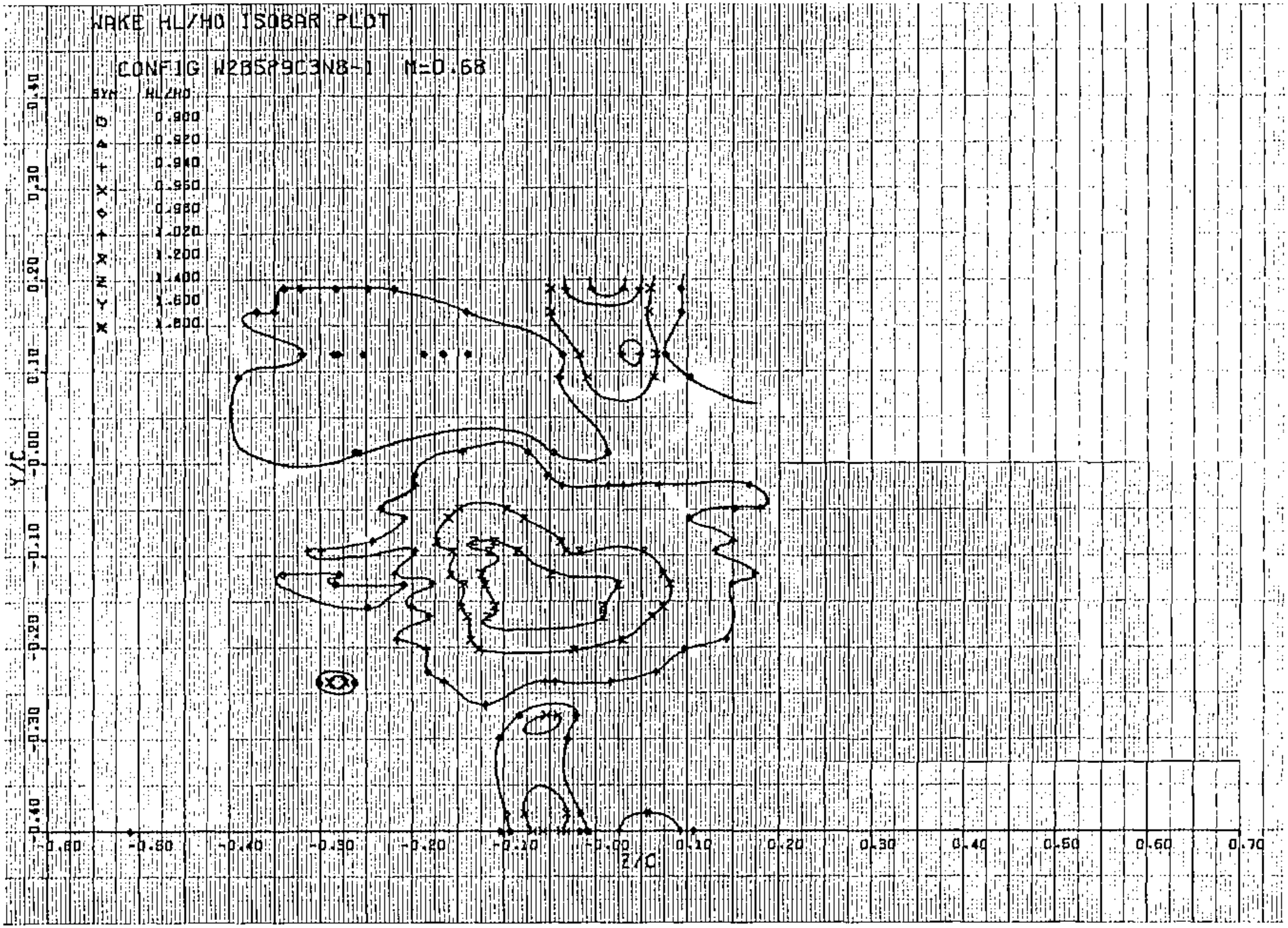

Figure 190. Isobar plot of USB nacelle-wing-jet wake pattern measured one chord length aft of trailing edge, $R_{NC} = 3.5 \times 10^6$, test 22, series 4, run numbers 475 - 489, $\alpha = 3°$

USB CRUISE PROGRAM

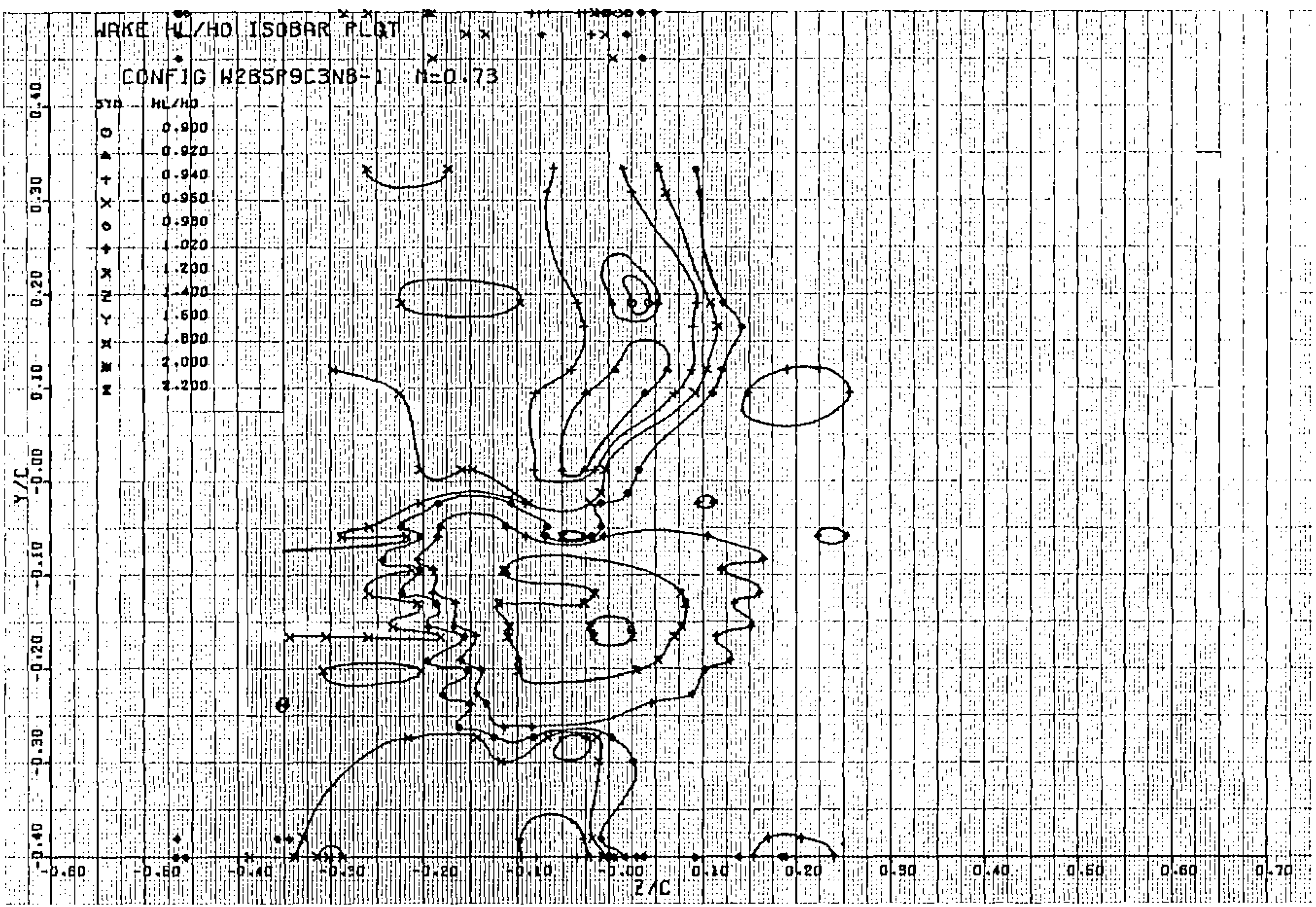

Figure 191. Isobar plot of USB nacelle-wing-jet wake pattern measured one chord length aft of trailing edge, $R_{NC} = 3.5 \times 10^6$, test 22, series 4, run numbers 502 - 515, $\alpha = 3^{\circ}$

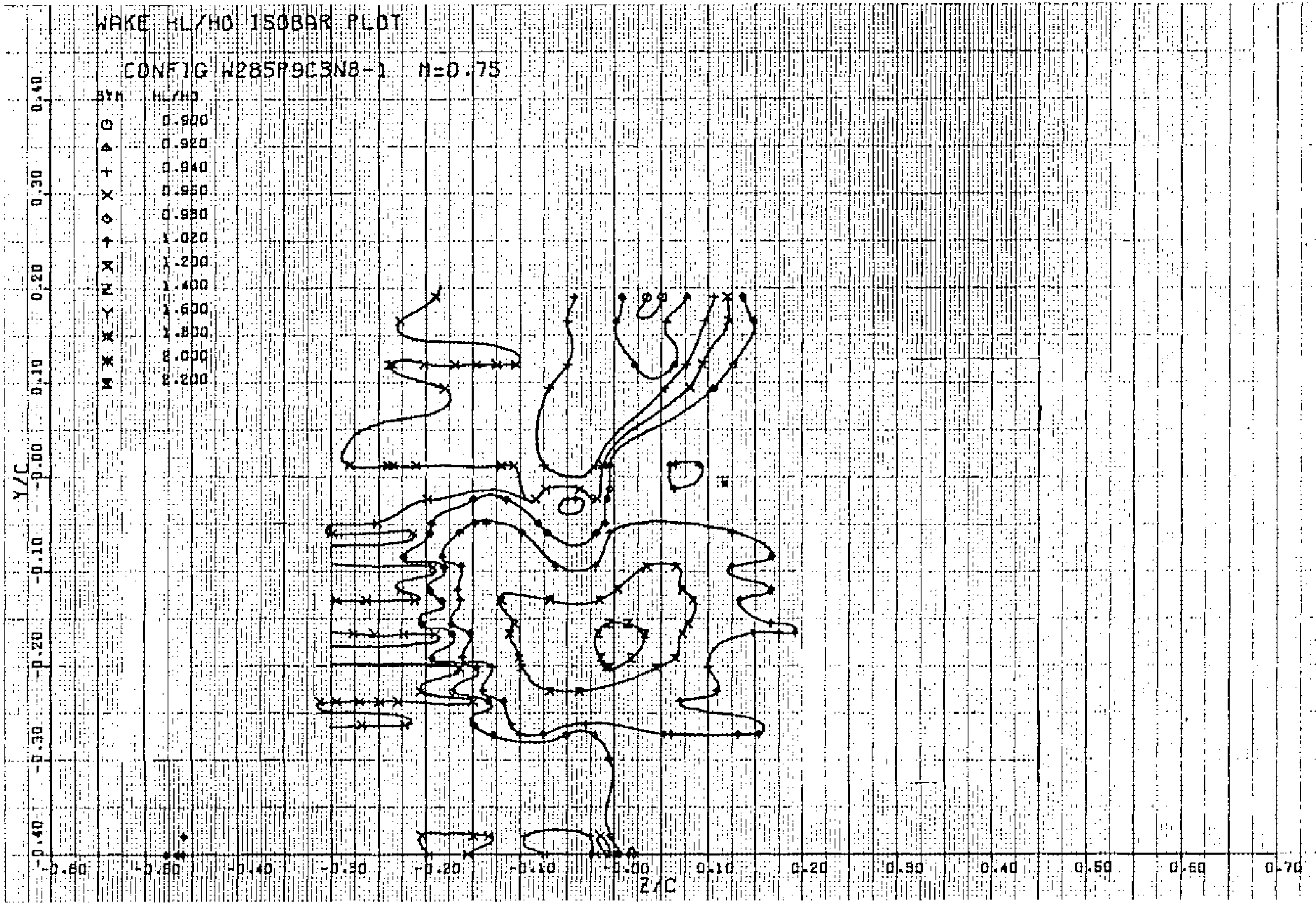

Figure 192. Isobar plot of USB nacelle-wing-jet wake pattern measured one chord length aft of trailing edge, $R_{NC} = 3.5 \times 10^6$, *test 22, series 4, run numbers 533 - 545,* $\alpha = 3^\circ$

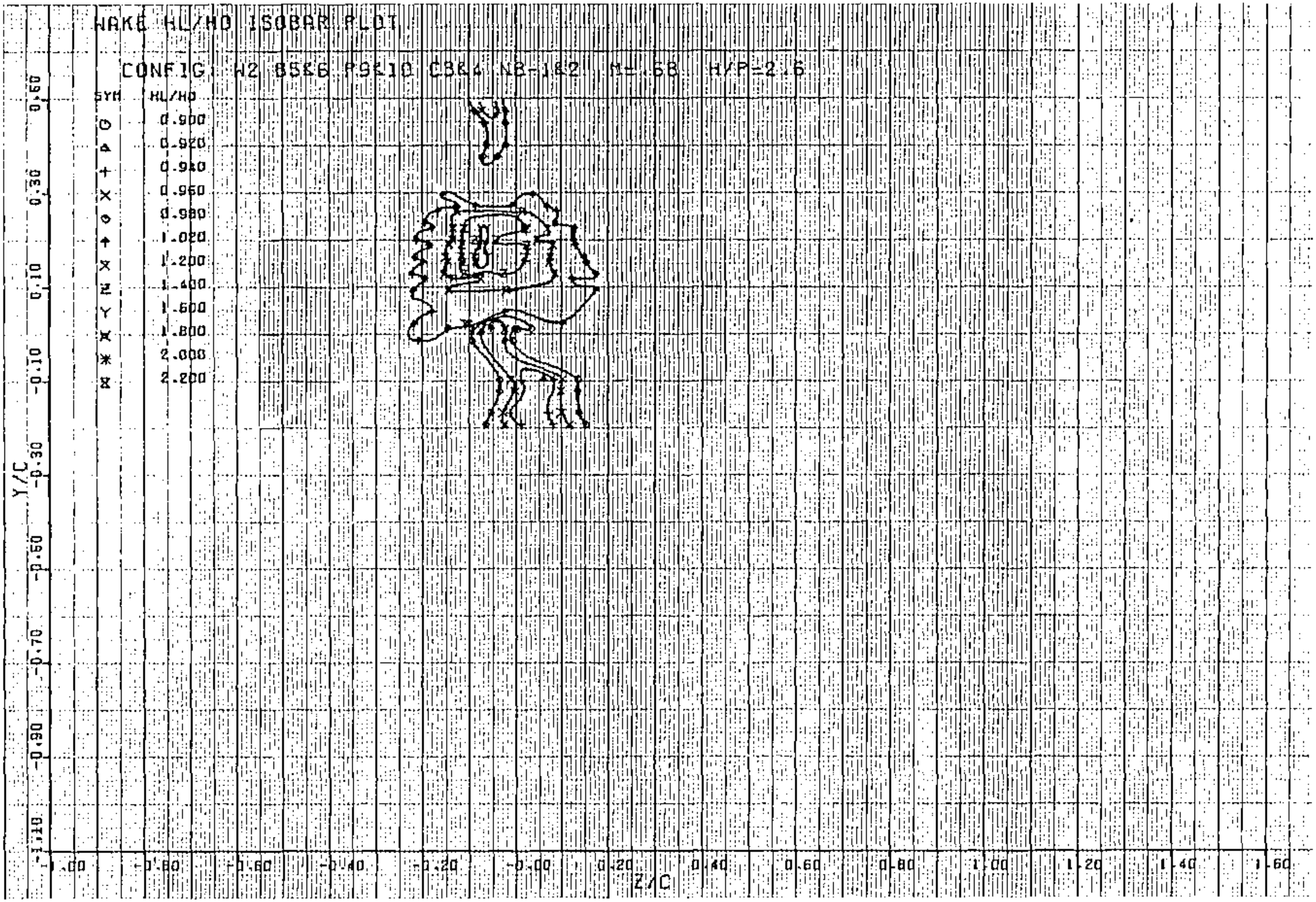

Figure 193. Isobar plot of USB nacelle-wing-jet wake pattern measured one chord length aft of trailing edge, $R_{NC} = 3.5 \times 10^6$, test 22, series 3, run numbers 355 - 367, $\alpha = 3^o$

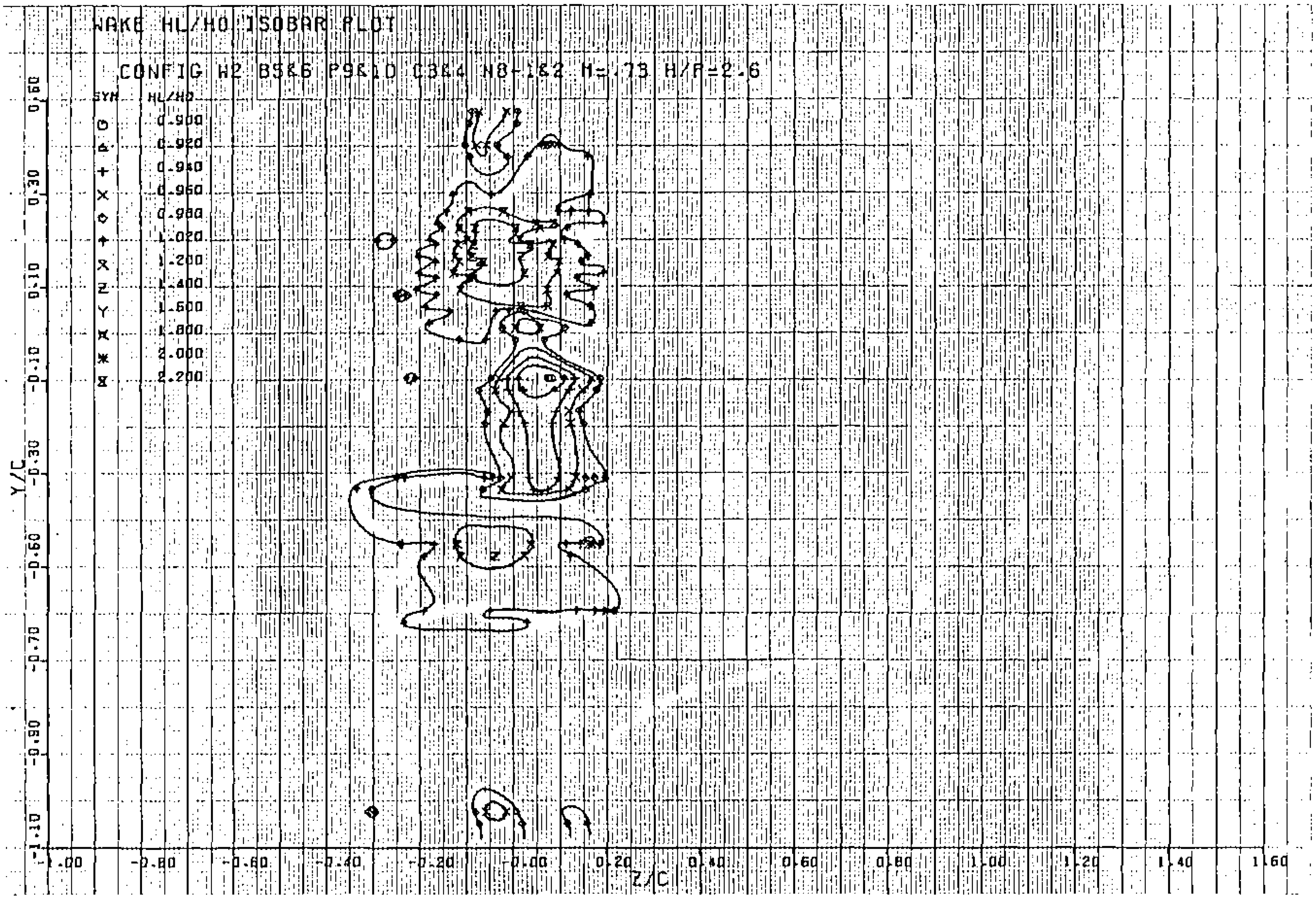

Figure 194. Isobar plot of USB nacelle-wing-jet wake pattern measured one chord length aft of trailing edge, $R_{NC} = 3.5 \times 10^6$, test 22, series 3, run numbers 277 - 297, $\alpha = 3^\circ$

USB CRUISE PROGRAM

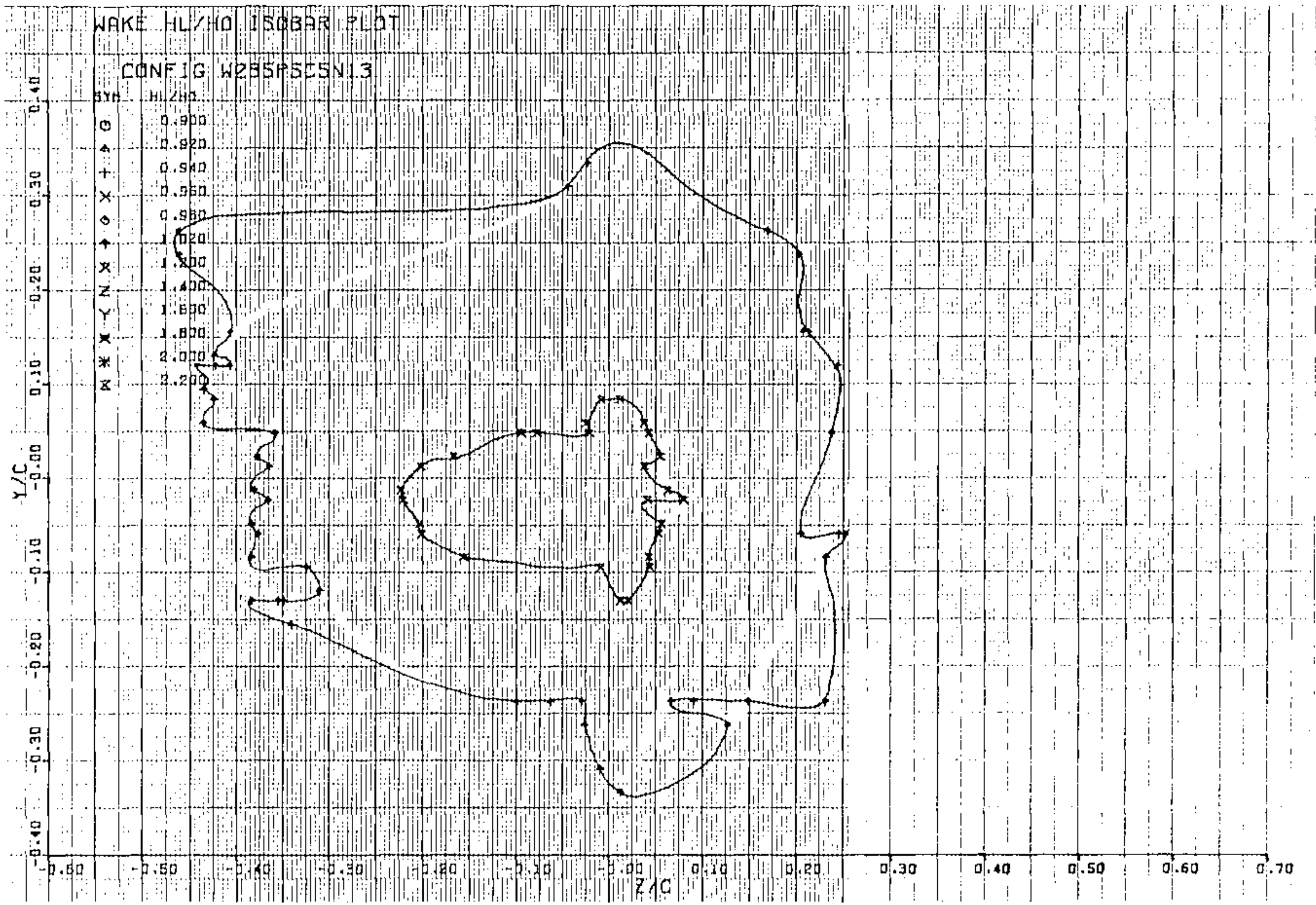

Figure 195. Isobar plot of USB nacelle-wing-jet wake pattern measured one chord length aft of trailing edge, $R_{NC} = 3.5 \times 10^6$, test 22, series 7, run numbers 662 - 674, $\alpha = 0$, $M_\infty = 0$, $H_j/p_\infty = 2.70$

Figure 196. Isobar plot of USB nacelle-wing-jet wake pattern measured one chord length aft of trailing edge, $R_{NC} = 3.5 \times 10^6$, test 22, series 7, run numbers 703 - 715, $\alpha = 3^o$, $M_\infty = 0.68$, $H_j/p_\infty = 2.56$

USB CRUISE PROGRAM

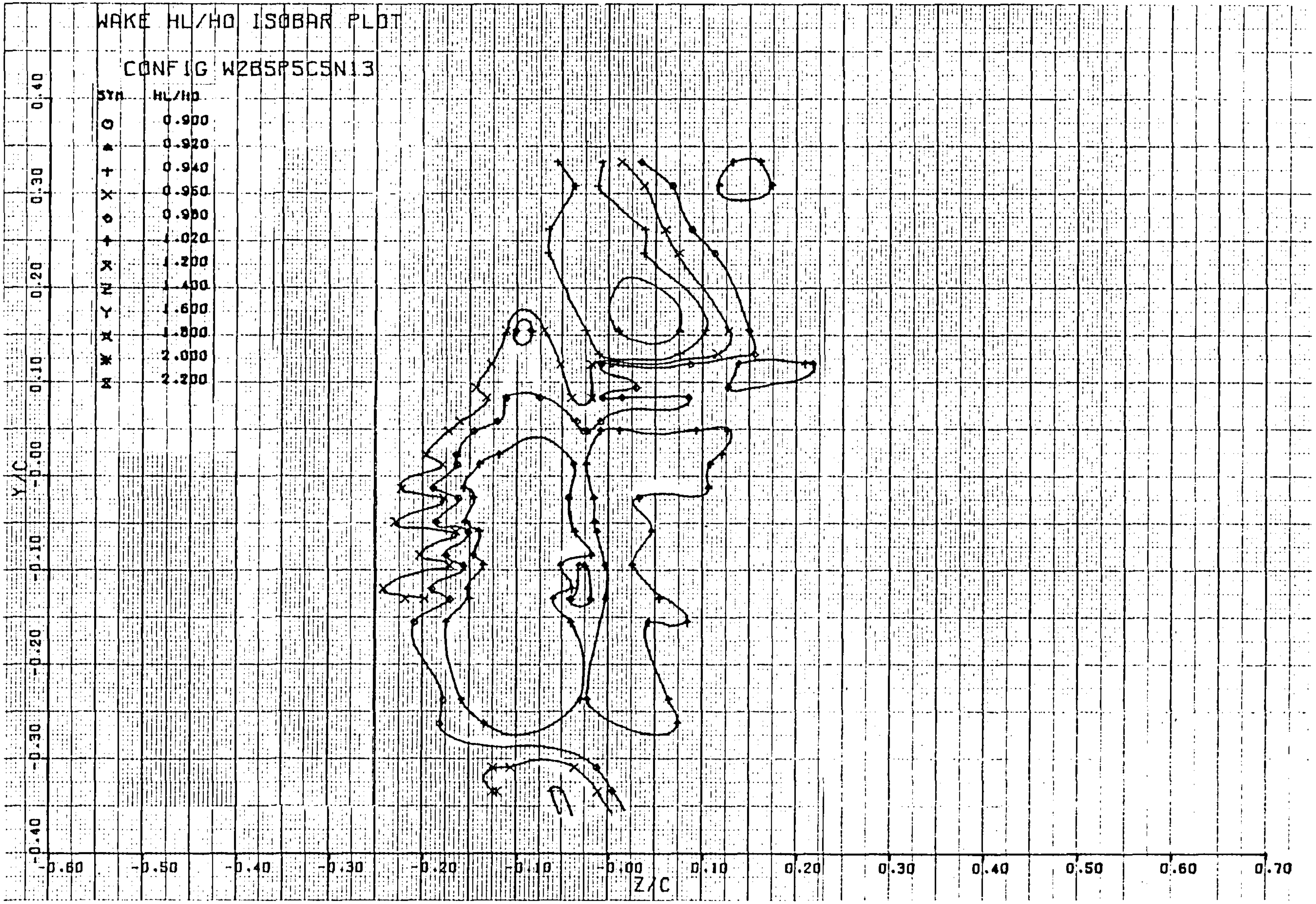

Figure 197. Isobar plot of USB nacelle-wing-jet wake pattern measured one chord length aft of trailing edge, $R_{NC} = 3.5 \times 10^6$, test 22, series 7, run numbers 690 - 702, $\alpha = 3^o$, $M_\infty = 0.73$, $H_j/p_\infty = 2.60$

7.0 REFERENCES

1. Braden, J. A., Hancock, J. P., and Hackett, J. E., "Exploratory Studies of the Cruise Performance of Upper-Surface Blown Configurations, Program Plan", Lockheed-Georgia Company, May 1, 1972.

2. Braden, J. A., Hancock, J. P., Burdges, K. P., and Hackett, J. E., "Exploratory Studies of the Cruise Performance of Upper Surface Blown Configuration, Experimental Program - Test Facilities, Model Design, Instrumentation, and Low-Speed High-Lift Tests," NASA CR-3192, 1979.

1. Report No.	2. Government Accession No.	3. Recipient's Catalog No.
CR-159135		

4. Title and Subtitle
EXPLORATORY STUDIES OF THE CRUISE PERFORMANCE OF UPPER-SURFACE BLOWN CONFIGURATIONS - Experimental Program, High-Speed Pressure Tests

5. Report Date
October 1979

6. Performing Organization Code

7. Author(s)
J. A. Braden, J. P. Hancock, J. E. Hackett, V. Lyman

8. Performing Organization Report No.
LG77ER0028

10. Work Unit No.

9. Performing Organization Name and Address
Lockheed-Georgia Company
86 South Cobb Drive
Marietta, Georgia 30063

11. Contract or Grant No.
NAS1-13871

13. Type of Report and Period Covered
Contractor Report

12. Sponsoring Agency Name and Address
National Aeronautics and Space Administration
Langley Research Center
Hampton, Virginia 23665

14. Sponsoring Agency Code

15. Supplementary Notes

Part of a Series of Reports Covering Various Phases of the USB Program:
CR-3193, CR-3192, CR-159134, CR-159135, CR-159136

16. Abstract

The present report provides basic pressure data obtained from an experimental study of upper-surface blown (USB) configurations at cruise. The high-speed (subsonic) experimental work, studying the aerodynamic effects of wing-nacelle geometric variations, was conducted around semi-span model configurations composed of diversified, interchangeable components. Power simulation was provided by high-pressure air ducted through closed forebody nacelles. Nozzle geometry was varied across size, exit aspect ratio, exit position and boattail angle. Both 3-D force and 2-D pressure measurements were obtained at cruise Mach numbers from 0.5 to 0.8 and at nozzle pressure ratios up to about 3.0. The experimental investigation was supported by an analytical synthesis of the system using a vortex lattice representation with first-order power effects. Results are also presented from a compatibility study in which a short-haul transport is designed on the basis of the aerodynamic findings in the experimental study as well as acoustical data obtained in a concurrent program. High-lift test data are used to substantiate the projected performance of the selected transport design.

17. Key Words (Suggested by Author(s))	18. Distribution Statement
Subsonic cruise performance Propulsion integration High-lift Transport design	Unclassified - Unlimited

19. Security Classif. (of this report)	20. Security Classif. (of this page)	21. No. of Pages	22. Price*
UNCLASSIFIED	UNCLASSIFIED	209	

* For sale by the National Technical Information Service, Springfield, Virginia 22161